Doctoral Thesis
for the academic degree of
Dr. rer. nat.

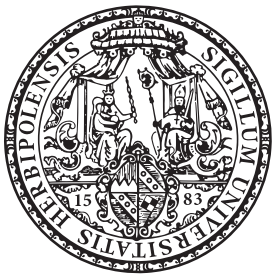

Universitätsklinikum
Würzburg

Establishment of a 3D tumour model and targeted therapy of *BRAF*-mutant colorectal cancer

submitted by
Florentin Philipp Baur
from Heilbronn

January 2018

conducted at
Chair Tissue Engineering & Regenerative Medicine
of the
University Hospital Würzburg

First Supervisor:
Prof. Dr. Heike Walles

Second Supervisor:
Prof. Dr. Thomas Dandekar

Submitted on: _____

Members of the promotion committee:

Chairperson: _____

First Supervisor: _____

Second Supervisor: _____

Date of public defence: _____

Date of receipt of certificates: _____

Tempus fugit.

"Omne adeo genus in terris hominumque ferarumque
et genus aequoreum, pecudes pictaeque volucres,
in furias ignemque ruunt: amor omnibus idem. ...
Sed fugit interea, fugit inreparabile tempus,
singula dum capti circumvectamur amore."

Vergilius Maro, Publius. *Georgicon*, III. 29 BC.

Contents

List of Figures

List of Tables

Abbreviations

Table 1: List of abbreviations

Abbreviation	**Meaning**
%	percent
©	copyright
®	registered
™	trademark
°C	degree Celsius
α-tubulin	alpha-tubulin
β-Cat.	beta-catenin
µl	microlitre
µM	micromolar ($\frac{\mu mol}{l}$)
µm	micrometer
2D	two-dimensional
3D	three-dimensional
3-HSD	3-α-hydroxysteroid dehydrogenase
5-FU	5-fluorouracil
A	Austria
Akt	AKT serine/threonine kinase 1, protein kinase B
Alcian blue-PAS stain	alcian blue-periodic acid-Schiff stain
APC	adenomatous polyposis coli gene
AML	acute myeloid leukaemia
APS	ammonium peroxydisulphate
ATP	adenosine triphosphate
BCR-ABL	breakpoint cluster region-Abelson proto-oncogene
BioVaSc®	biological vascularised scaffold (registered)
BRCA1	breast cancer 1 gene
BRAF	rapidly accelerated fibrosarcoma oncogene type B gene
BSA	bovine serum albumin (fraction V)

Table 1: List of abbreviations (continued)

Abbreviation	**Meaning**
Ca^{2+}	calcium ion
CAFs	cancer-associated fibroblasts
CC	co-culture
ccK18	caspase-cleaved cytokeratin 18
CD34	cluster of differentiation 34 molecule
CD38	cluster of differentiation 38 molecule, ADP-ribosyl cyclase 1
CD44	cluster of differentiation 44 molecule, Indian blood group
CD133	cluster of differentiation 133 molecule, prominin 1
CD166	cluster of differentiation 166 molecule, activated leukocyte cell adhesion molecule (ALCAM)
CH	Confoederatio Helvetica (Switzerland)
CICs	cancer-initiating cells
CIMP	cytosine-guanosine (CpG) island methylation phenotype
CIN	chromosomal instability
CK7	Cytokeratin-7
CK18	Cytokeratin-18
CK20	Cytokeratin-20
cm	centimetre
cm^2	square centimetre
CML	chronic myeloid leukaemia
CO_2	carbon dioxide
CpG	cytosine-guanosine
Col. IV	collagen type IV
CRC	colorectal cancer
CSCs	cancer stem cells
CTC	computed tomographic colonography
ctrl.	control
D	Deutschland (Germany)
DAB	3,3'-Diaminobenzidine
DAPI	4',6-diamidino-2-phenylindole

Table 1: List of abbreviations (continued)

Abbreviation	**Meaning**
ddH_2O	double-distilled water
DMEM	Dulbecco's modified Eagle medium
DMSO	dimethyl sulfoxide
DNA	deoxyribonucleic acid
DNase	deoxyribonuclease
e.g.	exempli gratia
E-Cad.	E-cadherin
ECM	extracellular matrix
EDTA	ethylenediaminetetraacetic acid
EGF	epidermal growth factor
EGFR	epidermal growth factor receptor
ELISA	enzyme-linked immunosorbent assay
EMT	epithelial-mesenchymal transition
EpCAM	epithelial cell adhesion molecule
et al.	et alii
Erk1/2	extracellular signal-related kinases 1/2, MAPK1
Fab domain	fragment antigen-binding domain
Fc region	fragment crystallisable region
FCS	foetal calf serum
FDA	Food and Drug Administration (of the United States)
FGFR	fibroblast growth factor receptor
Fig.	figure
FITC	fluorescein isothiocyanate
FOBT	faecal occult blood test
FOLFIRI	folinic acid (leucovorin), 5-fluorouracil and irinotecan
FOLFOX	folinic acid (leucovorin), 5-fluorouracil and oxaliplatin
g	gram
GB	Great Britain
h	hour(s)
H&E staining	haematoxylin and eosin staining
H_2O_2	hydrogen peroxide

Table 1: List of abbreviations (continued)

Abbreviation	**Meaning**
HER-2	human epidermal growth factor receptor 2
HCl	hydrochloric acid
HCV	hepatitis C virus
HGF	hepatocyte growth factor
HGFR	hepatocyte growth factor receptor, Met or c-Met
HNPCC	hereditary non-polyposis colorectal cancer (Lynch syndrome)
HRP	horseradish peroxidase
Hz	Hertz ($\frac{1}{s}$)
I	Italy
i.p.	intra-peritoneal
IF staining	immunofluorescence staining
IHC staining	immunohistochemical staining
kDa	kilo Dalton
kg	kilogram
KRAS	Kirsten rat sarcoma viral oncogene homologue gene
l	litre
M	molar ($\frac{mol}{l}$)
mA	milliampere
MAPK pathway	mitogen-activated protein kinase pathway
MC	monoculture
MEK	mitogen-activated protein kinase kinase (MAPKK)
Met	hepatocyte growth factor receptor (HGFR), c-Met
MET	mesenchymal-epithelial transition
Mg^{2+}	magnesium ion
mg	milligram
min	minute(s)
ml	millilitre
MLH1	mutL (*E. coli*) homologue 1, HNPCC2 gene
mM	millimolar ($\frac{mmol}{l}$)
mm	millimetre

Table 1: List of abbreviations (continued)

Abbreviation	Meaning
mm^2	square millimetre
MMR	mismatch-repair
MMR-D	mismatch-repair deficiency
ms	millisecond(s)
MSH2	mutS (*E. coli*) homologue 2, HNPCC1 gene
MSH6	mutS (*E. coli*) homologue 6 gene
MSI	microsatellite instability
MSS	microsatellite stability/stable
MTT	3-(4,5-dimethylthiazol-2-yl)-2,5-diphenyltetrazolium bromide
N	Norway
N_2	nitrogen
NaCl	sodium chloride
NAD(H)/NADP(H)	nicotinamide adenine dinucleotide/ nicotinamide adenine dinucleotide phosphate
NaF	sodium fluoride
neg. ctrl.	negative control
ng	nanogram
NIH	National Institute of Health (USA)
NL	Netherlands
nm	nanometre
PAS stain	periodic acid-Schiff stain
PBS	phosphate-buffered saline
PBS^-	phosphate-buffered saline without calcium/magnesium
PBS^+	phosphate-buffered saline with calcium/magnesium
PBS-T	phosphate-buffered saline with Tween-20
PCK	pan-cytokeratin
PD-1	programmed cell death 1, PDCD1
PD-L1	programmed cell death ligand-1
PDGFR	platelet-derived growth factor receptor
PenStrep	penicillin/streptomycin

Table 1: List of abbreviations (continued)

Abbreviation	**Meaning**
PI3K	phosphatidylinositol-4,5-bisphosphate 3-kinase
PMS2	postmeiotic segregation increased (*S. cerevisiae*) 2, HNPCC4 gene
PVDF	polyvinylidene difluoride
RAF-1	C-Raf proto-oncogene serine/threonine kinase, CRAF (see *BRAF*)
RAS	rat sarcoma proto-oncogene, GTPase (see *KRAS*)
RIPA	radio-immunoprecipitation assay
RNA	ribonucleic acid
rpm	revolutions per minute
RPMI-1640	Roswell Park Memorial Institute medium 1640
RT	room temperature
RTK	receptor tyrosine kinase
S	Sweden
SCID	severe combined immunodeficiency
SD	standard deviation
SDS	sodium dodecyl sulphate
SDS-PAGE	sodium dodecyl suphate-polyacrylamide gelelectrophoresis
SEM	standard error of the mean
SIS	small intestinal submucosa
SISmuc	small intestinal submucosa with mucosa
SMAD4	mothers against decapentaplegic homologue 4 (*Drosophila*), DPC4 gene
Tab.	table
TBS	tris-buffered saline
TBS-T	tris-buffered saline with Tween-20
TEMED	N'-tetramethylethylenediamine
TGF-β	transforming growth factor beta
TICs	tumour-initiating cells
TKI	tyrosine kinase inhibitor
TMB	3,3',5,5'-tetramethylbenzidine

Table 1: List of abbreviations (continued)

Abbreviation	**Meaning**
TP53	tumour suppressor p53 gene
U	unit(s)
US/USA	United States of America
USD	US Dollar
V	Volt(s)
v/v	volume per volume
v/w	volume per weight
VEGF	vascular endothelial growth factor receptor
Vim.	vimentin
WB	western blot

Summary/Zusammenfassung

Summary

Cancer remains after cardiovascular diseases the leading cause of death worldwide and an estimated 8.2 million people died of it in 2012 [1]. By 2030, 13 million cancer deaths are expected due to the growth and ageing of the population. Hereof, colorectal cancer (CRC) is the third most common cancer in men and the second in women with a wide geographical variation across the world.

Usually, CRC begins as a non-cancerous growth leading to an adenomatous polyp, or adenoma, arising from glandular cells. Yet less than 10 % of adenomas become malignant, they are generally considered to be the precursors of adenocarcinomas which account for approximately 96 % of all CRCs. Since screenings, e.g. colonoscopy, provide an unique opportunity for the early detection and removal of pre-cancerous polyps before they develop into a carcinoma, the risk of CRC-related death can be reduced up to 53 %. However, screening cannot prevent cancer from developing and most patients with CRC will have to have some type of surgery to remove the tumour. Additionally, adjuvant chemotherapy and/or radiation therapy may be recommended after surgery, but if distant metastases already exist, chemotherapy as well as radiation might be the only options left for treatment. Since research has brought about better understanding of the mechanisms of cancer development, novel treatments such as targeted therapy have emerged in the past decades.

Despite that, up to 95 % of anticancer drugs tested in clinical phase I trials do not attain a market authorisation and hence these high attrition rates remain a key challenge for the pharmaceutical industry, making drug development processes enormously costly and inefficient. Therefore, new preclinical *in vitro* models which can predict drug responses *in vivo* more precisely are urgently needed. Tissue engineering not only provides the possibility of creating artificial three-dimensional (3D) *in vitro* tissues, such as functional organs, but also enables the investigation of drug responses in pathological tissue models, that is, in 3D cancer models which are superior to conventional two-dimensional (2D) cell cultures on petri dishes and can overcome the limitations of animal models, thereby reducing the need for preclinical *in vivo* models.

In this thesis, novel 3D CRC models on the basis of a decellularised intestinal matrix were established. In the first part, it could be shown that the cell line SW480 exhibited different characteristics when grown in a 3D environment from those in conventional 2D culture. While the cells showed a mesenchymal phenotype in 2D culture, they displayed a more pronounced epithelial character in the 3D model suggesting an undergone mesenchymal-epithelial transition (MET). By adding stromal cells (fibroblasts), the cancer cells changed their growth pattern and built tumour-like structures together with the fibroblasts, thereby remodelling the natural mucosal structures of the scaffold. Additionally, the established 3D tumour model was used as a test system for treatment with standard chemotherapeutic 5-fluorouracil (5-FU). It could be shown that the drug sensitivity of the cancer cells was influenced by the fibroblasts which produced an increased drug sensitivity compared to mono-cultured tumour cells. Moreover, tumour growth was improved by dynamic culture conditions in a flow bioreactor where treatment response was more pronounced. These results led to an equally contributing authorship in the publication "Mimicking metastases including tumor stroma: A new technique to generate a three-dimensional colorectal cancer model based on a biological decellularized intestinal scaffold" of the journal Tissue Engineering Part C Methods [2].

The second part of the thesis focused on the establishment of a 3D *in vitro* test system for targeted therapy. The US Food and Drug Administration has already approved of a number of drugs for targeted therapy of specific types of cancer. For instance, the small molecule gefitinib (Iressa®) is applied in non-small cell lung cancer (NSCLC) patients harbouring an activating mutation of the epidermal growth factor receptor (EGFR). Another example is the small molecule vemurafenib (PLX4032, Zelboraf™) which demonstrated impressive response rates of 50–80 % in melanoma patients with a mutation of the rapidly accelerated fibrosarcoma oncogene type B (BRAF) kinase which belongs to the mitogen actived protein kinase (MAPK) signalling pathway. However, only 5 % of CRC patients harbouring the same BRAF mutation respond to treatment with vemurafenib. An explanation for this unresponsiveness could be a feedback activation of the upstream EGFR, reactivating the MAPK pathway which sustains a proliferative signalling. To test this hypothesis, the two early passage cell lines HROC24 and HROC87, both presenting the mutation $BRAF^{V600E}$ but differing in other mutations, were used and their drug response to vemurafenib and/or gefitinib was assessed in conventional 2D cell culture and compared to the more advanced 3D model. While HROC24 cells responded to the treatment with vemurafenib and its combination with gefitinib by an increase of apoptosis rate and the reduction of proliferation rate in 2D culture,

HROC87 cells responded only to gefitinib and the combination therapy but not to a vemurafenib treatment. Under 3D culture conditions, both cell lines showed a reduction of the proliferation rate only in the combination therapy approach. Furthermore, no significant differences between the various treatment approaches and the untreated control regarding apoptosis rate and viability for both cell lines could be found in the 3D tumour model which conferred an enhanced chemoresistance to the cancer cells. Because of the observed unresponsiveness to BRAF inhibition by vemurafenib as can be seen in the clinic for patients with BRAF mutations in CRC, the cell line HROC87 was used for further xenografting experiments and analysis of activation changes in the MAPK signalling pathway. It could be shown that the cells presented a reactivation of Akt in the 3D model when treated with both inhibitors, suggesting an escape mechanism for apoptosis which was not present in cells cultured under conventional 2D conditions. Moreover, the cells exhibited an activation of the hepatocyte growth factor receptor (HGFR, c-Met) in 2D and 3D culture, but this was not detectable in the xenograft model. This shows the limitations of *in vivo* models. The results suggest another feedback activation loop than that to the EGFR which might not primarily be involved in the resistance mechanism. This reflects the before mentioned high attrition rates in the preclinical drug testing.

Altogether, tissue engineering provides opportunities for the establishment of novel 3D test systems which can mimic the *in vivo* situation in the patient more precisely. The 3D tumour model offers a promising method for drug testing in the context of personalised medicine which might improve preclinical screening and help to reduce both the high attrition rates and animal experiments in future.

Zusammenfassung

Krebs ist nach Herz- und Kreislauferkrankungen die führende Todesursache weltweit und 2012 starben daran geschätzt 8,2 Millionen Menschen [1]. Für das Jahr 2030 werden 13 Millionen Krebstote erwartet, was auf das Bevölkerungswachstum und deren Überalterung zurückzuführen ist. Dabei ist das kolorektale Karzinom (engl. colorectal cancer, CRC) der dritthäufigste Krebs bei Männern und der zweithäufigste bei Frauen und weist eine große geographische Ungleichverteilung auf.

Für gewöhnlich entwickelt sich CRC aus einem nicht-kanzerösen Wachstum, das zu einem adenomatösen Polyp bzw. Adenom führt, welches aus Drüsenzellen hervorgeht. Obwohl weniger als 10 % der Polypen bösartig werden, wird vermutet, dass sie im Allgemeinen Vorläufer von Adenokarzinomen sind, die etwa 96 % aller CRCs ausmachen. Da Vorsorgeuntersuchungen, wie z.B. die Kolonoskopie, eine einzigartige Möglichkeit für die Früherkennung und Entfernung von präkanzerösen Polypen bieten, kann das Risiko an CRC zu sterben um bis zu 53 % gesenkt werden. Doch auch Vorsorgeuntersuchungen können die Krebentstehung nicht verhindern und die meisten CRC-Patienten werden sich einem chirurgischen Eingriff unterziehen müssen, um den Tumor zu entfernen. Zusätzlich kann eine adjuvante Chemotherapie und/oder Bestrahlung empfohlen werden. Wenn sich jedoch schon Metastasen gebildet haben, sind Chemotherapie und Bestrahlung häufig die einzigen Behandlungsmöglichkeiten. Da die Forschung in den vergangenen Jahrzehnten ein besseres Verständnis für die Mechanistik der Krebsentstehung hervorgebracht hat, entstanden neuartige Behandlungsformen, wie die zielgerichtete Krebstherapie.

Trotzdem erhalten bis zu 95 % der in der klinischen Phase I getesteten Krebsmedikamente keine Marktzulassung und dadurch bleiben die hohen Versagensraten, welche den Medikamentenentwicklungsprozess sehr kostenaufwendig und ineffizient machen, eine entscheidende Herausforderung für die pharmazeutische Industrie. Daher werden dringend neue präklinische *in vitro* Modelle, die bessere *in vivo* Wirkungsvorhersagen liefern, benötigt. Das Tissue Engineering bietet die Möglichkeit künstliche dreidimensionale (3D) *in vitro* Gewebe herzustellen, z.B. funktionelle Organe, aber es ermöglicht auch, die Reaktion auf ein Medikament in pathologischen Gewebemodellen, wie beispielsweise Krebsmodelle, zu untersuchen. Diese sind der konventionellen zweidimensionalen (2D) Zellkultur in Petrischalen überlegen und können die begrenzten Möglichkeiten von Tiermodellen erweitern, was zudem die Notwendigkeit für präklinische *in vivo* Modelle vermindert.

In der vorliegenden Arbeit wurden neuartige 3D CRC Modelle auf Basis einer dezellularisierten intestinalen Matrix entwickelt. Im ersten Teil konnte gezeigt

werden, dass die Zelllinie SW480 verschiedene Charakteristika bezüglich des Wachstums in der konventionellen 2D Zellkultur oder der 3D Umgebung aufwies. Im Gegensatz zu den mesenchymalen Eigenschaften der Zellen in der 2D Zellkultur, zeigten sie im 3D Modell einen betonteren epithelialen Charakter, was auf eine vollzogene mesenchymal-epitheliale Transition (MET) hindeutet. Durch das Hinzufügen von Stromazellen (Fibroblasten) änderten die Krebszellen ihr Wachstumsverhalten und sie bildeten zusammen mit den Fibroblasten tumorartige Strukturen aus, wobei die natürlichen Strukturen der Darmmatrix, Krypten und Villi, umgebaut wurden. Zusätzlich wurde das entwickelte 3D Tumormodell als Testsystem für das Standardchemotherapeutikum 5-Fluorouracil (5-FU) herangezogen und es konnte gezeigt werden, dass die Empfindlichkeit der Krebszellen auf die Substanz durch die Fibroblasten positiv beeinflusst wurden. Darüber hinaus verbesserten dynamische Kulturbedingungen in einem Flussreaktor das Tumorzellwachstum, was das Ansprechen auf die Behandlung deutlich hervorhob. Diese Ergebnisse sind Bestandteil einer geteilten Erstautorenschaft der Publikation „Mimicking metastases including tumor stroma: A new technique to generate a three-dimensional colorectal cancer model based on a biological decellularized intestinal scaffold“ in der Fachzeitschrift Tissue Engineering Part C Methods [2].

Der zweite Teil der Dissertation konzentrierte sich auf die Entwicklung eines 3D *in vitro* Testsystems für die zielgerichtete Behandlung. Es gibt schon eine Reihe von der US Food and Drug Administration zugelassenen Medikamente für die zielgerichtete Behandlung spezifischer Tumorentitäten. Das „small molecule“ Gefitinib (Iressa®) wird beispielsweise beim nicht-kleinzelligen Lungenkarzinom (engl. non-small cell lung cancer, NSCLC), das eine aktivierende Mutation des epidermalen Wachstumsfaktorrezeptors (engl. epidermal growth factor receptor, EGFR) aufweist, eingesetzt. Ein weiteres Beispiel ist Vemurafenib (PLX4032, Zelboraf™), das eindrucksvolle Ansprechraten von 50 – 80 % bei Melanompatienten mit Mutation der Kinase „accelerated fibrosarcoma oncogene type B“ (BRAF), welche zum „mitogen activated protein kinase“ (MAPK) Signaltransduktionsweg gehört, erzielte. Trotzdem sprechen nur 5 % der CRC-Patienten mit der gleichen BRAF-Mutation auf die Behandlung mit Vemurafenib an. Gründe für diese Unempfindlichkeit könnte eine Rückkoppelung zum aufwärtsgelegenen EGFR sein, der das Signal zur Proliferation aufrecht erhält. Um diese Hypothese zu überprüfen, wurden die zwei Zelllinien HROC24 und HROC87, die beide die $BRAF^{V600E}$-Mutation tragen aber sich in anderen Mutationen unterscheiden, mit Vemurafenib und/oder Gefitinib behandelt und das Ansprechen auf die Substanzen in der herkömmlichen 2D Zellkultur sowie im fortschrittlicheren 3D Modell verglichen. Im Gegensatz zur Zelllinie HROC24, die auf die Behandlung mit Vemurafenib oder dessen Kombination

mit Gefitinib in der 2D Zellkultur mit Erhöhung der Apoptoserate und Senkung der Proliferation ansprach, zeigten HROC87-Zellen eine Reaktion auf Gefitinib und die Kombinationstherapie. In 3D Kulturbedingungen zeigten beide Zelllinien eine Senkung der Proliferation nur im Kombinationstherapie-Ansatz. Außerdem wurden bei den 3D Modellen keine signifikanten Unterschiede zwischen den verschiedenen Behandlungsansätzen und der unbehandelten Kontrolle, hinsichtlich der Apoptoserate und Viabilität, gefunden. Das deutet auf eine erhöhte Chemoresistenz der Krebszellen in der 3D Umgebung hin. Wegen der vorhandenen Unempfindlichkeit der Zelllinie HROC87 gegenüber der BRAF-Inhibierung mit Vemurafenib, wie es auch in der Klinik im Fall von Patienten mit *BRAF*-Mutation des CRC beobachtet werden kann, wurden diese Zellen für weitere Xenograft-Experimente und Analysen von Aktivierungsunterschieden im MAPK-Signaltransduktionsweg herangezogen. Es wurde deutlich, dass die Zellen eine Reaktivierung von Akt im 3D Modell auf die Behandlung mit beiden Inhibitoren aufwiesen, was als ein Mechanismus zur Umgehung der Apoptose anzusehen ist, welcher jedoch nicht bei Zellen, die in 2D Zellkultur behandelt wurden, auftrat. Weiterhin zeigten die Zellen eine Aktivierung des „hepatocyte growth factor receptor“ (HGFR, c-Met) in 2D und 3D Zellkultur, der jedoch nicht im Xenograft-Modell zu sehen war, was die limitierte Übertragbarkeit von Ergebnissen des Tiermodells auf den Menschen verdeutlicht. Die erhaltenen Ergebnisse lassen vermuten, dass es einen anderen Rückkoppelungsmechanismus als zum EGFR, der wahrscheinlich nicht hauptsächlich für die Resistenzvermittlung verantwortlich ist, geben muss. Dies spiegelt wiederum die obenstehend erwähnten hohen Versagensraten in der präklinischen Medikamententestung wider.

Zusammengefasst kann das Tissue Engineering Möglichkeiten zur Herstellung und Entwicklung neuartiger 3D Testsysteme bieten, welche besser die *in vivo* Situation abbilden. Für eine Medikamententestung in Übereinstimmung mit personalisierter Medizin eröffnet das 3D Tumormodell vielversprechende Wege, welche in Zukunft das präklinische Screening verbessern sowie die hohen Versagensraten und Tierversuche vermindern könnten.

1 Introduction

1.1 The large intestine and colorectal cancer

The large intestine consists of the colon and the rectum (colorectum) forming the final part of the digestive tract. The colon itself can be anatomically divided into the proximal colon, consisting of the *caecum*, *colon ascendens* and *colon transversum*, as well as into the distal colon, consisting of the *colon descendens* and *colon sigmoideum*. Embryologically, the proximal colon derives from the midgut and the distal colon from the hindgut [3]. The average length of the colorectum for both sexes is 160.5 cm [4] and it resorbs daily about 1.5 litres of water and nutrients from food as it passes the colon [5]. The gastrointestinal wall which surrounds the lumen of the gastrointestinal tract is built up of four layers (from the lumen outwards): mucosa, submucosa, muscular layer (*muscularis propria*), and serosa [6]. The mucosa consists of the epithelium including glandular tissue, an underlying loose connective tissue, the *lamina propria*, which often contains mucosal glands, lymphoid follicles and plasma cells, as well as of the *lamina muscularis mucosae* for local movement of the mucosa. The submucosa presents a loose connective tissue layer containing larger blood vessels, lymphatics and nerves. The *muscularis propria* is made up of two muscular layers, an inner circular and an outer longitudinal layer which are responsible for peristalsis to move food down the gut. The serosa containing blood vessels, lymphatics and nerves is the outermost layer of loose connective tissue covered by the visceral peritoneum [6]. The renewal of the colonic epithelium takes 4–5 days in humans [7], and a homeostasis of epithelial proliferation and apoptosis allows normal epithelial regeneration. An imbalance of that renewal might lead to dysplastic and hyperplastic cell growth resulting in the development of either ulcers or carcinoma [8].

Colorectal cancer (CRC) is the third most common cancer in men and the second in women worldwide (fig. 1.1). In 2012, the estimated cancer incidence for CRC was 10.1 % (746,298 cases) in men and 9.2 % (614,304 cases) in women, with a wide geographical variation across the world where almost 55 % of the cases occur in more developed regions. Reasons for this distribution might be a prevalence of excess body weight as well as changes in lifestyle patterns that cause obesity, and an unhealthy diet high in fat and low in fibre as well

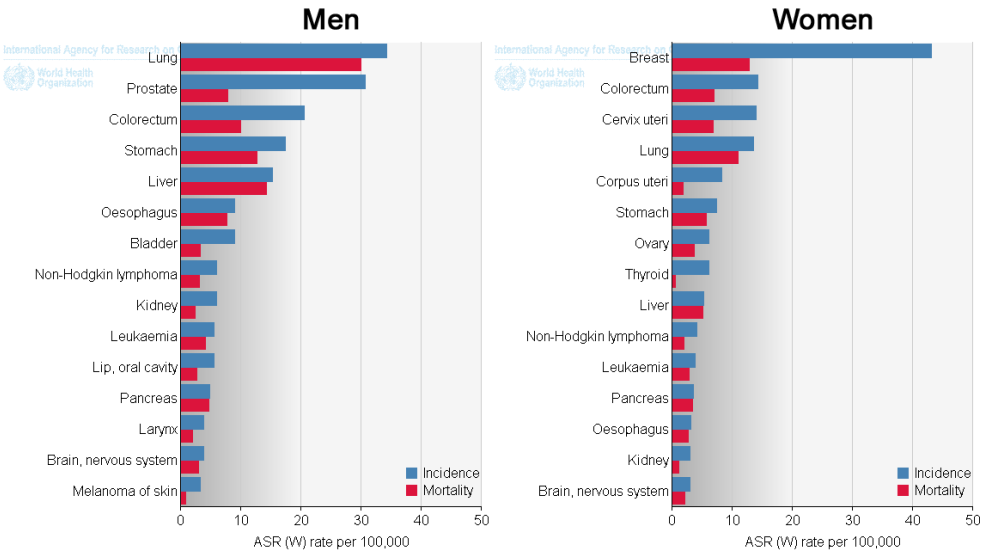

Figure 1.1: Estimated age-standardised cancer incidence and mortality rates worldwide for men and women in 2012. The age-standardised rate (ASR) shows an incidence for cancer of the colorectum of 20.6 in men and 14.3 in women, and therefore, colorectal cancer (CRC) is the third most common cancer in men and the second in women. Mortality rate for CRC is lower in both sexes (10.0 in men and 6.9 in women). Credit: The International Agency for Research on Cancer (IARC): GLOBOCAN 2012 [13]

as a sedentary lifestyle [9, 10]. With 694,000 deaths (8.5 % of the total), the estimated mortality for CRC was lower, but in less developed regions of the world, CRC was responsible for 52 % of the cancer-related deaths. This reflects a poor survival rate in these regions [11]. For 2017, the American Cancer Society estimates 95,520 new cases of colon cancer and 39.910 cases of rectal cancer in the US [12]. It could be shown that CRC does not occur in equal distribution along the colon. There are subsites with proportionally higher tumour occurrence: From 2009 to 2013, 41 % of all CRC patients in the US developed a tumour in the proximal colon, 22 % in the distal colon and 28 % in the rectum. The remaining 9 % developed cancer at other subsites [10]. For the period of 2006–2012, the mean 5-year relative survival rate in the US for all colon cancer stages was 66 % and for rectal cancer 68 % [10].

1.1.1 Development of CRC: Molecular pathways

Various hypotheses for the development of cancer exist, but stepwise genetic and/or epigenetic alterations in oncogenes are found to be responsible [14] and

a genetic model for colorectal tumorigenesis was proposed by Fearon & Vogelstein in 1990 [15]. Usually, CRC begins as a non-cancerous growth forming dysplastic tissue. Further growth leads to an adenomatous polyp, or adenoma, arising from glandular cells [16]. Adenomas are generally considered to be the obligate precursors of adenocarcinomas, yet less than 10 % of adenomatous polyps become malignant [17, 18]. As an adenoma becomes larger, genetic mutations as well as epigenetic changes may begin to accumulate, and the risk of cancer increases [19, 20]. An adenocarcinoma, which accounts for approximately 96 % of all CRCs [21], will eventually become invasive and can metastasise via blood and/or lymphatic vessels to distant body sites (fig. 1.2). The progression from a polyp to an invasive cancer may take up to 18 years. On average it takes nine years [22].

In recent years, it became evident that three molecular pathways are involved in CRC development [3, 23]: the suppressor pathway, the serrated pathway and the Lynch syndrome pathway. While sporadic CRCs usually develop by the first two pathways, the Lynch syndrome (hereditary non-polyposis colorectal cancer, HNPCC) pathway is hereditary and caused by an initial germline mutation in one copy of the mismatch repair (MMR) genes (*MLH1, MSH2, MSH6,* and *PMS2*). The loss of MMR gene function results in DNA replication errors which lead to characteristic microsatellite instability (MSI)-positive tumours.

The suppressor pathway develops through mutations in the adenomatous polyposis coli (*APC*) gene leading to chromosomal instability (CIN) and microsatellite stable (MSS) tumours. These account for up to 80 % of all sporadic CRC characterised by mutational activation of the Kirsten rat sarcoma viral oncogene homologue (*KRAS*) and successive loss of tumour suppressor proteins (APC, SMAD4 and TP53). These genetic alterations accumulate and lead to the proposed model for colorectal tumorigenesis described by Fearon & Vogelstein [14, 15], and is characteristic for left-sided CRC [3].

The serrated pathway is defined by an activating mutation of the rapidly accelerated fibrosarcoma oncogene type B (*BRAF*) and an aberrant cytosine-guanosine (CpG) island methylation phenotype (CIMP) which leads to transcriptional inactivation by hypermethylation and subsequent loss of gene functions by epigenetic silencing of the MMR gene *MLH1* resulting in MSI-positive tumours [24, 25]. Chan *et al.* found that 36 % of hyperplastic polyps, 20 % of admixed hyperplastic polyps/adenoma, and 100 % of serrated adenomas harboured a *BRAF* mutation [26]. Furthermore, the frequency of carcinomas arising via the serrated pathway is higher in the proximal colon and older females [27–29]. Activating mutations of *KRAS* and *BRAF* are almost always mutually exclusive and tumours only present one of the oncogenic mutations [23, 30]. Moreover, MSI-positive Lynch syndrome tumours rarely harbour a

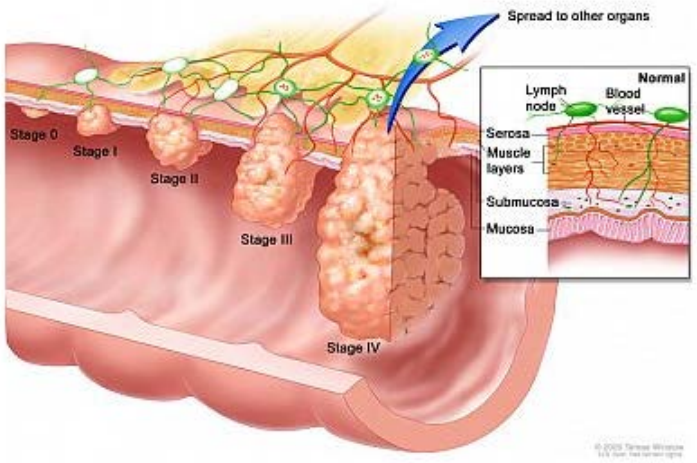

Figure 1.2: Stages of colorectal cancer (CRC). The development of CRC usually begins by a non-cancerous growth forming dysplastic tissue. Further cell growth (hyperproliferation) results in the formation of a (benign) polyp or adenoma (Stage 0). Ten percent of adenomatous polyps become malignant and an adenocarcinoma which invades into the *muscularis propria* develops (Stage I). Continuous growth leads to an increase of tumour volume and further tissue invasion into the serosa (Stage II) and visceral peritoneum (Stage III). Finally, cancer cells can metastasise via blood and/or lymphatic vessels (Stage IV). Credit: Advances in colorectal cancer research, National Institutes of Health (NIH), Bethesda [32]

BRAF mutation, which is a key marker to distinguish hereditary MSI-positive tumours from CIMP/MSI positive tumours [31] arising from the serrated pathway.

1.1.2 Screening and treatment of CRC

Screenings provide a unique opportunity for the early detection and removal of pre-cancerous polyps before they develop into a CRC [33]. There are structural examinations, such as flexible sigmoidoscopy, colonoscopy or computed tomographic colonography (CTC), and stool tests, e.g. the faecal occult blood test (FOBT), which are recommended by the American Cancer Society for CRC screening in men and women of age 50 and older [16]. Studies show that these screenings can reduce the CRC-related mortality of patients up to 53 % in case of colonoscopic polyectomy [34].

However, screening cannot prevent cancer from developing and most patients with CRC will have to have some type of surgery to remove the tumour, espe-

cially if the tumour has not spread to nearby lymph nodes or tissue. Adjuvant chemotherapy and/or radiation therapy may be recommended after surgery if the cancer has already spread to regional lymph nodes. It could be shown that 5-fluorouracil (5-FU)-based chemotherapies could improve survival in patients with stage III and high-risk stage II disease [35]. Yet, in case of already distant metastases, surgery may be an option to relieve or prevent blockage of the colon but is not recommended for all patients [16].

Conventional chemotherapeutic drugs are cytotoxic and not only target rapidly dividing cells such as cancer cells but also affect normal cells, for example cells of the intestinal epithelium and therefore have significant side effects. Most of the chemotherapeutic agents interfere with cell division or DNA synthesis. In use are alkylating agents (e.g. cisplatin, oxaliplatin, cyclophosphamide, gemcitabine, etc.), anti-metabolites (methotrexate, 5-FU), anthracyclines (doxorubicin, mitoxantrone, etc.), plant alkaloids (vincristine, vinblastine), and topoisomerase inhibitors (camptothecin, irinotecan, etc.) [36]. Common chemotherapy regimens used to treat advanced CRC (stage III) that has metastasised consist of folinic acid (leucovorin), 5-FU and irinotecan (FOLFIRI), or folinic acid, 5-FU and oxaliplatin (FOLFOX) [37].

In the past decades, research has brought better understanding of the mechanisms of cancer development and several hallmark capabilities of cancer cells have been established [38, 39], thus enabling therapeutic targeting such as the inhibition of the epidermal growth factor receptor (EGFR) to block sustaining proliferative signalling or the use of inhibitors of the vascular endothelial growth factor (VEGF) to block tumour angiogenesis.

1.2 Targeted therapy in cancer treatment

Targeted cancer therapies use compounds interfering with specific proteins involved in tumorigenesis and focusing on specific molecular changes which are uniquely found in particular cancers thereby inhibiting cancer cell growth and metastasis [36]. Currently, there are two types of novel approaches to treat cancer patients and to complement conventional therapies: small molecules and monoclonal antibodies. Small molecule inhibitors target kinases to prevent activation of signalling pathways dysregulated in cancer. Monoclonal antibodies affect the interactions between ligands and their receptors, either by blocking or by capturing and eliminating a protein, for example a growth factor, and thus preventing the activation of signalling pathways [36].

1.2.1 Patient stratification and biomarker identification

An important prerequisite for a targeted therapy is patient stratification because not all patients respond favourably to drugs and some patients do not benefit from their treatment. Stratification is the identification of a group of patients with shared "biological" characteristics by using molecular, biochemical and imaging diagnostic testing to select the optimal management for the patients and so to achieve the best possible outcome in terms of risk assessment and prevention as well as an optimal treatment outcome [40]. For personalised medicine, an understanding of disease mechanisms and drug actions is necessary. One approach for the identification of suitable targets is the use of biomarkers. These are defined by the European Commission Health Research Directorate as a biological characteristic of molecular, anatomic, physiologic, or biochemical nature [40]. Biomarkers act as indicators of a normal or pathogenic biological process and they allow assessing the pharmacological response to a therapeutic intervention. Such indicators are diagnostic biomarkers (HCV RNA after infection), susceptibility/risk biomarkers (BRCA1-breast cancer), prognostic biomarkers (HER-2-breast cancer), and predictive biomarkers (EGFR, BRAF) [40].

The breakpoint cluster region-Abelson proto-oncogene (BCR-ABL) is the most successful example of a predictive biomarker used as a clinically relevant drug target: This aberrant fusion protein caused by chromosomal translocation t9;22 (Philadelphia chromosome) with an unregulated tyrosine kinase domain is found in almost all chronic myeloid leukaemia (CML) patients [41, 42]. The small molecule inhibitor imatinib mesylate (Gleevec®) binds competitively to the activation site of BCR-ABL, which results in disruption of the tyrosine kinase potential. Approximately 98 % of CML patients respond completely to the treatment with imatinib [36].

1.2.2 Current targeted therapies of CRC

The US Food and Drug Administration (FDA) has already approved of a number of targeted therapies for the treatment of specific types of cancer [43]. For example, the small molecules gefitinib (Iressa®) and erlotinib (Tarceva®), which are tyrosine kinase inhibitors (TKIs) of the EGFR, are applied in non-small cell lung cancer (NSCLC) patients harbouring an activating *EGFR* mutation [44, 45]. In a subset of patients, it could be shown that treatment with these EGFR TKIs results in dramatic antitumour activity with response rates of 75 %, but that genetic assessment of the *EGFR* mutational status for individual patients should be included [46].

For the targeted treatment of CRC, there are five approvals of antibodies (cetuximab [47], panitumumab [48], bevacizumab [49], ramucirumab [50], and nivolumab [51]) and one approval of a small molecule (regorafenib [52]) as well as one approval of a recombinant fusion protein binding to VEGF and human immunoglobulin IgG1 (ziv-aflibercept [53]).

The antibodies cetuximab and panitumumab are applied in *KRAS* wildtype metastasised CRC (mCRC) patients who show EGFR (over-)expression. By binding to the EGFR, it can disrupt the oncogenic signalling from this receptor tyrosine kinase. If *KRAS* is mutated, as found in about 40 % of CRC [14, 54], an anti-EGFR treatment is compromised in case of constitutive *KRAS* activation. Therefore, *KRAS* is a predictive marker for anti-EGFR therapeutic strategies and is recommended to be tested in advance [55].

Bevacizumab is an antibody that binds VEGF, similar to ziv-aflibercept, and hence can block angiogenesis. It is approved for a first-line and second-line treatment of mCRC. An analogous approach to inhibiting angiogenesis makes use of the antibody ramucirumab which blocks the VEGF receptor 2.

The antibody nivolumab works as a checkpoint inhibitor and aims at stimulating the patient's immune system by blocking the programmed death 1 (PD-1) receptor of T cells which would get deactivated by tumour cells overexpressing its ligand PD-L1. Nivolumab is approved for unresectable or metastatic *BRAF* wildtype and *BRAF*-mutant CRCs.

The small molecule regorafenib is currently applied in mCRC patients who have been previously treated with a FOLFOX-based chemotherapy, an anti-VEGF therapy, and, if *RAS* wildtype, an anti-EGFR therapy. Regorafenib is an inhibitor of multiple membrane-bound (VEGFR, platelet-derived growth factor receptor (PDGFR), fibroblast growth factor receptor (FGFR), etc.) and intracellular kinases (RAF-1, BRAF, etc.) involved in normal cellular functions and in pathological processes such as oncogenesis, tumour angiogenesis, metastasis and tumour immunity.

1.2.3 *BRAF*-mutant CRC and malign melanoma

Activating *BRAF* mutations were described in a multitude of cancer entities (melanomas, CRCs, gliomas, lung cancers, sarcomas, ovarian carcinomas, breast cancers and liver cancers) by Davies *et al.* in 2002 and it was found that 80 % of the *BRAF* mutations were accounting for the single substitution of valine (V) by glutamic acid (E) at position 600 (V600E) [56]. This discovery led to attempts for targeting the mitogen-activated protein kinase (MAPK; RAF-MEK-ERK) signalling pathway for therapeutic purposes by focussing on the development of RAF and MEK kinase inhibitors, such as sorafenib. This

substance was the first RAF kinase inhibitor to be tested in clinical trials and is now FDA-approved for the treatment of renal cell carcinoma and hepatocellular carcinoma [57, 58]. However, no clinical benefit was observed concerning the inhibition of $BRAF^{V600E}$ signalling by sorafenib, which prompted the development of second-generation RAF inhibitors demonstrating elevated specificity for the V600E mutation [58–60].

Vemurafenib (PLX4032, Zelboraf™) is such a new BRAF inhibitor. It was approved in 2011 by the FDA for the treatment of patients with unresectable or metastatic melanoma harbouring the $BRAF^{V600E}$ mutation [61]. About 60 % of malign melanoma show this *BRAF* mutation and vemurafenib treatment resulted in impressive response rates of 50–80 % in these patients [62, 63]. In contrast, *BRAF* is found to be mutated in about 5–15 % of CRC patients [29, 56, 64], but only 5 % of these patients respond to the treatment with vemurafenib [65, 66]. An explanation for this unresponsiveness of *BRAF*-mutant CRC to BRAF inhibitors was described by Corcoran *et al.* and Prahallad *et al.* who found a feedback activation of the downstream kinase MEK to the EGFR and thus a reactivation of the MAPK signalling pathway [67, 68]. The authors suggested that patients might benefit from a combination therapy consisting of BRAF and EGFR inhibitors. Although this subject has already been investigated in a clinical trial (NCT01791309: vemurafenib and panitumumab combination therapy) completed in 2015, no results have been published, yet [69]. This approach constitutes a major part of this thesis which investigates the combination of the BRAF inhibitor vemurafenib and the EGFR inhibitor gefitinib in $BRAF^{V600E}$ mutated early-passage CRC cell lines. These are well characterised [70] and were kindly provided by PD Dr. M. Linnebacher (University Hospital Rostock) by using a novel three-dimensional (3D) tumour model.

1.3 Tissue engineering as a tool for the development of healthy and pathological *in vitro* models

In 1993, Langer & Vacanti commented that the new field of tissue engineering, which applies the principles of biology and engineering to the development of functional substitutes for damaged tissue, might be an alternative for the increasing need of donor organs by transplantation [71]. The principle of generating human tissues *in vitro* is based on co-culturing different human cell types isolated from biopsy material. After isolation, cells have to be expanded before they can be cultured on an appropriate 3D scaffold for differentiation, maturation and re-implantation. Moreover, these tissue-engineered 3D mod-

els can be used for the generation of *in vitro* test systems for an approach to personalised medicine (section 1.2.1).

The scaffolds used for tissue engineering consist of biomaterials which should be carefully selected, depending on the modelled tissue. They act as a synthetic extracellular matrix (ECM) that interacts with the cells on a molecular level [72], enabling the cells to remodel and/or produce their own ECM. Such scaffolds can be synthetically produced, e.g. ceramic scaffolds for bone regeneration and polymer-based electrospun scaffolds, or they can consist of biological materials, for example collagen, alginate-based substrates and chitosan [73]. Another approach is the use of decellularised natural complex tissues/organs, such as the patented *Biological Vascularised Scaffold* (BioVaSc®; DE:302014007893), which is obtained by decellularisation of porcine small intestine [74–77]. The preserved basal membranes and tissue architecture, including vascular structures, are unique features of that scaffold. A simplified version without preserved vessel structures is the small intestinal submucosa (SIS) with mucosa (SISmuc), which has been successfully used before in a lung cancer model [78] and in a standardised CRC model [2] that is a substantial part of this thesis.

1.3.1 Models for preclinical cancer research

The high attrition rates in drug development remain a key challenge for the pharmaceutical industry and up to 95 % of anticancer drugs tested in clinical phase I trials do not reach market authorisation, making the drug development process enormously costly and inefficient [79, 80]. Moreover, only 1 in 10,000 preclinical compounds ever reach the market and the total worldwide research and development costs for the pharmaceutical industry increased from USD 108 billion in 2006 to USD 141 billion in 2015 [79, 81]. Reasons for the reported high attrition rates are diverse and comprise amongst others lack of reliability of published data, biopharmaceutical issues including suboptimal pharmacokinetics and poorly predictive preclinical models in discovery research and preclinical testing [79, 81]. Alone 56 % of drugs fail due to lack of efficiency, followed by 28 % for reason of safety issues in phase II and phase III of clinical development [81]. Therefore, new preclinical models which can predict drug responses *in vivo* more precisely are urgently needed. Tissue engineering, or better "tumour engineering" as commented by Ghajar & Bissell [82], provides another application of artificial *in vitro* tissues aiming at the investigation of molecular principles of pathological alterations. Furthermore, the use of 3D models which are superior to conventional two-dimensional (2D) cell cultures of monolayers on petri dishes [72, 82, 83] can overcome the limitations of animal models and reduce the need for *in vivo* tests according to the principle of

the 3Rs (replacement, reduction and refinement) [84]. In the past years, there has been progress in the reduction of animal experiments within the European Union (EU) where about 11.5 million animals were used as *in vivo* models in 2011. This is a reduction of over half a million animals compared to 2008 [85]. With 60.9 % and 13.9 %, mice and rats were by far the most commonly used species [85]. However, experimental results may not be predictive for humans, so that intraspecies and not interspecies studies become necessary [86]. Even humanised mouse models expressing a human gene possess lots of proteins that are still animal proteins [87].

1.3.2 Modelling and analysing early steps of metastasis and invasion: Epithelial-mesenchymal transition (EMT)

Carcinomas are of epithelial origin and will eventually invade neighbouring tissue and/or metastasise into distant organs during disease progression. The changes occurring during this process termed as epithelial-mesenchymal transition (EMT) include the cells' loss of epithelial characteristics and their acquisition of mesenchymal properties, thereby gaining enhanced migratory capacity, invasiveness, elevated resistance to apoptosis and also greatly includes enhanced production of ECM components [88, 89]. EMT was originally described by Elizabeth Hay in 1995 as a mechanism of forming primary mesenchymal cells in mesoderm from primitive epithelium during gastrulation in the embryonal development [90] and it can be classified as three different subtypes: Type 1 generates diverse cell types of the mesenchyme during embryogenesis and organ development as described by Hay without causing fibrosis or induction of an invasive phenotype; type 2 is associated with tissue regeneration and inflammation during wound healing and fibrosis; type 3 occurs in neoplastic cells that have previously undergone genetic and epigenetic changes [89, 91]. Although these three classes of EMT represent distinct biological processes, common molecular mechanisms and multiple biochemical changes underlie this diverse programme which appears to be plastic and thus enabling a movement back and forth between epithelial and mesenchymal states, EMT and mesenchymal-epithelial transition (MET) [91]. However, in all contexts, EMT includes the loss of apical-basal cell polarity, the dissolution of cell-to-cell junctions, the reorganisation of the cytoskeletal architecture and changes in cell shape, the acquisition of a front-rear polarity, and the detachment or degradation of the underlying basement membrane and ECM components [92]. Several key signalling pathways contributing to this process exist, such as TGF-β and Wnt which are known inducers of EMT and promoters of stem cell maintenance [93].

A multitude of biomarkers is available for the examination of a cell's EMT state. These can be grouped as cell-surface proteins, cytoskeletal markers, ECM markers, transcription factors, and micro-RNAs [91]. The typical epithelial cell-surface protein E-cadherin which enables the development of cell-to-cell contacts is expressed in epithelial cells. Its expression is decreased in cells undergoing EMT. The cytoplasmic plaque protein β-catenin forms a complex with the intracellular domain of E-cadherin linking the cytoskeleton's actin filaments for stabilising the cell-to-cell contacts. If a cell undergoes EMT, β-catenin is dissociated from this complex and serves as a cotranscriptional activator, and as a result, nuclear localisation appears [91], and the cell-to-cell contacts are destabilised and single cells can leave the epithelial cell layer. Cytokeratins are another example for epithelial cytoskeletal markers. These are intermediate filaments and opposed to the mesenchymal intermediate filament protein vimentin. Vimentin expression is correlated with increased invasiveness and metastasis [94] and commonly used to identify cells undergoing EMT in cancers. A marker for ECM is collagen type IV. This is one of the principal basement membrane constituents among laminin, nidogen, and sulphated proteoglycans which become remodeled during EMT [91, 92].

Because conventional 2D culture approaches lack ECM, they cannot reflect these changes in the cells' phenotype which occur during disease progression from metastasis to invasion. But these alterations can be examined in the 3D tumour model and distinct differences in the expression of the EMT markers E-cadherin and vimentin as well as E-cadherin and β-catenin were found comparing 2D culture with 3D culture: the CRC cell line SW480 showed a more pronounced epithelial phenotype in 3D culture and a more mesenchymal phenotype in 2D culture [2]. By adding stromal cells, in particular fibroblasts, the cancer cells' EMT marker expression shifted towards a more epithelial phenotype indicating that the cells have undergone a MET process [2].

1.3.3 EMT and cancer stem cells: Indications for enhanced chemoresistance

As mentioned in section 1.1, the intestinal epithelium continuously renews itself by the activity of a population of tissue-specific stem cells [95]. These adult stem cells are long-lived and generate cellular progeny throughout life to regenerate the multiple specialised short-lived cells that ultimately perform tissue-specific functions [96].

Cancer stem cells (CSCs) were first described by Lapidot *et al.* in 1994 as cells that could initiate human acute myeloid leukaemia (AML) after transplantation into severe combined immunodeficiency (SCID) mice. They found that

only $CD34^+/CD38^-$ cells were able to form AML in mice, but that the fractions of $CD34^+/CD38^+$ and $CD34^-$ cells did not have these properties [97]. Later, (tumour-initiating) CSCs were reported in solid tumours such as breast cancer, brain cancer, hepatocellular carcinoma, pancreatic cancer, prostate cancer, and CRC [98–105]. In 2006, CSCs were defined as cells within a tumour that possess the capacity of self-renewal and of causing the heterogeneous lineages of cancer cells that compose the tumour, which clearly describes the relationship between CSCs and tumour-initiating cells (TICs), cancer-initiating cells (CICs) or normal stem cells [106]. The common characteristics of CSCs are (i) by defintion self-renewal and differentiation leading to heterogeneous lineage, (ii) a small number in cancer cells, (iii) chemoresistance, (iv) resistance to radiation therapy, (v) persistance in the resting phase of the cell cycle, (vi) high metastatic ability, (vii) sphere forming ability, (viii) expression of cancer stem cell markers, and (ix) high ATP-binding cassette (ABC) transporter expression [107].

For instance, the transmembrane glycoprotein CD166, or activated leukocyte cell adhesion molecule (ALCAM), is a cell surface marker and has been identified as an antigen which is shared by CRC stem cells [108]. CD166 can be found in colon cancer, lung cancer, breast cancer, melanoma and prostate cancer cells [109]. It has been suggested that CD166 is a key regulator of stemness in colon cancer cells and it has the potential to be used as a prognostic marker for the clinical management of CRC patients [110]. CD133 (Prominin 1) is another example. This is a pentaspan transmembrane glycoprotein expressed on adult stem cells where it is thought to function by maintaining stem cell properties and by suppressing differentiation [111]. In CRC, the expression of CD133 correlates with that of CD166 and it was shown that CD133 predicts low patient survival [108]. On the other hand, Lugli *et al.* found that a loss of membranous CD44, which is a cell-surface glycoprotein involved in cell-cell interactions, cell adhesion and migration as it binds to hyaluronic acid, and that a loss of CD166 expression is associated with aggressive tumour-related features, such as a more advanced tumour stage, vascular invasion and infiltrating tumour growth [112].

The correlation of CSCs and EMT has the effect that their signalling pathways boost both normal and CSC renewal and maintenance. There is evidence that metastatic cancer cells which have presumably undergone EMT may exhibit a CSC phenotype [93]. For example, it was found that disseminated breast cancer cells in pleural effusions were enriched by a $CD44^{high}/CD24^{low}$ CSC-like population [99]. Furthermore, studies have shown that EMT-associated emergence of CSCs occurs after an immune response because $CD8^+$ T-cells can induce dedifferentiation of breast cancer cells, resulting in the formation of

$CD44^{high}/CD24^{low}$ stem cell-like cells [93]. In conclusion, CSCs play crucial roles in cancer cell growth and metastasis. Targeting the population of CSCs and inhibiting EMT may result in novel therapeutic targets for cancer treatment [107].

1.4 Scope and aim of the thesis

Cancer remains one of the deadliest diseases worldwide and an estimated 8.2 million people died in 2012. By 2030, 13 million cancer deaths are expected, due to the growth and ageing of the population [1]. Conventional treatment of cancer includes surgical resection of a tumour and/or chemotherapy and radiation therapy. This shows limited benefits and usually has severe side effects on the patients [16]. Although increasing amounts of money are spent for research and development, attrition rates remain high and less than 5 % of the anticancer drugs tested in clinical trial phase I enter the market. Reasons for failure are diverse and comprise amongst others poorly predictive preclinical *in vitro* and *in vivo* models used in discovery research and preclinical testing [79–81]. Therefore new approaches are urgently needed.

It is known that the use of 3D models is superior to conventional 2D culture of cells in a monolayer and can thus overcome the limitations of animal models and reduce the need for *in vivo* tests [72, 82, 83]. Tissue engineering provides a tool for the development of artificial 3D *in vitro* test systems for an approach towards a personalised medicine, that can predict the efficacy and outcome of possible treatments more precisely. Patient stratification is a prerequisite for personalised medicine in the context of targeted therapy integrating biomarkers for the definition of suitable targets for cancer treatment [40]. It could be shown that patients with *BRAF*-mutated melanoma benefit from the treatment with the small molecule vemurafenib (PLX4032, Zelboraf™) which inhibits the oncogenic $BRAF^{V600E}$ signal, thus resulting in impressive response rates of 50–80 % [62, 63]. However, only 5 % of patients with CRC, and harbouring the same mutation of *BRAF* respond to the treatment with vemurafenib [65, 66]. This low response of CRC is thought to be caused by a feedback activation of the EGFR which re-activates the common MAPK signalling pathway leading to the observed unresponsiveness [67, 68]. By combining vemurafenib with the small molecule gefitinib which is approved for NSCLC with EGFR overexpression, this resistance should be eliminated and its investigation was a substantial aim of this study.

This thesis can be divided in two parts: First, the establishment of a 3D tumour model of the well-described CRC cell line SW480, including fibroblasts

as stromal cells, on the basis of a decellularised intestinal matrix and a treatment with the standard chemotherapy 5-FU. This was part of a publication [2]. Secondly, a targeted therapy of two *BRAF*-mutated CRC early-passage cell lines in conventional 2D culture and 3D culture as well as the comparison with mouse xenograft models. The here presented 3D *in vitro* test systems may provide a more reliable tool for the evaluation and prediction of possible treatments and may as well help to reduce animal experiments and their huge costs in preclinical research.

2 Materials & Methods

2.1 Materials

2.1.1 Equipment

Table 2.1: List of equipment and devices

Equipment/Device	**Producer/Supplier**
Analytical balances:	
Kern ABJ 220-4M,	Kern & Sohn GmbH,
Kern EG 2200-2NM	Balingen-Frommern (D)
Aspiration device (VacuBoy)	Integra Biosciences, Fernwald (D)
Autoclaves:	
Systec DX-45	Systec GmbH, Wettenberg (D)
Systec VX-150	Systec GmbH, Wettenberg (D)
Tecnoclav	Integra Biosciences AG, Zizers (CH)
Bioreactor board	Chair of Tissue Engineering & Regenerative Medicine, Würzburg (D)
Blotting chambers:	
Biometra Fastblot B44	Biometra GmbH, Göttingen (D)
Peqlab PerfectBlue™	VWR Life Science Competence Center,
Sedec M	Erlangen (D)
Cell freezing container (Mr. Frosty™)	VWR, Darmstadt (D)
Cell incubator (37°C, 5% CO_2)	Heraeus, Hanau (D)
Centrifuges:	
Centrifuge 5417R	Eppendorf, Hamburg (D)
Multifuge X12	Thermo Fisher Scientific, Dreieich (D)
Multifuge X1R	Thermo Fisher Scientific, Dreieich (D)
Rotilabo	Carl Roth GmbH, Karlsruhe (D)
Cold storage room (4°C)	Genheimer, Höchberg (D)
Cooling plate Leica EG1150 C	Leica, Wetzlar (D)

Table 2.1: List of equipment and devices (continued)

Equipment/Device	Producer/Supplier
Digital camera	Canon, Krefeld (D)
Embedding cassette printer VCP-5001	Vogel Medizintechnik, Gießen (D)
Freezers:	
-80°C HFU586 Basic	Heraeus, Hanau (D)
-20°C Comfort	Liebherr, Biberach a.d. Riss (D)
Fume hood	Prutscher Laboratory Systems, Neudörfl (A)
Gel chambers:	
Peqlab PerfectBlue™ Dual Gel Chamber (Twin S)	VWR Life Science Competence Center, Erlangen (D)
Heat sealer ME400HC	Pro-System Verpackungstechnik GmbH, Schönbrunn-Schwanheim (D)
Hand tally counter	neoLab, Heidelberg (D)
Hazardous material cabinet	MSG Produkte, Schöllkrippen (D)
Hot air sterilizer	Memmert, Schwabach (D)
Ice machine AF-80	Scotsman, Milano (I)
Imaging station FluorChem Q	Biozym Scientific GmbH, Hessisch Oldendorf (D)
Immersion thermostat for water bath	Lauda, Lauda-Königshofen (D)
Laboratory dish washer	Miele, Gütersloh (D)
Laminar flow cabinet Safe2020	Thermo Fisher Scientific, Dreieich (D)
Liquid nitrogen storage tank MVE 815 P190	German-cryo, Jüchen (D)
Magnetic stirrer with integrated heater 720-HPS	VWR, Darmstadt (D)
Microplate reader Tecan Infinite® M200	Tecan, Crailsheim (D)
Microscopes:	
Bright field (Axio Lab.A1)	Carl Zeiss Microscopy GmbH, Göttingen (D)
Confocal (SP8)	Leica, Wetzlar (D)
Fluorescence (BZ-9000)	Keyence, Neu-Isenburg (D)

Table 2.1: List of equipment and devices (continued)

Equipment/Device	**Producer/Supplier**
Multichannel pipette plus	Eppendorf, Hamburg (D)
Multistep pipette	Brand, Wertheim (D)
Neubauer cell counting chamber (hemocytometer)	Marienfeld GmbH & Co. KG, Lauda-Königshofen (D)
Object slide printer VSP-5001	Vogel Medizintechnik, Gießen (D)
Orbital shaker KM-2 Akku	Edmund Bühler GmbH, Hechingen (D)
Paraffin embedding module EG1150H	Leica, Wetzlar (D)
Peristaltic pump	Ismatec, Wertheim-Mondfeld (D)
pH-Meter	Mettler Toledo, Gießen (D)
Pipettes: 0.5 - 10μl, 10 - 100μl, 100 - 1000μl	Eppendorf, Hamburg (D)
Pipette tamping machine	BellCo Glass Dunn, Asbach (D)
Pipetting aid (accu-jet® pro)	Brand, Wertheim (D)
Power supply units: Peqlab EV202 (Blotting), EV243 (Electrophoresis)	VWR Life Science Competence Center, Erlangen (D)
Pressure sensor: reusable transducer SP844	HJK Sensoren + Systeme GmbH & Co. KG, Merching (D)
Pump tubing cassette	Ismatec, Wertheim-Mondfeld (D)
Refrigerator (MediLine)	Liebherr, Biberach a.d. Riss (D)
Rocking platform shaker	VWR, Darmstadt (D)
Rotating mixer	neoLab, Heidelberg (D)
Sliding microtome (Leica SM2010 R)	Leica, Wetzlar (D)
Spin tissue processor (Microm STP120)	Thermo Fisher Scientific, Dreieich (D)
Steamer (MultiGourmet)	Braun, Kronberg/Taunus (D)
Thermomixer (comfort)	Eppendorf, Hamburg (D)
Timer	Carl Roth GmbH, Karlsruhe (D)
Tissue drying oven TDO66	Medite GmbH, Burgdorf (D)

Table 2.1: List of equipment and devices (continued)

Equipment/Device	Producer/Supplier
Tissue float bath GFL1052	GFL Gesellschaft für Labortechnik mbH, Burgwedel (D)
Vortexer (Genie)	Carl Roth GmbH, Karlsruhe (D)
Water purification system (MilliQ®)	Merck-Millipore, Darmstadt (D)

2.1.2 Consumables

Table 2.2: List of consumable materials

Material	Producer/Supplier
Air filter, sterile (16596-HYK)	Sartorius AG, Göttingen (D)
Aluminium foil	Carl Roth GmbH, Karlsruhe (D)
Blotting membranes: Nitrocellulose (Protran) Polyvinylidene difluoride (PVDF)	 Whatman, Maidstone (GB) Millipore, Schwalbach (D)
Cell culture flasks ($150cm^2$, $75cm^2$, $25cm^2$)	TPP Techno Plastik Products AG, Trasadingen (CH)
Cell culture multiwell plates (6-well, 12-well, 24-well, 96-well)	TPP Techno Plastik Products AG, Trasadingen (CH)
Cell scraper	Sarstedt, Nümbrecht (D)
Cell strainer ($70\mu m$, $100\mu m$)	BD Biosciences, Heidelberg (D)
Centrifuge tubes ($15ml$, $50ml$)	Greiner Bio-One, Frickenhausen (D)
Chamber slides (8-well, glass)	Nunc, Wiesbaden (D)
Cling film	Toppits, Minden (D)
Cover slips for object slides (24x60mm)	Menzel-Gläser, Braunschweig (D)
Cover slips (round, ⌀ $12mm$)	Marienfeld GmbH & Co. KG, Lauda-Königshofen (D)

Table 2.2: List of consumable materials (continued)

Material	**Producer/Supplier**
Cryo tubes (1.8ml)	Nunc, Wiesbaden (D)
Disposable pipettes ($5ml$, $10ml$, $25ml$, $50ml$)	Greiner Bio-One, Frickenhausen (D)
Disposal bags	Hartenstein, Würzburg (D)
Embedding cassettes	Klinipath, Duiven (NL)
Embedding filter paper	Labonord, Mönchengladbach (D)
Gloves: Latex Nitrile	 Cardinal Health, Kleve (D) Medline International Germany GmbH (D)
Grease pencil	Dako, Hamburg (D)
Microtome disposable blades (Type A35)	pfm Medical, Köln (D)
Object slides: Uncoated (26x16x1mm) Polysine™ (25x75x1mm)	 Menzel, Braunschweig (D) Langenbrinck, Emmendingen (D)
O-rings (sealing rings)	Dichtelemente arcus GmbH, Seevetal (D)
Parafilm® M	Carl Roth GmbH, Karlsruhe (D)
Pasteur pipettes	Brand, Wertheim (D)
Petri dishes (145x20mm, 6x20mm)	Greiner Bio-One, Frickenhausen (D)
Pipette tips: 0.5 - 10μl, 10 - 100μl, 100 - 1000μl	Eppendorf, Hamburg (D)
Pressure dome: sterile and disposable dome 844-28	Memscap AS, Skoppum (N)
PTFE thread seal tape (BS7786:1995 Grade L, 12m x 12mm x 0,075mm)	Hydrasun Ltd., Aberdeen (GB)
Pump tubing (large: SC0746, small: SC0736)	Ismatec, Wertheim-Mondfeld (D)
Scalpel blades (rounded)	Bayha, Tuttlingen (D)
Silicone tube (9531.1)	Carl Roth GmbH, Karlsruhe (D)

Table 2.2: List of consumable materials (continued)

Material	Producer/Supplier
Sterile filter (attachment for disposable syringes): Diameter $50mm$, Pore size $0.2\mu m$	Sartorius Stedium Biotech, Göttingen (D)
Syringes ($20ml, 50ml$)	BD Biosciences, Heidelberg (D)
Transparent sterilized pack	Melag, Berlin (D)
Vasofix® Safety: 18G (4269136S-01) 20G (4269110S-01)	B.Braun Melsungen AG, Melsungen (D)
Weighing dish	Hartenstein, Würzburg (D)
Whatman filter paper	Hartenstein, Würzburg (D)

2.1.3 Laboratory Materials

Table 2.3: List of laboratory materials

Material	Producer/Supplier
Beakers ($250ml, 500ml, 1l, 2l, 5l$)	
glass	Schott, Mainz (D)
plastic	Bürkle GmbH, Bad Bellingen (D)
Cell crowns for static three-dimensional culture	Chair of Tissue Engineering & Regenerative Medicine, Würzburg (D)
Centrifuge tube racks	neoLab, Heidelberg (D)
Cold protection gloves	VWR, Darmstadt (D)
Funnels	Hartenstein, Würzburg (D)
Glass cuvettes with lid (100x90x80mm)	Mercateo, München (D)
Glass pipettes ($2ml, 5ml, 10ml, 25ml$)	Brand, Wertheim (D)
Humidity chamber	Chair of Tissue Engineering & Regenerative Medicine, Würzburg (D)
Laboratory bottles ($50ml$, $100ml$, $250ml$, $500ml$, $1000ml$, $2000ml$)	Brand, Wertheim (D)

Table 2.3: List of laboratory materials (continued)

Material	**Producer/Supplier**
Magnetic stirring bars	Hartenstein, Würzburg (D)
Magnetic stirring bar retriever	Hartenstein, Würzburg (D)
Measuring cylinders ($50ml$, $100ml$, $250ml$, $500ml$, $1000ml$)	
glass	Brand, Wertheim (D)
plastic	Vitlab GmbH, Großostheim (D)
Object slide racks (glass, stainless steel)	Mercateo, München (D)
Protective goggles	neoLab, Heidelberg (D)
Reaction tube racks	neoLab, Heidelberg (D)
Scalpel blade handles	Bayha, Tuttlingen (D)
Small components for bioreactor (Luer lock adapters, etc.)	Nordson Medical, Loveland (USA)
Spatula	Hartenstein, Würzburg (D)
Spoon spatula	Hartenstein, Würzburg (D)
Spray flasks (70% Ethanol, Descosept)	Hartenstein, Würzburg (D)
Stainless steel casting moulds for embedding tissue (24x37x9mm)	Labonord, Mönchengladbach (D)
Sterile filter (attachment for laboratory bottles)	Hartenstein, Würzburg (D)
Tweezers (round, curved, flat)	Assistent, Sondheim (D)
Volumetric flasks with plug ($250ml, 500ml, 1l, 2l, 5l$)	Hirschmann Laborgeräte GmbH, Eberstadt (D)

2.1.4 Chemicals & Solutions

2.1.4.1 General chemicals and solutions

Table 2.4: List of general chemicals and solutions

Chemical/Solution	Producer/Supplier	Catalog No.
3-(4,5-Dimethylthiazol-2-yl)-2,5-diphenyltetrazolium-bromide (MTT)	Serva, Heidelberg (D)	20395.01
4',6-Diamidino-2-phenyl-indoldihydrochloride (DAPI)	Sigma-Aldrich, München (D)	D9542
5-Fluorouracil (5-FU) $10\,mM$	Selleckchem, München (D)	S1209
Acetone ($\geq 99.5\,\%$)	Carl Roth GmbH, Karlsruhe (D)	5025.5
Acrylamide/Bisacrylamide Rotiphorese® Gel 30 (37.5:1)	Carl Roth GmbH, Karlsruhe (D)	3029.1
Albumine Fraction V (BSA)	Carl Roth GmbH, Karlsruhe (D)	90604-29-8
Alcian blue staining solution (1 %, pH 2 with acetic acid)	Morphisto Evolutionsforschung und Anwendung GmbH, Frankfurt/Main (D)	10126.00500
Ammonium persulphate (APS, $(NH_4)S_2O_8$)	Carl Roth GmbH, Karlsruhe (D)	9592.1
β-Mercaptoethanol	Carl Roth GmbH, Karlsruhe (D)	4227.1
Bromophenol blue (sodium salt)	Carl Roth GmbH, Karlsruhe (D)	A512.1
BSA protein standard ($2\,mg/ml$)	Sigma-Aldrich, München (D)	P083410x1ML
Calcium chloride ($CaCl_2$)	VWR, Darmstadt (D)	1.02391.1000
Chloral hydrate	VWR, Darmstadt (D)	22682.265
Chloroform ($CHCl_3$)	Sigma-Aldrich, München (D)	372978-1L
Citric acid monohydrate	VWR, Darmstadt (D)	1.00244.1000
DAPI Fluoromount-G™	SouthernBiotech, Birmingham (USA)	SBA-0100-20

Table 2.4: List of general chemicals and solutions (continued)

Chemical/Solution	Producer/Supplier	Catalog No.
Descosept® AF	Dr. Schumacher GmbH, Melsungen (D)	00-311-050
Deoxycholic acid sodium salt ($\geq 98\,\%$)	Carl Roth GmbH, Karlsruhe (D)	3484.2
Dimethyl sulfoxide (DMSO)	Sigma-Aldrich, München (D)	D2438-50ML
Donkey serum	BIOZOL Diagnostica Vertrieb GmbH, Eching (D)	ECL-ECS0217D
Dulbecco's Modified Eagle Medium (DMEM) ($4.5\,g/l$ D-Glucose) + GlutaMax™-I	Gibco® Life Technologies™, Darmstadt (D)	32430-027
Dulbecco's Modified Eagle Medium/F-12 (DMEM/F-12) + GlutaMax™-I	Gibco® Life Technologies™, Darmstadt (D)	31331-028
Eosin Y	Sigma-Aldrich, München (D)	E4009-5G
Ethanol:		
absolute	Carl Roth GmbH, Karlsruhe (D)	9056.4
96 %, denatured	Carl Roth GmbH, Karlsruhe (D)	T171.4
Ethylenediamintetraacetic acid (EDTA-$Na_2 \cdot 2H_2O$)	Sigma-Aldrich, München (D)	E5134-1KG
Foetal calf serum (FCS):	Lonza, Köln (D)	Lot N° 8SB016
	Bio'N'Sell, Feucht (D)	Lot N° BS196368, BS196369, BS210601.5
Formaldehyde/Formalin, phosphate buffered (4%, pH7)	Carl Roth GmbH, Karlsruhe (D)	P087.3

Table 2.4: List of general chemicals and solutions (continued)

Chemical/Solution	Producer/Supplier	Catalog No.
Gefitinib (Iressa®)	Tocris Bioscience, Bristol (GB)	3000
Glycerol	Carl Roth GmbH, Karlsruhe (D)	3783.1
Glycine	Carl Roth GmbH, Karlsruhe (D)	3908.3
Haematoxylin solution	Carl Roth GmbH, Karlsruhe (D)	3816.1
Hydrochloric acid (HCl):		
37 % (fuming)	Carl Roth GmbH, Karlsruhe (D)	4625.2
1 M volumetric standard solution	Carl Roth GmbH, Karlsruhe (D)	K025.1
6 M volumetric standard solution	Carl Roth GmbH, Karlsruhe (D)	0281.1
Hydrogen peroxide (30%)	Sigma-Aldrich, München (D)	216763-500ML
Incidin® plus	Ecolab Healthcare, Monheim/Rhein (D)	3011520
Magnesium chloride hexahydrate ($MgCl_2 \cdot 6H_2O$)	Carl Roth GmbH, Karlsruhe (D)	HN03.3
Methanol	Sigma-Aldrich, München (D)	34860-2.5R
Milk powder	Carl Roth GmbH, Karlsruhe (D)	T145.3
Minimum Essential Medium Eagle (MEME) + GlutaMax™-I	Gibco® Life Technologies™, Darmstadt (D)	41090-028
Mounting media:		
Entellan®	Merck Chemicals GmbH, Darmstadt (D)	107960
Mowiol® 4-88	Sigma-Aldrich, München (D)	81381

Table 2.4: List of general chemicals and solutions (continued)

Chemical/Solution	Producer/Supplier	Catalog No.
N,N,N,N'-Tetramethyl-ethylenediamine (TEMED)	Carl Roth GmbH, Karlsruhe (D)	2367.2
Non-essential amino acids (NEAA)	Invitrogen, Darmstadt (D)	11140-035
Nonidet® P40 (NP40)	AppliChem GmbH, Darmstadt (D)	A1694
Paraffin	Carl Roth GmbH, Karlsruhe (D)	6642.6
Penicillin/Streptomycin (PenStrep, 100x conc.)	Sigma-Aldrich, München (D)	P4333
Periodic acid (1 %)	Morphisto Evolutionsforschung und Anwendung GmbH, Frankfurt/Main (D)	11415.01000
Phosphate buffered saline (PBS):		
powder (w/o Ca^{2+} and Mg^{2+})	Biochrom GmbH, Berlin (D)	L182-50
solution (w/ Ca^{2+} and Mg^{2+})	Sigma-Aldrich, München (D)	D8662
solution (w/o Ca^{2+} and Mg^{2+})	Sigma-Aldrich, München (D)	D8537
Potassium alum ($KAl(SO_4)_2 \cdot 12H_2O$)	VWR, Darmstadt (D)	1.01047.1000
Potassium chloride (KCl)	Merck Chemicals GmbH, Darmstadt (D)	1049361000
Protein marker: ProSieve® QuadColor™ ($4.6 - 300kDa$)	Lonza, Köln (D)	193837
Roswell Park Memorial Institute Medium 1640 (RPMI 1640) + GlutaMax™-I	Gibco® Life Technologies™, Darmstadt (D)	61870-010

Table 2.4: List of general chemicals and solutions (continued)

Chemical/Solution	Producer/Supplier	Catalog No.
Schiff's reagent	Merck KGaA, Darmstadt (D)	107907/2
Sodium azide (NaN_3)	Carl Roth GmbH, Karlsruhe (D)	4221.1
Sodium chloride ($NaCl$)	Carl Roth GmbH, Karlsruhe (D)	HN00.3
Sodium dodecyl sulphate (SDS)	Carl Roth GmbH, Karlsruhe (D)	CN30.3
Sodium fluoride (NaF)	Sigma-Aldrich, München (D)	201154-5G
Sodium hydrogen carbonate ($NaHCO_3$)	Carl Roth GmbH, Karlsruhe (D)	HN01.2
Sodium hydroxide ($NaOH$):		
Pellets	Carl Roth GmbH, Karlsruhe (D)	6771.3
1 M volumetric standard solution	Carl Roth GmbH, Karlsruhe (D)	K021.1
5 M volumetric standard solution	Carl Roth GmbH, Karlsruhe (D)	KK71.1
Sodium iodate ($NaIO_3$)	AppliChem GmbH, Darmstadt (D)	A5027
Sodium orthovanadate ($NaVO_4$)	Sigma-Aldrich, München (D)	S6508-10G
Sodium pyruvate ($100mM$)	Invitrogen, Darmstadt (D)	11360-039
Total bile acids assay control	Diazyme Europe GmbH, Dresden (D)	DZ042A-Con
Tris base	Sigma-Aldrich, München (D)	T6066-5KG
Triton™ X-100	Sigma-Aldrich, München (D)	X100-1L
Trypan blue 0.4 %	Sigma-Aldrich, München (D)	T8154-100ML
Tween®-20	Sigma-Aldrich, München (D)	P7949-500ML

Table 2.4: List of general chemicals and solutions (continued)

Chemical/Solution	Producer/Supplier	Catalog No.
Vemurafenib (PLX4032)	Selleckchem, München (D)	S1267
Xylene	Carl Roth GmbH, Karlsruhe (D)	9713.3

2.1.4.2 Media, buffers and solutions for cell culture

Table 2.5: List of media, buffers and solutions for cell culture

Medium/Buffer/Solution	Composition	
0.05 % Trypsin/EDTA working solution	10 ml	Trypsin/EDTA 0.5 % (10x)
	90 ml	PBS^- solution stored at 4°C
5-Fluorouracil stock solution	10 mM	in 1ml DMSO (stored at -80°C)
Collagenase solution (500 U/ml CDU)	1000 mg	Collagenase NB4
	436 ml	DMEM sterile filtered (stored at -20°C)
Dispase II solution (2 U/ml)	1000 mg	Dispase II powder (min. 0.5 U/mg)
	250 ml	PBS^- sterile filtered (stored at -20°C)
DNase I solution	100 mg	DNase I (grade II)
	300 ml	PBS^+ with 1% PenStrep freshly prepared prior to use
Fibroblast culture medium	10 % (v/v)	FCS
	1 mM	Sodium pyruvate
	in	Dulbecco's Modified Eagle Medium (DMEM), pH7.2 (stored at 4°C)
Gefitinib stock solution	10 mg	Gefitinib (Iressa®)

Table 2.5: List of media, buffers and solutions for cell culture (continued)

Medium/Buffer/Solution	**Composition**	
($100\,mM$)	$224\,\mu l$	DMSO aliquoted (stored at -20°C, no re-freezing)
HROC24 and HROC87 culture medium	10 % (v/v) in	FCS Dulbecco's Modified Eagle Medium/F-12 (DMEM/F-12), pH 7.2 (stored at 4°C)
MTT reagent	$3\,mg/ml$	3-(4,5-Dimethylthiazol- 2-yl)-2,5-diphenyl- tetrazolium- bromide (MTT) solved in ultrapure water (MilliQ®)
MTT solution ($1\,mg/ml$)	1 volume 2 volumes	MTT reagent ($3\,mg/ml$) cell specific culture medium prepared immediately before use
PBS$^-$	$9.55\,g$ in $1\,l$	PBS powder (w/o Ca^{2+} and Mg^{2+}) Ultrapure water (MilliQ®) pH 7.2, autoclaved before use (stored at 4°C) *or* PBS solution without Ca^{2+}, Mg^{2+}
PBS$^-$/EDTA	$1\,l$ $0.2\,g$	PBS$^-$ Na_2-EDTA $\cdot$ 2 H_2O pH 7.2, autoclaved before use (stored at 4°C) *or*
	$500\,ml$	PBS solution without Ca^{2+}, Mg^{2+}

Table 2.5: List of media, buffers and solutions for cell culture (continued)

Medium/Buffer/Solution	**Composition**	
	500 μl	0.5 M Na_2-EDTA · 2 H_2O
PBS^+	1 l	PBS^-
	0.1 g	$MgCl_2 \cdot 6\, H_2O$
	0.1 g	$CaCl_2$
		or
		PBS solution with Ca^{2+}, Mg^{2+}
SW480 culture medium	10 % (v/v)	FCS
	in	Roswell Park Memorial Institute Medium 1640 (RPMI 1640), pH7.2 (stored at 4°C)
Vemurafenib stock solution (50 mM)	10 mg	Vemurafenib (PLX4032)
	408 μl	DMSO
		aliquoted (stored at -80°C, no re-freezing)

2.1.4.3 Buffers and solutions for histology and immunohistology

Table 2.6: List of buffers and solutions for histology and immunohistology

Buffer/Solution	**Composition**	
Antibody diluent	5 % (w/v)	Bovine serum albumine (BSA)
	in	PBS^-
		sterile filtered
		(stored at 4°C)
Blocking solution	5 % (v/v)	Donkey serum
	in	Antibody diluent
		freshly prepared prior to use
Citrate buffer stock solution	42 g/l	Citric acid monohydrate
(10x concentrated)	17.6 g/l	$NaOH$ pellets
	in	ddH_2O
		pH 6.0 (stored at RT)
Citrate buffer working	10 % (v/v)	Citrate buffer stock solution
solution	in	ddH_2O
Embedding solution (aqueous)	0.1 %	DAPI
	in	Mowiol® 4-88
		(stored at -20°C)
Eosin	10 mg/ml	Eosin Y
	in	ddH_2O
		(stored at RT)
Hemalum	1.2 g/l	Haematoxylin
	0.2 g/l	$NaIO_3$
	20 g/l	Potassium alum
	20 g/l	Chloral hydrate
	1 g/l	Citric acid monohydrate
	in	ddH_2O
		used after four weeks of maturation
		(stored at RT)
HCl-Ethanol (H&E staining)	6.85 % (v/v)	HCl, 1 M
	in	Ethanol, 50 %
		(stored at RT)
Hydrogen peroxide 3 %	10 % (v/v)	H_2O_2 30 %

Table 2.6: List of buffers and solutions for histology and immunohistology (continued)

Buffer/Solution	**Composition**	
(H_2O_2)	in	ddH_2O prepared immediately before use
Permeabilisation solution	0.2 % (v/v)	Triton™ X-100
	in	PBS^- (stored at RT)
Tris-EDTA buffer stock	12.11 g/l	Tris base
solution (10x concentrated)	3.72 g/l	Na_2-EDTA
	in	Ultrapure water (MilliQ®) pH 9.0 (stored at RT)
Tris-EDTA buffer working	10 % (v/v)	Tris-EDTA buffer stock solution
solution	in	Ultrapure water (MilliQ®) (stored at RT)
Washing buffer (PBS-T)	10 % (v/v)	Washing buffer stock solution
	0.5 % (v/v)	Tween®-20
	in	ddH_2O (stored at RT)
Washing buffer stock solution	1370 mM	$NaCl$
(PBS, 10x concentrated)	26.8 mM	KCl
	14.5 mM	KH_2PO_4
	64.6 mM	$Na_2PO_4 \cdot 2H_2O$
	in	ddH_2O pH 7.2, autoclaved before use (stored at RT)

2.1.4.4 Buffers and solutions for protein chemistry

Table 2.7: List of buffers and solutions for protein chemistry

Buffer/Solution	Composition	
Antibody diluent	5 % (w/v)	Milk powder
	0.1 % (v/v)	NaN_3, 10 %
	in	Washing buffer (TBS-T)
		(stored at 4°C)
		or
	5 % (w/v)	Albumine Fraction V
		(BSA)
	0.1 % (v/v)	NaN_3, 10 %
	in	Washing buffer (TBS-T)
		(stored at 4°C)
Blocking solution	5 % (w/v)	Milk powder
	in	Washing buffer (TBS-T)
		(stored at 4°C)
Electrophoresis buffer	10 % (v/v)	Electrophoresis buffer
		stock solution
	in	Ultrapure water
		(MilliQ®)
		(stored at RT)
Electrophoresis buffer stock	1920 mM	Glycine
solution (10x concentrated)	250 mM	Tris base
	1.5 % (w/v)	SDS
	in	Ultrapure water
		(MilliQ®)
		(stored at RT)
Laemmli buffer	1.5 M	Tris base, pH 6.8
(5x concentrated)	10 % (v/v)	Glycerol
	5 % (v/v)	β-Mercaptoethanol
	2 % (w/v)	SDS
	0.01 % (w/v)	Bromophenol blue
		Na-salt
		(stored at -20°C)
Lower Tris	1.5 M	Tris base, pH 8.8
(4x concentrated)	0.4 % (w/v)	SDS
		(stored at RT)
Lysis buffer: modified RIPA	137 mM	$NaCl$
	50 mM	NaF

Table 2.7: List of buffers and solutions for protein chemistry (continued)

Buffer/Solution	Composition	
	20 mM	Tris base, pH 8.0
	2 mM	EDTA
	10 % (v/v)	Glycerol
	1.0 % (v/v)	Nonidet® P40
	0.5 % (w/v)	Deoxycholic acid sodium salt
	0.1 % (w/v)	SDS
	in	Ultrapure water (MilliQ®) (stored at 4°C) added immediately before use:
	1 mM	Na_3VO_4
	1	Protease inhibitor cocktail tablet per 10 ml of lysis buffer
Separation gel 10 % (for two gels)	2.5 ml	Lower Tris (4x conc.)
	3.3 ml	Acrylamide/Bisacrylamide
	2.2 ml	Ultrapure water (MilliQ®)
	2.0 ml	Glycerol
	14 μl	APS, 40 %
	14 μl	TEMED prepared immediately before use
Stacking gel 5 % (for two gels)	1.25 ml	Upper Tris (4x conc.)
	0.5 ml	Acrylamide/Bisacrylamide
	3.2 ml	Ultrapure Water (MilliQ®)
	12 μl	APS, 40 %
	12 μl	TEMED prepared immediately before use
Stripping buffer (mild)	1.5 % (w/v)	Glycine
	0.1 % (w/v)	SDS
	1.0 % (v/v)	Tween®-20

Table 2.7: List of buffers and solutions for protein chemistry (continued)

Buffer/Solution	**Composition**	
	in	Ultrapure water (MilliQ®) pH 2.2 (stored at RT for up to two weeks)
Washing buffer (TBS-T)	10 %	Washing buffer stock solution
	0.5 %	Tween®-20
	in	ddH_2O (stored at RT)
Washing buffer stock solution (TBS, 10x concentrated)	1500 mM	$NaCl$
	500 mM	Tris base
	in	Ultrapure Water (MilliQ®) pH 7.6 (stored at RT)
Upper Tris (4x concentrated)	0.5 M	Tris base, pH 6.8
	0.4 % (w/v)	SDS (stored at RT)

2.1.5 Enzymes

Table 2.8: Enzymes used in cell culture and protein chemistry

Enzyme	Description	Producer/Supplier
Collagenase lyophilisate	Collagenase NB4 or Clostridiopeptidase A from *Clostridium histolyticum*. Protease specific for collagen, degenerates extracellular matrix.	Serva, Heidelberg (D), Cat. No. 17454.01
Dispase II, powder	Dispase II is an amino-endo peptidase from *Bacillus polymyxa*. This neutral protease hydrolyses N-terminal peptide bonds of non-polar amino acid residues. Used for dissociation of dermis and epidermis.	Thermo Fisher Scientific, Dreieich (D), Cat. No. 17105041
Deoxyribonuclease I (DNase I)	DNase I (grade II) is a double-strand-specific endonuclease from bovine pancreas. Used for DNA degradation in the preparation of the SISmuc.	Roche, Penzberg (D), Cat. No. 10104159001
Protease inhibitor cocktail (tablets)	Contains several protease inhibitors to protect proteins from degradation while lysing cells; inhibits aspartic proteases as well as serine, cysteine, and metalloproteases.	Roche, Penzberg (D), Cat. No. 04693116001
Trypsin/EDTA stock solution, 0.5 % (10x concentrated)	Trypsin is a serine protease used to digest cell adherence molecules and therefore to detach cells from their culture vessel.	Invitrogen, Darmstadt (D), Cat. No. 15400-054

2.1.6 Kits

Table 2.9: List of kits used

Kit	Description	Producer
CellTiter-Glo® Luminescent Cell Viability Assay	Kit for the determination of cell viability in culture based on metabolically active cells (ATP quantitation).	Promega, Mannheim (D), Cat. No. G7570
DC Protein Assay	Kit for the determination of total protein concentration in lysates (Lowry based).	BioRad, München (D), Cat. No. 500-0112
IHC-Kit DCS SuperVision 2 HRP	Two-step polymer system for immunohistochemical staining with horse radish peroxidase (HRP) and 3,3'-diaminobenzidine (DAB) using secondary anti-mouse and anti-rabbit antibodies.	DCS Innovative Diagnostik-Systeme GmbH & Co. KG, Hamburg (D), Cat. No. PD000KIT
M30 CytoDeath™ ELISA	One step *in vitro* immunoassay for the quantitative determination of apoptosis in cultured human, monkey or bovine epithelial cells expressing the intermediate filament protein keratin 18 (K18).	Peviva, Bromma (S), Cat. No. 10900
ProteomeProfiler™ Human Phospho-Kinase Array	Array for parallel screening and detection of 43 kinase phosphorylation sites from cell lysates.	R&D Systems, Inc., Minneapolis (USA), Cat. No. ARY003B
ProteomeProfiler™ Human Phospho-RTK Array Kit	Array for simultaneous screening and detection of 49 different phosphorylated human receptor tyrosine kinases (RTKs) from cell lysates.	R&D Systems, Inc., Minneapolis (USA), Cat. No. ARY001B

Table 2.9: List of kits used (continued)

Kit	Description	Producer
Total Bile Acids Assay Kit	Assay for the quantitative determination of total bile acids. Used for controlling the bile acids residues of the SISmuc after decellularisation with deoxycholic acid.	Diazyme Europe GmbH, Dresden (D), Cat. No. DZ042A-K
WesternBright™ Quantum Chemiluminescence Substrate	Kit consisting of two reaction reagents for the detection of HRP-based chemiluminescence in the development of western blotting membranes.	Biozym Scientific GmbH, Hessisch Oldendorf (D), Cat. No. 541015

2.1.7 Antibodies

Table 2.10 lists all antibodies used for immunofluorescence stainings (IF), immunohistochemistry stainings (IHC) and western blotting (WB). The used amounts of the antibodies are specified as absolute concentrations or applied dilutions.

Table 2.10: List of antibodies used for immunofluorescence (IF), immunoperoxidase staining with DAB (DAB) and western blotting (WB)

Antibody	Clone	Host	Conc./ Dilution	Producer
Akt (pan)	C67E7	Rabbit	1:1000 (WB)	Cell Signaling Technology, Beverly, MA (USA), Cat. No. 4691
Alexa Fluor® 555 anti-Mouse IgG (H+L)	—	Donkey	$2\,mg/ml$, 1:400 (IF)	Thermo Fisher Scientific, Dreieich (D), Cat. No. A-31570

Table 2.10: List of antibodies used for immunofluorescence (IF), immunoperoxidase staining with DAB (DAB) and western blotting (WB)(continued)

Antibody	**Clone**	**Host**	**Conc./ Dilution**	**Producer**
Alexa Fluor® 555 anti-Rabbit IgG (H+L)	—	Donkey	2 mg/ml, 1:400 (IF)	Thermo Fisher Scientific, Dreieich (D), Cat. No. A-31572
Alexa Fluor® 647 anti-Mouse IgG (H+L)	—	Donkey	2 mg/ml, 1:400 (IF)	Thermo Fisher Scientific, Dreieich (D), Cat. No. A-31571
Alexa Fluor® 647 anti-Rabbit IgG (H+L)	—	Donkey	2 mg/ml, 1:400 (IF)	Thermo Fisher Scientific, Dreieich (D), Cat. No. A-31573
α-Tubulin	DM1A	Mouse	1:2000 (WB)	Cell Signaling Technology, Beverly, MA (USA), Cat. No. 3873
β-Catenin	E247	Rabbit	1:100 (IF)	Abcam pcl, Cambridge (GB), Cat. No. 32572
CD44	EPR1013Y	Rabbit (IgG)	1:250 (DAB), 1:100 (IF)	Abcam pcl, Cambridge (GB), Cat. No. 51037
CD133	17A6.1	Mouse (IgG2aκ)	1 mg/ml, 1:500 (DAB)	Merck Chemicals GmbH, Darmstadt (D), Cat. No. MAB4399
CD166	MOG/07	Mouse (IgG2a)	1:160 (DAB)	Abcam pcl, Cambridge (GB), Cat. No. 49496
CDX2	EPR2764Y	Rabbit (IgG)	1:500 (DAB), 1:100 (IF)	Abcam pcl, Cambridge (GB), Cat. No. 76541

Table 2.10: List of antibodies used for immunofluorescence (IF), immunoperoxidase staining with DAB (DAB) and western blotting (WB)(continued)

Antibody	**Clone**	**Host**	**Conc./ Dilution**	**Producer**
Cytokeratin 7 (CK7)	RCK105	Mouse (IgG1)	1:1000 (DAB), 1:100 (IF)	Abcam pcl, Cambridge (GB), Cat. No. 9021
Cytokeratin 18 (CK18)	DC10 (6)	Mouse	1:100 (IF)	Dako Denmark A/S, Glostrup (DK), Cat. No. M7010
Cytokeratin 20 (CK20)	K_S20.8	Mouse	1:500 (DAB), 1:100 (IF)	Dako Denmark A/S, Glostrup (DK), Cat. No. M7019
Cytokeratin, pan (PCK)	C-11 +PCK-26+CY-90+KS-1A3+M20 +A53-B/A2	Mouse	1:50 (IF)	Sigma-Aldrich, München (D), Cat. No. C2562
E-Cadherin	36/E-Cadherin	Mouse	250 $\mu g/ml$, 1:100 (IF)	BD Transduction Laboratories, Heidelberg (D), Cat. No. 610181
EGFR	D38B1	Rabbit	1:1000 (WB)	Cell Signaling Technology, Beverly, MA (USA), Cat. No. 4267
EpCAM	B302	Mouse (IgG1)	300 $\mu g/ml$, 1:300 (DAB)	Abcam pcl, Cambridge (GB), Cat. No. 8601

Table 2.10: List of antibodies used for immunofluorescence (IF), immunoperoxidase staining with DAB (DAB) and western blotting (WB)(continued)

Antibody	**Clone**	**Host**	**Conc./ Dilution**	**Producer**
Erk1/2 (p44/p42)	137F5	Rabbit	1:1000 (WB)	Cell Signaling Technology, Beverly, MA (USA), Cat. No. 4695
Ki67	SP6	Rabbit	1:100 (IF)	Abcam pcl, Cambridge (GB), Cat. No. 166667
Met/HGFR	D1C2	Rabbit	1:1000 (WB)	Cell Signaling Technology, Beverly, MA (USA), Cat. No. 8198
Phospho-Akt (Ser473)	D9E	Rabbit	1:1000 (WB)	Cell Signaling Technology, Beverly, MA (USA), Cat. No. 4060
Phospho-EGFR (Tyr1068)	Y68	Rabbit	1:10000 (WB)	Abcam pcl, Cambridge (GB), Cat. No. 32430
Phospho-Erk1/2 (Thr202/Tyr204)	D13.14.4E	Rabbit	1:2000 (WB)	Cell Signaling Technology, Beverly, MA (USA), Cat. No. 4370
Phospho-Met (Tyr1234/1235)	D26	Rabbit	1:1000 (WB)	Cell Signaling Technology, Beverly, MA (USA), Cat. No. 3077
Vimentin	EPR3776	Rabbit	$150\,\mu g/ml$, 1:100 (IF)	Abcam pcl, Cambridge (GB), Cat. No. 92547

2.1.8 Biological material

2.1.8.1 Cell lines

Table 2.11: List of cell lines

Cell line	Description	Source
HROC24	A xenopatient-derived early-passage cell line established from a grade 2 primary adenocarcinoma of the colon ascendens of a 98-year-old Caucasian man. TNM stage: T2N0M0. Epithelial adherently growing cells.	University of Rostock, Division of Molecular Oncology and Immunotherapy, Rostock (D)
HROC87	A xenopatient-derived early-passage cell line established from a grade 3 primary adenocarcinoma of the colon ascendens of a 76-year-old Caucasian woman. TNM stage: T3N0M0. Epithelial adherently growing cells.	University of Rostock, Division of Molecular Oncology and Immunotherapy, Rostock (D)
SW480	A colon adenocarcinoma cell line established from a grade 4 tumour (Duke class B) of a 50-year-old Caucasian man. Epithelial adherently growing cells.	Leibniz-Institut DSMZ, Braunschweig (D), Cat. No. ACC-313

The patient-derived early-passage cell line **HROC24** was obtained (either patient-derived or by xenografting) from a primary adenocarcinoma of the colon ascendens (TNM stage: G2T2N0M0) of a 98-year-old male who was not treated before. HROC24 cells harbour mutations in exon 15 of *APC* and the point mutation V600E in the kinase *BRAF*, though, they are wildtype for *KRAS* and *TP53*. The tumour cells show a spontaneous mismatch-repair deficiency (spMMR-D) in all six markers analysed and display a high-degree CpG island methylator phenotype (CIMP), including *MLH1* promoter methylation [70, 113].

The patient-derived early-passage cell line **HROC87** was obtained through xenografting from a primary adenocarcinoma of the colon ascendens (TNM stage: G3T3N0M0) of a 76-year-old female without prior therapy. HROC87 cells are classified as sporadic MMR-D and show as well as HROC24 cells *MLH1* promoter methylation [70]. In contrast to the cell line HROC24, HROC87 cells

harbour mutations in exons 6 and 7 of *TP53*, but present a wildtype in *APC* while both cell lines bear the $BRAF^{V600E}$ mutation [70]. In both cell lines, β-catenin is not translocated to the nucleus.

The cell line **SW480** was established from the tumour of a 50-year-old Caucasian man with colon adenocarcinoma (grade 4, Duke class B) in 1973 by Albert Leibovitz [114, 115]. The endothelial-like adherent cells grow in monolayers and express the oncogenes *c-MYC, K-RAS, H-RAS, N-RAS, MYB, SIS* and *FOS*. The expression of p53 protein is elevated in these cells [116].

2.1.8.2 Porcine material: SISmuc

The small intestinal submucosa (SIS) is derived from the biological vascularised scaffold BioVaM® or BioVaSc® [74, 117] consisting of a decellularised jejunum segment of the German landrace pig (Deutsche Landrasse). It is composed of a dense layer of cross-linked collagen and elastin fibers preserving the vascular basement membrane and elastica interna [74, 118]. Experimental protocols for its preparation have been published previously [74, 75, 77, 117–119].

In contrast, the biological scaffold SISmuc still implies the mucosa (muc) of the former jejunum while the mesentery with the vascular tree from the completely decellularised explant is removed after the decellularisation procedure preserving the mucosal tissue layer, including crypt, villi and the basement membrane structure [2, 78].

Materials, chemicals and further equipment used for the decellularisation of the SISmuc are summarised in table 2.12.

Table 2.12: List of materials, equipment and chemicals/solutions for the decellularisation of the SISmuc

Material	**Equipment**	**Chemical/Solution**
Breathing mask	Analytical balance	DNase I ($300\,mg/ml$) in PBS^+ 1 % (v/v) PenStrep
Clips	Beakers	Deoxycholic acid sodium salt ($22.5\,g/l$) in ultrapure water
Disposable pipettes	Cold storage room	PBS powder ($9.55\,g/l$, w/o Ca^{2+}, Mg^{2+}) in ultrapure water
Instrument tray	Freezer (-20°C)	PBS^+ solution
Pipette tips	Magnetic stirrer	Penicillin/Streptomycin (PenStrep, 100x concentrated)

Table 2.12: List of materials, equipment and chemicals/solutions for the decellularisation of the SISmuc (continued)

Material	Equipment	Chemical/Solution
Peristaltic pump	Measuring cylinders	Ultrapure water (MilliQ®)
Pump tubing	Pipettes	
Reaction tubes	Pipetting aid	
Silicon tubes	Pump tubing cassette	
Tube adapters	Pressure sensor	
Weighing dishes	Rocking platform shaker	
	Volumetric flasks	

2.1.8.3 Human material

For higher complexity of the tumour model, co-culture experiments with human primary dermal fibroblasts were conducted. The fibroblasts were isolated from prepuces or the skin of the thigh of donors with different age according to approval by the Institutional Ethics Committee of the University Hospital Würzburg (approval number 182/10).

2.1.8.4 Animals for xenografting experiments

Male NMRI Foxn1nu mice were used for xenografting experiments with the cell line HROC87. All experiments were conducted by the lab of PD Dr. M. Linnebacher at the University Hospital Rostock.

2.1.9 Software & Programmes

Table 2.13: List of computer software and programmes

Software	**Description**	**Developer/ Manufacturer**
Adobe Photoshop 7.0	Image processing	Adobe Systems Inc., San Jose (USA)
AlphaView FluorChem Q 3.2.2	Imaging and analysis tool for protein and nucleotide gels	ProteinSimple, San Jose (USA)
BZ Analyzer	Software for microscopy	Keyence Corporation, Neu-Isenburg (D)
ImageJ 1.50i	Image processing	Wayne Rasband, National Institute for Health (USA)
LaTeX	Typesetting/Document preparation system	LaTeX Project Public License, Mainz (D)
Microsoft Excel 2013	Spreadsheet processing	Microsoft Corporation, Redmond (USA)
OriginPro 8.6	Data analysis and graphing software	OriginLab Corporation, Northampton (USA)
Pressure control	Software for controlling the pump speed in the bioreactor board	Chair of Tissue Engineering & Regenerative Medicine, Würzburg (D)
R 3.3.0	Software for statistical computing	The R Foundation for Statistical Computing, Vienna (A)

2.2 Methods

2.2.1 Cell culture techniques

To ensure sterile conditions, all cell culture techniques were performed under a class II laminar flow safety cabinet. Prior to work, all surfaces of the laminar flow safety cabinet were decontaminated thoroughly by spraying the disinfectant Descosept® AF or 70 % ethanol, considering a residence time of about 2–5 min, after the lead time of the laminar flow safety cabinet of 10–15 min. All disposable materials were sterile and all laboratory materials as well as all solutions were sterilised by autoclaving or sterile-filtering, respectively.

Cells were cultured at 37°C, 5 % CO_2 and 96 % relative humidity in an incubator. Daily, the cells were monitored microscopically for their morphology and growth speed as well as for possible contaminations. The cell culture media did not contain any antibiotics during under conventional 2D cell culture conditions or under 3D static cell culture conditions in cell crowns. Only for bioreactor experiments it was added. FCS was not heat-inactivated. The media were changed every 2–3 days. Cell cultures were tested regularly by PCR for mycoplasma contamination.

2.2.1.1 Culturing cell lines in conventional 2D cell culture

HROC24 cells were cultured in Dulbecco's Modified Eagle Medium/F12 (DMEM/F12) containing 10 % (v/v) FCS. 1.5–3·10^5 cells were seeded in a T75 culture flask and grown until they reached 70–90 % confluency, yielding about 2–4·10^6 cells/75 cm^2.

HROC87 cells were cultured in DMEM/F12 containing 10 % (v/v) FCS. 3–5·10^5 cells were seeded in a T75 culture flask and grown until they reached 70–90 % confluency, yielding about 2–4·10^6 cells/75 cm^2.
SW480 cells were cultured in Roswell Park Memorial Institute 1640 (RMPI 1640) medium containing 10 % (v/v) FCS. 1.5–3·10^5 cells were seeded in a T75 culture flask and grown until they reached 70–90 % confluency, yielding about 2– 4·10^6 cells/75 cm^2.

2.2.1.2 Freezing and thawing of cells

To preserve a stock of cell lines and primary cells, they were frozen at a low passage number. After having reached a confluency of 80–90 %, cells were detached from their culture flask by trypsinisation (see 2.2.1.3). Subsequently, cells were counted (see 2.2.1.4) and the cell concentration was adjusted to 1·10^6 cells/ml with cell-specific culture medium. 1 ml of this cell suspension

was pipetted per cryo tube, further, 10 % (v/v) FCS and 10 % (v/v) DMSO were added. To prevent damage of the cells due to DMSO, cells should be frozen as fast as possible using the freezing container "Mr. Frosty". This container ensures a gentle freezing process by cooling down 1°C/min; it was immediately put at -80°C for at least 24 hours before transferring the cryo tubes into the liquid nitrogen tank at -180°C for long-term storage.

To start cell culture, a cryo tube with frozen cells was swayed gently in a water bath at 37°C until only a small piece of ice remained. Thereafter, the suspension was poured into 10 ml of pre-warmed cell-specific culture medium and centrifuged at 1200 rpm for 5 min. After aspirating the supernatant to remove all DMSO, the cells were resuspended in 10 ml of fresh culture medium and put in the culture flask. The next day, a medium change was performed. The thawed cells were passaged at least once before they were used for experiments.

2.2.1.3 Passaging cells

At a confluency of 70–90 %, the cells had to be passaged to prevent overgrowing, this was performed once or twice per week. First, the culture medium in the flask was aspirated and the cells were washed once with PBS^-/EDTA to remove medium residues. To assure a gentle detachment, the cells were then pre-incubated for 5 min with 5 ml PBS^-/EDTA at 37°C. Next, 5 ml of 0.05 % Trypsin/EDTA solution was added and the cells were incubated for 3 min at 37°C. The detachment of the cells from the bottom of the culture flask was monitored by microscopy and the enzymatic reaction was stopped by adding 2 ml FCS or 5–10 ml cell-specific culture medium. The cell suspension was then transferred to a 50 ml centrifuge tube and the empty culture flask was rinsed with 3–5 ml PBS^-/EDTA to detach and to collect remaining cells. After pooling, the suspension was centrifuged at 1200 rpm for 5 min and the supernatant aspirated. The pellet was resuspended in 5–10 ml of cell-specific medium and the cell number and vitality was assessed by using a hemocytometer (Neubauer counting chamber, see 2.2.1.4). If the cells were still not separating and forming clusters, e.g. HROC87 cells, they were passed through a 70 µm cell sieve. An adequate amount of cells (see 2.2.1.1) was then seeded into a new culture flask. Cells were kept in culture for a maximum of three months and 20 passages from the time point of thawing.

2.2.1.4 Determination of cell number and vitality

Cell number and vitality were determined by using trypan blue staining and a hemocytometer (Neubauer counting chamber). For this purpose, an aliquot

of the cell suspension was mixed carefully with 0.4 % trypan blue solution and 10 µl of this solution were applied to the edge of the coverslip of the Neubauer counting chamber. By capillary action, the solution was sucked into the void and filled the chambers completely. The living cells appeared shiny and colourless whereas dead cells were stained dark and blue. All living cells were counted in the four quadrants of the Neubauer counting chamber and the cell number per millilitre was calculated using the specific chamber volume ($0.1\,mm^3$) and the dilution factor (e.g. 2 for a 1:2 dilution with 0.4 % trypan blue) according to the following formula:

$$\bar{x}_{LC} \cdot V_{CF} \cdot DF = CC$$

$\bar{x}_{LC}$: mean of living cells per quadrant
V_{CF} : volume, chamber factor ($10^4/ml$)
DF : dilution factor (trypan blue)
CC : cell concentration [$cells/ml$]

Cell vitality was calculated as the quotient of living cells and total cells counted.

2.2.1.5 Cell culture on chamber slides/cover slips

To compare cell characteristics of 2D cultured cells and 3D cultured cells, they were seeded on glass chamber slides and round glass cover slips (⌀ 12mm), respectively, for immunohistochemical (IHC) or immunofluorescence stainings (IF).

$1{\cdot}10^4$ cells in 400 µl of their specific culture medium were seeded into each of the eight wells of a glass chamber slide and cultured until they reached a confluency of 30–50 % prior to the start of treatment with vemurafenib and/or gefitinib. After the treatment period of 3 days, the cells were fixed for 10 min using 4 % solution and stained subsequently for different specific markers, e.g. the proliferation marker Ki67, or the fixed cells were covered and stored under sterile PBS^- at 4°C until IHC/IF staining. Cells were fixed 5–7 days after seeding, reaching a confluency of about 70–80 % in the control sample.

For the glass cover slips, $2.5–5{\cdot}10^4$ cells were seeded in 1 ml cell-specific culture medium in 24-well plates and cultured the same way as cells seeded on glass chamber slides.

2.2.1.6 Cell culture on Petri dishes and well plates

Petri dishes (⌀ 6 cm) were used for biochemical analyses (see 2.2.6). HROC24 and HROC87 cells were seeded at a density of $3–5{\cdot}10^5$ per dish. Cells were

cultured until reaching a confluency about 30–50 % before the treatment with vemurafenib and gefitinib started for 1–3 days.

Well plates were used for comparison of treated and untreated 2D cell culture to 3D cell culture on SISmuc. For experiments determining the rate of growth, $2{\cdot}10^5$ HROC24 cells and $3{\cdot}10^5$ HROC87 cells, respectively, were seeded in 1 ml per well in a 12-well plate and cultured as well as treated identically as the cells in Petri dishes. On each day after the beginning of the treatment, cells were detached by trypsinisation and counted with a hemocytometer (see 2.2.1.4) to assess the cell number.

For viability tests such as on the glycolysis metabolism based MTT test (see 2.2.3), 24-well plates were used and $1{\cdot}10^5$ HROC24 cells and $1.55{\cdot}10^5$ HROC87 cells, respectively, were seeded in 1 ml per well with culturing and treatment time according to cells cultured on Petri dishes.

2.2.1.7 Static 3D culture of cells on SISmuc

To compare conventional 2D with 3D cell culture, a scaffold is needed for the cells to grow on and inside. For this purpose, the collagen-based scaffold SISmuc (see 2.1.8.2) was used and cells were seeded on the mucosal side. Cells were cultured for up to 14 days with a medium change every 2–3 days. Treatment with inhibitors occurred in the last 72 h of culture before fixing or lysing the cells on the scaffold and using them for further analyses (see figure 2.5).

Prior to seeding with cells, the SISmuc had to be fixed between two metal cylinders, “cell crowns”, in order to keep it on its position while culturing in 12-well plates. To prevent the matrix from touching the bottom of the well plate the outer and larger metal cylinder possessed little stands. The fixation of the SISmuc into a cell crown is illustrated in figures 2.1 and 2.2. First, a piece of SISmuc (fig. 2.2 A) was cut open with a scalpel on a sterile Petri dish under a laminar flow safety cabinet (fig. 2.2 B/C) and opened up so that the luminal side of the scaffold was facing upwards (fig. 2.2 D). After cutting off an appropriate size from the SISmuc (fig. 2.2 E/F) it was imposed on the smaller inner metal cylinder using tweezers (fig. 2.2 G) and fixed with the outer larger metal cylinder by pushing the outer over the inner cylinder (fig. 2.2 H). Subsequently, the cell crown was put upside down with the aperture facing upwards into a 12-well plate (fig. 2.2 I) and submerged with cell-specific culture medium in order to equilibrate the matrix. The well plate was incubated over night at 37°C and 5 % CO_2 before seeding the cells. Usually, $1 \cdot 10^5$ cells in 500 µl culture medium were seeded per cell crown and another 500 µl culture medium were added 2 h later into the inner compartment. 1.5 ml of culture medium were filled immediately before seeding into the outer compartment.

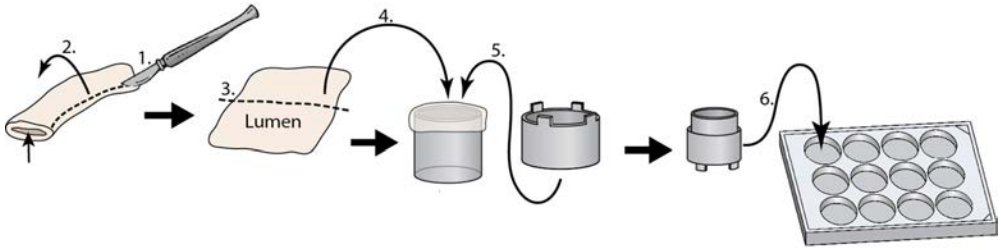

Figure 2.1: Schematic drawing of the fixation of the SISmuc into a "cell crown". At first, the scaffold was cut open with a scalpel (1.) and opened up (2.) so that the luminal side faced upwards. An adequate piece of the matrix was cut off (3.) then imposed on the smaller inner metal cylinder (4.) with the luminal side facing downwards and fixed with the larger outer metal cylinder (5.) before putting the whole "cell crowns" upside down into a 12-well plate (6.). The cells were seeded onto the mucosal side of the scaffold after one day of equilibration in culture medium. (Drawing by N. Wirth)

For co-culture experiments with fibroblasts, $1 \cdot 10^5$ cells from each cell type were seeded together. Medium change was performed every 2–3 days and cells were cultured for 14 days before either fixing them with 4 % formalin and embedding in paraffin for histological/immunohistological staining or lysing for biochemical analyses or using the tumour model for viability assays such as MTT test, respectively (see figure 2.5).

2.2.1.8 Dynamic 3D culture of cells on SISmuc

For the dynamic 3D culture, the SISmuc was fixed into "cell crowns" at first as described in section 2.2.1.7 and as shown in figures 2.1 and 2.2. Cells were seeded 3 days before mounting the scaffold into a flow bioreactor system in order to ensure adhesion of the cells onto the matrix. The flow bioreactor system consisted of the reactor body comprising three chambers for the pre-seeded scaffolds and three culture medium reservoir bottles which were connected to the reactor body via silicone tubes. A pump tubing for each of the three chambers was inserted with tube adaptors between silicone tubes and attached to the peristaltic pump of the bioreactor board with pump tubing cassettes (fig. 2.4 O/P).

Prior to insertion of the SISmuc into the flow bioreactor, all parts of the bioreactor system were autoclaved. The scaffold was transferred from the cell crown to the bioreactor using sterile tweezers by removing the larger outer metal cylinder. Afterwards, the SISmuc, still sticking to the smaller inner metal cylinder

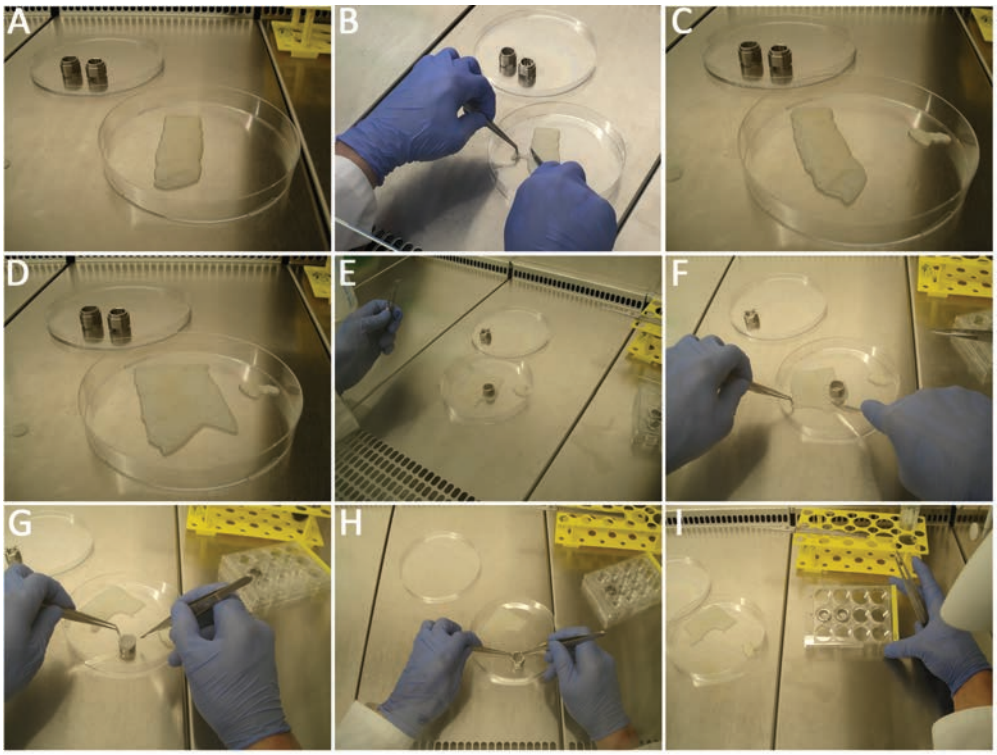

Figure 2.2: Demonstration of fixing the SISmuc into a "cell crown". A piece of SISmuc was put on a sterile Petri dish under a laminar flow safety cabinet (A) and cut open on one edge with a scalpel (B). After opening up (C and D), the inner metal cylinder of the cell crown was put on the luminal side of the SISmuc (E) and an adequate piece of the matrix was cut off (F). The scaffold was then imposed upside down (with the luminal side facing downwards) on the smaller metal cylinder (G) and fixed with the larger outer metal cylinder (H) so that the luminal side was facing upwards. The cell crowns were put into a 12-well plate (I) and incubated at least over night in cell-specific culture medium before seeding the cells.

(fig. 2.4 D), was placed into one of the bioreactor's chambers (fig. 2.4 E). After removing the smaller inner metal cylinder of the cell crown, the scaffold was stretched and smoothed gently with tweezers to ensure the proper fixation between the other half of the reactor body (fig. 2.4 F). O-rings were inserted between the two halves of the reactor body (fig. 2.4 G/H) to tighten the system and to prevent culture medium from leaking out. Subsequently, the two halves were placed onto each other and screwed together tightly (fig. 2.4 I/J) thereby creating two compartments with a volumetric capacity of approximately 2 ml each separated by the SISmuc seeded with cells (see fig. 2.3). Thereafter, the silicone tubes were attached to the reactor body by screwing the Luer-lock adaptors (fig. 2.4 K/L/M/N) and the culture medium reservoirs were filled with 40 ml of cell culture medium each. After placing the flow bioreactor system into the incubator, the pump tubing cassettes were attached to the peristaltic pump of the bioreactor board (fig. 2.4 O/P). A constant flow was applied and culture medium was pumped through the chambers with a speed of 3.8 ml/min [2]. Gas exchange was provided by the silicone tubes allowing oxygen and carbon dioxide to pass via diffusion. A medium change was performed after 7 days of dynamic culture and cells were kept in the flow bioreactor system for 14 days before fixing the SISmuc in 4 % formalin and embedding in paraffin for histological and immunohistological analyses, respectively.

2.2.1.9 Treatment schemes for 2D and 3D cell culture

SW480 cells in monoculture (MC) as well as in co-culture (CC) with fibroblasts were treated in static and dynamic 3D culture with 5-fluorouracil (5-FU). The 5-FU stock solution of 10 mM was diluted in culture medium to a final concentration of 25 µM. The static 3D tumour models were treated with 5-FU on day 7, 10, and 13. Dynamically cultured models were treated on day 7 and 11 with 25 µM 5-FU. The tissue was fixed in 4 % formalin on day 14 and embedded in paraffin for immunohistochemistry [2].

HROC24 cells and HROC87 cells were treated either with 1 µM vemurafenib (PLX4032, Zelboraf®) or 1 µM gefitinib (Iressa®) or with a combination of both inhibitors, and compared to the untreated control group regarding cell number, proliferation, apoptosis rate, marker expression and/or biochemical changes in the activation of protein kinases.

For 2D cell culture, cells were seeded on Petri dishes or well plates and cultured until they reached a confluency of 30–50 % before treatment start, usually 1–3 days after seeding. The cell culture medium supernatant was collected (t_0), frozen at -80°C and replaced by fresh medium with or without inhibitors (control). The following day, a sample of 100–300 µl supernatant was drawn for

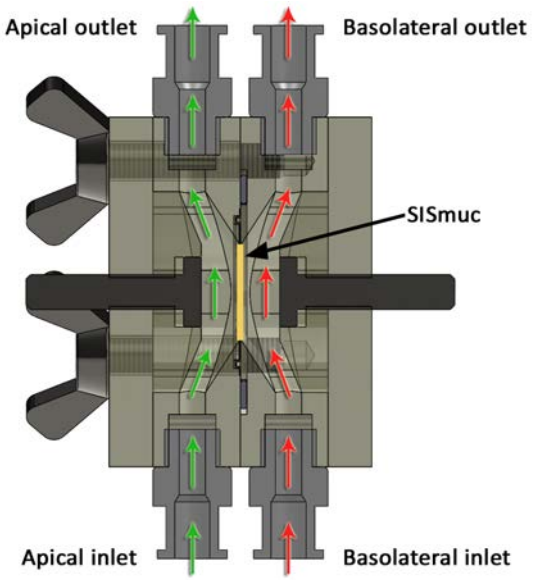

Figure 2.3: Sectional view of a compartment of the flow bioreactor. The culture medium flow direction is depicted by arrows, medium from the reservoir is pumped through the apical inlet leaving the flow bioreactor at the apical outlet. Thereafter, the culture medium flows through a loop (not shown) entering the basolateral inlet and leaving the reactor at the basolateral outlet which is connected to the culture medium reservoir. The SISmuc with cells (beige/yellow) is fixed between the two halves of the flow bioreactor. (Drawing by T. Schwarz)

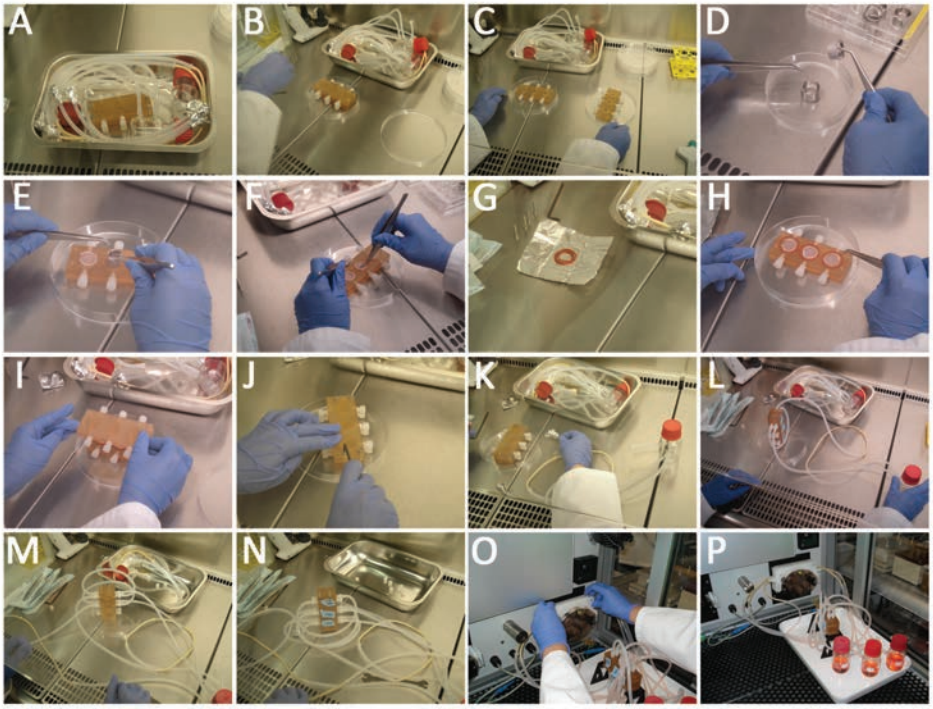

Figure 2.4: Assembling of the flow bioreactor. First, the autoclaved parts of the flow bioreactor were unpacked under a laminar flow safety cabinet (A). The flow bioreactor body was placed on a sterile Petri dish (B) and, after unscrewing, one of its halves was put aside (C). A "cell crown" was unfixed (D) and the inner smaller metal cylinder with the scaffold was put subsequently on the aperture of the flow chamber (E) in order to place carefully the scaffold (F). To ensure tightness, O-rings (G) where inserted between the two halves of the reactor body surrounding the scaffolds (H) followed by closing the bioreactor body (I) and screwing them tightly together (J). Afterwards, the circuit was assembled for each of the three chambers by screwing the Luer-lock adaptors (K, L, M and N). The cell culture medium reservoir bottles were filled with 40 ml of culture medium (not shown) and all parts were put onto a tray and placed into the bioreactor board. The pump tubings were fixed into the pump tubing cassettes and clamped to the peristaltic pump (O). A constant flow was set and the cells were cultured dynamically for 14 days (P).

Table 2.14: Treatment schedule for 2D (upper panel) and 3D (lower panel) culture. For 2D culture, first treatment ($\lightning_1$) was on day 1 or day 2 after cell seeding ($\odot$) depending on cell density, and repeated 48 h later ($\lightning_2$). In contrast, the beginning of the treatment for 3D culture ($\lightning_1$) took place on day 11 followed by the second treatment after 48 h on day 13 ($\lightning_2$). Medium change ($\circlearrowleft$) was performed every 2–3 days.

Day	0	1	2	3	4	5
Action	$\odot$	$\lightning_1$	...	$\lightning_2$	Stop	|
	$\odot$	...	$\lightning_1$	...	$\lightning_2$	Stop

Day	0	1	2	3	4	5	6	7	8	9	10	11	12	13	14
Action	$\odot$	...	...	$\circlearrowleft$	...	$\circlearrowleft$	...	$\circlearrowleft$	...	...	$\circlearrowleft$	$\lightning_1$	...	$\lightning_2$	Stop

determining apoptosis rate using M30-ELISA (see 2.2.4) at time point 24 h ($t_{24.1}$), frozen at -80°C and was replaced by the same amount of fresh medium with inhibitors. The second day after onset of medication, the complete supernatant was collected in order to determine apoptosis rate (t_{48}), frozen at -80°C and refilled with culture medium plus inhibitors; the cells were further incubated for another day encompassing in total 72 h ($t_{24.2}$) of treatment. For the calculation of the apoptosis rate at time point t_{72}, the measured values of t_{48} and $t_{24.2}$ were added (see figure 2.5).

For static 3D cell culture, cells were seeded on the SISmuc (see 2.1.8.2, 2.2.1.7 and 2.2.2.1) and cultured for 10 days before treatment started, with medium change every second day. As for the 2D culture, the treatment period lasted 72 h and supernatants were collected for each time point mentioned and stored at -80°C for the subsequent determination of the apoptosis rate. The treatment schedule for 2D as well as 3D culture is represented in table 2.14. An overview of the read-out parameters after treatment of 3D cell culture is given in figure 2.5 on page 55.

2.2.2 Preparation of biological materials

2.2.2.1 Porcine material: SISmuc

All animals received human care in compliance with the Guide for Care and Use of Laboratory Animals published by the National Institutes of Health (NIH publication No. 85-23, revised 1996) after approval by the institutional board

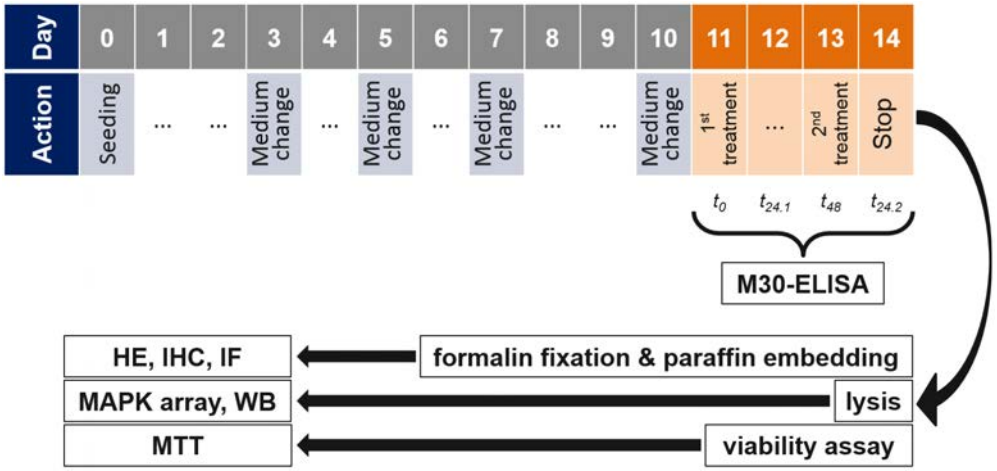

Figure 2.5: Overview of the treatment schedule for the 3D tumour model and the performed read-outs. On day 11, the cell culture supernatant was collected for the M30-ELISA prior to treatment. This value was used as a baseline for apoptosis (t_0). Twenty-four hours after the beginning of the treatment, another sample was drawn ($t_{24.1}$). The second treatment was applied on day 13 after collecting the supernatant of time point t_{48}. On day 14, sample $t_{24.2}$ was collected for determining the apoptosis rate before either fixing the tumour model with 4 % formalin prior to its embedding in paraffin for histological analyses, or lysing it for western blot analysis, or performing viability assays such as the MTT test. The value of measured cleaved cytokeratin 18 (M30) for time point t_{72} was calculated by adding t_{48} and $t_{24.2}$. (H&E: haematoxylin-eosin staining, IHC: immunohistochemistry, IF: immunofluorescence, WB: western blot)

of animal protection. Surgeries were performed at the Center for Experimental Molecular Medicine (ZEMM) Würzburg. The donor piglets (3 months old, 15–25 kg) were anaesthetised (trapanal, fentanyl), heparinised (1000 IE/kg) and sacrificed by an anaesthesia overdose (T61®) before explanting the jejunum with its supplying artery. After explantation, the ileum was stored in PBS^- 1 % (v/v) PenStrep at 4°C until decellularisation of the tissue.

After rinsing the lumen with PBS^- to remove all faeces, the blood vessels were perfused via the cannulated feeding artery with 500 ml PBS^- 1 % (v/v) PenStrep at 80 mmHg to remove remaining blood, followed by an incubation over night at 4°C in PBS^- 1 % (v/v) PenStrep on a rocking platform shaker.

Prior to decellularisation, the tissue was thoroughly rinsed with PBS^-, followed by perfusion of the cannulated artery with 500 ml PBS^- at 80 mmHg to remove all antibiotics. Subsequently, the lumen was filled with sodium deoxycholate solution (22.5 g/l) and perfusion at 80 mmHg was started until two litres were pumped through the blood vessels with changing the solution in the lumen after 500 ml had passed through the vessels, followed by washing with 2000 ml PBS^- at 100 mmHg with changing the PBS solution in the lumen after 500 ml had passed through the vessels. After the perfusion was finished, a sample for the determination of the remaining bile acid content was drawn and frozen at -20°C. The SISmuc was incubated over night at 4°C on a rocking platform shaker with fresh sodium deoxycholate solution.

On the following day, the SISmuc was perfused with 3000 ml PBS^- without antibiotics and the solution in the lumen was changed after 500 ml passed through the vessels. After separation of the mesentery with the vascular tree, the SISmuc was cut into pieces of 8 – 10 cm length and washed 3x with 300 ml PBS^- with 1 % (v/v) PenStrep, for 1–2 h each, prior to over night incubation at 4°C with DNase I (300 mg/ml with 1 % (v/v) PenStrep in PBS^+) on a rocking platform shaker.

For the determination of residual bile acid, a sample of the buffer solution was drawn and frozen at -20°C. To remove antibiotics, the SISmuc was washed again 3x with 300 ml PBS^-, for 30 min each, at 4°C before sterilisation by gamma ray treatment (25 kGy; BBF Sterilisationsservice GmbH, Rommelshausen). After sterilisation, a sample for the determination of residuary bile acid was drawn under sterile conditions, and frozen at -20°C, followed by a change of the PBS^- solution (without antibiotics). The SISmuc was stored at 4°C until use.

Quantitative determination of residual bile acid deriving from deoxycholic acid was performed by use of the total bile acids assay kit (Diazyme Europe GmbH, Dresden). It measures the contents of bile acids by enzyme cycling on basis of a redox reaction oxidising bile acids and reducing thio-NAD to thio-

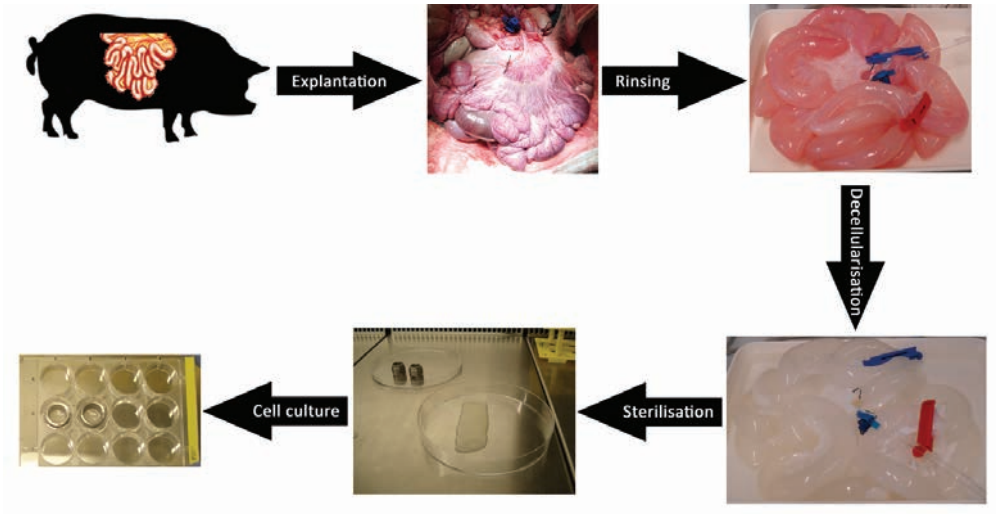

Figure 2.6: Preparation of the porcine collagen-based matrix SISmuc. After explantation, the lumen of the ileum was rinsed with PBS^- in order to remove faeces followed by perfusion of its cannulated supplying artery with PBS^- 1 % PenStrep to remove remaining blood. The following day, decellularisation was started by perfusion with deoxycholic acid solution and rinsing with PBS^-. After removal of the mesentery, the SISmuc was cut in´to pieces of 8 – 10 cm length and shipped for sterilisation by gamma ray treatment. Thereafter, the SISmuc was ready for use in cell culture.
(Graphics adapted from http://www.keyword-suggestions.com/aWxldW0gYW5hdG9teQ, last access: 08-08-2016)

NADH via the enzyme 3-α-hydroxysteroid dehydrogenase (3-α-HSD) thereby changing the absorbance at 405 nm. The samples deriving from the washing buffers were measured to ensure as far as possible the removal of deoxycholic acid in the scaffold. All assay procedures were conducted according to the manufacturer's instructions by a technician.

2.2.2.2 Human material

For the isolation of human primary fibroblasts, prepuces were stored in PBS^- 1 % (v/v) PenStrep for transport. Upon arrival, they were washed three times with PBS^+. After removal of fat and connective tissue, the prepuces were cut into pieces of 2–3 mm with a scalpel and washed again three times with PBS^+ prior to over night incubation with dispase II solution (2 U/ml, 5–10 ml for 6 cm^2) at 4°C in a Petri dish. From the transport medium, 3 ml were taken for sterile control and incubated at 37°C and 5 % CO_2 in a T25 cell culture flask.

After removing the epidermis using sterile tweezers on the following day, the dermis was washed with PBS^- and cut with a scalpel into pieces of 1–

2 mm width prior to an incubation for 45 min at 37°C with collagenase solution (500 U/ml, 10 ml). After centrifugation at 1200 rpm for 5 min, the remaining pellet was resuspended in 10 ml fibroblast culture medium followed by another centrifugation step at 1200 rpm for 5 min. The pellet was resuspended in 2 ml fibroblast culture medium with 1 % (v/v) PenStrep and transferred into a T75 cell culture flask allowing the dermis pieces to adhere.

The following day, 3–6 ml of fibroblast culture medium with 1 % PenStrep were added carefully without dermis pieces being detached from the bottom of the culture flask. After one week of culture, the antibiotics in the culture medium were omitted. Medium change was performed every 2 – 3 days. The fibroblasts growing out of the dermis tissue were allowed to reach a confluency about 80–90 % before splitting. The fibroblasts were used for experiments immediately or frozen and stored in a liquid nitrogen tank at -180°C. They were used no longer than passage 6.

2.2.2.3 Animals for xenografting experiments

All animal experiments with male NMRI Foxnu1nu mice were conducted by the lab of PD Dr. M. Linnebacher at the University Hospital Rostock. After injection of HROC87 cells into both flanks of 20 mice, the tumour cells were allowed to grow. The mice were grouped into five animals per experimental approach (control group, vemurafenib group, gefitinib group and combination therapy group) and kept for the treatment time of 21 days. Tumour volume was measured at day 0, day 3, day 8, day 10, day 17, and day 21 of treatment. Mice in the control group received an i.p. injection of 28 µl DMSO three times per week. Mice in the vemurafenib group received 417 mg/kg vemurafenib *ad libitum*. Gefitinib was administered by i.p. injection of 100 mg/kg three times per week. Mice of the combination therapy group received both drugs analogue to the mono-treatments.

On day 23 after onset of therapy, the animals were sacrificed and the tumours were resected. After documentation of the tumour weights, the tumours were divided and half was frozen at -80°C and half was fixed in 4 % formalin. Further (immuno-)histochemical and western blot analyses of the xenograft tumours were performed at the Chair of Tissue Engineering & Regenerative Medicine of the University Hospital Würzburg.

2.2.3 Cell viability assays: MTT and CellTiter-Glo®

3-(4,5-Dimethylthiazol-2-yl)-2,5-diphenyltetrazolium bromide (MTT) is a tetrazolium salt that changes its color from yellow to purple when being meta-

bolically reduced to formazan by NADH/NADPH-dependent enzymes of the endoplasmic reticulum and to a lesser extent by the enzyme succinate dehydrogenase of the mitochondrial complex II [120, 121]. Hence this reaction is dependent on metabolic active cells, the MTT assay is suitable for the qualitative and quantitative assessment of the cells' viability to compare different treatments with a control sample. The formed water-insoluble formazan is retained as crystals within the cells' cytoplasm and is therefore cell invasive. These insoluble formazan crystals could be dissolved and extracted with isopropanol which can be used for quantitation by photometric absorptiometry [120].

The MTT assay was performed after having finished the treatment of the cells with inhibitors (see table 2.14), for 2D culture in 12-well or 24-well plates and for 3D culture in 12-well plates. First, the MTT stock solution (3 mg/ml) was diluted 1:3 with cell-specific culture medium yielding 1 mg/ml MTT working solution. After aspirating the cell culture supernatant, 1 ml of the MTT working solution was pipetted into each well of the 12-well or 24-well plates, respectively, for 2D culture and for 3D cell culture, 1.5 ml of MTT working solution was pipetted outside and 1 ml was pipetted inside the "cell crown". The cells were then incubated for 4 hours at 37°C and 5 % CO_2. Subsequently, the solution was aspirated and for 3D culture, the "cell crown" was rinsed carefully with PBS^+ to avoid cells being washed away; for 2D culture, only the MTT working solution was removed without any washing step. Afterwards, the extraction of the formazan crystals within the cells was conducted using isopropanol 0.04 N HCl. For 3D culture, the SISmuc was unfixed from the "cell crown" and transferred into a 6-well plate and incubated with 2 ml of extraction solution for 1 hour at RT or over night at 4°C, respectively, on an orbital platform shaker after sealing the well plate with Parafilm M® in order to prevent evaporation of the organic solvent isopropanol. For 2D culture, 1 ml of extraction solution was pipetted into each well and incubated as for the extraction of 3D culture samples. Afterwards, the solution was collected in a 15 ml centrifugation tube and re-extraction with another 2 ml of extraction solution (for 2D culture 1 ml) was performed for 30 min on an orbital platform shaker at RT. The extraction process was repeated as far as necessary with 1 ml of isopropanol 0.04 N HCl (for 2D culture 500 µl) until the scaffold or the cells, respectively, were completely white in colour. The extracts of the same sample were pooled and after mixing well 200 µl were pipetted into a 96-well cell culture plate (in triplicates). For the blank value, 200 µl of isopropanol 0.04 N HCl were applied and the absorbance was measured at 570 nm with subsequent subtraction of the measured aborbance at reference wavelength at 630 nm using a microplate reader. The relative viability could be calculated as

the rate of the absorbance of tested inhibitors and the untreated control sample.

The CellTiter-Glo® luminescent cell viability assay (Promega) is based on the quantitation of ATP present in viable cells. This assay is determined for the use in conventional 2D culture. Here, 96-well plates were used and cells were seeded in triplicates and treated with inhibitors as mentioned in table 2.14. After 72 hours of treatment, the lyophilisate and supplied buffer of the assay were mixed and applied onto the cells according to the manufacturer's instructions. The resulting luminescence was measured after 10 min in a microplate reader. The viability could be calculated as the rate of relative luminescence units of tested inhibitors and the untreated control sample.

2.2.4 Enzyme-linked immunosorbent assay (ELISA): Measurement of apoptosis in epithelial cells using M30

Apoptosis, a process of the programmed cell death, can be initiated by an intrinsic (e.g. cell stress) as well as by an extrinsic (e.g. triggering cell death receptors) pathway, both inducing proteases (caspases) to degrade cellular proteins and to cleave DNA. Usually, the intrinsic pathway is defective in cancer cells leading to their uncontrolled proliferation and hereby to tumour growth. Chemotherapeutics such as the cytotoxic drug cisplatin interfere with the cells' DNA repair mechanisms and by this can trigger apoptosis via the intrinsic pathway. Enzyme inhibitors, also known as small molecules, such as gefitinib (Iressa®) or vemurafenib (Zelboraf®) block the EGFR or BRAF/MEK/ERK pathway, respectively, inducing apoptosis. For this reason, an evaluation of the apoptosis rate can be used for determining the effectiveness of different treatments.

Cytokeratin 18 (K18) is an intermediate filament protein expressed in epithelial cells and is cleaved by caspase-9 in early apoptosis as well as by caspase-3 and caspase-7 during the execution phase [122]. The M30 CytoDeath™ ELISA (Peviva) quantitatively measures apoptosis in epithelial cells which express K18. The mouse monoclonal IgG2b antibody M30 recognises the neo-epitope K18Asp396 which is exposed after caspase cleavage [123]. The caspase-cleaved K18 (ccK18) is formed after induction of apoptosis and released into the extracellular compartment due to secondary necrosis of apoptotic bodies, it can be measured in the cell culture supernatant. As a solid-phase sandwich enzyme immunoassay, ccK18 is captured by the pre-coated antibody M6. Measurement of ccK18 only is ensured by horseradish peroxide (HRP)-conjugated M30 binding to Asp396 and reacting with the chromogenic substrate 3,3',5,5'-tetramethylbenzidine (TMB) resulting in formation of diimines and a colour

change. The resulting colour intensity is directly proportional to the ccK18 concentration and can be measured by absorptiometry.

The M30-ELISA was performed according to the manufacturer's instructions using cell culture supernatants of cells being cultured under 2D and 3D conditions (see tab. 2.14 on p. 54 and fig. 2.5 on p. 55). Supernatants were collected over the time of interest and were frozen at -80°C. 25 µl of supernatant, diluted with cell culture medium as required, and the provided standard solutions were applied per well in duplicates to the ELISA microplate. 75 µl of M30-HRP conjugate were added to each well and the plate was covered with a special foil prior to incubation on an orbital platform shaker at RT for 4 h. The plate was washed five times using 200 µl washing buffer per well and 200 µl TMB was pipetted into each well followed by 20 min incubation in the dark. The reaction was stopped with 50 µl 1 M sulphuric acid and after mixing, the absorbance was measured immediately at 450 nm. For calculation, the measured absorbance of the standards was used to define a sigmoidal standard curve as fitting algorithm and the ccK18 concentration of the samples was determined in units per litre (U/l). For 2D culture, apoptosis rate was calculated as the quotient of ccK18 concentration of a treated sample to the untreated control. For 3D culture, the measured ccK18 concentration for each sample was divided by its corresponding ccK18 concentration directly before start of the treatment start in order to normalise all measured values to the basal apoptosis rate in each single cell crown. Subsequently, the relative increase of apoptosis could be calculated as the rate of treated samples and the untreated control.

2.2.5 Histology

2.2.5.1 Fixation of cells on chamber slides/cover slips (2D) and on SISmuc (3D)

In order to use cells or tissues for histological as well as immunohistological analyses they have to be fixed with a fixative to preserve their morphology and to prevent potential autolysis reactions. For this purpose, a 4 % formaldehyde solution is commonly used. Hereby, primary amino groups in proteins become cross-linked. Shorter fixation times ensure a reversible reaction of cross-linking while longer fixation times promote an irreversible cross-linking. Especially for immunohistological analyses, the reversible fixation process is of importance due to the possible de-masking of antigen epitopes of interest recognised by antibodies which might not detect their cross-linked target because of structural changes.

Prior to fixation, cells on chamber slides or cover slips and SISmuc were washed with PBS^- after aspirating the cell culture medium in order to remove all cell debris. Chamber slides and cover slips were fixed for 10 min with 4 % formalin at RT, cells on SISmuc were incubated for 2 h in 4 % formalin at RT to assure proper fixation of the tissue. Afterwards, the fixative was removed and cells on chamber slides or cover slips were washed with PBS^- and either used directly for staining or stored in PBS^- at 4°C for up to 4 weeks until staining. The fixed SISmuc was prepared for embedding in paraffin (section 2.2.5.2) before performing histological and immunohistological staining.

2.2.5.2 Paraffin embedding and microtome sectioning

Fixed SISmuc samples were removed from the "cell crowns" and spread onto embedding filter papers after cutting off excess matrix that was not seeded with cells. Each folded filter paper with SISmuc inside was then inserted into an embedding cassette and stored in deionised water until starting the spin tissue processor (Thermo Fisher Scientific) which performed automatised paraffin infiltration over night. The paraffin embedding procedure is summarised in table 2.15.

Subsequently, the embedding cassettes were pre-incubated in the paraffin bath of the heated paraffin embedding module (Leica) for approximately 30 min prior to cutting the scaffold into 2–3 single stripes. These pieces of a SISmuc sample were blocked within a stainless steel casting mould with the cutting edges facing downwards and all pieces arranged in parallel next to each other.

With a sliding microtome, tissue sections were cut with a thickness of 3 µm and mounted onto a microscope glass slide for transferring it to a tissue float

bath (50°C) in order to flatten the section. After re-mounting the tissue sections, the microscope glass slides were put into a tissue drying oven at 37°C over night. Afterwards, they were either directly deparaffinised or stored up to one month before use for histological or immunohistological analyses. Uncoated microscope glass slides were used for H&E staining and alcian blue-PAS stain (see 2.2.5.4 and 2.2.5.5), polylysine-coated object slides were used for immunohistochemical staining (see 2.2.5.6).

Table 2.15: Program of the spin tissue processor for paraffin embedding over night.

Step	**Solution**	**Time [min]**
Washing out fixative	Deionised water	60
Ascending alcohol series for dehydration	Ethanol 50 %	60
	Ethanol 70 %	60
	Ethanol 80 %	60
	Ethanol 96 %	60
	Isopropanol I	60
	Isopropanol II	60
Removing alcohol from tissue	Isopropanol/Xylene (1:2)	60
	Xylene I	60
	Xylene II	60
Infiltrating tissue with paraffin	Paraffin I	90
	Paraffin II	90

2.2.5.3 Deparaffinisation of tissue sections on microscope glass slides

The paraffin embedded tissue sections had to be deparaffinised and rehydrated before performing histological or immunohistological staining. Prior to deparaffinisation, the microscope glass slides with tissue sections were incubated at 60°C for 30–60 min in a tissue drying oven in order to melt the paraffin. Subsequently, the microscope glass slides were put in xylene to dissolve the paraffin followed by a descenting alcohol series for rehydration. After rehydrating, the tissue must not run dry. The deparaffinisation was performed according to table 2.16.

Table 2.16: Deparaffinisation procedure for tissue sections on microscope glass slides. After rehydration, the sections must not run dry and has to be kept in water or washing buffer.

Step	**Solution**	**Time [min]/Action**
Melting paraffin at 60°C		30–60
Deparaffinisation of the tissue sections	Xylene I	10
	Xylene II	10
Descending alcohol series for rehydration	Ethanol 96 % I	Slewing up and down 3–5x
	Ethanol 96 % II	Slewing up and down 3–5x
	Ethanol 70 %	Slewing up and down 3–5x
	Ethanol 50 %	Slewing up and down 3–5x
	Deionised water	Slewing until disturbances clear

2.2.5.4 Haematoxylin-Eosin (H&E) staining

The haematoxylin and eosin (H&E) staining is the most widely used stain for histological sections of biopsies such as tumours in medical diagnosis. Haematoxylin is a compound extracted from the logwood tree *Haematoxylum campechianum* and is used for the formulation of hemalum: its oxidation product hematein forms a complex with aluminium ions. Hemalum stains basophilic structures of the cell in blue (e.g. the nuclei) whereas eosin Y colours acidophilic cellular structures and the extracellular matrix in red (e.g. cytoplasmic proteins and collagen fibres). Therefore, the H&E staining serves as an overview staining.

After deparaffinisation (see tab. 2.16), the microscope glass slides with the tissue sections were incubated in hemalum and rinsed in deionised water until no colour has been washed out any more. If the staining with hemalum was too dark it had to be differentiated with a solution of hydrochloric acid and ethanol. After rinsing in deionised water, the tissue sections were blued with tap water providing cations (Mg^{2+} and Ca^{2+}) which are responsible for the blueing reaction. Subsequently, the glass slides were incubated shortly in eosin followed by rinsing in deionised water. The tissue sections were then either dehydrated by an ascending alcohol series with successive mounting of the microscope glass slide using the mounting media Entellan® or they were air-dried and dipped into xylene before mounting with Entellan® and a cover slip. The mounted object slides were dried under a fume hood over night prior to microscopy. The H&E staining procedure is described in detail in table 2.17.

Table 2.17: H&E staining protocol following dehydration for mounting the microscope glass slides with the organic mounting medium Entellan®. (dd H_2O: distilled deionised water)

Step	**Solution**	**Time [min]/Action**
Staining basophilic structures	Hemalum	6–8
	dd H_2O	Until solution is clear
Differentiating hemalum (optional)	HCl-Ethanol	Dipping 3–5x
	dd H_2O	Dipping 3–5x
Blueing of hemalum	Tap water	5
Staining acidophilic structures	Eosin	1
	dd H_2O	Until solution is clear
Ascending alcohol series for dehydration	Ethanol 70 %	Dipping 3–5x
	Ethanol 96 %	2
	Isopropanol I	5
	Isopropanol II	5
	Xylene I	5
	Xylene II	5
Mounting with cover slip	Entellan®	

2.2.5.5 Alcian blue-periodic acid-Schiff stain (Alcian-PAS stain)

Alcian blue is a water soluble strong alkaline dye which is able to react with acidic mucopolysaccharids, e.g. sulphated mucins and hyaluronic acid. These mucopolysaccharids appear in mucus producing goblet cells within the epithelium of the gastrointestinal tract. The combination of alcian blue stain with periodic acid-Schiff (PAS) staining allows to additionally detect polysaccharides (glycogen) and neutral mucosubstances (glycoproteins, glycolipids and proteoglycans) which are usually found in connective tissues and basal laminae. Periodic acid oxidises the glycol moieties from polysaccharides to aldehydes reacting with Schiff's reagent which leads to a purple-magenta colour. Mucosubstances are not only present in healthy tissue but also in adenocarcinomas which often secrete neutral mucins.

Before conducting the alcian-PAS stain, the tissue sections on the microscope glass slides had to be deparaffinised (see 2.2.5.3). The tissue sections were first incubated for 10 min in 1 % alcian blue solution followed by rinsing in tap water. Subsequently, the PAS stain was performed. Cell nuclei were counter-stained with hemalum and, after dehydration of the samples, the glass slides were mounted with Entellan® and a cover slip. Mounted object slides were dried under a fume hood over night before microscopy. The alcian-PAS staining procedure is summarised in table 2.18.

2.2.5.6 Immunohistochemistry (IHC): Immunoperoxidase staining with DAB and Immunofluorescence

A specific antigen is recognised and labelled by antibodies in IHC. The fragment antigen-binding (Fab) domain of a primary antibody binds to its target structure on the antigen exposing the antibody's fragment crystallisable (Fc) region. The labelling can be performed with the aid of secondary antibodies which are either conjugated to enzymes such as horseradish peroxidase (HRP) processing chromogenic substrates or they are linked to a fluorochrome like fluorescein isothiocyanate (FITC) and can be detected by excitation with a certain wavelength. The secondary antibodies bind with their Fab domain to the primary antibody's Fc region enabling the identification of the antigen and its location in the cell or tissue.

Table 2.18: Alcian-PAS staining protocol. Alcian blue stains acidic mucopolysaccharids in blue and PAS stains neutral mucosubstances in purple-magenta.

Step	**Solution**	**Time [min]/ Action**
Staining acidic mucopolysaccharids	Alcian blue 1 %	10
	Tap water	3
	Deionised water	Dipping 3–5x
Staining neutral mucosubstances	Periodic acid 0.5 %	10
	Tap water	3
	Deionised water	Dipping 3–5x
	Schiff's reagent	30
	Tap water	10
	Deionised water	Dipping 3–5x
Counterstain of nuclei	Hemalum	2
	Tap water	5
	Deionised water	Dipping 3–5x
Ascending alcohol series for dehydration	Ethanol 70 %	Dipping 3–5x
	Ethanol 96 %	2
	Isopropanol I	5
	Isopropanol II	5
	Xylene I	5
	Xylene II	5
Mounting with cover slip	Entellan®	

Immunoperoxidase staining with DAB

In the immunoperoxidase staining, the enzyme HRP processes the substrate 3,3'-diaminobenzidine (DAB) resulting in the deposition of a brown colouring which can be analysed by light microscopy. The used kit DCS Super Vision 2 HRP contained secondary antibodies linked to a HRP-conjugated micropolymer for signal enhancement and could detect mouse as well as rabbit primary antibodies.

IHC staining with DAB was performed on tissue sections as well as on chamber slides or cover slips. For staining intracellular antigens, cells on chamber slides or cover slips had to be permeabilised for 5 min using a solution of 0.2 % Triton™ X-100 in PBS^{-} prior to incubation with the primary antibody in order to make the antigens accessible; for antigens inside the plasma membrane (transmembrane proteins), the permeabilisation step could be skipped. Tissue sections had to be deparaffinised and rehydrated (see section 2.2.5.3) before transferring into deionised water. During fixation of SISmuc samples, the proteins of the tissue were cross-linked and therefore, epitopes of the antigens had to be retrieved either enzymatically or by heat-induction to assure the recognition of the primary antibody's target antigen. For the heat-induced antigen retrieval, tissue sections were heated (∼100°C) for 20 min either in citrate buffer (pH 6.0) or in Tris-EDTA buffer (pH 9.0) depending on the primary antibody used. For the successive administration of small volumes of antibodies and solutions (50–100 µl) in each of the following steps, tissue sections were then encircled with a grease pencil. Incubation with antibodies and solutions were performed at RT in a humidity chamber to prevent drying-out. Endogenous peroxidases which are able to process DAB resulting in false-positive stain were blocked with 3 % hydrogen peroxide. Washing steps were carried out in glass cuvettes on a rocking platform shaker. For negative controls, antibody diluent was applied instead of diluted primary antibodies. For isotype controls, antibodies of the same species and isotype according to the primary antibody were used and applied with the same concentration as the respective primary antibody (see table 2.10). After DAB stain, cell nuclei were counterstained with hemalum and prepared for mounting with Entellan® by performing the ascending alcohol series for dehydration. The immunoperoxidase staining procedure with DAB is summarised in table 2.19.

Table 2.19: Immunoperoxidase staining protocol using the chromogenic substrate DAB.

Step	**Solution**	**Time [min]**
Blocking endogenous peroxidases	3 % H_2O_2	10
Washing	PBS-T	5
Incubation with primary antibody	Diluted primary antibodies	60
Washing (3x)	PBS-T	5
Incubation with secondary antibody (Amplifying I)	DCS enhancer solution	10
Washing (3x)	PBS-T	5
Incubation with polymer (Amplifying II)	DCS polymer solution	20
Washing (3x)	PBS-T	5
Detection with DAB	DAB solution	3–5
Washing	PBS-T	Dipping 3–5x
Counterstain of cell nuclei	Hemalum	0.5–1
Blueing	Tap water	1–1.5
Stop of blueing	Deionised water	
Ascending alcohol series for dehydration	Ethanol 70 %	Dipping 3–5x
	Ethanol 96 %	2
	Isopropanol I	5
	Isopropanol II	5
	Xylene I	5
	Xylene II	5
Mounting with cover slip	Entellan®	

Immunfluorescence (IF): Immunostaining with fluorochrome

Immunofluorescence staining technique uses either a direct detection of the antigen of interest by primary antibodies labelled with a fluorochrome or indirectly by secondary antibodies, labelled with a fluorochrome, detecting the primary antibody. In this work, the indirect detection method was used and secondary antibodies labelled with the dyes Alexa Fluor® 555 or Alexa Fluor® 647 were applied. By using primary antibodies of different species, co-localisation of different antigens within the same sample could be achieved if the secondary antibodies were conjugated to different fluorochromes. A fluorochrome can be excited by light of a distinct wavelength causing the electrons to shift to a higher energy level. The fall-back of the electrons to their base level causes an emission of light of longer wavelength.

IF staining was performed on tissue sections as well as on cells grown on chamber slides or cover slips. Tissue sections had to be deparaffinised as described in section 2.2.5.3 and heat-induced antigen retrieval was performed as mentioned in the paragraph "immunoperoxidase staining with DAB". Cells grown on chamber slides or cover slips had to be permeabilised with 0.2 % Triton® X-100 prior to blocking with donkey serum and incubation with primary antibodies. After antigen retrieval, tissue sections were encircled with a grease pencil and 2D as well as 3D samples were incubated for 20 min with 5 % donkey serum in order to reduce background staining by blocking unspecific binding sites for the secondary antibody. Primary antibodies were diluted 1:100 (if not otherwise indicated, see tab. 2.10) with antibody diluent and incubated in a humidity chamber at 4°C over night. For IF staining of cells grown on cover slips, primary antibodies were diluted 1:200 and 200 µl of this solution were applied to each sample in a 24-well plate which was incubated at 4°C over night on a rocking platform shaker. Secondary antibodies were diluted 1:400 in antibody diluent and incubated in a humidity chamber for 60 min at room temperature. For double stainings, the primary as well as the secondary antibodies were combined in one single tube and applied to the sample. Washing steps were performed on a rocking platform shaker at room temperature, either in glass cuvettes for tissue sections or directly in a 24-well plate for cover slips. For negative control, antibody diluent without any antibodies was applied. After staining, samples were mounted with Mowiol® 4-88 0.1 % DAPI for counterstaining of the cell nuclei. The protocol for immunofluorescence staining is described in table 2.20.

Table 2.20: Immunofluorescence staining protocol using the indirect detection with secondary antibodies conjugated to fluorochromes.

Step	Solution	Time [min]
Blocking to reduce background	5 % Donkey serum	20
Incubation with primary antibody	Diluted primary antibody	over night (4°C)
Washing (3x)	PBS-T	5
Incubation with secondary antibody	Secondary antibody (1:400)	60
Washing (3x)	PBS-T	5
Mounting with cover slip	Mowiol 4-88® 0.1 % DAPI	

2.2.5.7 Proliferation rate: Ki-67 index

The proliferation rate was assessed by immunofluorescence staining against the marker Ki-67. This protein is expressed during all active phases of the cell cycle (late G_1, S, G_2 and mitosis) but absent in quiescent cells (G_0) [124].

After the staining procedure as mentioned in 2.2.5.6, six high-power fields (HPF) with a 20x magnification of the microscopy samples were recorded digitally and the total cell number was evaluated by counting manually all cell nuclei with the programme ImageJ. Subsequently, the Ki-67 positive cells were counted and the proportion was calculated as the percentage of positive cells to the total cell number.

2.2.6 Biochemistry

2.2.6.1 Cell lysis

For protein analysis using western blot (protein immunoblot), proteins have to be extracted from the cells. Depending on the protein's location within the cell (e.g. nucleus, cytoplasm or cell membrane), the appropriate lysis buffer has to be chosen for this purpose. In this work, a modified radioimmunoprecipitation assay (RIPA) buffer was used in order to extract not only nuclear proteins but also cytoplasmic and cell membrane proteins.

For the analysis of conventional 2D cell culture, cells were cultured in 6 cm Petri dishes (see 2.2.1.6). After 72 h of treatment, cells were gently washed twice with ice-cold PBS^- to remove remaining cell culture medium and serum. Still on ice, 800 µl of modified RIPA were pipetted into each sample and incubated

subsequently for 30 min on an orbital platform shaker at 4°C. After scraping the Petri dish with a cell scraper, the lysate was collected and centrifuged for 10 min at 10,000 g and 4°C. Afterwards, the supernatant was transferred to a new 1.5 ml reaction tube and either used directly for the determination of the total protein concentration or frozen at -80°C for further use.

After treatment, cells grown on SISmuc (see 2.2.1.7) were washed twice with ice-cold PBS^{-} before detaching the scaffolds from the "cell crowns" and transferring them to 6-well plates on ice. 800 µl of lysis buffer were added to each sample following an incubation for 30 min at 4°C on an orbital platform shaker. Subsequently, the SISmuc was scratched gently with a cell scraper to remove remaining cells within the scaffold. After centrifugation for 10 min at 10000 g and 4°C, the supernatant was transferred into a new 1.5 ml reaction tube and either used directly for determination of total protein concentration or frozen at -80°C for further use.

2.2.6.2 Determination of total protein concentration

In order to reach the same protein concentation in each sample of western blot analysis, the protein concentration of each cell lysate has to be determined. Here, the Lowry-based DC Protein Assay kit (Bio-Rad) was used for the colorimetric protein measurement [125]. Based on the reaction of proteins with an alkaline copper solution, the subsequent reduction of folin reagent leads to its colour change which can be measured by photometry. The colour intensity is proportional to the amount of solved proteins.

For calibration, standard samples were prepared using a 2 mg/ml standard solution of bovine serum albumin (BSA) which was diluted with ultrapure water (0–2000 µg/ml). 5 µl of all standard samples and cell lysates were pipetted in duplicates into a 96-well plate. Additionally, one aliquot of each cell lysate sample was diluted with ultrapure water (1:2–1:5) and included to the measurement in order to stay in the standard range of 0–2000 µg/ml. Ultrapure water served as a blank.

Each time, the alkaline copper solution was freshly prepared by mixing reagents A (copper solution) and S (surfactant) at the ratio of 50:1. 25 µl of the alkaline copper solution were added to each well followed by 200 µl/well of reagent B (folin). After incubation for 15 min in the dark at room temperature, the samples were measured by photometry at 750 nm. With the standard samples, a standard curve was generated and the protein concentrations of the lysates could be calculated.

As in 3D cell cultures, the concentration of proteins deriving from the scaffold was high, an unseeded SISmuc was included as a blank. The protein concentra-

tion was subtracted from the samples to ensure that same amounts of cellular proteins as in 2D cell culture were applied for western blot analysis.

2.2.6.3 Human Phospho-RTK Array Kit & Human Phospho-Kinase Array Kit

To identify kinases affected by treatment in the signal transduction pathway, the ProteomeProfiler™ Human Phospho-Kinase Array and Human Phospho-RTK Array Kit by R&D were used for screening. The phospho-kinase array contained 43 different antibodies against phosphorylated kinases. The RTK array consisted of a membrane spotted with 49 different antibodies against phosphorylated receptor tyrosine kinases (RTKs).

Phospho-kinase array: All reagents and samples were prepared for use according to the manufacturer's instructions. Cells were lysed by using the kit's lysis buffer 6 (800 µl, as mentioned in section 2.2.6.1) after rinsing the cells with PBS^-. After determination of the total protein concentration (see 2.2.6.2), 200–600 µg of total protein were adjusted with lysis buffer to a maximum volume of 334 µl lysate per array set (membranes A and B), followed by an incubation over night at 4°C on a rocking platform shaker. After three washing steps, the membranes were incubated with biotinylated detection antibodies for 2 h at RT on a rocking platform shaker, and after washing, incubation with diluted streptavidin-HRP for 30 min at room temperature was performed before visualisation by using a chemoluminescence substrate. Pictures were made by using the imaging station FluorChem Q.

RTK array: All reagents and samples were prepared for use according to the manufacturer's instructions. Cells were lysed by using the kit's lysis buffer 17 (800 µl, see 2.2.6.1) after rinsing the cells with PBS^-. 100–300 µg of total protein were adjusted with array buffer 1 to a maximum volume of 1.5 ml after determining the total protein concentration (see 2.2.6.2). Membranes were incubated with the diluted lysates over night at 4°C on a rocking platform shaker and washed three times the following day. Subsequently, incubation for 2 h with anti-phospho-tyrosine-HRP antibodies was performed on a rocking platform shaker at room temperature. Phospho-RTKs were detected by chemoluminescence and recorded with the imaging station FluorChem Q.

2.2.6.4 Chloroform-methanol precipitation

Chloroform-methanol precipitation according to Wessel & Flügge [126] was performed in order to enrich the low contents of phospho-proteins, which cannot be detected if their amount is below the detection range within the total protein

amount. Further, proteins were purified by removal of lysis buffer salts which improved their separation during gel electrophoresis.

After determination of total protein concentration (see 2.2.6.2), 100 µg of total protein was adjusted with ultrapure water to a maximum volume of 100 µl. Subsequently, 400 µl methanol were added and the lysate was mixed briefly. After adding 100 µl chloroform and 300 µl ultrapure water, the solution split into an organic (chloroform) and aqueous (methanol/water) phase. The samples were mixed and centrifuged for 10 min at 14000 rpm. The aqueous phase was carefully discarded without losing the proteins which concentrated on the formed interphase. 800 µl methanol were added followed by mixing and centrifugation for 10 min at 14000 rpm. The supernatant was discarded and the protein pellet was dried in an incubator at 37°C for 15–30 min. Afterwards, the pellet was dissolved in 15 µl ultrapure water and 5 µl Laemmli buffer, and heated for 5 min at 95°C for denaturing proteins. Samples were either used directly for SDS-PAGE and western blot (see 2.2.6.5) or stored at -20°C until use.

2.2.6.5 Western blot

Western blot is used for the detection of specific proteins of interest allowing their semi-quantitative analysis. By comparison of samples treated with an inhibitor to an untreated control, activation and/or suppression of distinct proteins in the signalling transduction pathway (e.g. EGFR, Met, Akt and Erk1/2) can be observed. For this, the proteins in a cell or tissue lysate have to be separated by size using gel electrophoresis. In this work, sodium dodecyl sulphate polyacrylamide gel electrophoresis (SDS-PAGE) was used to separate proteins. The detergent SDS denatures, unfolds and linearises the proteins. Further, SDS imparts the proteins a negative charge allowing their migration in the applied electrical field towards the (positive) anode. Small proteins migrate faster in the polyacrylamide gel than proteins of greater size with the result that proteins are spread in their length or size, respectively. The migration speed is dependent on the gel's content of polyacrylamide and the applied electric current. Here, a 10 % separation gel was used and electrophoresis was performed with 25 mA per gel for approximately 1 h. Prior to loading, samples were prepared by chloroform-methanol precipitation for enrichment of the protein content in the lysates and for purification (see 2.2.6.4). 5 µl of protein ladder and 18 µl of sample (90 µg) with an equal amount of total protein were loaded into the lanes of the stacking gel. Table 2.21 lists the components of the stacking and separation gel. Gels were always prepared freshly each time.

In order to detect the proteins of interest, they have to be immobilised and accessible for antibodies. Therefore, the proteins within the gel were transferred by semi-dry electroblotting onto a membrane made of nitrocellulose or polyvinylidene difluoride (PVDF). A stack of three Whatman papers, the blotting membrane, the gel and three Whatman papers was made after pre-soaking in transfer buffer and put in the blotting chamber. The western blot was performed for 2 h with 1 mA/cm^2 and voltage was limited to 11 V. After the transfer, the membrane was incubated in 5 % milk TBS-T for 1 h at room temperature in order to block unspecific binding sites on the membrane. Subsequently, the membrane was cut into stripes according to the protein sizes that should be detected and the stripes were incubated with the primary antibodies over night at 4°C in 50 ml centrifuge tubes on a rolling platform shaker. On the following day, the membrane stripes were washed three times with TBS-T for 5–10 min each followed by incubation with the HRP-conjugated secondary antibody for 1 h at room temperature. After successive washing with TBS-T for 10 min (3x each), the membrane stripes were incubated for 1 min with developing solution and analysed with the imaging station FluorChem Q. The membrane stripes with the size of the loading control α-tubulin were stripped and re-probed with the respective antibody over night at 4°C.

Stripping was performed by washing the membranes twice for 10 min with mild stripping buffer, twice for 10 min with PBS^- and twice for 5 min with TBS-T. Afterwards, the membranes were re-blocked in 5 % mild TBS-T for 30 min on a rocking platform shaker at RT and subsequently incubated over night with the antibody for the loading control. Next day, the membranes were washed, incubated with the secondary antibody and analysed as described before.

Table 2.21: Composition of the stacking and separation gel for SDS-PAGE. Indications for one gel.

Solution/ Chemical	**Stacking gel (5 %)**	**Separation gel (10 %)**
Upper Tris	1.25 ml	—
Lower Tris	—	2.5 ml
Acrylamide/Bisacrylamide (37.5:1)	0.5 ml	3.3 ml
Ultrapure water	3.2 ml	2.2 ml
Glycerol	—	2.0 ml
TEMED	12 µl	14 µl
APS 40 %	12 µl	14 µl

3 Results

3.1 Characterisation of the SISmuc: H&E staining and alcian blue-PAS stain

H&E staining and alcian blue-periodic acid Schiff (alcian-PAS) stain were performed for the characterisation of the unseeded scaffold.

Haematoxylin stains cell nuclei in purple and eosin dyes the extracellular matrix as well as cytoplasmic proteins in pink. After the decellularisation process (see 2.2.2.1), all porcine cells were removed and only the extracellular matrix is remaining. The preserved morphology of the mucosa's structures (crypts and villi) for two different batches of SISmuc is shown in figure 3.1. Natural batch-to-batch variations in the thickness of the SISmuc can be observed, SISmuc 21/22 (fig. 3.1 A/C) shows a thicker sub-mucosal layer compared to SISmuc 47/48 (fig. 3.1 B/D).

Alcian blue stains acidic mucopolysaccharides (e.g. mucus producing goblet cells) in blue while PAS reacts with neutral mucosubstances, such as found in connective tissue and basal laminae, colouring them in pink. Figure 3.2 shows an alcian-PAS stain in four magnifications (4x, 10x, 20x and 40x) of two different batches of SISmuc without cells. The batch-to-batch variation in the scaffold's thickness can be noticed in figure 3.2 C/D and E/F, while the occurrence of pink stain shows preserved connective tissue and basal laminae lining all former crypt and villi structures (fig. 3.2 E/F/G/H, black arrowheads). Especially at the transition from the mucosa to the sub-mucosa, the strong pink colouring indicates stacked basal laminae which derive from the former *lamina muscularis mucosae*. Former vessels within the sub-mucosa present clearly stacked basal laminae (fig. 3.2 E/G, white arrowheads).

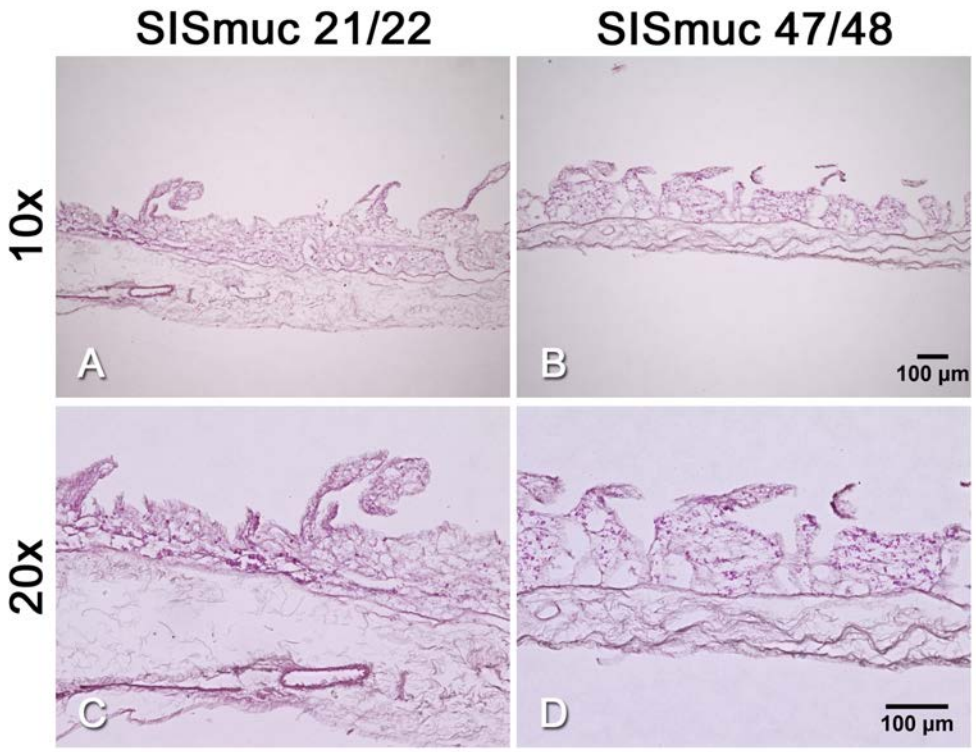

Figure 3.1: H&E staining of two different batches of SISmuc without cells. The extracellular matrix is stained in pink (eosin) and cell nuclei are stained in blue (haematoxylin). No cells can be found after decellularisation, neither in the mucosa nor in the sub-mucosa. The former structures of the mucosa (villi and crypts) were preserved during the decellularisation process. The scale bar for the 10x (A/B) and 20x (C/D) magnifications measure 100 µm each.

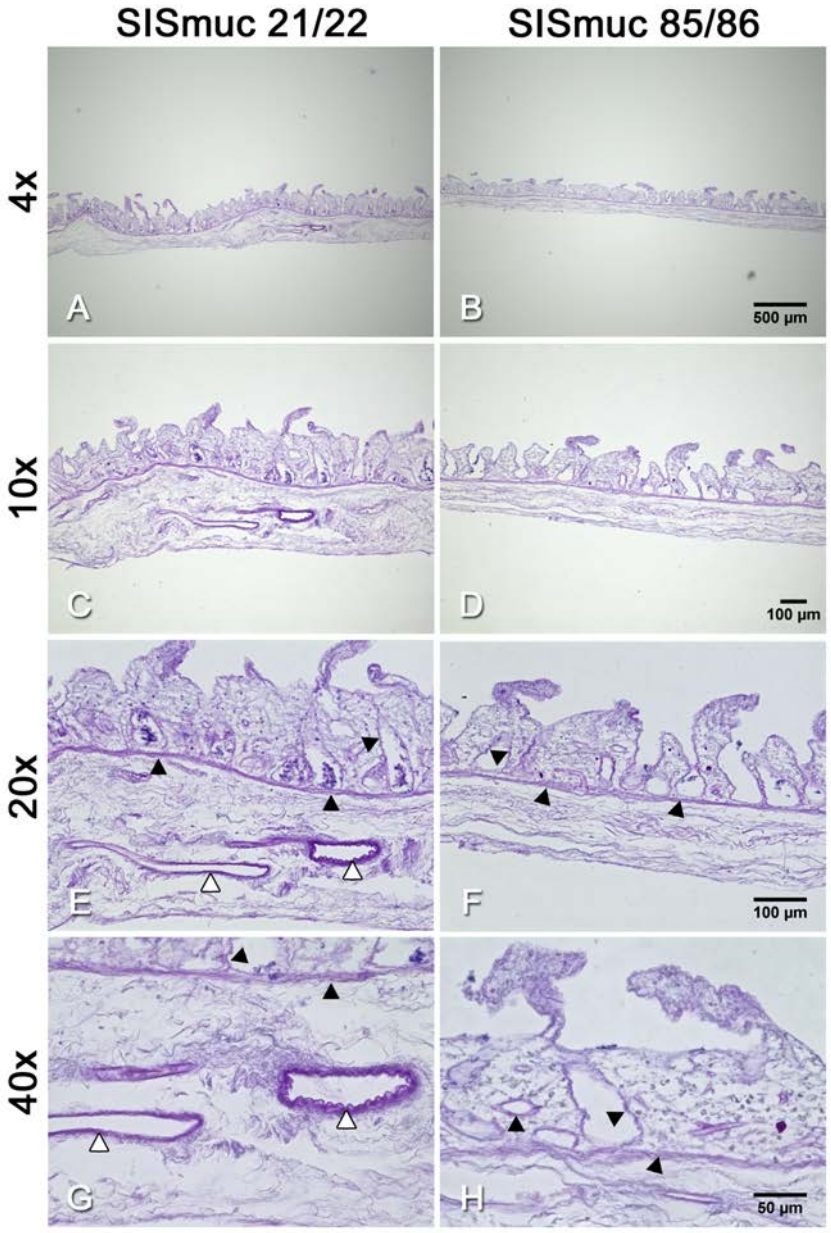

Figure 3.2: Alcian-PAS stain of two different batches of SISmuc without cells. An overview of the SISmuc is given in A and B (4x, scale bar 500 µm). The natural batch-to-batch variation in the scaffold's thickness can be observed in the 10x magnification (C/D, scale bar 100 µm). The 20x (E/F, scale bar 100 µm) and 40x (G/H, scale bar 50 µm) magnifications show that the connective tissue and basal laminae are preserved (pink colour, black arrowheads). Former vessels within the sub-mucosa can be found to be stained in pink-violett indicating basal laminae (white arrowheads, E/G).

3.2 Establishment and standard treatment of a 3D colorectal cancer model

The cell line SW480 was chosen for the establishment and standard treatment of a 3D colorectal cancer model. For this, the tumour cells were characterised by H&E staining and stained for the EMT markers E-cadherin/β-catenin and pan-cytokeratin/vimentin by immunofluorescence in conventional 2D culture and static 3D culture as well as under dynamic 3D conditions. Furthermore, fibroblasts were added as stromal cells to investigate their role in tumour growth. For the assessment of changes of the scaffold's collagen structure including its basement membranes, double staining for pan-cytokeratin and collagen IV were performed. Finally, the tumour model was treated with the standard chemotherapeutic 5-fluorouracil (5-FU). These results were also published in the scientific journal Tissue Engineering Part C (Mary Ann Liebert, Inc.) [2].

3.2.1 Characterisation and morphology of SW480 cells

For characterisation of SW480 cells, H&E stainings and immunofluorescence stainings for pan-cytokeratin (PCK) and vimentin as well as E-cadherin and β-catenin were performed. The remodelling of the scaffold's collagen structure including its basal laminae was assessed by double staining against pan-cytokeratin and collagen IV.

3.2.1.1 H&E staining of a 3D tumour model with SW480 cells and fibroblasts

Dynamically cultured SW480 cells, fibroblasts and the co-culture of both cells are displayed in figure 3.3. In the mono-culture (MC) of SW480 cells, the cells grew in dense clusters on top of the mucosa and inside the former crypts (A/D). Some of the tumour cells detached due to medium shear stress, moved to the subucosa via the medium flow and adhered there (A/D). The scaffold's natural structure with villi and crypts was still preserved in SW480 MC (A/D). Fibroblast MC resulted in smoothing of the SISmuc and thereby remodelling the villi and crypts (B/E). SW480 co-culture (CC) showed a completely remodelled mucosa structure (C/F). Fibroblasts and tumour cells formed an irregular tumour mass on top of the scaffold (C/F).

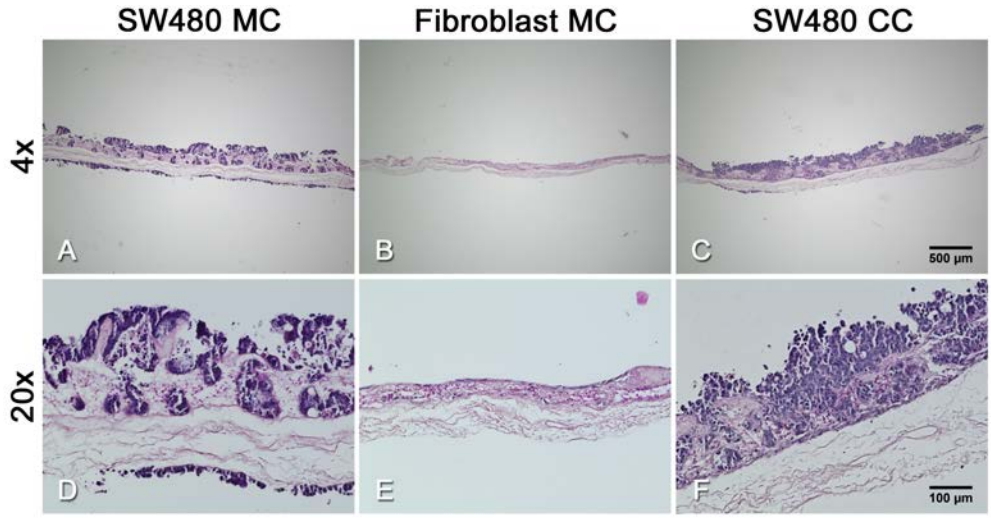

Figure 3.3: H&E staining of dynamically cultured SW480 cells (A/D) and fibroblasts (B/E) in mono-culture (MC) as well as in co-culture (CC) of both cells (C/F). SW480 cells in MC grew in dense clusters on the mucosal side and inside the former crypts (A/D). Some tumour cells detached due to shear stress and moved to the submucosa; the scaffold's natural structure with villi and crypts was still preserved (A/D). Fibroblast MC resulted in flattening the SISmuc and thereby remodelling villi and crypts (B/E). The mucosal structure was completely remodelled in the SW480 CC and tumour cells and fibroblasts formed an irregular tumour mass on top of the scaffold (C/F). Scale bars: 4x magnification 500 µm, 20x magnification 100 µm.

3.2.1.2 Analysing of the EMT markers E-cadherin/β-catenin and pan-cytokeratin/vimentin

SW480 cells and fibroblasts were stained by immunofluorescence against the epithelial-mesenchymal transition (EMT) markers E-cadherin/β-catenin and pan-cytokeratin (PCK)/vimentin.

In conventional 2D MC (fig. 3.4 A–D), most of the SW480 cells expressed the epithelial intermediate filament protein PCK (B) as well as the mesenchymal intermediate filament protein vimentin (C). There were only some single cells negative for vimentin which can be observed in the overlay of fluorescence images (D). Fibroblast MC (E–H) showed PCK-negative (F) and vimentin-positive (G) cells which displayed a flattened and spindle-like cell shape. In the CC of SW480 cells and fibroblasts, only the SW480 cells were PCK-positive (J) and few of the tumour cells were vimentin-positive (K/L) compared to SW480 MC. In 2D culture, fibroblasts and SW480 cells grew tightly packed side by side and only some single tumour cells grew on top of a fibroblast layer (L).

In static 3D culture (fig. 3.5), SW480 cells (A–D) were growing monolayer-like forming small cell clusters expressing PCK (B) and vimentin (C). Fibroblasts cultured in MC on the SISmuc (E–H) were stained for vimentin (G). They grew on top of the scaffold but did not migrate into the former mucosa. The CC of both cell types (I–L) exhibited an altered growth pattern and fibroblasts migrated into the former mucosa surrounding SW480 cells which formed dense cell clusters.

SW480 MC in dynamic 3D culture resulted in an increased growth of tumour cells which were positive for PCK but negative for vimentin (fig. 3.6 A–D). The cells formed tumour-like cell masses and filled the former crypts of the matrix. In the fibroblast MC (E–H), the fibroblasts were positive for vimentin (G). They did not migrate into the former mucosa but grew on top of the scaffold. This growth pattern was altered in the SW480 CC (I–L) and fibroblasts migrated into the mucosa while SW480 cells formed dense tumour-like cell clusters growing on top of the scaffold as well as within the scaffold surrounded by fibroblasts.

E-cadherin/β-catenin expression of SW480 cells in static 3D culture is illustrated in figure 3.8 A–D. SW480 cells were stained for E-cadherin (B) and some single cells exhibited expression of β-catenin in the cell nuclei (C). The MC of fibroblasts (E–H) did neither express E-cadherin (F) nor β-catenin (G). The CC of both cells (I–L) displayed the E-cadherin positive SW480 cells (J) but no β-catenin expression (K) could be observed.

In dynamic 3D culture (fig. 3.9), total cell number was increased compared to static 3D culture (fig. 3.8 A–D). The cells exhibited E-cadherin expression (B)

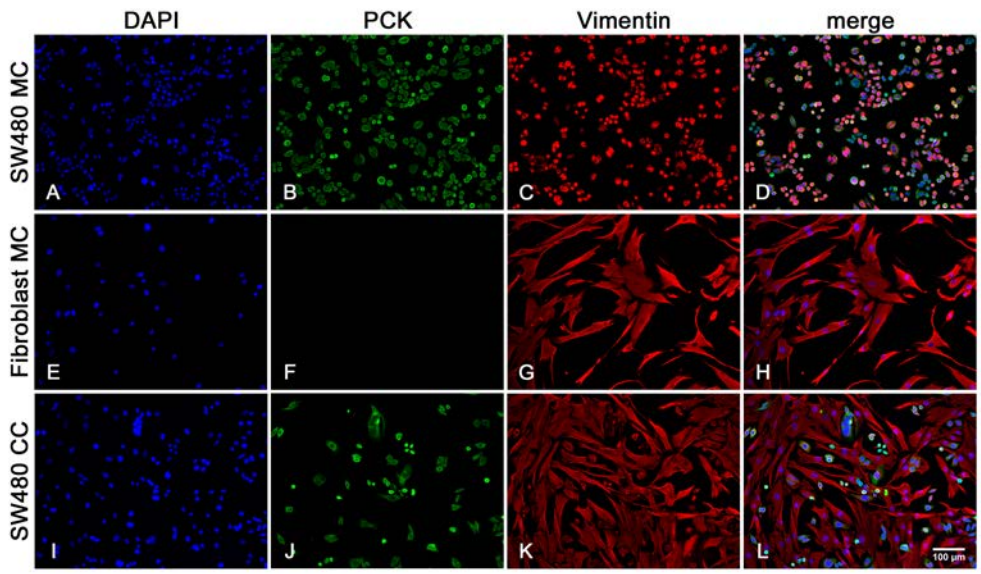

Figure 3.4: Immunofluorescence staining for the EMT markers PCK/vimentin of monocultures (MC) of SW480 cells and fibroblasts cultured in conventional 2D culture as well as of their respective co-culture (CC). SW480 MC (A–D) displays SW480 cells which were stained positively for PCK (B) and vimentin (C). In contrast, fibroblasts (E–H) did not express PCK (F) but vimentin (G). The SW480 CC (I–L) shows PCK-positive tumour cells (J) with some single cells stained for vimentin (K, small round-shaped cells). The DAPI channel (A/E/I) shows the cell nuclei, the overlay of all channels is shown in merge (D/H/L). Scale bar in L: 100 µm for A to L.

and there were more β-catenin positive cells in the dynamic 3D MC (fig. 3.9 C) than in static 3D culture (fig. 3.8 C). SW480 cells grew in cell clusters inside the crypts and built multilayers on top of the scaffold. Some single tumour cells grew also on the basal side of the submucosa (A–D). The fibroblast MC (E–H) was negative for both markers. The CC of SW480 cells and fibroblasts (I–L) showed dense tumour-like cell masses. SW480 cells were E-cadherin positive (J) and cells located at the margin of the tumour-like mass were strongly β-catenin positive (K).

3.2.1.3 Analysis of matrix remodelling: Collagen IV immunohistochemistry

The preserved basal laminae of the scaffold SISmuc could be represented by immunofluorescence staining for collagen IV which is found primarily in the basal lamina. Figure 3.10 displays dynamic 3D cultures of SW480 cells (A–D)

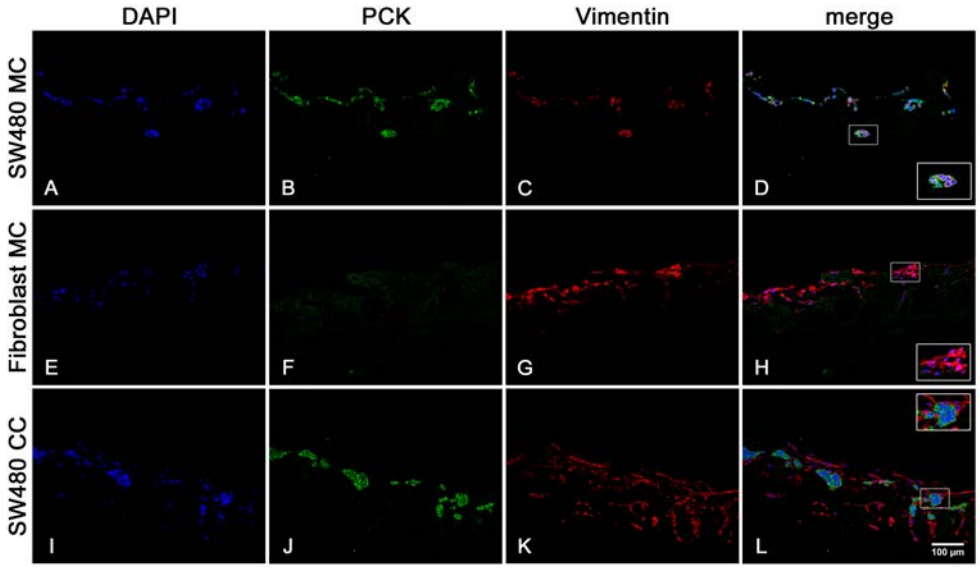

Figure 3.5: Immunofluorescence staining for the EMT markers PCK/vimentin of monocultures (MC) of SW480 cells and fibroblasts cultured in static 3D culture as well as of their respective co-culture (CC). SW480 MC (A–D) illustrates that the tumour cells exhibited PCK (B) and vimentin (C) expression. Vimentin expression (G) could be detected only in the fibroblast MC (E–H), where the cells grew on the scaffold, but no PCK expression could be detected. In the SW480 CC (I–L), SW480 cells were surrounded by fibroblasts which grew on top of the scaffold and also migrated into the former mucosa. The DAPI channel (A/E/I) shows the cell nuclei, the overlay of all channels is shown in merge (D/H/L). Scale bar in L: 100 µm for A to L.

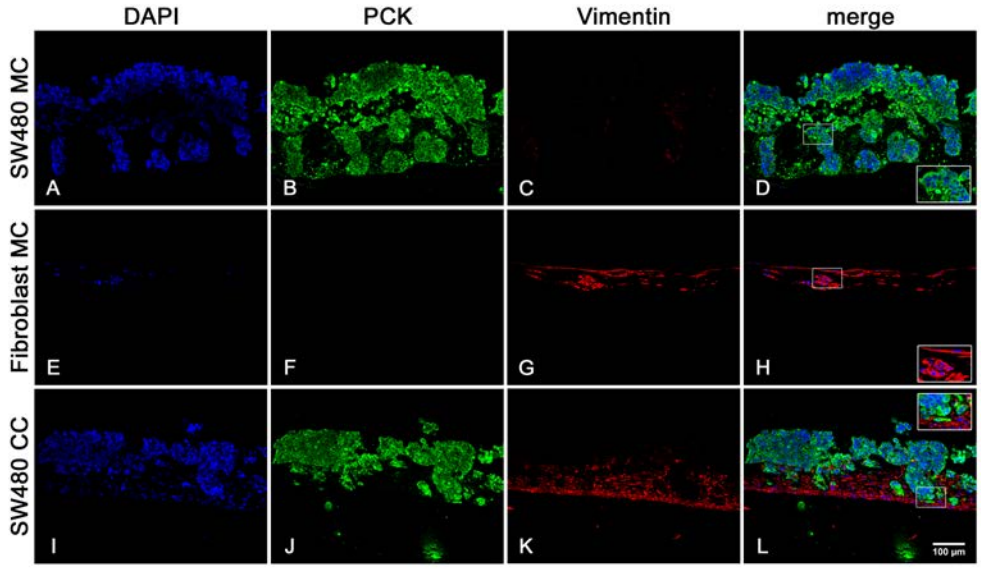

Figure 3.6: Immunofluorescence staining for the EMT markers PCK/vimentin of monocultures (MC) of SW480 cells and fibroblasts cultured in dynamic 3D culture as well as of their respective co-culture (CC). SW480 MC (A–D) exhibited dense tumour clusters which grew on top of the scaffold and inside the former crypts. The tumour cells expressed PCK (B) but no vimentin (C). Fibroblast MC (E–H) displayed vimentin (G) expression and the cells grew mainly on top of the scaffold. SW480 CC (I–L) showed that the fibroblasts migrated into the mucosa and SW480 cells grew in tumour-like cell masses on top of the scaffold as well as within former crypts surrounded by fibroblasts. The DAPI channel (A/E/I) shows the cell nuclei, the overlay of all channels is shown in merge (D/H/L). Scale bar in L: 100 µm for A to L.

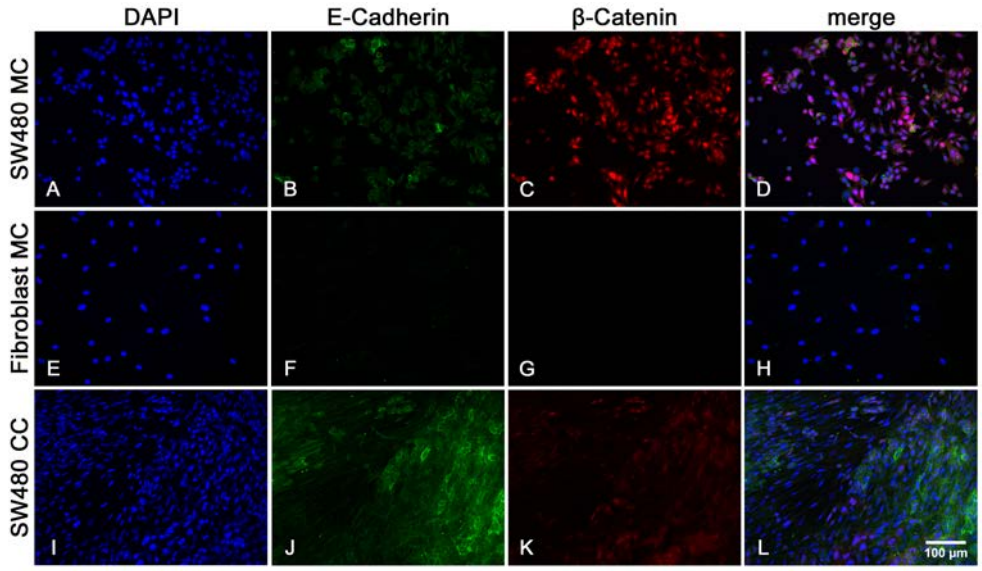

Figure 3.7: Immunofluorescence staining against the EMT markers E-cadherin/β-catenin of monocultures (MC) of SW480 cells and fibroblasts cultured in conventional 2D culture as well as of their respective co-culture (CC). SW480 cells in MC (A–D) weakly expressed E-cadherin (B) and only cells having a direct contact to each other expressed this protein at the cell membrane. B-catenin was localised within the cell nuclei (C) and most SW480 cells expressed this protein (D). In the fibroblast MC (E–H), both EMT markers could not be detected. The SW480 CC (I–L) showed lighter staining of E-cadherin (J) and β-catenin (K) compared to the SW480 MC (B and C). Scale bar in L: 100 µm for A to L.

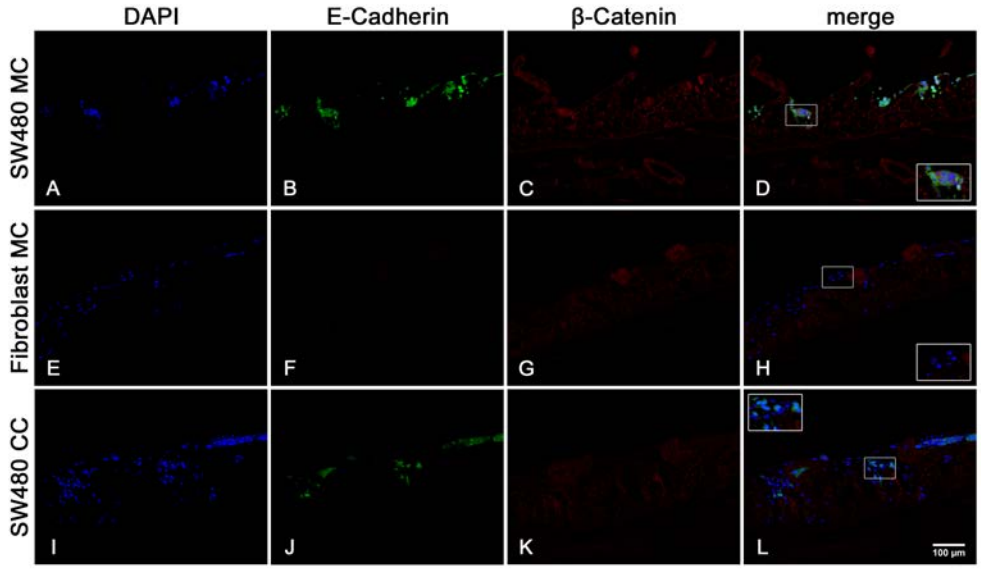

Figure 3.8: Immunofluorescence staining for the EMT markers E-cadherin/β-catenin of monocultures (MC) of SW480 cells and fibroblasts cultured in static 3D culture as well as of their respective co-culture (CC). SW480 MC (A–D) illustrates that the tumour cells exhibited E-cadherin (B) and β-catenin (C) expression. The MC of fibroblasts did neither express E-cadherin (F) nor β-catenin (G). SW480 cells in CC were E-cadherin positive (J) but no β-catenin expression (K) could be detected. The DAPI channel (A/E/I) shows the cell nuclei, the overlay of all channels is shown in merge (D/H/L). Scale bar in L: 100 µm for A to L.

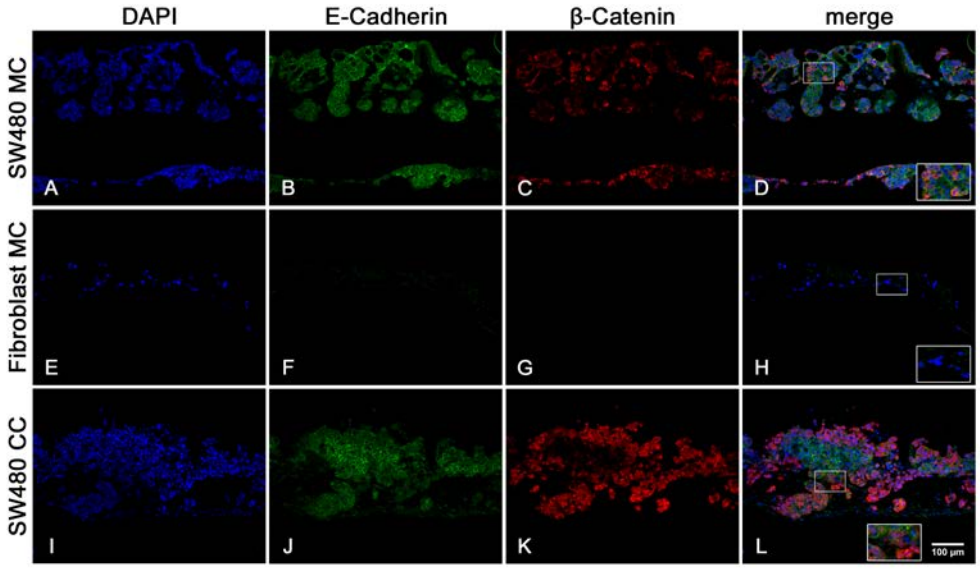

Figure 3.9: Immunofluorescence staining for the EMT markers E-cadherin/β-catenin of monocultures (MC) of SW480 cells and fibroblasts cultured in dynamic 3D culture as well as of their respective co-culture (CC). SW480 MC (A–D) presented an increased growth of E-cadherin positive tumour cells (B). Some single SW480 cells were also β-catenin positive (C). Fibroblasts (E–H) did neither express E-cadherin (F) nor β-catenin (G). The tumour cells in SW480 CC (I–L) displayed E-cadherin expression (J) as well as β-catenin positive cells (K) at the margins of the tumour-like cell mass. The DAPI channel (A/E/I) shows the cell nuclei, the overlay of all channels is shown in merge (D/H/L). Scale bar in L: 100 µm for A to L.

and fibroblasts (E–H) in monoculture as well as the co-culture (I–L) of both cell types.

Dynamic MC of SW480 cells resulted in an enhanced tumour cell growth. The cells filled the former crypts of the scaffold and built multilayers on the former villi of the scaffold (A–D). The tumour cells alone did not change the collagen structure with the basement membrane indicated by the collagen IV staining (C) which showed clearer outlines of the former crypts (c) compared to the more diffuse staining in the CC (k). The fibroblast MC (E–H) caused a remodelling of the scaffold by flattening the former villi and crypt structures. In the CC of SW480 cells and fibroblasts (I–L), this remodelling was more pronounced by the invasive tumour cells growth (J) and more diffuse collagen IV staining (K) compared to the SW480 MC.

3.2.2 Standard chemotherapeutic treatment of a 3D colorectal carcinoma model

The 3D SW480 CC model was treated with the standard chemotherapeutic 5-FU and changes in the expression of PCK and vimentin were assessed by immunofluorescence staining.

Figure 3.11 displays the results of the treatment with 25 µM 5-FU of SW480 cells and fibroblasts in static 3D MC and CC as well as in dynamic 3D CC. SW480 cells in static 3D MC did not respond to the treatment with 5-FU (E) in comparison to the untreated control (A). Also, fibroblasts in static 3D MC were not affected by the treatment with the chemotherapeutic (F). The static CC of SW480 cells and fibroblast resulted in formation of dense cell aggregates (C) which were reduced by the treatment with 5-FU (G). This effect was even more pronounced in the dynamic CC where treatment caused a remarkable reduction of the tumour cell mass (H) when compared to the untreated control (D). These results were published in the article “Mimicking metastases including tumor stroma: A new technique to generate a three-dimensional colorectal cancer model based on a biological decellularized intestinal scaffold” in the journal Tissue Engineering Part C Methods [2].

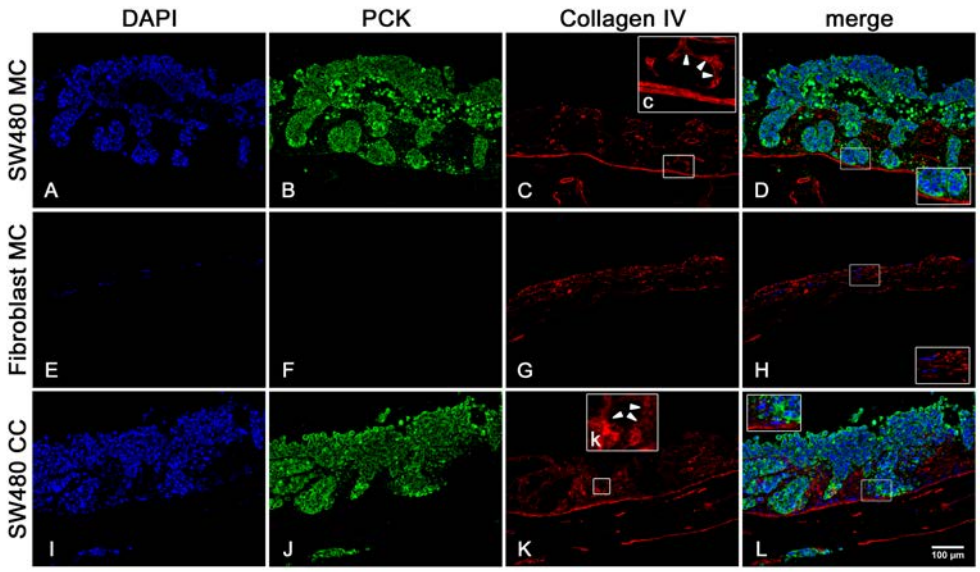

Figure 3.10: Immunofluorescence staining for PCK and collagen IV of SW480 cells (A–D) and fibroblasts (E–H) cultured in monoculture (MC) and their respective co-culture (CC, I–L) in dynamic 3D culture. Dynamic culture enhanced SW480 tumour cell growth and cells filled the former crypts and built multilayers on the former villi. The collagen structure with the basement membrane, which is shown by the collagen IV staining (C), was not changed by the tumour cells alone. The former crypts were still sharply outlined by collagen IV (c, arrowheads). Fibroblast MC resulted in a remodelling of the scaffold, they flattened the villi and crypt structures and hence the basement membrane (G). The former crypts in the SW480 CC were completely remodelled indicated by the infiltrating tumour cell growth (J) and diffuse collagen IV staining (K) which did not show sharp margins outlining the former crypts (k, arrowheads). Scale bar in L: 100 µm for A to L.

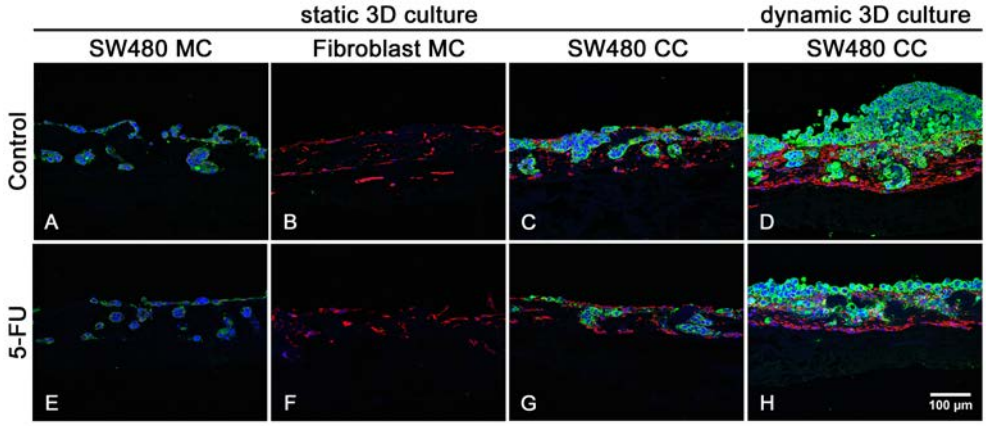

Figure 3.11: Immunofluorescence staining against PCK (*green*) and vimentin (*red*) of the 3D tumour models treated with 5-fluorouracil (5-FU). There were no differences visible for SW480 cells cultured in static 3D monoculture (MC) after treatment with 25 µM 5-FU (E) compared to the untreated control (A). Fibroblast MC (B) did neither show a reduction of the cell number after treatment (F). In the static 3D SW480 co-culture (CC), a reduction of the tumour cell number could be observed after treatment with 5-FU (G). This response could also be seen in the dynamic SW480 CC (D and H). Scale bar in H: 100 µm for A to H.

3.3 Targeted therapy of a 3D tumour model of *BRAF*-mutant colorectal carcinoma

At first, the two *BRAF*-mutant early passage CRC cell lines HROC24 and HROC87 were characterised in conventional 2D cell culture and 3D cell culture according to their morphology, expression of colon adenocarcinoma-specific markers, expression of tumour stem cell markers, expression of EMT markers and proliferation index. Furthermore, cells were treated with the BRAF inhibitor vemurafenib (PLX4032, Zelboraf™) and/or the EGFR inhibitor gefitinib (Iressa®). For assessment of the treatment's success, the used read-out parameters were apoptosis (M30-ELISA), viability (MTT assay) and changes in the signal transduction pathway (phospho-kinase arrays, western blot) as well as (immuno-) histological analyses such as Ki67 staining for the evaluation of the proliferation rate. Two different FCS batches were used for the experiments and revealed different growth and drug response.

Additionally, xenografting experiments were performed with HROC87 cells in mice and subsequently treated with vemurafenib and/or gefitinib (done by the lab of PD Dr. M. Linnebacher, University Hospital Rostock). Here, the

read-out parameters were tumour volume and weight as well as proliferation and changes in the signalling pathway, besides the assessment of EMT markers by IHC staining.

3.3.1 Characterisation and morphology of the two *BRAF*-mutant early passage CRC cell lines HROC24 and HROC87

3.3.1.1 Morphological characterisation of cells and 3D tissues using H&E staining

In conventional 2D cell culture, HROC24 cells grew in monolayers forming scattered cell colonies which tended to form loose clusters, single cells showed a spindle-like morphology while others appeared round in shape (fig. 3.12 A/E and C/G). The cells displayed an evenly distributed monolayer-like growth on the SISmuc in static 3D culture and filled the former crypts of the mucosa (fig. 3.12 B/F and D/H). HROC24 cells did not show any differences between the two different FCS batches N° 8SB016 and N° BS196368 concerning growth and morphology, neither in 2D culture (fig. 3.12 A/C and E/G) nor in static 3D culture (fig. 3.12 B/D and F/H).

The cell line HROC87 grew in dense clusters forming multi-layered cell aggregates in 2D culture which seemed spheroid-like (fig. 3.12 I/M and K/O). The cells appeared mostly in a spindle-like morphology while the cell aggregates consisted of round-shaped cells for FCS Lot N° 8SB016 (fig. 3.12 I/M). In comparison, HROC87 cells displayed a less scattered growth and a more round-shaped morphology with dense cell aggregates when cultured in cell culture medium with FCS Lot N° BS196368 (fig. 3.12 K/O). In static 3D culture, the cells grow in irregularly scattered multi-layered clusters on the SISmuc (fig. 3.12 J/N and L/P). As for HROC24 cells, HROC87 cells grew into the former crypts of the mucosa. In contrast, HROC87 cells did not form any monolayers, regardless of the used FCS (fig. 3.12 B/F vs. J/N, D/H vs. L/P). The cell morphology did not change comparing the two FCS batches, but less HROC87 cells grew on the SISmuc when cultured in cell culture medium with 10 % FCS Lot N° BS196368 (fig. 3.12 J/N vs. L/P).

Additionally, an overview of a static 3D tumour model with HROC87 cells cultured in two different FCS batches is displayed in figure 3.13. The cells grew better yielding a higher cell number in cell culture medium containing FCS Lot N° 8SB016 compared to FCS Lot N° BS196368. The scaffold's margins are flattened (fig. 3.13, black arrowheads) because of its fixation in the "cell crown" (see 2.2.1.7).

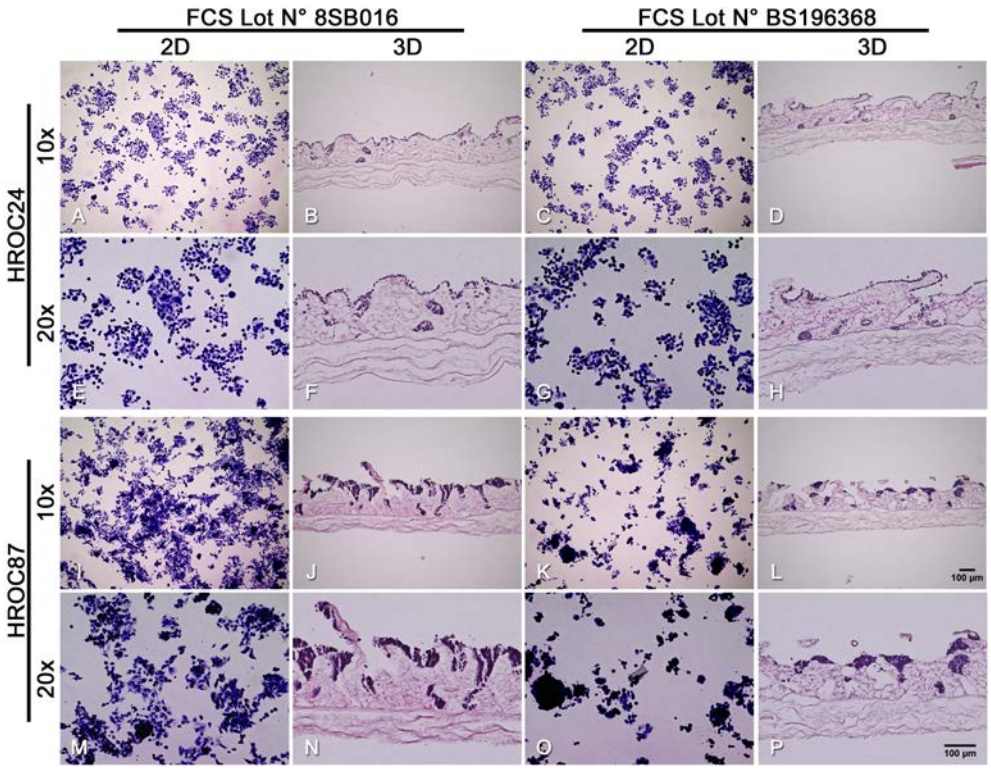

Figure 3.12: H&E staining of HROC24 and HROC87 cells cultured with two different FCS batches on glass coverslips (2D) and on SISmuc (3D, static). Two different magnifications (10x: A/B/C/D and I/J/K/L, 20x: E/F/G/H and M/N/O/P, scale bar 100 µm each) are shown. HROC24 cells grew in 2D culture as a monolayer forming scattered cell colonies (A/E and C/G). In static 3D culture, they formed monolayers and filled the former crypts of the SISmuc (B/F and D/H). HROC87 cells showed a multi-layered and clustered growth for 2D culture (I/M and K/O) and 3D culture (J/N and L/P). They did not tend to grow evenly scattered as HROC24 cells under static 3D culture conditions. There are no remarkable differences between the two FCS batches for HROC24 cells cultured in 2D (A/C and E/G) and 3D (B/D and F/H) concerning cell growth, density and morpholgy. In contrast, HROC87 cells grew more scattered with the FCS Lot N° 8SB016 in 2D culture compared to the dense formed clusters with FCS Lot N° BS196368 (I/K and M/O). In static 3D culture, HROC87 cells showed a similar multi-layered morpholgy for the two FCS batches, though the cells formed bigger cell clusters with FCS Lot N° 8SB016 (J/L and N/P). Scale bar in L (10x): 100 µm for A–D and I–L. Scale bar in P (20x): 100 µm for E–H and M–P.

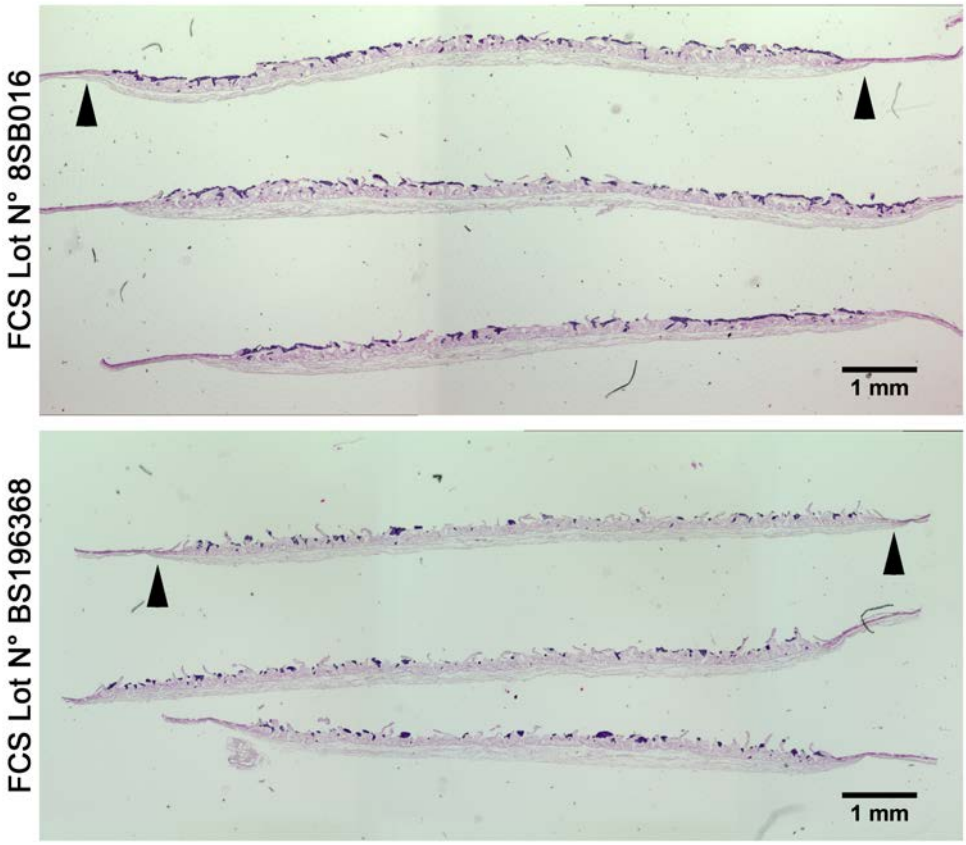

Figure 3.13: Overview of the full length of the SISmuc (H&E staining). Shown are HROC87 cells cultured under static 3D culture conditions in cell culture medium with two different FCS batches. More cells grew with FCS Lot N° 8SB016. The scaffold was fixed in a "cell crown" therefore the ends (black arrowheads) are flattened and not covered with cells. Scale bars measure 1 mm each.

3.3.1.2 Mucines, connective tissue and basal laminae: Alcian-PAS stain

Figure 3.14 shows an alcian-PAS stain of sections of the static 3D tumour models with HROC24 cells (A/E/I) and HROC87 cells (B/F/J) as well as sections of native tissues of an adenocarcinoma of the colon (C/G/K) and a healthy colon (D/H/L). The cell nuclei are coloured in dark blue, mucus-producing cells in light blue (fig. 3.14 H/J/L, white arrowheads) and connective tissue/basal laminae in pink.

As shown for the unseeded SISmuc (fig. 3.2), the basal laminae of the static 3D tumour model are stained in pink. Both cell lines, HROC24 and HROC87 cells, did not cross the lamina muscularis mucosae (fig. 3.14 I/J) but stayed on the surface of the SISmuc or inside the former crypts. The sections of the colon adenocarcinoma showed irregularly distributed cancer and stromal cells within the tissue but glandular structures still can be observed (fig. 3.14 C/G/K). There are basal membranes but not as developed as in healthy colon or the SISmuc. Mucus-producing cells were present in the healthy colon (fig. 3.14 H/L, white arrowheads) and to a lesser extend in the HROC87 tumour model (fig. 3.14 J). Those cells were scattered in the adenocarcinoma (fig. 3.14 K, light blue"hollow" vacuoles within the cells). There could be found necrotic debris within the lumina of adenocarcinomatous glands of the tumour (fig. 3.14 C/G/K, black stars). Scale bar in D (10x): 100 µm for A–D. Scale bar in H (20x): 100 µm for E–H. Scale bar in L (40x): 100 µm for I–L.

3.3.1.3 CDX2, CK7 and CK20: Marker for colorectal adenocarcinoma

CDX2, CK7 and CK20 are the most widely used immunohistochemical markers for colorectal adenocarcinoma [23].

The enteric differentiation marker CDX2 was heterogeneously expressed in both HROC24 (fig. 3.15 A/B/C/D) and HROC87 (fig. 3.16 A/B/C/D) cells, regardless of the cells being cultured in conventional 2D culture or static 3D culture (FCS Lot N° 8SB016). The same heterogeneous expression of CDX2 was found in a section of a colon adenocarcinoma (fig. 3.17 C) which displayed a more intensive staining compared to the 3D tumour model (fig. 3.17 A/B). In the healthy colon, CDX2 expression was restricted to the apical enterocytes being fully differentiated (fig. 3.17 D).

Both cell lines, HROC24 and HROC87, were negative for the marker CK7 independent of the cells being cultured in conventional 2D (fig. 3.15 E/F and fig. 3.16 E/F) or static 3D conditions (fig. 3.15 G/H and fig. 3.16 G/H). Furthermore, neither the colon adenocarcinoma (fig. 3.17 G) nor the healthy colon (fig. 3.17 H) did exhibit any CK7 expression.

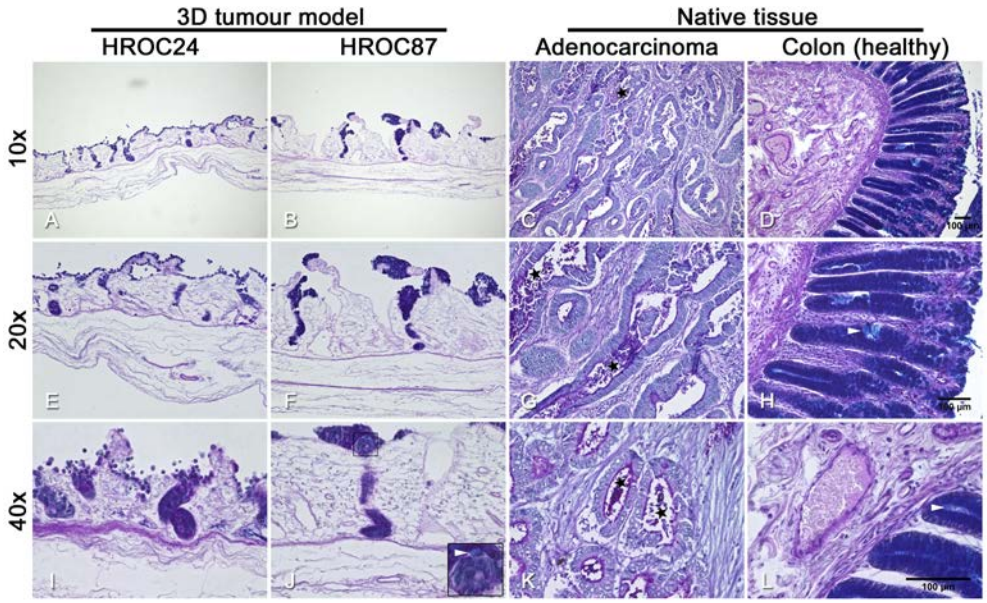

Figure 3.14: Alcian-PAS stain of the static 3D tumour models (A/E/I and B/F/J, FCS Lot N° 8SB016) and native tissues of a colon adenocarcinoma (C/G/K) as well as of a healthy colon (D/H/L). Cell nuclei are stained in dark blue, acidic mucopolysaccharides in light blue (H/J/L, white arrowheads) and connective tissue/basal laminae in pink-violett. Necrotic debris was found within the lumina of adenocarcinomatous glands of the tumor tissue (C/G/K, black stars). The scale bars measure 100 µm for each magnification (10x, 20x and 40x).

The expression of CK20 varied in both cell lines and most HROC24 cells as well as HROC87 cells were negative for this marker in 2D culture (fig. 3.15 I/J and fig. 3.16 I/J). As in conventional 2D cell culture, most of HROC24 cells were negative for CK20 in static 3D culture and only single cells expressed this marker (fig. 3.15 K/L). In static 3D culture, there were no HROC87 cells found positive for CK20 (fig. 3.16 K/L). Figure 3.17 on page 100 displays a comparison of the CK20 expression of the 3D tumour models (I/J) and native tissues (K/L). The colon adenocarcinoma (fig. 3.17 K) exhibited a moderate to strong staining for CK20 whereas only enterocytes expressed this marker in the healthy colon (fig. 3.17 L).

No differences were found between the two FCS batches N° 8SB016 and N° BS196368 regarding the expression of CDX2 and CK7 for both HROC24 and HROC87 cells in conventional 2D cell culture (fig. 3.18 and fig. 3.19). However, the CK20 expression differed between the two FCS batches and there were more CK20 positive HROC24 cells cultured with the FCS Lot N° BS196368 compared to Lot N° 8SB016 (fig. 3.18 G/H and P/Q). Especially, the cell line HROC87 showed more CK20 positive cells when cultured with FCS Lot N° BS196369 (fig. 3.19 G/H) than with Lot N° 8SB016 (fig. 3.19 P/Q). The negative controls (neg. ctlr.; secondary antibodies only, fig. 3.18 and fig. 3.19 C/F/I/ L/O/R) displayed the specificity of the used primary antibodies against the antigens CDX2, CK7 and CK20.

In static 3D culture, HROC24 cells exhibited a similar marker expression which did not change for CDX2 (fig. 3.20 A/B and J/K) and CK7 (fig. 3.20 D/E and M/N). Differences between the two FCS batches were only found for the expression of CK20: more HROC24 cells expressed this marker when cultured with FCS Lot N° BS196368 (fig. 3.20 P/Q) compared to FCS Lot N° 8SB016 (fig. 3.20 G/H). As for cell line HROC24 cultured in static 3D culture, HROC87 cells did not show any differences in the expression of CDX2 (fig. 3.21 A/B and J/K) and CK7 (fig. 3.21 D/F and M/N) between the two FCS batches. However, single CK20 positive HROC87 cells could be detected when cultured with FCS Lot N° BS196368 (fig. 3.21 P/Q) in comparison to FCS Lot N° 8SB016 where no cell was found to be positive for this marker (fig. 3.21 G/H). The negative controls (neg. ctlr.; secondary antibodies only, fig. 3.20 and fig. 3.21 C/F/I/L/O/R) displayed the specificity of the used primary antibodies against the antigens CDX2, CK7 and CK20. The CDX2 antibody showed crossreactivity with the porcine SISmuc indicated by the light staining of the scaffold in comparison to the negative control.

Dynamically cultured HROC24 cells and HROC87 cells showed an increased tumour cell growth than in static 3D culture. CDX2 was stained only in single

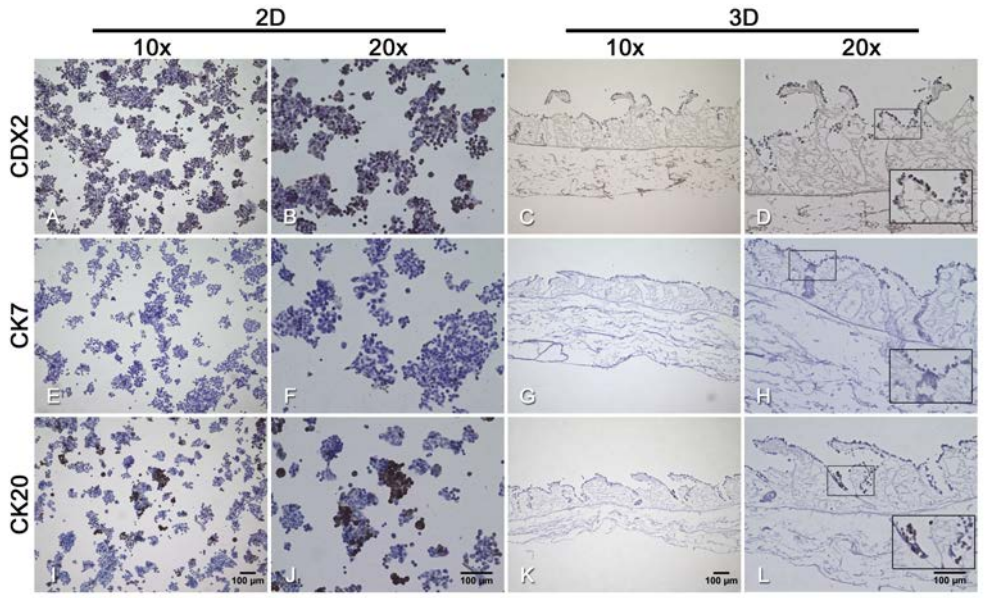

Figure 3.15: Immunohistochemical (DAB) staining for the colorectal adenocarcinoma markers CDX2, CK7 and CK20 in HROC24 cells cultured in conventional 2D culture (A/B, E/F and I/J) and static 3D culture (C/D, G/H and K/L; FCS Lot N° 8SB016). CDX2 expression was heterogeneous in 2D culture (A/B) as well as 3D culture (C/D), whereas CK7 expression could not be detected in any cells (E/F/G/H). The expression of CK20 was irregular distributed and most cells were negative for this marker in 2D culture (I/J). Especially in static 3D culture (K/L), there were less cells positive for CK20 than in 2D culture. Scale bars in I and K (10x): 100 µm for A/E/I and C/G/K. Scale bars in J and L (20x): 100 µm for B/F/J and D/H/L.

HROC24 cells (fig. 3.22 A/D) whereas more HROC87 cells could be detected for the expression of this marker staining predominantly the cell nuclei (fig. 3.22 G/J). The marker CK7 could neither be detected in HROC24 cells nor in HROC87 cells (fig. 3.22 B/E and H/K). In both cell lines, there were some heterogeneously distributed cells stained for CK20 (fig. 3.22 C/F and I/L). In comparison to static 3D culture (fig. 3.20 and 3.21), there are more cells CK20 positive in dynamic 3D culture.

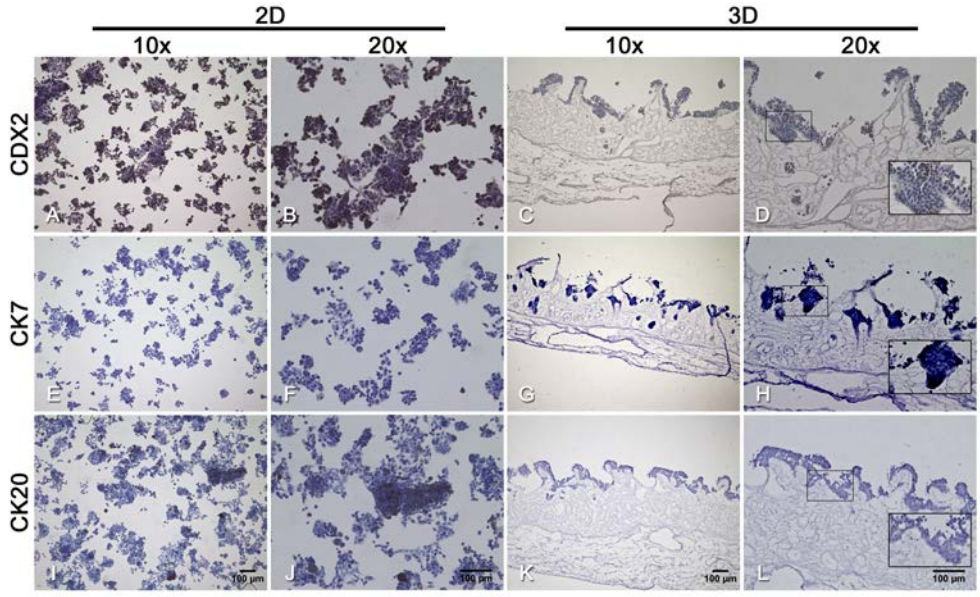

Figure 3.16: Immunohistochemical (DAB) staining for the colorectal adenocarcinoma markers CDX2, CK7 and CK20 in HROC87 cells cultured in conventional 2D culture (A/B, E/F and I/J) and static 3D culture (C/D, G/H and K/L; FCS Lot N° 8SB016). In 2D culture, about half of the HROC87 cells were positive for CDX2 (A/B), whereas less cells expressed this marker in static 3D culture (C/D). All cells were negative for CK7 (E/F/G/H). Only single cells were found to be stained for the marker CK20 in 2D culture (I/J) and no cells were found to be stained for CK20 in static 3D culture (K/L). Scale bars in I and K (10x): 100 µm for A/E/I and C/G/K. Scale bars in J and L (20x): 100 µm for B/F/J and D/H/L.

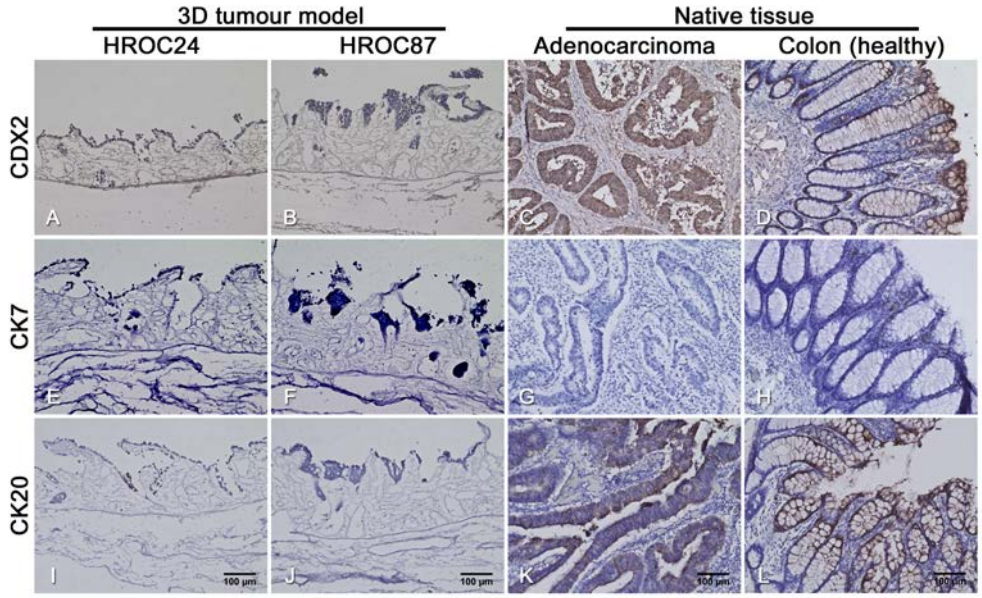

Figure 3.17: Immunohistochemical (DAB) staining for the colorectal carcinoma markers CDX2, CK7 and CK20 in HROC24 and HROC87 cells cultured under static 3D culture conditions (FCS Lot N° 8SB016) as well as in a colon adenocarcinoma and healthy colon. Most of the cells in the shown section of the colon adenocarcinoma were positive for CDX2 (C) in contrast to the static 3D tumour models (A/B) where only single cells expressed this marker of enteric differentiation. In the healthy colon, CDX2 expression is restricted to the differentiated enterocytes (D). The expression of CK7 could not be detected, neither in the static 3D tumour models (E/F) nor in the colon adenocarcinoma (G) nor in the healthy colon (H). There were only single cells stained for CK20 in the HROC24 tumour model (I) whereas no HROC87 cells expressed this marker in static 3D culture (J). The section of the colon adenocarcinoma showed moderate to strong staining for CK20 (K). In the healthy colon, only enterocytes expressed this marker (L). Scale bars in I, J, K, L: 100 µm for A to L.

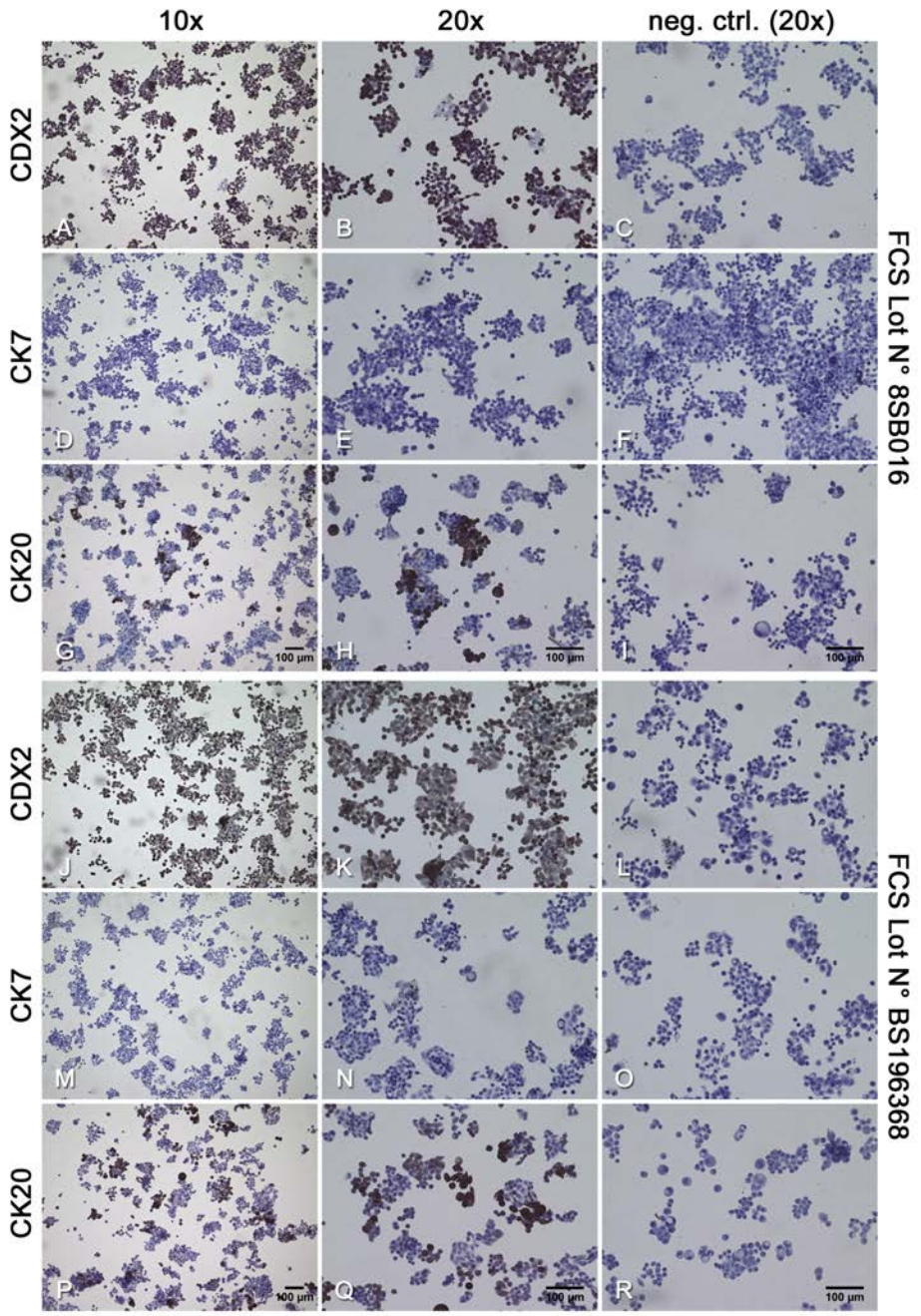

Figure 3.18: Immunohistochemical staining (DAB) for CDX2, CK7 and CK20 for HROC24 cells cultured with two different FCS batches (Lot N° 8SB016 and Lot N° BS196368) in conventional 2D cell culture. The expression of CDX2 (A/B/J/K) and CK7 (D/E/M/N) did not differ between the FCS batches. There were more cells positive for CK20 when being cultured with FCS Lot N° BS196368 (P/Q) compared to Lot N° 8SB016 (G/H). The negative control (neg. ctrl.; secondary antibodies only, C/F/I/L/O/R) confirmed the specificity for the primary antibodies. Scale bars in G and P (10x): 100 µm for A/D/G and J/M/P. Scale bars in H, I, Q, R (20x): 100 µm for B/C/E/F/H/I and K/L/N/O/Q/R.

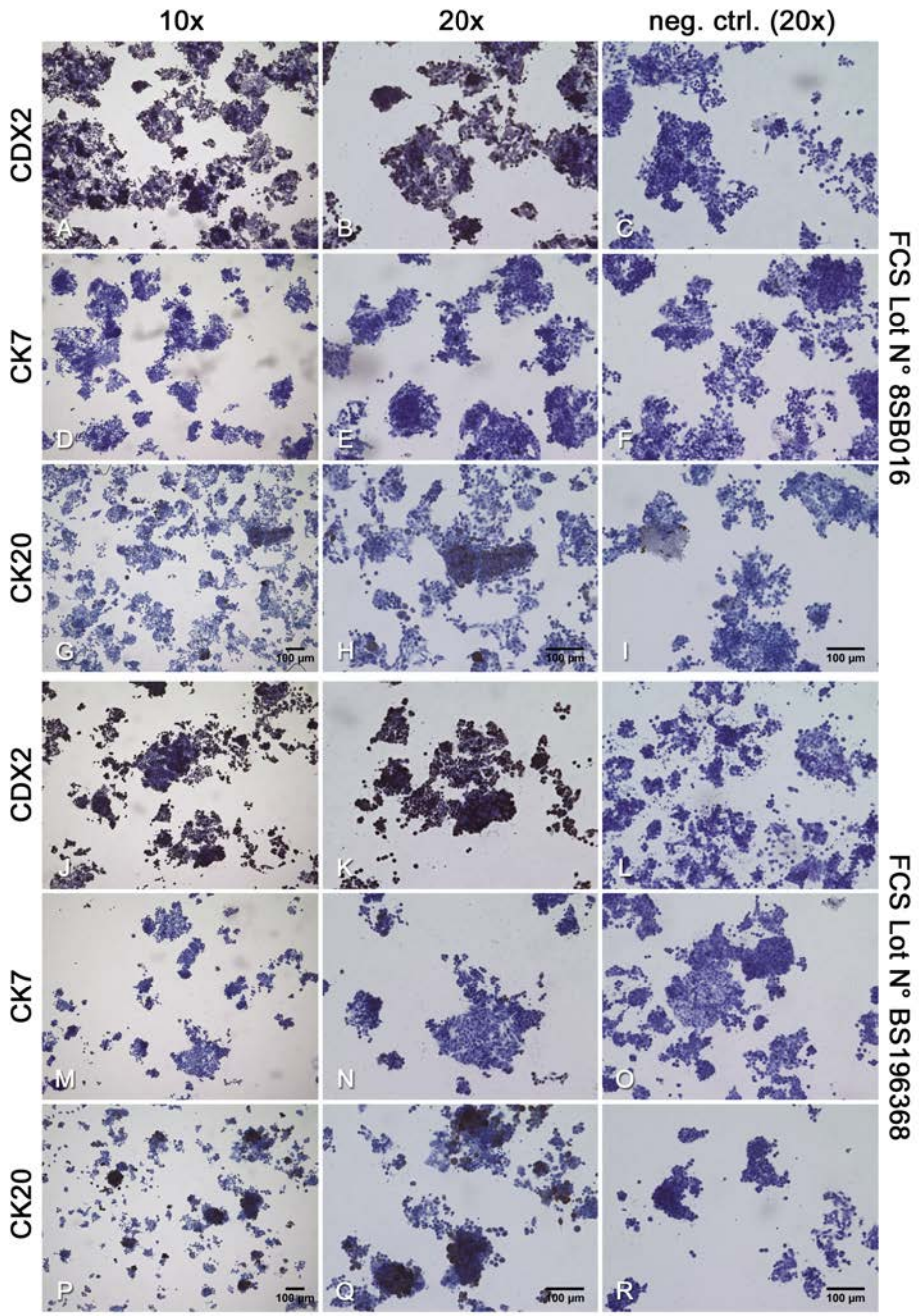

Figure 3.19: Immunohistochemical staining (DAB) for CDX2, CK7 and CK20 for HROC87 cells cultured with two different FCS batches (Lot N° 8SB016 and Lot N° BS196368) in conventional 2D cell culture. The expression of CDX2 (A/B/J/K) and CK7 (D/E/M/N) did not differ between the FCS batches. There were more cells positive for CK20 when being cultured with FCS Lot N° BS196368 (P/Q) compared to Lot N° 8SB016 (G/H). The negative control (neg. ctrl.; secondary antibodies only, C/F/I/L/O/R) confirmed the specificity for the primary antibodies. Scale bars in G and P (10x): 100 µm for A/D/G and J/M/P. Scale bars in H, I, Q, R (20x): 100 µm for B/C/E/F/H/I and K/L/N/O/Q/R.

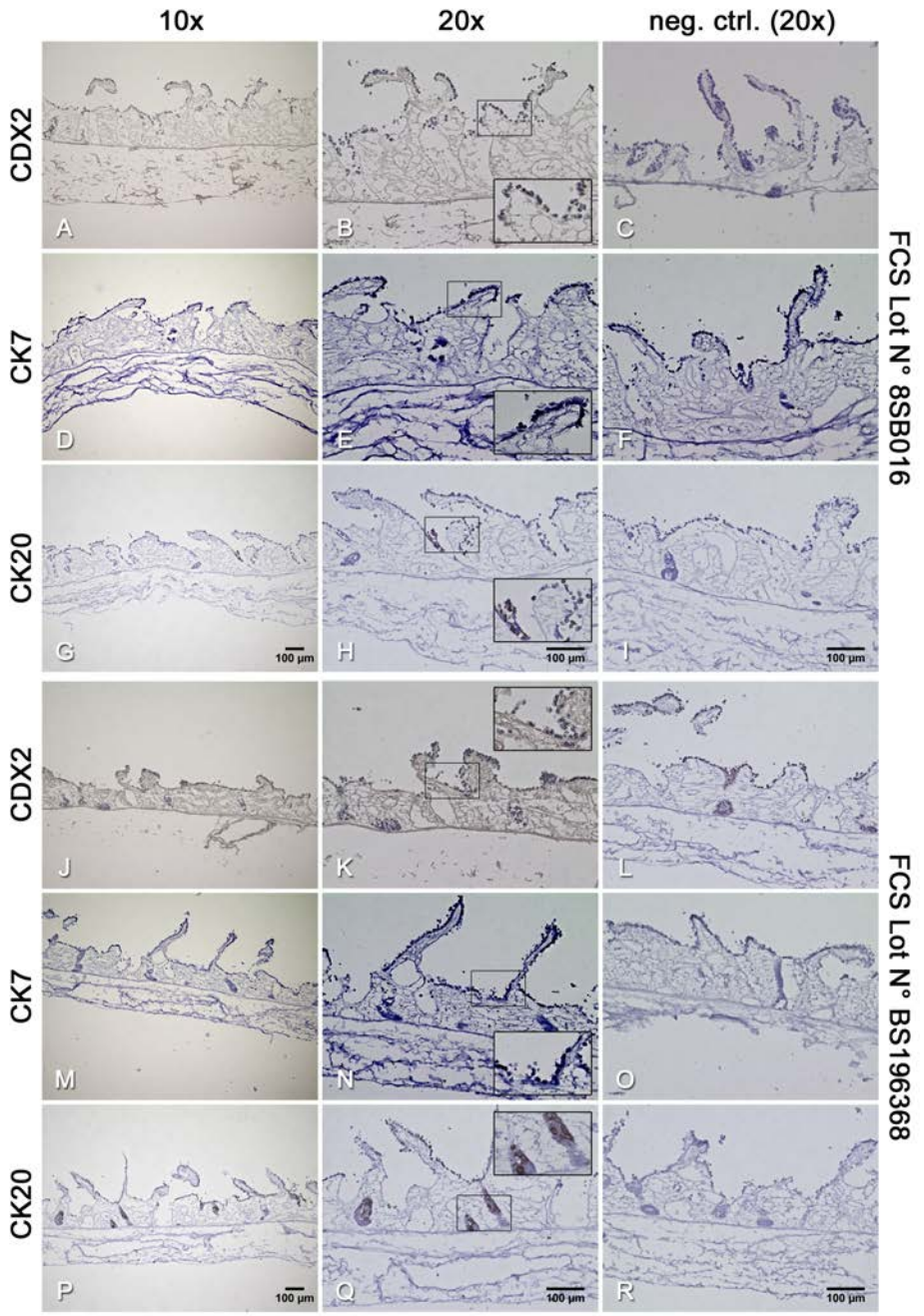

Figure 3.20: Immunohistochemical staining (DAB) for CDX2, CK7 and CK20 for HROC24 cells cultured with two different FCS batches (Lot N° 8SB016 and Lot N° BS196368) in static 3D culture. There were no differences between the two FCS batches regarding the expression of CDX2 (A/B and J/K) or CK7 (D/E and M/N). However, there were more CK20 positive HROC24 cells when being cultured with FCS Lot N° BS196368 (P/Q) compared to FCS Lot N° 8SB016 (G/H). The negative control (neg. ctrl.; secondary antibodies only, C/F/I/L/O/R) showed the specificity for the primary antibodies. Scale bars in G and P (10x): 100 µm for A/D/G and J/M/P. Scale bars in H, I, Q, R (20x): 100 µm for B/C/E/F/H/I and K/L/N/O/Q/R.

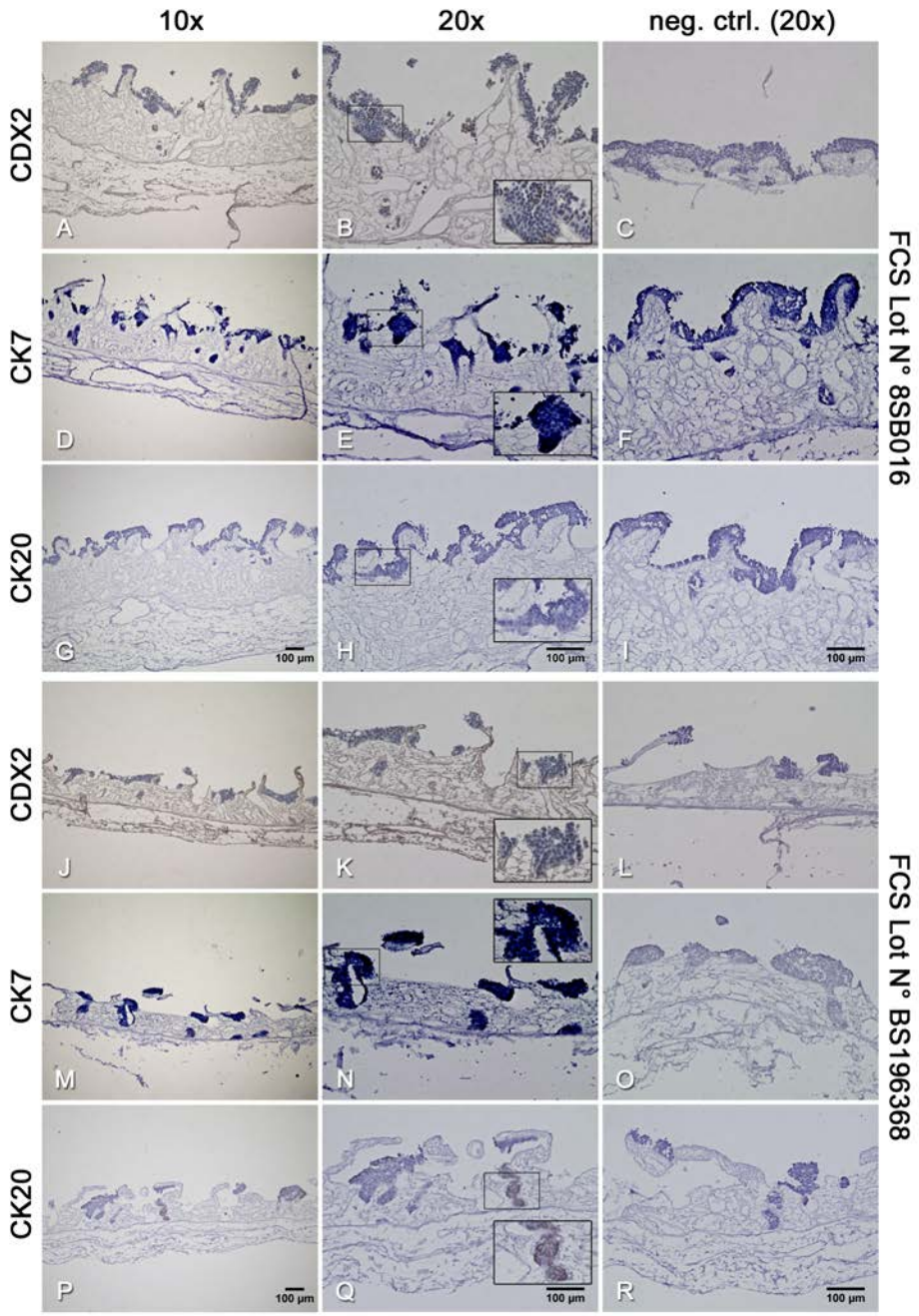

Figure 3.21: Immunohistochemical staining (DAB) for CDX2, CK7 and CK20 for HROC87 cells cultured with two different FCS batches (Lot N° 8SB016 and Lot N° BS196368) in static 3D culture. There were no differences between the two FCS batches regarding the expression of CDX2 (A/B and J/K) or CK7 (D/E and M/N). The CK20 expression differed between FCS Lot N° 8SB016 (G/H, all cells negative) and FCS Lot N° BS196368 (P/Q, single cells positive). The negative control (neg. ctrl.; secondary antibodies only, C/F/I/L/O/R) showed the specificity for the primary antibodies. Scale bars in G and P (10x): 100 µm for A/D/G and J/M/P. Scale bars in H, I, Q, R (20x): 100 µm for B/C/E/F/H/I and K/L/N/O/Q/R.

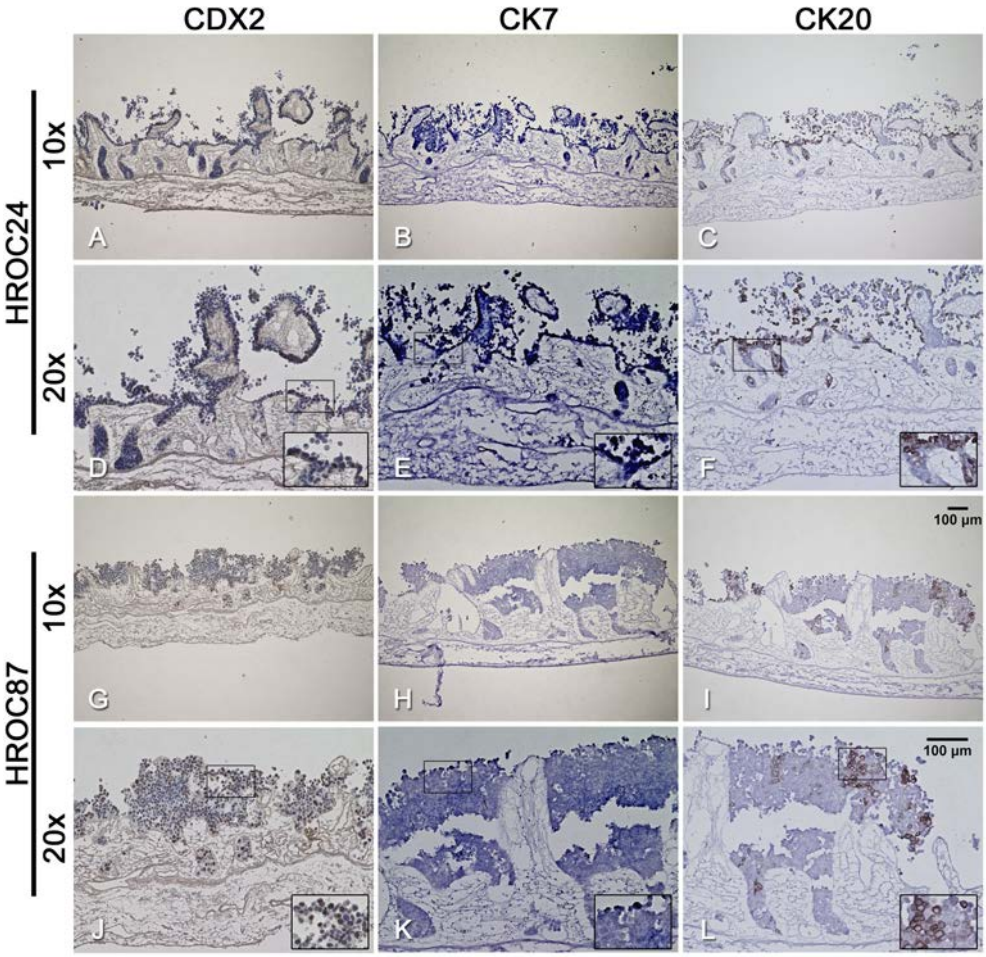

Figure 3.22: Immunohistochemical staining (DAB) for CDX2, CK7 and CK20 of HROC24 cells (A–F) and HROC87 cells (G–L) cultured in dynamic 3D conditions (FCS Lot N° BS196368). There were only few HROC24 cells detected to be stained for CDX2 (A/D). In contrast, more HROC87 cells were expressing CDX2 with staining of the cell nuclei (G/J). The marker CK7 could neither be detected in HROC24 cells (B/E) nor in HROC87 cells (H/K). Single HROC24 and HROC87 cells, which were heterogeneously distributed, showed expression of CK20 (C/F and I/L). Scale bar in I (10x): 100 µm for A–C and G–I. Scale bar in L (20x): 100 µm for D–F and J–L.

3.3.1.4 IHC stainings of the tumour stem cell markers CD44, CD133, CD166, and EpCAM

The cancer cells' expression of the putative tumour stem cell markers CD44, CD133, CD166 and EpCAM is thought to be correlated with increased resistance against chemotherapy and the ability to initiate distant metastases [127].

CD44 was neither expressed by HROC24 cells (fig. 3.23 A/B and M/N) nor HROC87 cells (fig. 3.24 A/B and M/N) in conventional 2D culture independent on the used FCS. Both cell lines neither expressed the marker CD166 (fig. 3.23 and 3.24 G/H and S/T). There were no differences concerning the expression of the markers CD133 (fig. 3.23 and 3.24 D/E and P/Q) and EpCAM (fig. 3.23 and 3.24 J/K and V/W) between the two FCS batches N° 8SB016 and N° BS196368. The negative control (neg. ctrl.; secondary antibodies only, fig. 3.23 and 3.24 C/F/I/L and O/R/U/X) revealed the primary antibodies' specificity for the antigens CD44, CD133, CD166 and EpCAM.

In comparison, both cell lines showed an expression of all the investigated tumour stem cell markers in static 3D culture. Figures 3.25 and 3.26 display IHC stainings with DAB for HROC24 cells cultured with the two FCS batches Lot N° 8SB016 and N° BS196368. The staining for CD44 (fig. 3.25 A–C and G–I), CD133 (fig. 3.25 D–F and J–L), CD166 (fig. 3.26 A–C and G–I), and for EpCAM (fig. 3.26 D–F and J–L) did not differ between the two used FCS batches. The cell line HROC24 built monolayers on top of the SISmuc as well as partially filled the former crypts. The cells on top of the scaffold showed a stronger staining of the investigated markers than of the cells grown inside the former crypts. Especially, this was pronounced in the staining for EpCAM where only the cells grown on top of the SISmuc were found to be stained (fig. 3.26 D/E and J/K).

The cell line HROC87 did not grow as a monolayer but in multilayered cell clumps scattered on top of the scaffold. They showed a tendency to grow inside the former crypts of the SISmuc. As for HROC24 cells, HROC87 cells cultured in static 3D conditions showed expression of all examined tumour stem cell markers which did not differ between the used FCS. Cells on top of the scaffold and on the margins of cell clumps showed a strong staining for CD44 (fig. 3.27 A–C and G–I) as well as for CD133 (fig. 3.27 D–F and J–L). The cells were all stained for the marker CD166 independent of the used two FCS batches in static 3D culture (fig. 3.28 A–C and G–I). There were neither differences found between the two FCS batches for the expression of EpCAM which could only be detected in cells at the margin of the cell clumps while cells within were not stained (fig. 3.26 D–F and J–L).

Dynamically cultured HROC24 and HROC87 cells displayed an enhanced tumour cells growth (fig. 3.29). HROC24 cells grew monolayer-like as in static 3D culture but they showed a tendency for higher agglomeration and they completely filled the former crypts of the scaffold (fig. 3.29 A–H). Especially, the cell line HROC87 showed an increased growth forming huge cell masses on top of the SISmuc and within the former crypts (fig. 3.29 I–P). The staining for CD44 of both cell lines (fig. 3.29 A/E and I/M) was weaker in comparison to the static cultured 3D models (fig. 3.25 A/B and 3.27 A/B). CD44 expression could be detected mainly in cells at the margin of cell masses on the apical side of the SISmuc and cells within were found to be only light stained at the cell membrane (fig. 3.29A/E and I/M). Both cell lines, HROC24 and HROC87 cells, showed a strong staining of CD133 with cells being stained in the cytoplasm and/or in the nucleus (fig. 3.29 B/I and J/N). CD166 displayed a heterogeneous distribution of stained cells with expression at the cell membrane (fig. 3.29 C/G and K/O). EpCAM expression was detected in HROC24 cells growing in monolayers and in few cells growing inside the former crypts, with a tendency for stronger staining of cells at the margins (fig. 3.29 D/H). Only single cells of the cell line HROC87 could be stained for EpCAM which mainly was expressed by cells grown on the apical side of the cell masses (fig. 3.29 L/P).

A comparison of conventional 2D cell culture and static 3D culture for both cell lines cultured with FCS Lot N° 8SB016 is displayed in figures 3.30 and 3.31. Here, the markers CD44 and CD166 were expressed by HROC24 cells (fig. 3.30 C/D and K/L) as well as by HROC87 cells (fig. 3.31 C/D and K/L) in contrast to the conventional 2D culture (fig. 3.30 and 3.31 A/B and I/J).

The expression of the tumour stem cell markers was heterogeneous in the sections of the colon adenocarcinoma (fig. 3.32 C/G/K/O). The tumour stroma was CD44-positive and tumour cells partially expressed this antigen (fig. 3.32 C) whereas in the healthy colon (fig. 3.32 D) only stromal cells were stained for CD44. In the static 3D tumour models of HROC24 cells (fig. 3.32 A) and HROC87 cells (fig. 3.32 B), CD44 was expressed by both cell lines. The staining against the marker CD133 in the colon adenocarcinoma (fig. 3.32 G) was weaker in comparison to the 3D tumour models (fig. 3.32 E/F) or the healthy colon (fig. 3.32 H) in which only enterocytes were detected to be stained. Furthermore, not all tumour cells within the colon adenocarcinoma were CD166-positive, some tumour cells were not stained at all (fig. 3.32 K). However, both cell lines within the 3D tumour model expressed CD166 (fig. 3.32 I/J), but not all HROC87 cells (J) were stained. In the healthy colon, CD166 expression was restricted to the crypts' cells (fig. 3.32 L). The expression of the marker EpCAM was restricted to the outer cells of the cell layers of the 3D tumor

models and cells in the center of the cell masses were negative (fig. 3.32 M/N). The staining for EpCAM in the colon adenocarcinoma was weaker and only single cells were detected to be stained (fig. 3.32 O). In the healthy colon, not all of the enterocytes within the crypts expressed this marker (fig. 3.32 P).

The stainings for the tumour stem cell markers of both, static and dynamic, HROC87 3D culture models and the respective xenograft tumour models are displayed in figure 3.33. CD44 showed a strong staining in the static 3D model (fig. 3.33 A) and a lighter staining in dynamically cultured HROC87 cells (E). For static and dynamic 3D culture, the cell membranes were predominantly stained for CD44. In both examined xenograft tumours (I and M), only few cells were expressing CD44. CD133 expression was heterogeneously distributed in all tumour models with less cells stained in the xenografts (fig. 3.33 B, F and J/K). Especially in the dynamic 3D culture, the cells showed a more pronounced CD133 staining of the cell nuclei (F). The staining for CD166 did not differ between static and dynamic 3D culture (fig. 3.33 C and G) in contrast to the strongly stained xenograft tumours (K and O). Only the apical cells showed an expression of EpCAM in the static and dynamic 3D models (fig. 3.33 D and H) and most of the cells were negative for this marker. In the xenograft tumours, EpCAM was similarly stronger stained at the tumour's margins (fig. 3.33 L and P), but xenograft tumour 2 was additionally stained throughout the tumour tissue (P). Altogether, the xenograft tumours presented a more diffuse morphology including stromal cells of murine origin compared to the more dense tumour cell aggregates in the 3D models.

3.3.1.5 Analysis of EMT in the models: The expression of E-Cadherin/β-Catenin and Pan-Cytokeratin/Vimentin

The expression of the EMT markers E-cadherin/β-catenin and PCK/vimentin of both cell lines, HROC24 and HROC87, was analysed by IF double stainings of cells cultured in conventional 2D culture and static 3D culture.

Figure 3.34 represents an immunofluorescence staining for E-cadherin and β-catenin in HROC24 cells (A–H) as well as HROC87 cells (I–P) cultured in conventional 2D culture (A–D and I–L) and static 3D culture (E–H and M–P). The co-localisation of both proteins in the merged channels (D/H/L/P) resulted in a yellow staining where both markers were co-localised. Especially, HROC87 cells displayed an increased co-localisation of E-cadherin and β-catenin in the apical cells of the dense cell clusters in 3D cell culture (fig. 3.34 P).

The immunofluorescence stainings of HROC24 and HROC87 cells for PCK and vimentin are depicted in figure 3.35 for cells being cultured in conventional 2D as well as static 3D culture. Both cell lines expressed the epithelial marker

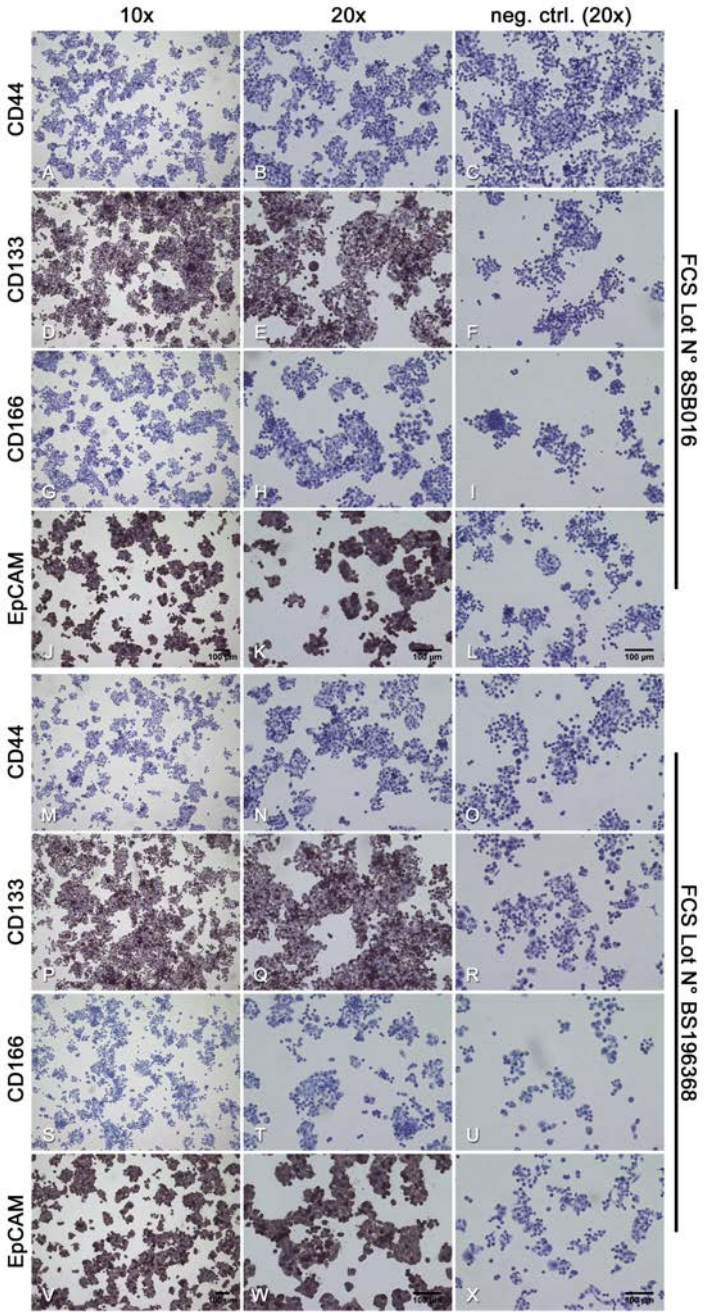

Figure 3.23: Immunohistochemical staining (DAB) for the tumour stem cell markers CD44, CD133, CD166, and EpCAM in conventional 2D culture of HROC24 cells. Neither the markers CD44 (A/B and M/N) nor CD166 (G/H and S/T) were expressed in any cell independent of the used FCS batches. However, the cells showed staining for the markers CD133 (D/E and P/Q) and EpCAM (J/K and V/W) in both FCS batches. The negative control (neg. ctrl.; secondary antibodies only, C/F/I/L and O/R/U/X) confirmed the specificity for the used primary antibodies. Scale bars in J, V: 100 µm for A/D/G/J and M/P/S/V. Scale bars in K, L and W, X: 100 µm for B/C/E/F/H/I/K/L and N/O/Q/R/T/U/W/X.

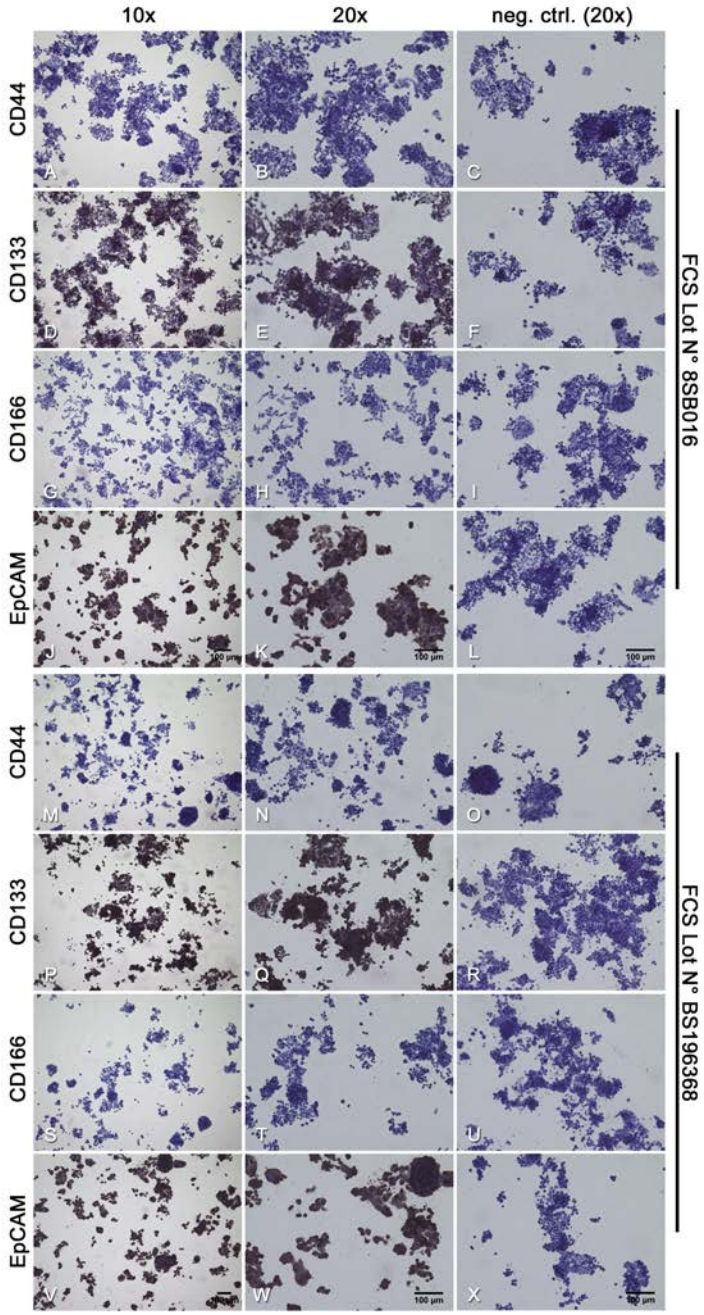

Figure 3.24: Immunohistochemical staining (DAB) for the tumour stem cell markers CD44, CD133, CD166, and EpCAM in conventional 2D culture of HROC87 cells. Neither the marker CD44 (A/B and M/N) nor CD166 (G/H and S/T) were expressed in any cell independent of the used FCS batches. However, the cells were stained for the markers CD133 (D/E and P/Q) and EpCAM (J/K and V/W) in both FCS batches. The negative control (neg. ctrl.; secondary antibodies only, C/F/I/L and O/R/U/X) revealed the specificity for the used primary antibodies. Scale bars in J, V (10x): 100 µm for A/D/G/J and M/P/S/V. Scale bars in K, L, W, X (20x): 100 µm for B/C/E/F/H/I/K/L and N/O/Q/R/T/U/W/X.

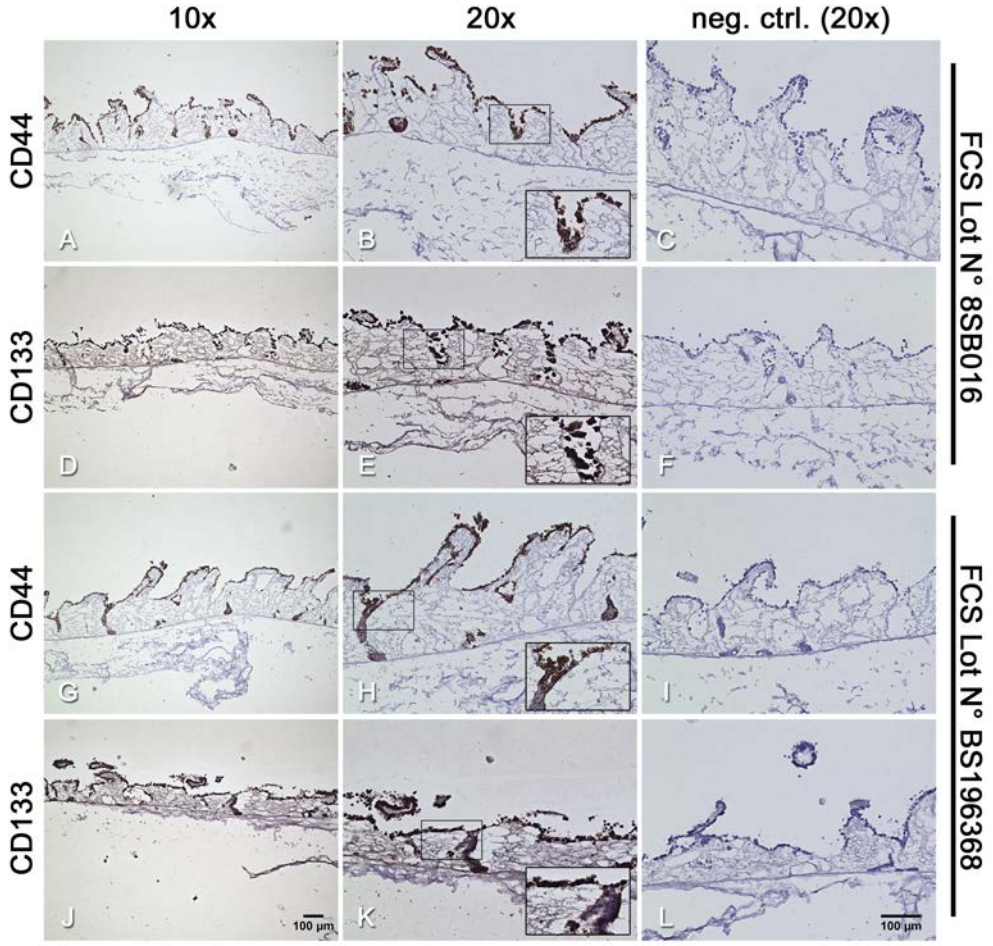

Figure 3.25: Immunohistochemical staining (DAB) for the tumour stem cell markers CD44 and CD133 of HROC24 cells cultured in static 3D culture with two different FCS batches (FCS Lot N° 8SB016 and N° BS196368). The staining of both markers, CD44 (A/B and G/H) and CD133 (D/E and J/K), displayed that almost all cells were stained independent of the used FCS. The negative control (neg. ctrl.; secondary antibodies only, C/F/I/L) confirmed the specificity for the used primary antibodies. Scale bar in J (10x): 100 µm for A/D/G/J. Scale bar in L (20x): 100 µm for B/C/E/F/H/I/K/L.

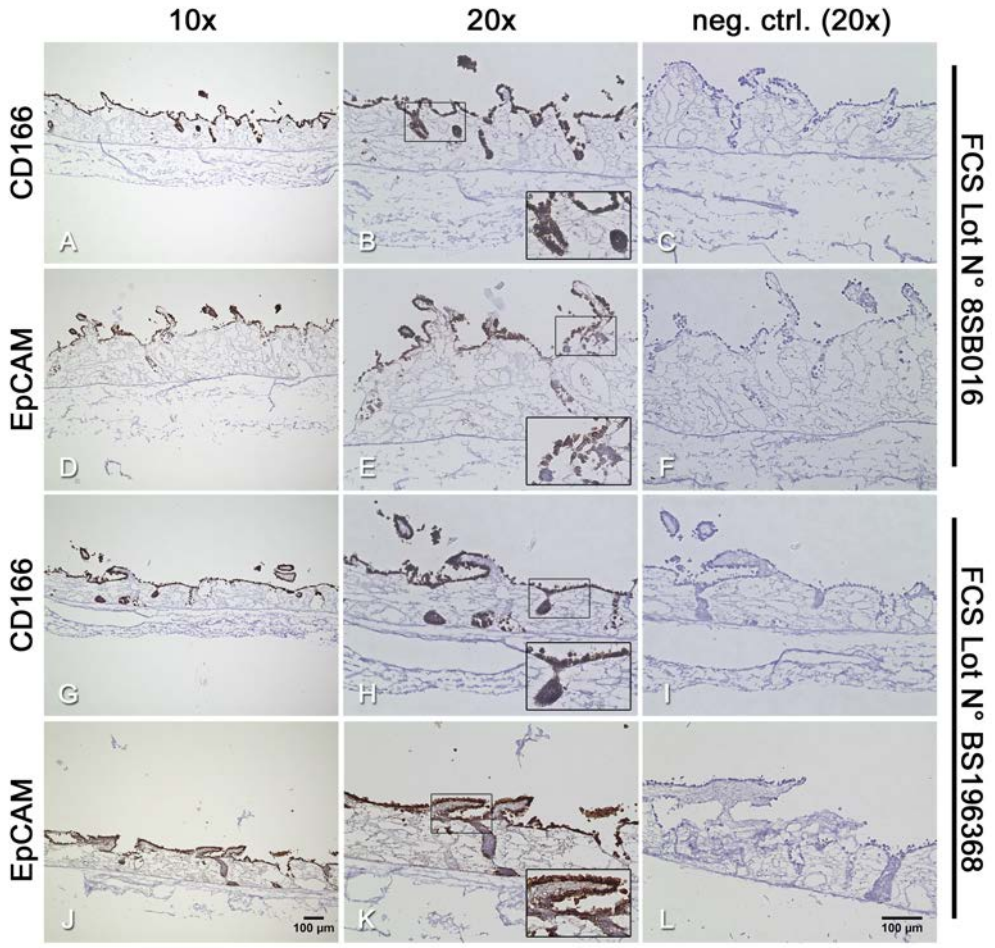

Figure 3.26: Immunohistochemical staining (DAB) for the tumour stem cell markers CD166 and EpCAM of HROC24 cells cultured in static 3D culture with two different FCS batches (FCS Lot N° 8SB016 and N° BS196368). CD166 (A/B and G/H) was expressed by almost every cell with a tendency to a stronger staining on top of the scaffold. EpCAM expression (D/E and J/K) was restricted to cells at the margin of cell masses and cells grown on top of the SISmuc. The negative control (neg. ctrl.; secondary antibodies only, C/F/I/L) confirmed the specificity for the used primary antibodies. Scale bar in J (10x): 100 µm for A/D/G/J. Scale bar in L (20x): 100 µm for B/C/E/F/H/I/K/L.

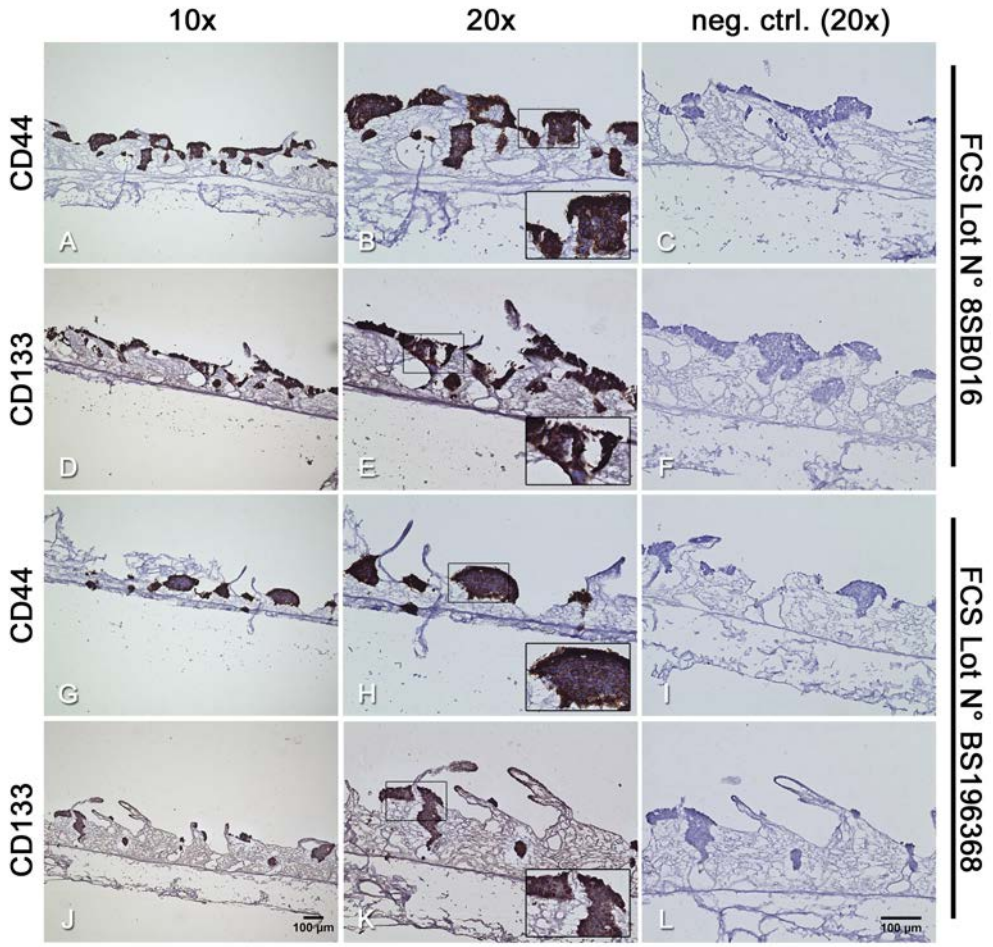

Figure 3.27: Immunohistochemical staining (DAB) for the tumour stem cell markers CD44 and CD133 of HROC87 cells cultured in static 3D culture with two different FCS batches (FCS Lot N° 8SB016 and N° BS196368). The staining of both markers, CD44 (A/B and G/H) and CD133 (D/E and J/K), displayed that most of the cells were stained independent of the used FCS. Staining of the markers was stronger at the margins of the cell masses than within. The negative control (neg. ctrl.; secondary antibodies only, C/F/I/L) confirmed the specificity for the used primary antibodies. Scale bar in J (10x): 100 µm for A/D/G/J. Scale bar in L (20x): 100 µm for B/C/E/F/H/I/K/L.

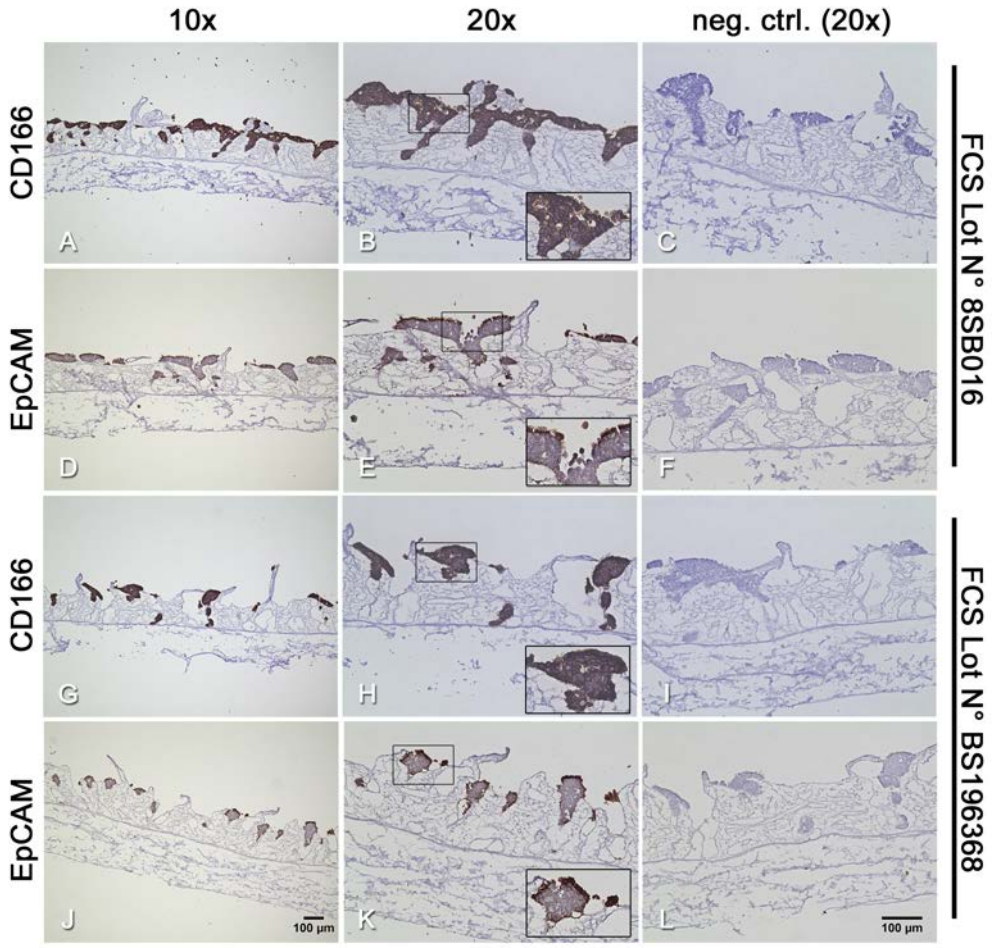

Figure 3.28: Immunohistochemical staining (DAB) for the tumour stem cell markers CD166 and EpCAM of HROC87 cells cultured in static 3D culture with two different FCS batches (FCS Lot N° 8SB016 and N° BS196368). CD166 (A/B and G/H) was expressed by most of the cells with a tendency to a stronger staining on top of the scaffold. EpCAM expression (D/E and J/K) was restricted to cells at the margin of cell masses and cells grown on top of the SISmuc. The negative control (neg. ctrl.; secondary antibodies only, C/F/I/L) confirmed the specificity for the used primary antibodies. Scale bar in J (10x): 100 µm for A/D/G/J. Scale bar in L (20x): 100 µm for B/C/E/F/H/I/K/L.

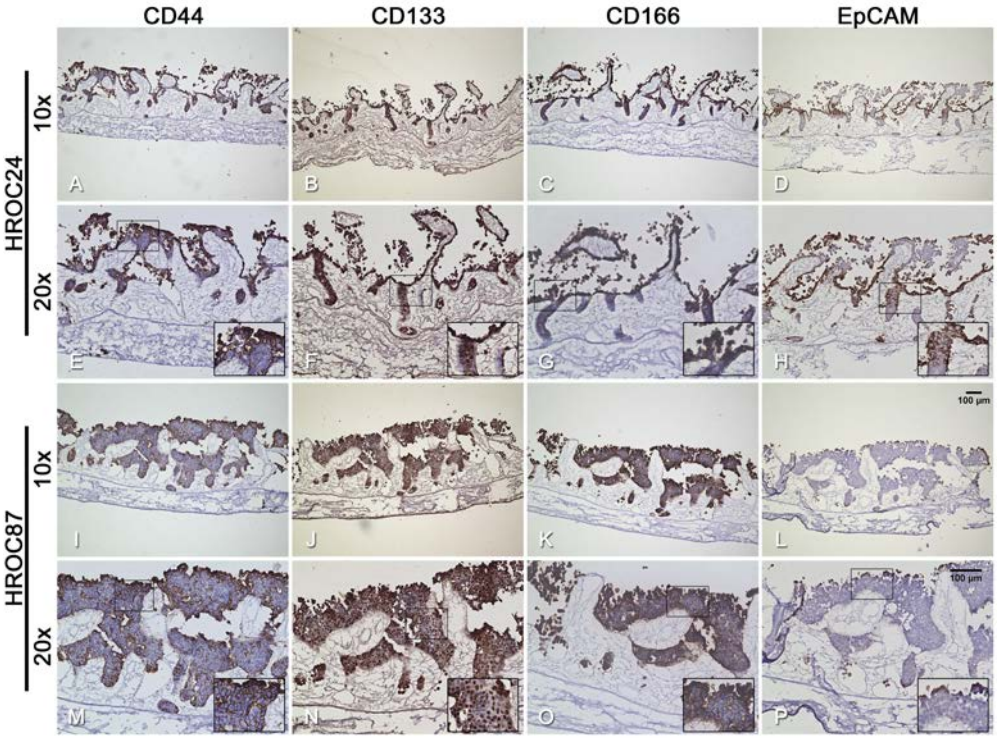

Figure 3.29: Immunohistochemical staining (DAB) for the tumour stem cell markers CD44, CD133, CD166, and EpCAM of HROC24 cells (A–H) as well as HROC87 cells (I–P) cultured in dynamic 3D culture (FCS Lot N° BS196368). CD44 expression was pronounced in cells grown at the margins of the cell masses (A/E and I/M). CD133 showed a strong staining which could be detected in the cells' cytoplasm and nuclei (B/F and J/N). CD166 displayed a heterogeneous distribution of stained cells (C/G and K/O). EpCAM expression was detected in HROC24 cells growing in monolayers and in few cells growing inside the former crypts (D/H). Only few EpCAM-positive HROC87 cells were found (L/P) and the expression of EpCAM could only be detected in cells grown at the apical side of cell clumps. Scale bar in L (10x): 100 µm for A–D and I–L. Scale bar in P (20x): 100 µm for E–H and M–P.

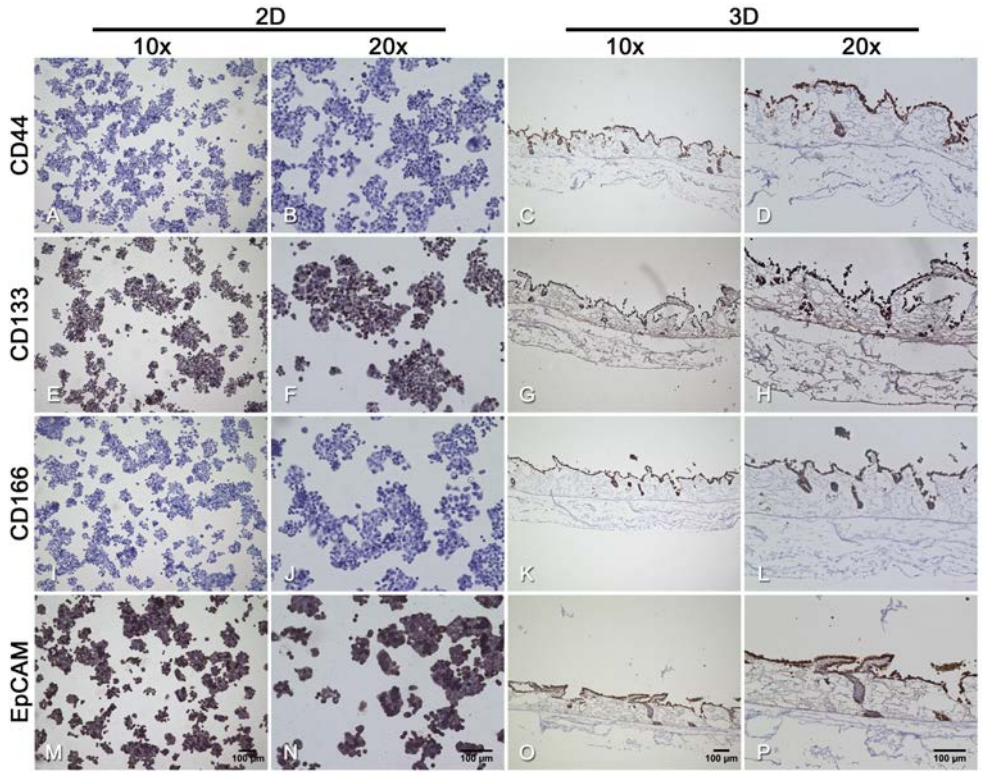

Figure 3.30: Immunohistochemical staining (DAB) for the tumour stem cell markers CD44, CD133, CD166, and EpCAM of HROC24 cells cultured in conventional 2D culture and in static 3D culture (FCS Lot N° 8SB016). The cells were positive for CD44 in 3D culture (C/D) but they did not express CD44 in 2D culture (A/B). CD166 was stained in the same pattern (I/J and K/L). Both markers, CD133 (E/F/G/H) and EpCAM (M/N/O/P), were expressed in 2D culture as well as in 3D culture. Scale bars in M and O (10x): 100 µm for A/E/I/M and C/G/K/O. Scale bars in N and P (20x): 100 µm for B/F/J/N and D/H/L/P.

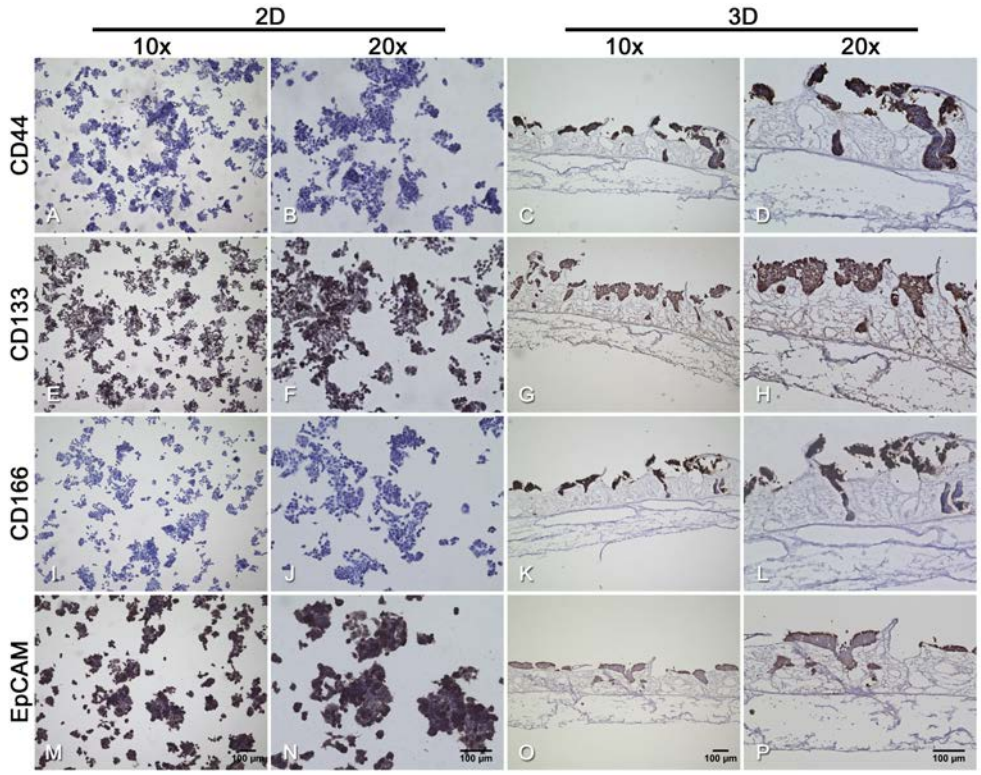

Figure 3.31: Immunohistochemical staining (DAB) for the tumour stem cell markers CD44, CD133, CD166, and EpCAM of HROC87 cells cultured in conventional 2D culture and in static 3D culture (FCS Lot N° 8SB016). The cells were positive for CD44 in 3D culture (C/D) but they did not express CD44 in 2D culture (A/B). CD166 was stained in the same pattern (I/J and K/L). Both markers, CD133 (E/F/G/H) and EpCAM (M/N/O/P), were expressed in 2D culture as well as in 3D culture. Scale bars in M and O: 100 µm for A/E/I/M and C/G/K/O. Scale bars in N and P: 100 µm for B/F/J/N and D/H/L/P.

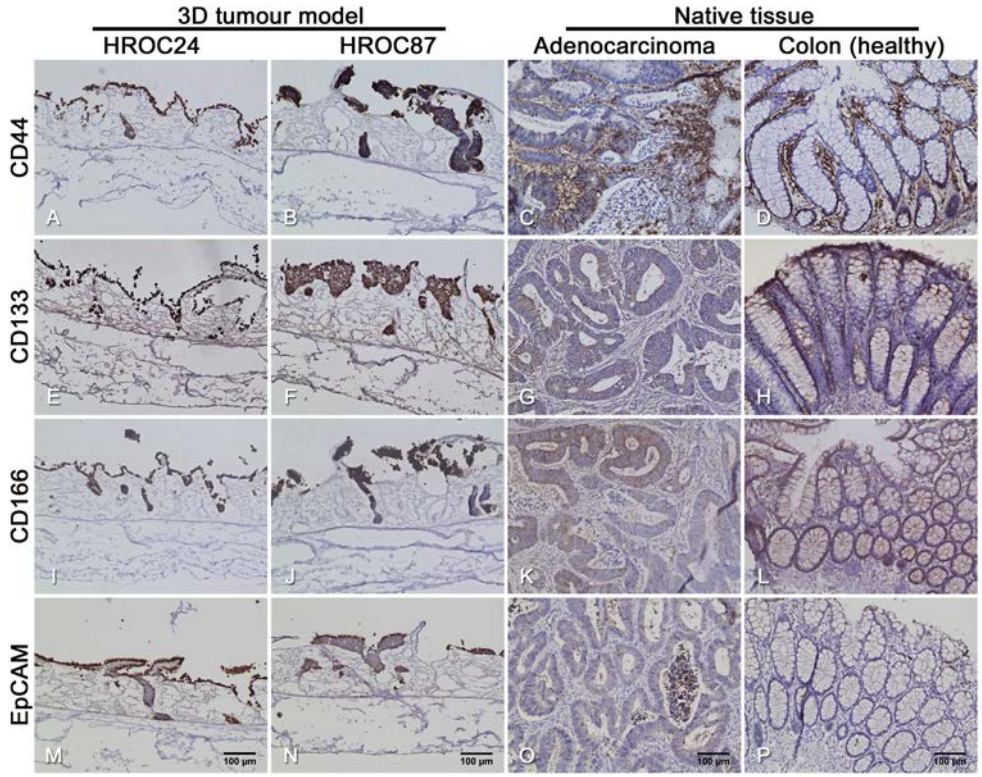

Figure 3.32: Immunohistochemical staining (DAB) for the tumour stem cell markers CD44, CD133, CD166, and EpCAM of the static 3D tumour models (HROC24 and HROC87 cells, FCS Lot N° 8SB016) and native tissues (colon adenocarcinoma and healthy colon). CD44 was expressed by HROC24 cells (A) and HROC87 cells (B), its expression in the colon adenocarcinoma (C) was heterogeneous and not all tumour cells were positive for this marker. In the healthy colon, only stromal cells were positive for CD44 only (D). Both 3D tumour models expressed the marker CD133 (E/F) whereas in the colon adenocarcinoma (G) only single cells were marked positively; the healthy colon (H) displayed CD133-positive enterocytes. Most of HROC24 and HROC87 cells were stained for CD166 (I and J) in contrast to the section of the colon adenocarcinoma in which not all cells expressed this marker (K). The enterocytes in the section of the healthy colon were stained CD166-positive (L). The 3D tumour models showed staining for the marker EpCAM (M and N) but the tumour cells of the colon adenocarcinoma were stained more lightly (O), and the enterocytes of the healthy colon (P) were almost not stained. Scale bars in M, N, O, and P: 100 µm for A to P.

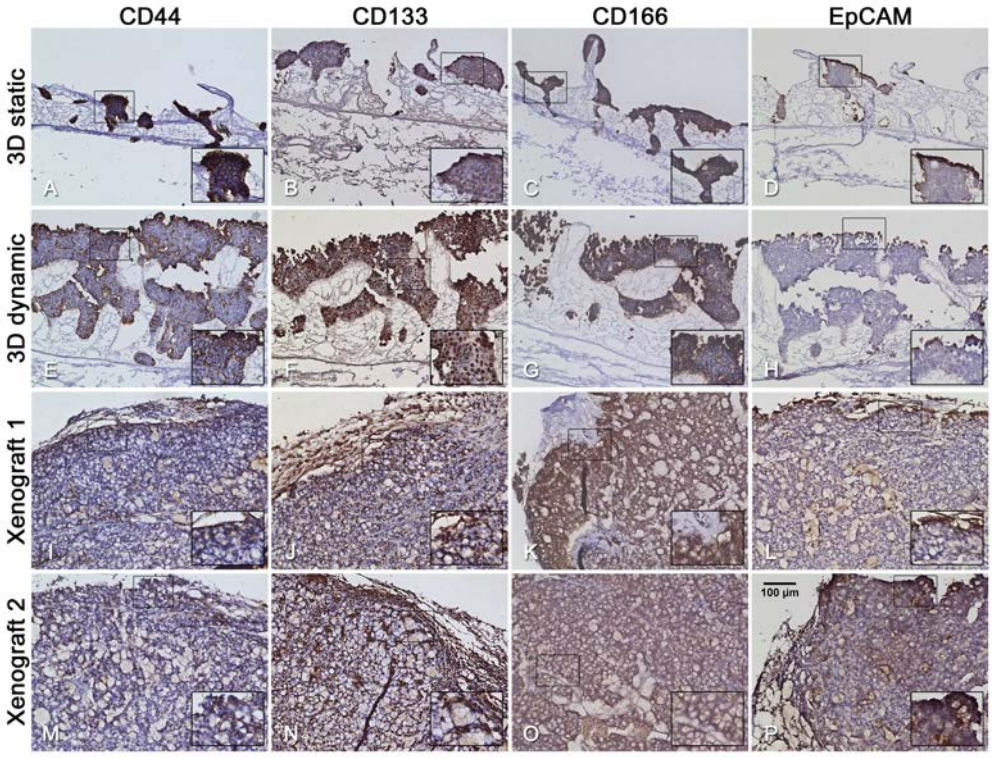

Figure 3.33: Immunohistochemical staining (DAB) for the tumour stem cell markers CD44, CD133, CD166, and EpCAM of HROC87 cells cultured in static and dynamic 3D conditions (FCS Lot N° BS196368) as well as of two representative HROC87 xenograft models. In comparison to the static (A) and dynamic (E) 3D model, only few cells were stained for CD44 in the xenograft tumours (I/M). The staining for the marker CD133 was more pronounced in the dynamic 3D culture (F) than in the static model (B) where most of the cells were only light stained. The xenograft tumours (J/N) showed a stronger staining with a heterogeneous distribution of CD133 expressing cells. The CD166 staining intensity and pattern was comparable for the static (C) and dynamic (G) 3D culture. However, in the xenograft tumours (K/O), there could be observed a strong staining for CD166 of the tumour cells. The expression of EpCAM was limited to apical cells in both, static (D) and dynamic (H), 3D tumour models and most of the cells were not stained. Both shown xenograft models (L/P) displayed a comparable strong staining, with the xenograft 1 (L) showing expression of EpCAM mainly at the tumour's margins while xenograft 2 (P) was stained heterogeneously throughout the tumour tissue. Scale bar in P (20x): 100 µm for A to P.

PCK in 2D culture (fig. 3.35 B and J) and 3D culture (fig. 3.35 F and N) whereas no vimentin expression could be detected in any cell (fig. 3.35 C/G and K/O).

The comparison of the cell line HROC87 (2D and static 3D culture) and the respective mouse xenograft model as well as a colon adenocarcinoma is displayed in figure 3.36. HROC87 cells expressed PCK in conventional 2D culture (E) as well as static 3D culture (F) but no vimentin expression could be detected. In the xenograft model of the cell line HROC87 (C/G/K/O), the tumour cells were positive for PCK (G). Some cells which are probably stromal cells of murine origin expressed vimentin (K). The colon adenocarcinoma (D/H/L/P) revealed PCK expression of the tumour cells (H) and vimentin expression in the tumour stroma (L). The exemplary tumour of the xenograft model had a spongy morphology (O) and the cells did not form such dense clusters as in the static 3D model and the colon adenocarcinoma.

3.3.2 Testing a targeted therapy commonly used in the clinic: Vemurafenib and Gefitinib

The *BRAF*-mutant CRC cell lines HROC24 and HROC87 were treated in monotherapy with the EGFR inhibitor gefitinib (Iressa®) or the BRAF inhibitor vemurafenib (PLX4032, Zelboraf®) and with the combination of both drugs as mentioned in 2.2.1.9. The cells' response was assessed by several read-outs including (immuno-)histological analyses (morphological changes, changes in marker expression, proliferation), apoptosis and biochemical methods (western blot).

3.3.2.1 Morphological changes and EMT marker expression caused by the different treatments

For the testing of morphological changes of the single cells and of the cell aggregates after treatment, a H&E staining was performed. The H&E staining for both cell lines, HROC24 and HROC87, cultured with two different FCS batches is displayed in figures 3.37 and 3.38.

For FCS Lot N° 8SB016 (fig. 3.37 A–H), HROC24 cells grew in monolayers on the whole surface of the SISmuc as well as inside the crypts of the former mucosa in the untreated control (A/E) and when treated with gefitinib (B/F). In contrast, the cell monolayer was discontinuous after treatment with vemurafenib (C/G) and total cell number was decreased on the scaffold. Only few cells survived when treated with a combination of both drugs (D/H). When cultured in medium containing FCS Lot N° BS196368 (I–P), the cell monolayers were

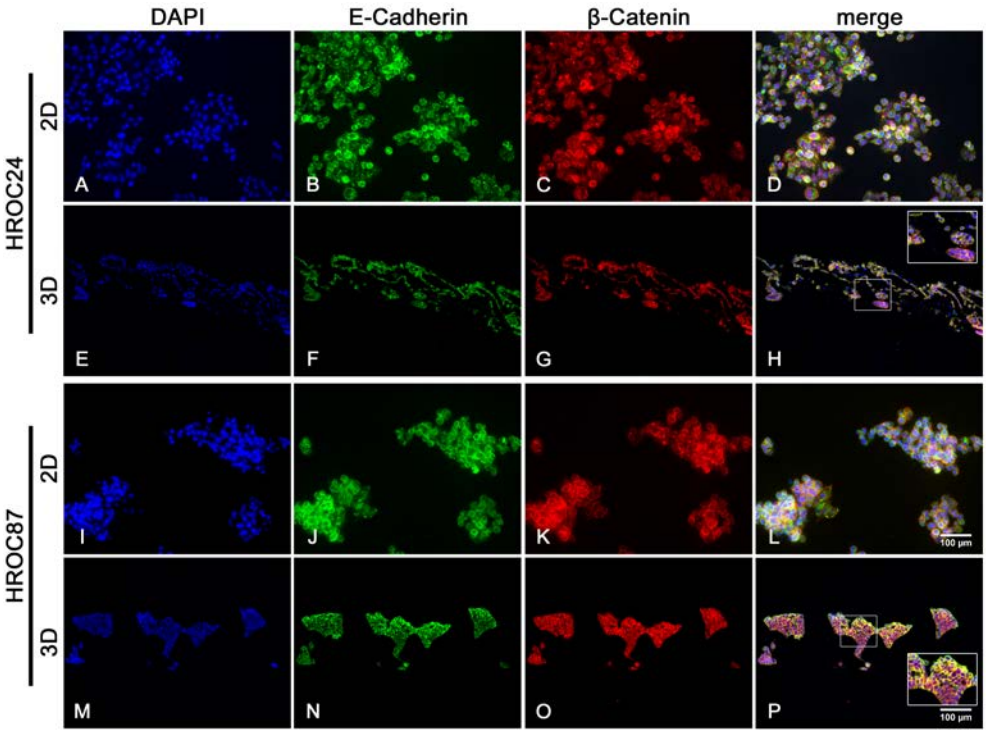

Figure 3.34: Immunofluorescence staining for E-cadherin and β-catenin in HROC24 and HROC87 cells cultured in conventional 2D and static 3D culture (FCS Lot N° 8SB016). E-Cadherin as well as β-catenin were expressed by both cell lines in 2D culture (B/C and J/K) and 3D culture (F/G and N/O). The co-localisation of both proteins is displayed in yellow when the different channels are merged (D/H and L/P). The DAPI channel (A/E and I/M) shows the cell nuclei. Scale bars in L and P: 100 µm for A to P.

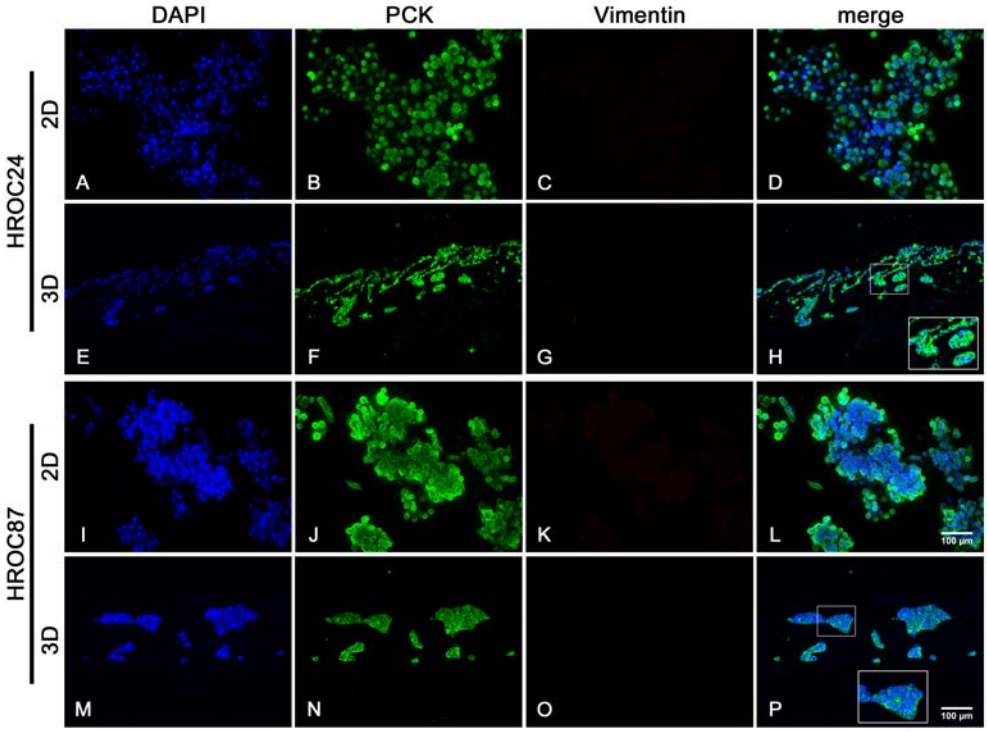

Figure 3.35: Immunofluorescence staining for pan-cytokeratin (PCK) and vimentin in HROC24 and HROC87 cells cultured in conventional 2D and static 3D culture (FCS Lot N° 8SB016). PCK was expressed in both cell lines in 2D culture (B and J) and 3D culture (F and N). The mesenchymal marker vimentin could not be detected in any cell (C/G and K/O). The DAPI channel (A/E and I/M) displays the cell nuclei. Scale bars in L and P: 100 µm for A to P.

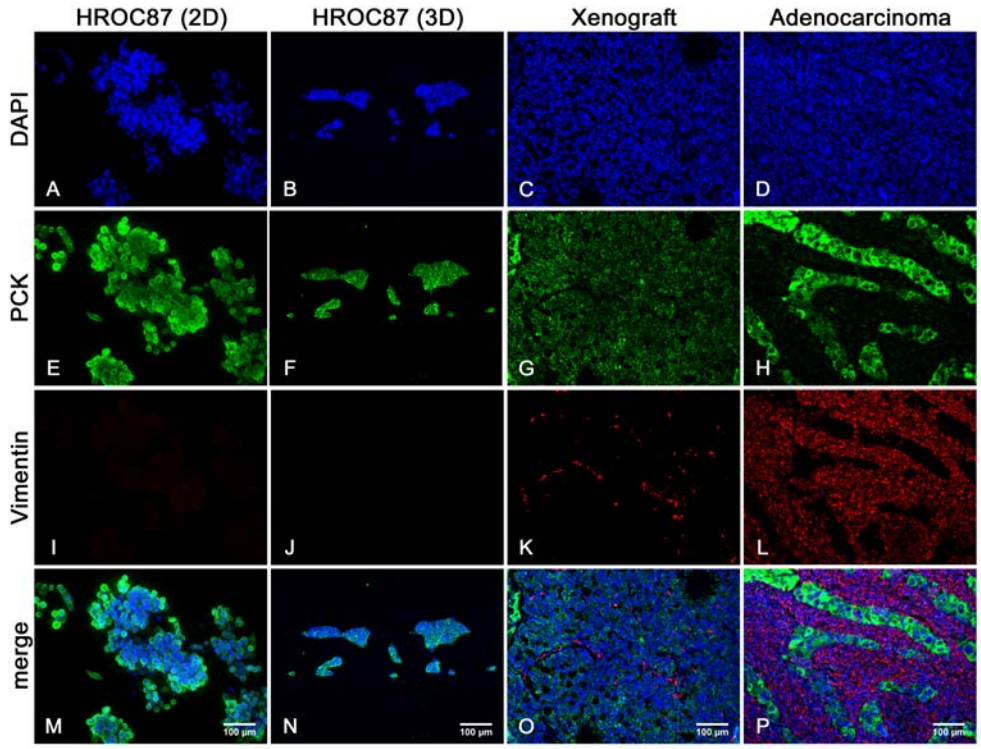

Figure 3.36: Immunofluorescence staining for pan-cytokeratin (PCK) and vimentin in HROC87 cells cultured in conventional 2D cell culture (A/E/I/M) and static 3D culture (B/F/J/N), as well as in a xenograft tumour (C/G/K/O) and in a colon adenocarcinoma (D/H/L/P). HROC87 cells expressed the epithelial marker PCK in 2D culture (E) and 3D culture (F) but not the mesenchymal intermediate filament protein vimentin (I and J). As for the 3D tumour model, HROC87 cells showed expression of PCK in the xenograft (G). Furthermore, there were some single cells positive for vimentin (K), probably stromal cells of murine origin. Also, the tumour cells in the colon adenocarcinoma expressed PCK (H) resembling the cell clusters in the 3D tumour model (F). In contrast, the adenocarcinoma exhibited a vimentin-positive tumour stoma (L). The DAPI channel (A–D) displays the cell nuclei, merged channels are shown in subfigures M/N/O/P. Scale bars in M, N, O, and P: 100 µm for A to P.

discontinuously in the control (I/M) and in the group treated with gefitinib (J/N). There were less HROC24 cells left after vemurafenib treatment (K/O) and the combination therapy (L/P) as compared to the untreated control or the cells treated with gefitinib.

In contrast to the cell line HROC24, HROC87 cells grew in multi-layers forming dense cell clusters and partially filled the former crypts of the mucosa (fig. 3.38). For cells cultured in medium containing FCS Lot N° 8SB016 (A–H), there was no significant reduction of the cell number of cells being treated with gefitinib (B/F), vemurafenib (C/G) and the combination therapy (D/H), respectively, when compared to the untreated control (A/E). In contrast, cells cultured with FCS Lot N° BS196368 (I–P) showed less cell clusters and in total there were less cells visible on the scaffold. There were no differences between cells treated with gefitinib (J/N) or vemurafenib (K/O) and the untreated control (I/M). Only the combination of both drugs (L/P) decreased the cell number and single cells were scattered over the SISmuc.

The immunofluorescence stainings for the EMT markers E-cadherin and β-catenin in HROC24 cells are shown in figure 3.39. The cells were cultured in static 3D culture with medium containing FCS Lot N° 8SB016. E-cadherin (E–H) expression did not change when the cells were treated with gefitinib (F), vemurafenib (G) or a combination of both drugs (H) compared to the untreated control (E). B-catenin (I–L) staining was lighter within the vemurafenib (K) or combination therapy (L) group in comparison to the untreated control (I) and gefitinib (J). Co-localisation of both proteins can be observed in the merged channels (M–P). Especially, the control and gefitinib group showed a co-localisation resulting in a shift to yellow (M/N).

E-cadherin expression did not change during treatment with gefitinib, vemurafenib or a combination of both drugs when compared to the control in HROC87 cells (fig. 3.40 E–H). In comparison, β-catenin expression was weaker in the combination therapy group (L) than in the untreated control (I), gefitinib (J) or vemurafenib (K) group. Both proteins were co-localised in some cells (M–P).

The epithelial marker PCK was expressed in HROC24 cells (fig. 3.41 E–H) as well as in the cell line HROC87 (fig. 3.42 E–H). The PCK expression did not change during treatment with gefitinib (F), vemurafenib (G) or the combination of both drugs (H) compared to the control (E).

The intermediate filament protein vimentin could not be detected in the cell line HROC24 (fig. 3.41 I–L). In comparison, vimentin was detected in HROC87 cells treated with vemurafenib (fig. 3.42 K) but not in the control (I) or the

gefitinib (J) and the combination therapy (L) group, respectively.

In static 3D CC with dermal fibroblasts, PCK expression did not change during treatment (fig. 3.43 E–H) as observed in the MC. Fibroblasts were stained for vimentin (fig. 3.43 I–L). There were no differences between the cells treated with gefitinib, vemurafenib or the combination of both drugs visible.

3.3.2.2 Analysis of proliferation in 3D tumour models: Ki-67 as a marker for proliferation

Proliferation was assessed by immunofluorescence staining for the marker Ki-67 which is expressed during all active phases of the cell cycle (late G_1, S, G_2 and mitosis) but it is absent in quiescent cells (G_0).

Figure 3.44 displays stainings for Ki-67 in the cell lines HROC24 (A–F) and HROC87 (G–L) as well as in two sections of a colon adenocarcinoma (M–R). Cells cultured in conventional 2D culture (A–C and G–I) showed a high proliferation rate indicated by a positive signal for Ki-67 in nearly every cell. In comparison, there were less cells expressing Ki-67 when cultured in static 3D culture (D–F and J–L). The two sections of a colon adenocarcinoma (M–R) demonstrated a heterogeneous distribution of proliferating cells within the tumour similar to the 3D tumour model where areas with more or less proliferating cells can be found.

After treatment with gefitinib (Gef.), vemurafenib (Vem.) or the combination of both drugs (Gef.+Vem.), the total cell number of HROC24 cells decreased in conventional 2D cell culture (fig. 3.45 A–D) but the cells were still proliferating after the different treatments (B–D). In the 3D tumour model, HROC24 cells exhibited a discontinuous monolayer when treated with vemurafenib (G) or the combination therapy (H) compared to the untreated control (Ctrl., E) and the gefitinib group (F), respectively. The cell line HROC87 showed no response to any treatment (N–P) in comparison to the untreated control (M) when cultured in static 3D culture.

The quantitation of Ki-67-positive cells (Ki-67 index) and the cell number per image for HROC24 and HROC87 cells are shown in figures 3.46 and 3.47, respectively.

In conventional 2D culture, HROC24 cells displayed a median Ki-67 index of 94.2 % in the control, 93.1 % when treated with gefitinib, 85.4 % with vemurafenib, and 81.2 % with both drugs (fig. 3.46 A). In comparison, proliferation was decreased in static 3D culture. The cells showed a median Ki-67 index of 13.9 % in the control, 11.6 % in the gefitinib group, 11.9 % in the vemurafenib group,

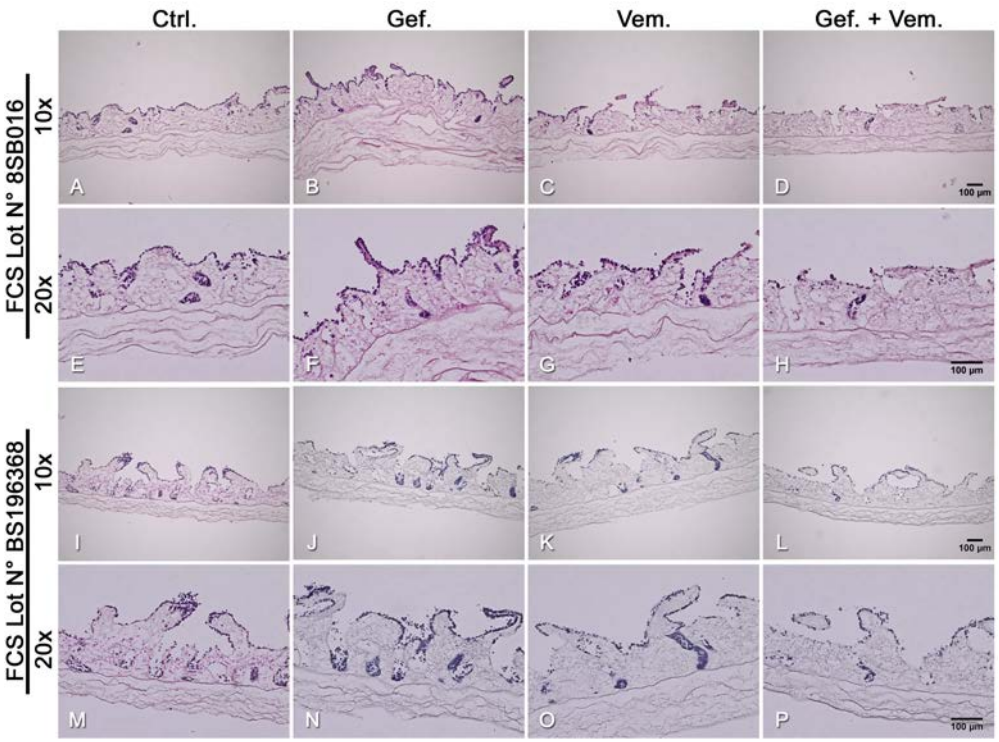

Figure 3.37: H&E staining of the static 3D tumour model of HROC24 cells treated with gefitinib (Gef., B/F/J/N) or vemurafenib (Vem., C/G/K/O) or a combination of both drugs (Gef.+Vem., D/H/L/P) for two different FCS batches. In FCS Lot N° 8SB016 (A–H), the cells filled the former crypts of the mucosa and grew in monolayers covering the SISmuc in the untreated control (Ctrl., A/E) as well as when treated with Gef. (B/F). The cells did not cover completely the scaffold after treatment with Vem. (C/G) compared to the Ctrl. and Gef. When treated with a combination of both drugs, only few cells survived (D/H). In FCS Lot N° BS196368 (I–P), the cell monolayer was not as pronounced as in cells cultured with FCS Lot N° 8SB016. Scale bars in D and L (10x): 100 µm for A–D and I–L. Scale bars in H and P (20x): 100 µm for E–H and M–P.

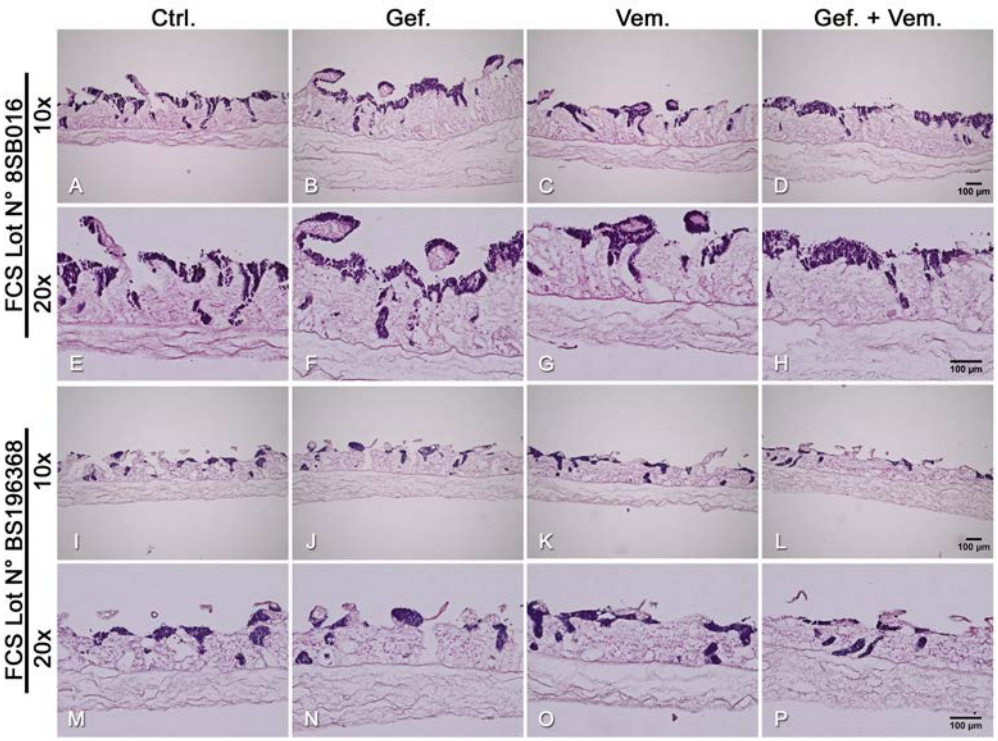

Figure 3.38: H&E staining of the static 3D tumour model of HROC87 cells treated with gefitinib (Gef., B/F/J/N) or vemurafenib (Vem., C/G/K/O) or a combination of both drugs (Gef.+Vem., D/H/L/P) for two different FCS batches. In FCS Lot N° 8SB016 (A–H), the tumour cells grew multi-layered forming dense clusters. The treatment with Gef. (B/F), Vem. (C/G) or the combination therapy (D/H) did not significantly reduce the cell number compared to the untreated control (Ctrl., A/E). In contrast, there were less cells on the scaffold when cultured with medium containing FCS Lot N° BS196368 (I–P). Also, there was no difference between the Ctrl. (I/M) and the cells being treated with Gef. (J/N) and Vem. (K/O) monotherapy, respectively. Only in the combination therapy (L/P), there were single cells left on the SISmuc. Scale bars in D and L (10x): 100 µm for A–D and I–L. Scale bars in H and P (20x): 100 µm for E–H and M–P.

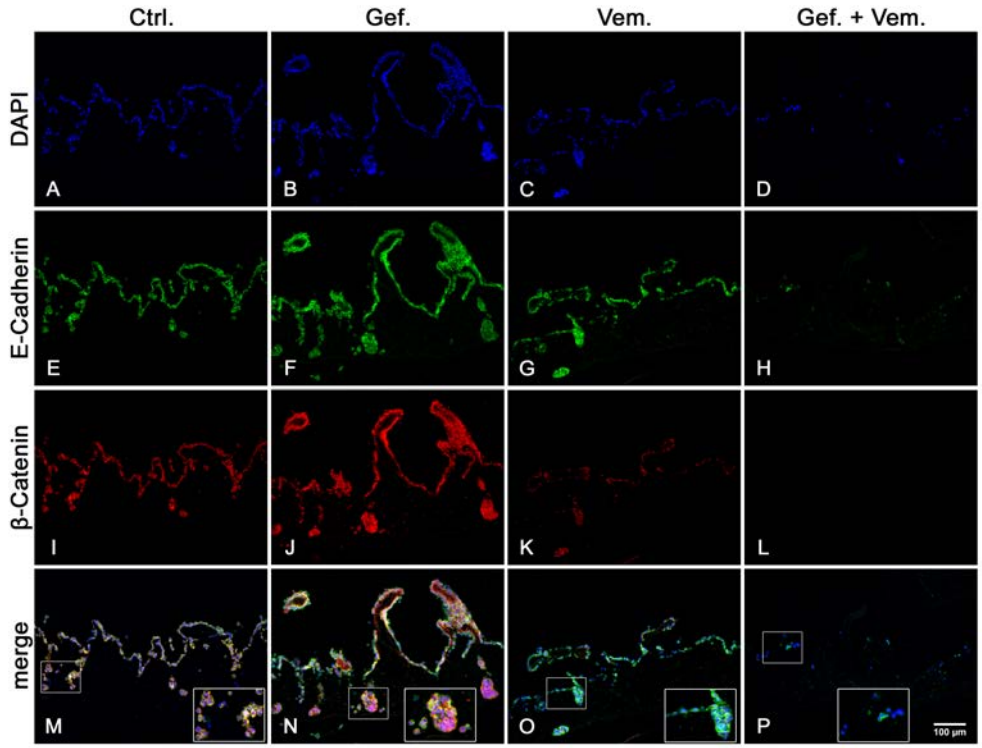

Figure 3.39: Immunofluorescence stainings for E-cadherin/β-catenin of the cell line HROC24 cultured in static 3D culture and treated with gefitinib (Gef., B/F/J/N) or vemurafenib (Vem., C/G/K/O) or a combination of both drugs (Gef.+Vem., D/H/L/P; FCS Lot N° 8SB016). The cells expressed E-cadherin (E–H) as well as β-catenin (I–L). In the untreated control (Ctrl., I) and with Gef. (J) treated cells, there were more cells positive for β-catenin compared to cells treated with Vem. (K) or the combination therapy (L). E-cadherin expression did not change during any treatment (E–H). The DAPI channel shows the cell nuclei (A–D). The overlay of all channels is displayed in merge (M–P). Especially, the Ctrl. and Gef. showed a co-localisation of both proteins resulting in a yellow staining. Scale bar in P: 100 µm for A to P.

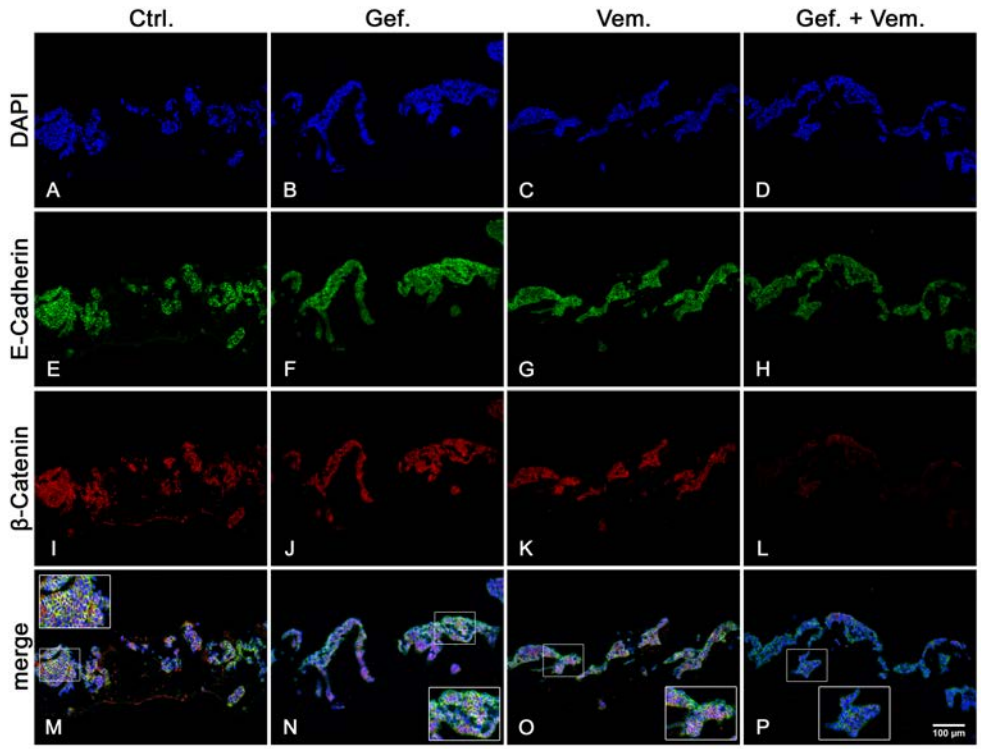

Figure 3.40: Immunofluorescence stainings for E-cadherin/β-catenin of the cell line HROC87 cultured in static 3D culture and treated with gefitinib (Gef., B/F/J/N) or vemurafenib (Vem., C/G/K/O) or a combination of both drugs (Gef.+Vem., D/H/L/P; FCS Lot N° 8SB016). The cells expressed E-cadherin (E–H) as well as β-catenin (I–L). In the untreated control (Ctrl., I) and with Gef. (J) or Vem. (K) treated cells, there were more cells positive for β-catenin compared to cells treated with the combination therapy (L). E-cadherin staining did not change during any treatment (E–H). The DAPI channel shows the cell nuclei (A–D). The overlay of all channels is displayed in merge (M–P). Scale bar in P: 100 µm for A to P.

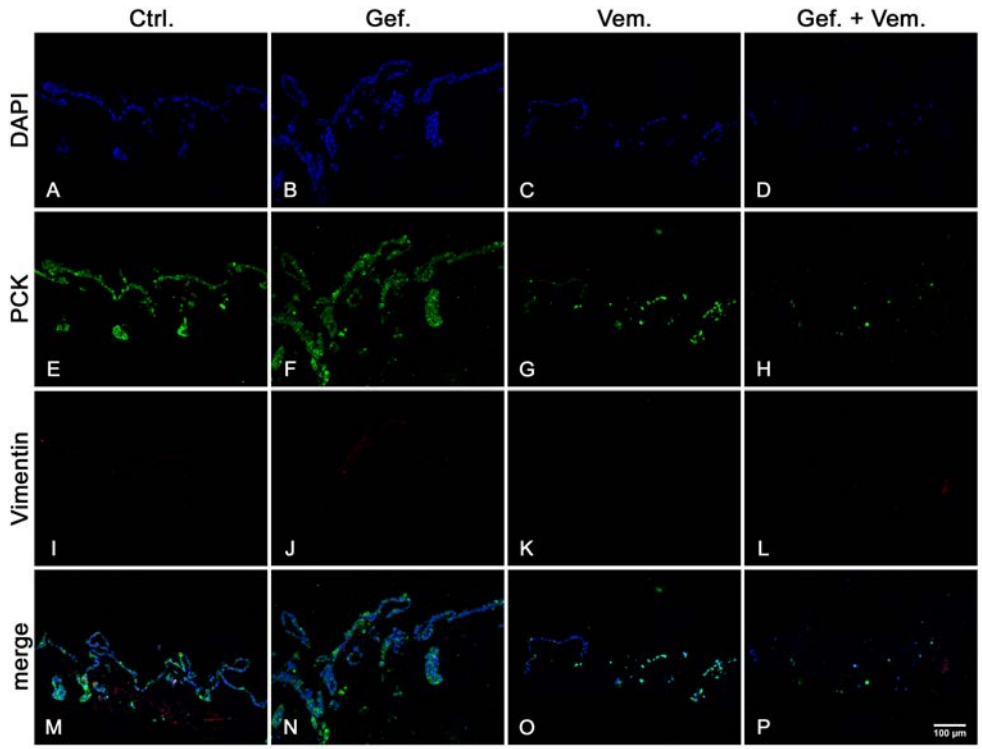

Figure 3.41: Immunofluorescence stainings for pan-cytokeratin (PCK) and vimentin of the cell line HROC24 cultured in static 3D culture and treated with gefitinib (Gef., B/F/J/N) or vemurafenib (Vem., C/G/K/O) or a combination of both drugs (Gef.+Vem., D/H/L/P; FCS Lot N° 8SB016). There were more cells in the untreated control (Ctrl., A/E/I/M) and after treatment with Gef. left (B/F/J/N) than in the group treated with Vem. (C/G/K/O) or Gef.+Vem. (D/H/L/P). The cells expressed PCK (E–H) but no vimentin (I–L). The cell nuclei were counterstained with DAPI (A–D). Scale bar in P: 100 µm for A to P.

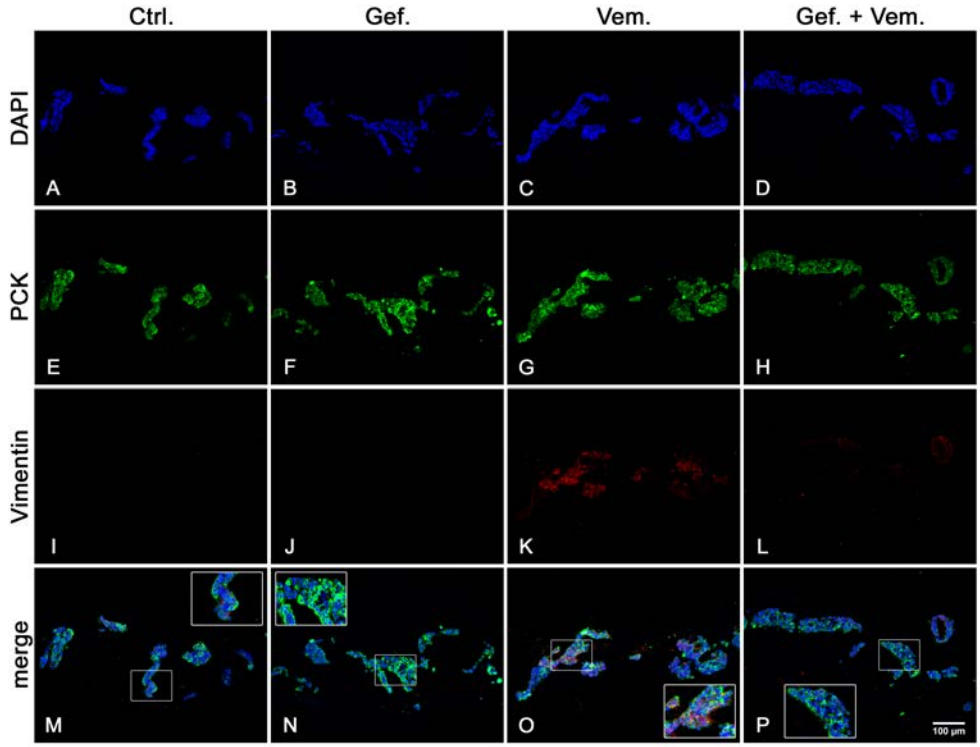

Figure 3.42: Immunofluorescence stainings for pan-cytokeratin (PCK) and vimentin of the cell line HROC87 cultured in static 3D culture and treated with gefitinib (Gef., B/F/J/N) or vemurafenib (Vem., C/G/K/O) or a combination of both drugs (Gef.+Vem., D/H/L/P; FCS Lot N° 8SB016). The cells expressed PCK (E–H) in all treatment groups. Vimentin expression was detected only in Vem.-treated cells (K) but not in the untreated control (Ctrl., I) or in the Gef. (J) or combination therapy (L) group. The cell nuclei were counterstained with DAPI (A–D). Scale bar in P: 100 µm for A to P.

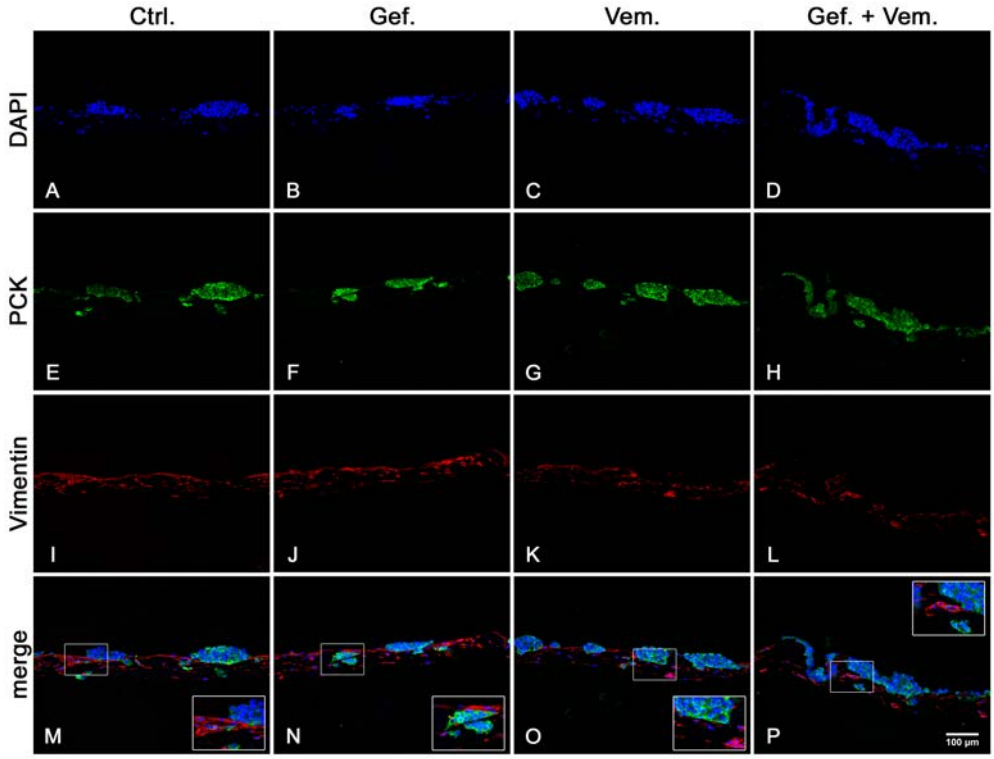

Figure 3.43: Immunofluorescence stainings for pan-cytokeratin (PCK) and vimentin of the cell line HROC87 co-cultured with dermal fibroblasts in static 3D culture (FCS Lot N° 8SB016) and treated with gefitinib (Gef., B/F/J/N) or vemurafenib (Vem., C/G/K/O) or the combination of both drugs (Gef.+Vem., D/H/L/P). The tumour cells expressed PCK (E–H) and fibroblasts expressed vimentin (I–L). There were no differences visible between the single treatment approaches when compared to the untreated control (Ctrl., A/E/I/M). The cell nuclei were counterstained with DAPI (A–D). Scale bar in P: 100 µm for A to P.

and 3.78 % in the combination treatment group (B). The median cell number per image in 2D culture was 420.0 in the control, 232.5 when treated with gefitinib, 72.5 with vemurafenib, and 65.0 with both drugs (C). The variability of cells per image was less in static 3D culture (D) with a median cell number of 182.5 in the control, 215.0 in the gefitinib group, 144.5 in the vemurafenib group, and 120.0 in the combination therapy. Using the pairwise Wilcoxon test with Bonferroni correction, significant differences were found for the Ki-67 index between the control and vemurafenib group ($p = 1.1 \cdot 10^{-7}$) as well as between the control and combination therapy ($p = 5.7 \cdot 10^{-7}$) for 2D cell culture (A, $n = 3$). The control and combination therapy were significantly different in Ki-67 index for static 3D culture (B, $p = 7.9 \cdot 10^{-11}$, $n = 5$). In 2D culture, there were significant differences for the cell number per image (C, $n = 3$) found between the control and vemurafenib ($p = 6.2 \cdot 10^{-6}$) as well as between the control and the combination of both drugs ($p = 3.2 \cdot 10^{-5}$), the difference between the control and gefitinib was not significant ($p = 0.0730$). The cell number per image of the control and vemurafenib ($p = 0.0319$) as well as of the control and combination therapy ($p = 8.1 \cdot 10^{-6}$) differed significantly in static 3D culture (D, $n = 5$).

The median Ki-67 index of the cell line HROC87 cultured in conventional 2D culture (fig. 3.47 A, $n = 3$) was 97.0 % in the control, 94.2 % in gefitinib, 97.2 % in vemurafenib, and 91.0 % in the combination therapy. In static 3D culture, the cells' proliferation rate was decreased with a median Ki-67 index of 24.2 % in the control, 20.4 % in gefitinib, 25.5 % in vemurafenib, and 13.8 % in the combination of both drugs (B, $n = 5$). The median cell number per image was 181.0 in the control, 180.5 in gefitinib, 198.0 in vemurafenib, and 168.0 in the combination therapy for 2D culture (C, $n = 3$). The variability in the cell number per image decreased in static 3D culture (D, $n = 5$), a median cell number per image of 252.0 was observed in the control, 200.0 in the gefitinib group, 200.0 in the vemurafenib group, and 191.5 in the combination treatment group. Significant differences in conventional 2D culture for the Ki-67 index (A, $n = 3$) were assessed between the control and gefitinib ($p = 0.04601$) as well as between the control and combination therapy ($p = 0.00012$) by pairwise Wilcoxon test with Bonferroni correction. In static 3D culture (B, $n = 5$), only the control and combination therapy were significantly different in Ki-67 index ($p = 0.003$). There were no significant differences regarding the cell number per image for HROC87 cells neither in 2D nor 3D culture (C and D).

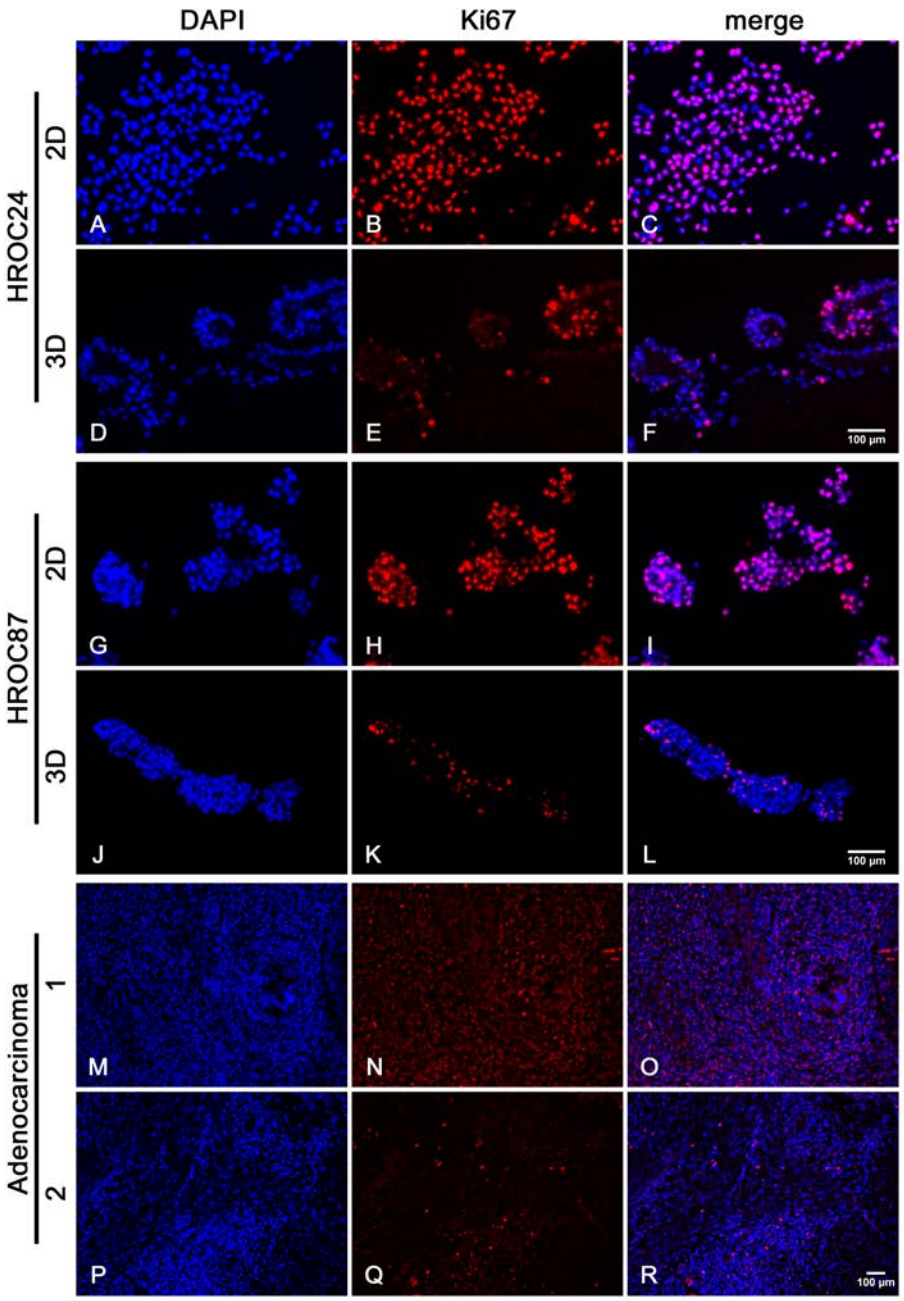

Figure 3.44: Immunofluorescence staining for the proliferation marker Ki-67 in HROC24 cells (A–F) and HROC87 cells (G–L) as well as in two sections (1 and 2) of a colon adenocarcinoma (M–R). Both cell lines were cultured in conventional 2D and static 3D culture (FCS Lot N° 8SB016). In 2D culture (A–C and G–I), nearly all cells expressed Ki-67 (B and H) indicating a high proliferation. In comparison, less cells were Ki-67-positive in static 3D culture (D–F and J–L). The colon adenocarcinoma showed a heterogeneous distribution of proliferating cells within the tumour similar to the 3D tumour model. Scale bars in F and L: 100 µm for A to L. Scale bar in R: 100 µm for M to R.

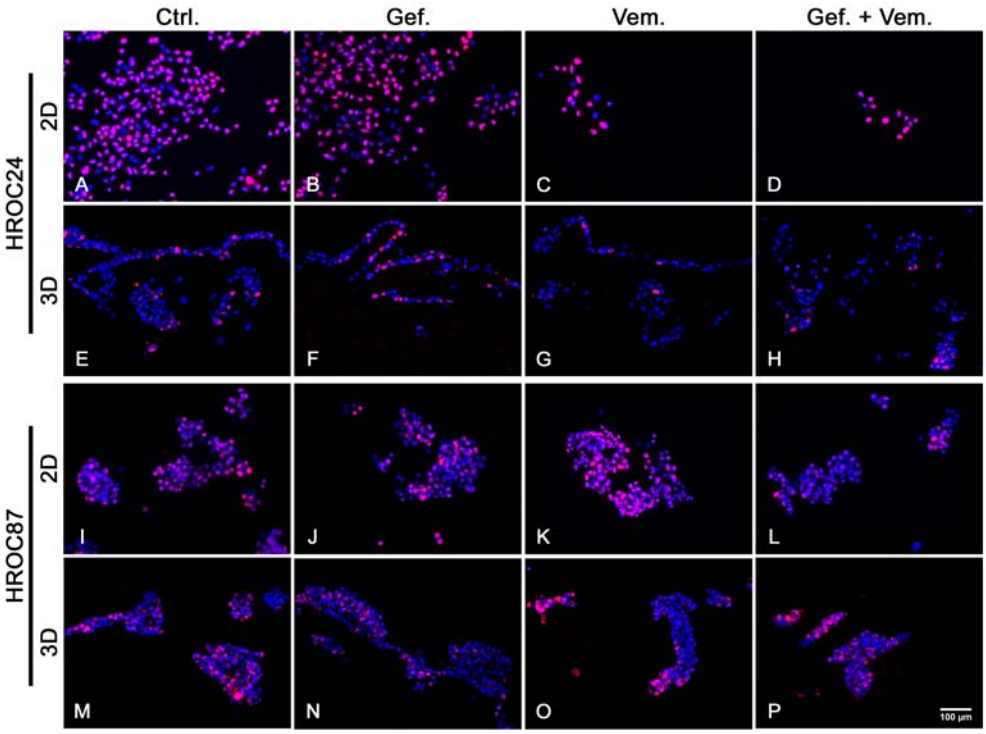

Figure 3.45: Immunofluorescence staining for the proliferation marker Ki-67 in HROC24 cells (A–H) and HROC87 cells (I–P) being treated with gefitinib (B/F/J/N), vemurafenib (C/G/K/O) or a combination of both drugs (D/H/L/P). In 2D culture, the HROC24 cell number decreased when treated with vemurafenib (Vem., C) and the combination therapy (Gef.+Vem., D) compared to the control (Ctrl., A) and gefitinib treatment (Gef., B). The cells still showed a positive Ki-67 signal when treated. In static 3D culture (E–H), the cell number did not decrease as much as in 2D culture (A–D). The cell number of HROC87 cells did not decrease neither in 2D culture (I–L) nor in 3D culture (M–P). There were more Ki-67-positive HROC87 cells in 3D culture than in 2D culture. Scale bar in P: 100 µm for A to P.

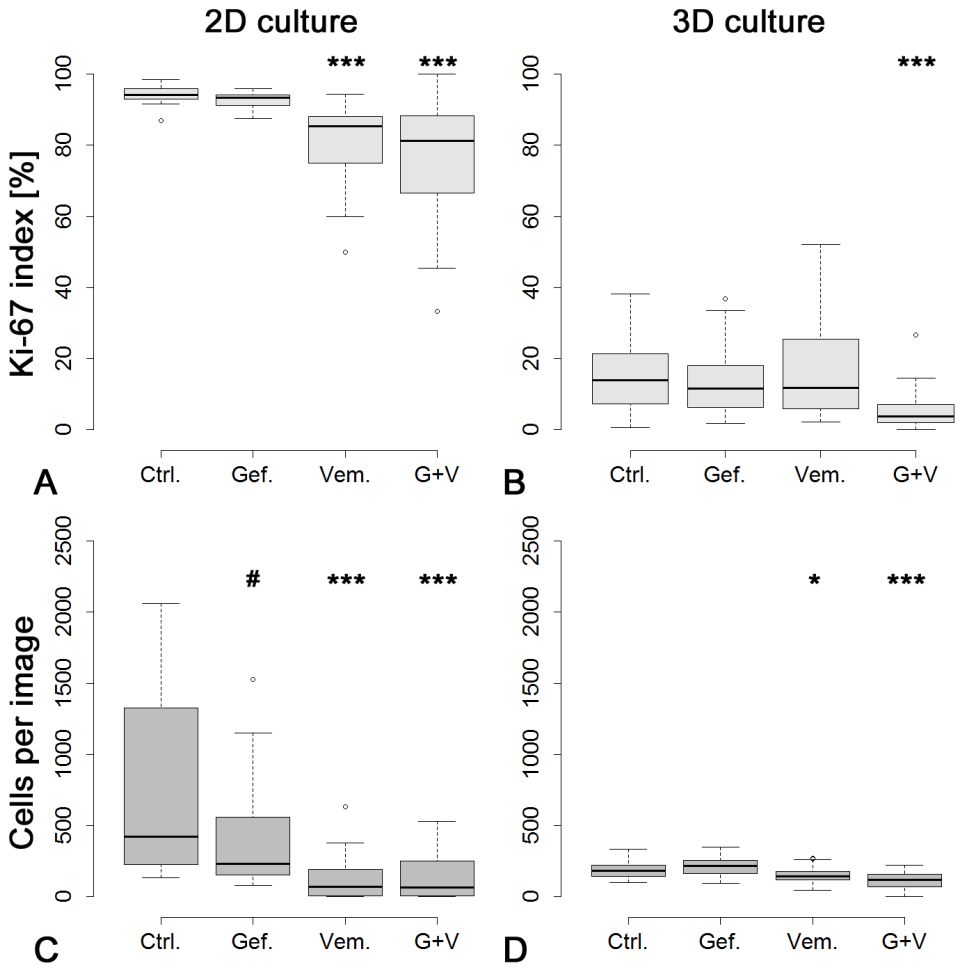

Figure 3.46: Ki-67 index of HROC24 cells cultured in 2D and 3D culture (FCS Lot N° 8SB016) and treated with gefitinib, vemurafenib and a combination of both drugs. In 2D culture (n = 3), the cell line HROC24 displayed a median Ki-67 index (A) of 94.2 % in the control compared to 93.1 % when treated with gefitinib, 85.4 % with vemurafenib, and 81.2 % with both drugs. Proliferation decreased in static 3D culture (B, n = 5) with a median of 13.9 % in the control, 11.6 % in gefitinib, 11.9 % in vemurafenib, and 3.78 % in the combination therapy. The median cell number per image in 2D culture (C) was 420.0 in the control, 232.5 in gefitinib, 72.50 in vemurafenib, and 65.00 in the combination therapy. In static 3D culture, the median cell number per image (D) was 182.5 in the control, 215.0 in gefitinib, 144.5 in vemurafenib, and 120.0 in the combination treatment. (Ctrl. = control, Gef. = gefitinib, Vem. = vemurafenib, G+V = combination of gefitinib and vemurafenib; statistical significance values by pairwise Wilcoxon test with Bonferroni correction: # $0.05<p<0.1$, * $p<0.05$, ** $p<0.01$, *** $p<0.001$)

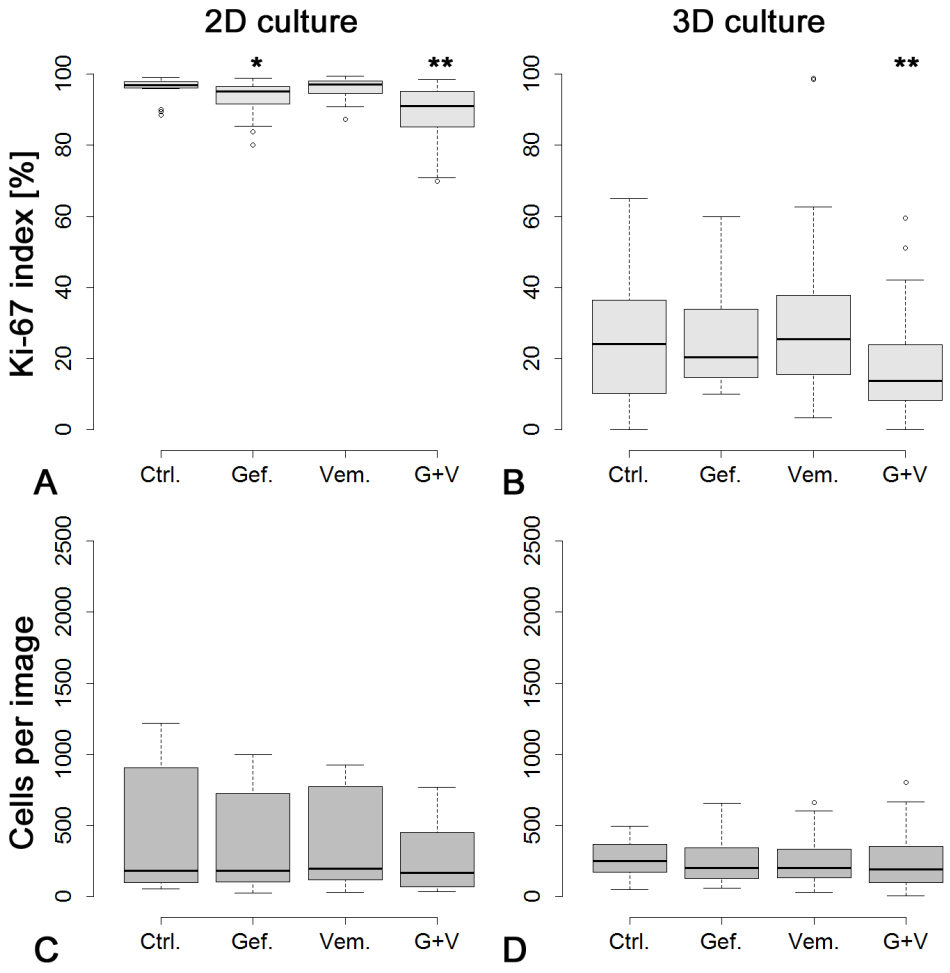

Figure 3.47: Ki-67 index of HROC87 cells cultured in 2D and 3D culture (FCS Lot N° 8SB016) and treated with gefitinib, vemurafenib and a combination of both drugs. In 2D culture (n = 3), the cell line HROC87 displayed a median Ki-67 index (A) of 97.0,% in the control compared to 95.2 % when treated with gefitinib, 97.2 % with vemurafenib, and 91.0 % with both drugs. Proliferation decreased in static 3D culture (B, n = 5) with a median Ki-67 index of 24.2 % in the control, 20.4 % in gefitinib, 25.5 % in vemurafenib, and 13.8 % in the combination therapy. The median cell number per image in 2D culture (C) was 181.0 in the control, 180.5 in gefitinib, 198.0 in vemurafenib, and 168.0 in the combination therapy. In static 3D culture, the median cell number per image (D) was 252.0 in the control, 200.0 in gefitinib, 200.0 in vemurafenib, and 191.5 in the combination treatment. (Ctrl. = control, Gef. = gefitinib, Vem. = vemurafenib, G+V = combination of gefitinib and vemurafenib; statistical significance values by pairwise Wilcoxon test with Bonferroni correction: # 0.05<p<0.1, * p<0.05, ** p<0.01, *** p<0.001)

3.3.2.3 Determination of the apoptosis rate by M30 ELISA

Apoptosis rate was assessed by the M30 CytoDeath™ ELISA (see 2.2.4 on page 60) which detects caspase-cleaved cytokeratin 18 (CK18). Both cell lines, HROC24 and HROC87, expressed the epithelial intermediate filament protein CK18 in 2D culture and static 3D culture (fig. 3.48). In 2D culture, most of the cells were stained for CK18 and only single cells showed no signal (A–C and G–I). The CK18 expression in 3D culture (D–F and J–L) was more homogeneous than in 2D culture. The negative control (M–R) showed the primary antibody's specificity for CK18.

The fold increase of apoptosis in HROC24 cells and HROC87 cells after treatment with inhibitors is presented in figures 3.49 and 3.50, respectively.

In conventional 2D culture with FCS Lot N° 8SB016, the cell line HROC24 responded 48 h after treatment with gefitinib by a median 0.92-fold increase in apoptosis, vemurafenib treatment resulted in a median 4.49-fold increase and the combination of both drugs induced a median 5.47-fold increase in apoptosis (fig. 3.49 A). After 72 h of treatment, there were median 1.02-fold, 1.94-fold and 1.71-fold increase in apoptosis for gefitinib, vemurafenib and the combination therapy, respectively (A). In 3D culture with the same FCS batch (B), apoptosis increased median by 1.42-fold with gefitinib, 1.43-fold with vemurafenib and 1.79-fold with combination treatment after 24 h. After 48 h, the median increase of apoptosis was 1.24-fold in gefitinib, 1.35-fold in vemurafenib and 1.70-fold in combination therapy treated cells (B). 72 h after treatment, apoptosis increased to 1.41-fold in gefitinib, 1.64-fold in vemurafenib and to 2.09-fold in the combination of both drugs (B). For 2D culture with FCS Lot N° BS196368 (C), HROC24 cells responded after 48 h with a median increase in apoptosis of 1.01-fold in gefitinib, 2.22-fold in vemurafenib and 2.72-fold in their combination. After 72 h, the median fold increase in apoptosis was 1.15 in gefitinib, 1.84 in vemurafenib and 1.95 in the combination therapy (C). The median fold increase in apoptosis for HROC24 cells cultured in 3D culture with FCS Lot N° BS196369 was 0.69 in gefitinib, 0.94 in vemurafenib and 2.35 in the combination treatment after 24 h (D). Apoptosis rate increased further after 48 h, to a median of 1.11 in gefitinib, 1.60 in vemurafenib and 2.45 in the combination of both drugs (D). After 72 h, the cells showed a median fold increase in apoptosis of 1.10 in gefitinib, 1.79 in vemurafenib and 3.14 in the combination treatment.

Significant differences from the untreated control were assessed by pairwise student's t-test with Bonferroni correction and found 48 h after treatment in 2D culture with FCS Lot N° 8SB016 for vemurafenib ($p = 0.0462$) and the combination therapy ($p = 0.0029$). For FCS Lot N° BS196368, there were significant differences after 48 h between the control and vemurafenib ($p = 0.0118$, $n = 3$) as

well as between the control and the combination treatment ($p = 0.0013$, $n = 3$). In static 3D culture with FCS Lot N° 8SB016 ($n = 4$), there were no significant differences detectable in comparison to FCS Lot N° BS196368. Here, the combination therapy displayed a significant increase in apoptosis for the combination therapy after 24 h ($p = 0.009$), 48 h ($p = 0.0002$) and 72 h ($p = 0.00028$, $n = 4$). Vemurafenib treatment showed tendency for an increased apoptosis rate after 72 h ($p = 0.0595$).

Figure 3.50 A displays the fold increase in apoptosis of HROC87 cells for conventional 2D culture with FCS Lot N° 8SB016. Gefitinib treatment resulted in a median fold increase of 1.96, vemurafenib in 1.15 and the combination therapy in 2.50 after 48 h. After 72 h, the median fold increase in apoptosis was 1.85 in gefitinib, 1.07 in vemurafenib and 2.06 in the combination of both drugs. In static 3D culture with FCS Lot N° 8SB016 (B), the cell line HROC87 showed a median fold increase in apoptosis of 0.94 in gefitinib, 1.62 in vemurafenib and 1.95 in the combination therapy after 24 h of treatment. Apoptosis rate increased 48 h after treatment with gefitinib to median 2.49-fold, with vemurafenib to 2.54-fold and with both drugs to 2.29-fold. After 72 h, gefitinib treated cells had a median 4.14-fold increase in apoptosis, vemurafenib treated cells 3.90-fold and the combination of both inhibitors 2.86-fold. For HROC87 cells cultured in 2D culture with FCS Lot N° BS196369 (C), there was a median fold increase in apoptosis of 1.25 in gefitinib treated cells, 1.10 in vemurafenib and 1.26 in the combination therapy after 48 h. The apoptosis rate did not increase further after 72 h: 1.21-fold with gefitinib, 1.08-fold in vemurafenib and 1.24-fold in combination of both drugs. For 3D culture with the same FCS batch (D), gefitinib induced a median 1.31-fold, vemurafenib 1.16-fold and both drugs 1.62-fold increase in apoptosis 24 h after treatment. After 48 h, the median apoptosis rate increased to 1.98 in gefitinib, 1.47 in vemurafenib and to 2.12 in the combination therapy. The median fold increase in apoptosis after 72 h was 2.10 in gefitinib, 1.57 in vemurafenib and 2.09 in the combination treatment.

Statistical analysis by pairwise student's t-test with Bonferroni correction resulted in significant differences in 2D culture with FCS Lot N° 8SB016 between the control and the combination therapy after 48 h as well as after 72 h ($p = 0.002$ and $p = 0.017$, $n = 7$). In static 3D culture with FCS Lot N° 8SB016, there were no differences between the untreated control and treated cells. There was a tendency after 24 h for an increased apoptosis rate in the combination treatment ($p = 0.07$, $n = 5$) compared to the untreated control. For FCS Lot N° BS196368, there were no significant differences detectable between the treatments and the control ($n = 9$).

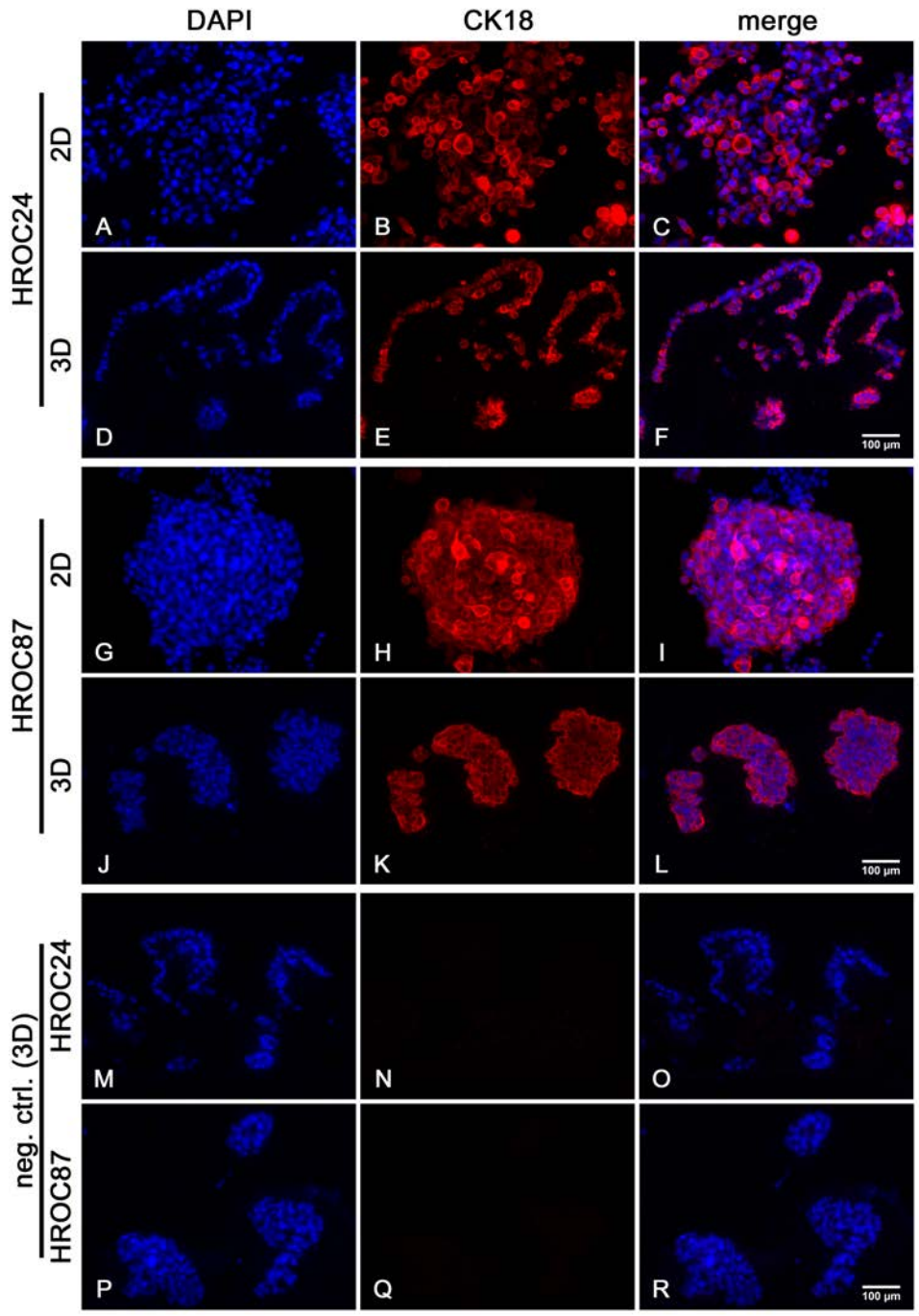

Figure 3.48: Immunofluorescence staining for cytokeratin 18 (CK18) in HROC24 (A–F) and HROC87 (G–L) cells cultured in conventional 2D culture (A–C and G–I) as well as static 3D culture (D–F and J–L) with FCS Lot N° 8SB016. For both cell lines, the negative control (neg. ctrl., secondary antibody only, M–R) reveals the specificity of the primary antibodies. The DAPI channel shows the cell nuclei. Scale bars in F, L, and R: 100 µm for A to R.

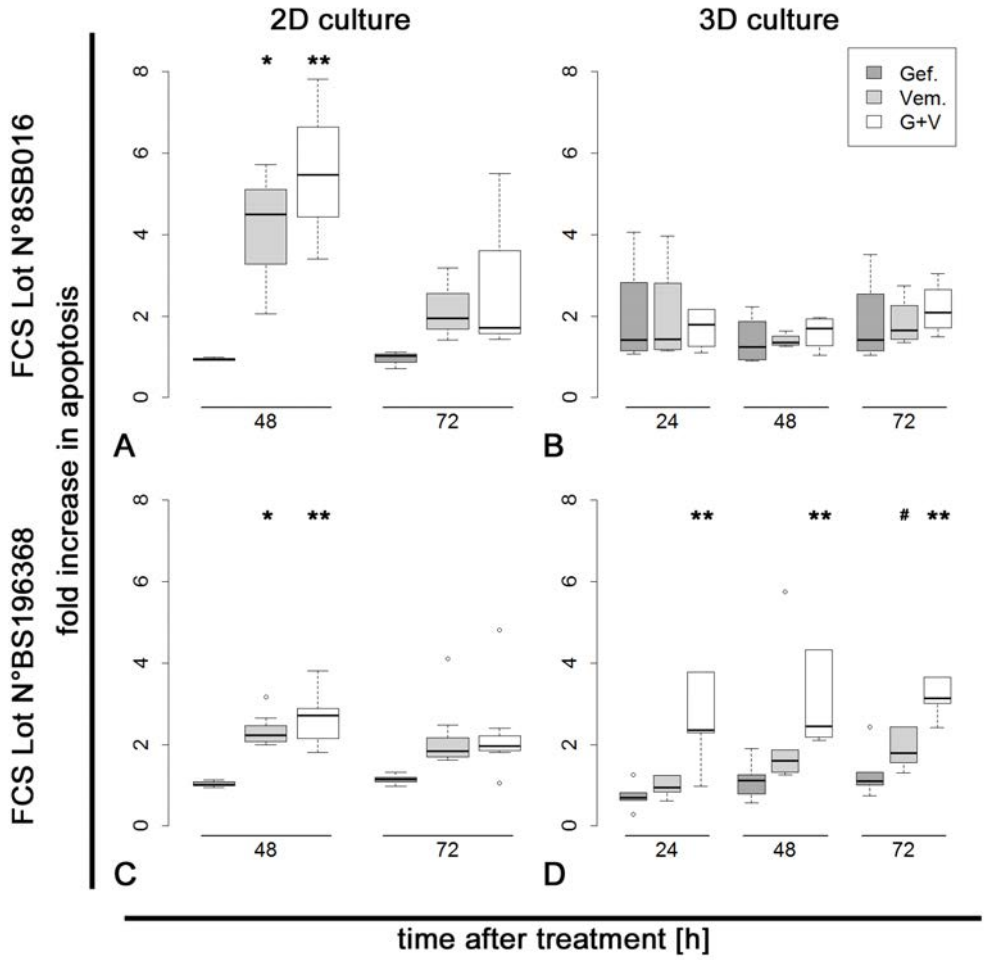

Figure 3.49: Apoptosis rate of HROC24 cells cultured in conventional 2D culture (A/C, n = 3) and static 3D culture (B/D, n = 4) with the two different FCS batches Lot N° 8SB016 (A/B) and Lot N° BS196368 (C/D). The cells were either treated with gefitinib (Gef.) or vemurafenib (Vem.) or a combination of both drugs (G+V). Apoptosis was measured in 2D culture 48 h and 72 h after treatment. In 3D culture, apoptosis was measured 24 h, 48 h and 72 h after treatment. The boxplots display the fold increase in apoptosis compared to the control. (Statistical significance values by pairwise student's t-test with Bonferroni correction: # $0.05<p<0.1$, * $p<0.05$, ** $p<0.01$, *** $p<0.001$)

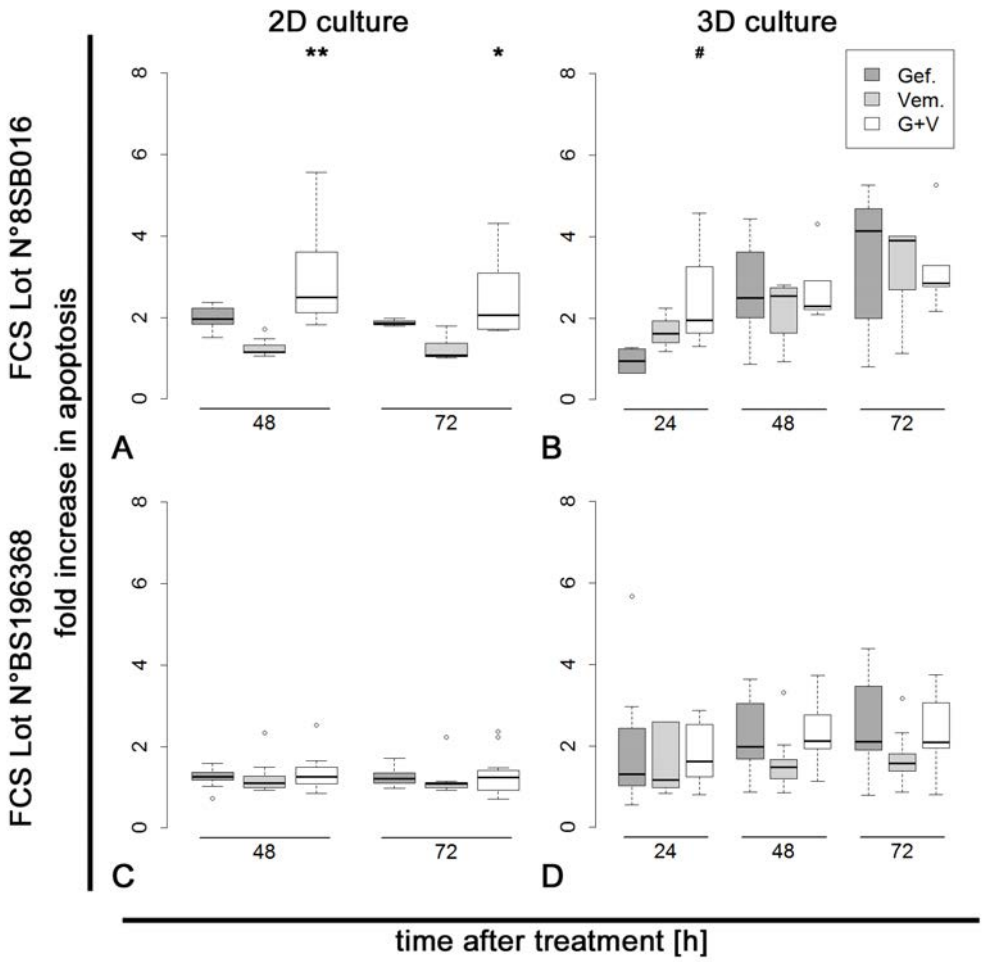

Figure 3.50: Apoptosis rate of HROC87 cells cultured in conventional 2D culture (A, n = 7 and C, n = 11) and static 3D culture (B, n = 5 and D, n = 9) with the two different FCS batches Lot N° 8SB016 (A/B) and Lot N° 196368 (C/D). The cells were either treated with gefitinib (Gef.) or vemurafenib (Vem.) or a combination of both drugs (G+V). Apoptosis was measured in 2D culture 48 h and 72 h after treatment. In 3D culture, apoptosis was measured 24 h, 48 h and 72 h after treatment. The boxplots display the fold increase in apoptosis compared to the control. (Statistical significance values by pairwise student's t-test with Bonferroni correction: # $0.05<p<0.1$, * $p<0.05$, ** $p<0.01$, *** $p<0.001$)

3.3.2.4 Analysis of cell viability using CellTiter-Glo® and MTT test

The CellTiter-Glo® viability assay is based on quantitation of ATP present in cells cultured in conventional 2D culture (see 2.2.3 on page 58). Figure 3.51 displays the results of the viability assay for HROC24 cells (A) and HROC87 cells (B) treated with gefitinib, vemurafenib or a combination of both drugs (n = 3, FCS Lot N° 8SB016). Presented are the percentages of the mean viability of the untreated control. Gefitinib treated HROC24 cells showed a mean viability of 99.5 %, with vemurafenib treatment 28.3 % and with the combination therapy 15.5 % (A). Significant differences were found between the control and vemurafenib ($p = 5.1 \cdot 10^{-9}$) as well as between the control and combination treatment ($p = 1.4 \cdot 10^{-9}$) using the pairwise student's t-test with Bonferroni correction.

The cell line HROC87 (fig. 3.51 B) showed a mean viability of 71.7 % after gefitinib treatment, 67.1 % and 37.6 % when treated with vemurafenib and the combination of both drugs, respectively. Statistical analysis by pairwise student's t-test revealed significant differences between the untreated control and gefitinib ($p = 0.03813$), between the control and vemurafenib ($p = 0.01772$) as well as between the control and the combination treatment ($p = 0.00025$).

The 3-(4,5-Dimethylthiazol-2-yl)-2,5-diphenyltetrazoliumbromide (MTT) assay is based on the cells' glycolysis metabolism (see 2.2.3 on page 58). Because this viability assay was developed for conventional 2D culture, its use had to be validated first in 3D cultured cells. Therefore, the deviations of different experimental approaches were evaluated regarding the absorbance at 570 nm. The standard deviation of four different "cell crowns" was 7.37 % in HROC24 cells and 3.34 % in HROC87 cells (fig. S1).

The results of a quantitative MTT test are displayed in figure 3.52 for HROC24 cells and HROC87 cells cultured in conventional 2D culture and static 3D culture. Gefitinib treatment did not result in any viability reduction of cell line HROC24, neither in 2D culture (A, 102.2 %) nor in 3D culture (B, 101.2 %). HROC24 cells responded to vemurafenib treatment with a decline of the viability to 4.8 % (A) and 72.4 % (B) in conventional 2D culture and static 3D culture, respectively. The combination therapy led to a mean viability of 2.1 % in 2D culture (A) and to 58.4 % viability in static 3D culture (B). Significant differences in viability were found in 2D culture (A) between the control and vemurafenib ($p = 4.5 \cdot 10^{-10}$) as well as between the control and the combination treatment ($p = 3.6 \cdot 10^{-10}$) by pairwise student's t-test with Bonferroni correction.

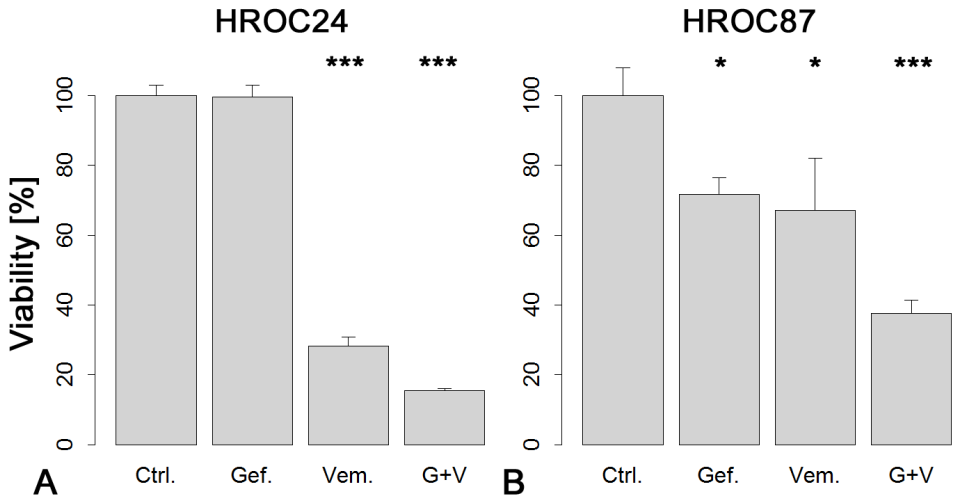

Figure 3.51: CellTiter-Glo® viability assay for HROC24 cells and HROC87 cells cultured in conventional 2D culture and treated for 72 h with the inhibitors gefitinib (Gef.), vemurafenib (Vem.) or a combination of both drugs (G+V, FCS Lot N° 8SB016). Viability is displayed as the percentage of the untreated control (Ctrl.). In HROC24 cells (A, n = 3), the cells showed a mean viability of 99.5 % when treated with gefitinib, 28.3 % with vemurafenib and 15.5 % with the combination therapy. The cell line HROC87 (B, n = 3) demonstrated a decrease in viability to 71.7 % with gefitinib, 67.1 % with vemurafenib and 37.6 % with both drugs. The error bars show the standard deviation of the mean. (Statistical significance values by pairwise student's t-test with Bonferroni correction: # 0.05<p<0.1, * p<0.05, ** p<0.01, *** p<0.001)

The cell line HROC87 declined in viability after gefitinib treatment to 71.2 %, after vemurafenib to 80.7 % and after the combination of both drugs to 46.0 % in 2D culture (fig. 3.52 C). In static 3D culture (D), the mean viability decreased to 79.4 %, 92.8 % and 70.1 % when treated with gefitinib, vemurafenib and the combination therapy, respectively. There were significant differences in viability between the control and gefitinib ($p = 2.7 \cdot 10^{-6}$), between the control and vemurafenib ($p = 5.5 \cdot 10^{-5}$) and between the control and the combination of both drugs ($p = 1.9 \cdot 10^{-8}$) in 2D culture (C) but not in 3D culture.

3.3.2.5 Analysis of signalling pathways via RTK array, phospho-kinase array and western blot

Both cell lines, HROC24 and HROC87, were screened by RTK arrays (fig. S2) and phospho-kinase arrays (fig. S3, R&D Systems) for activation changes of

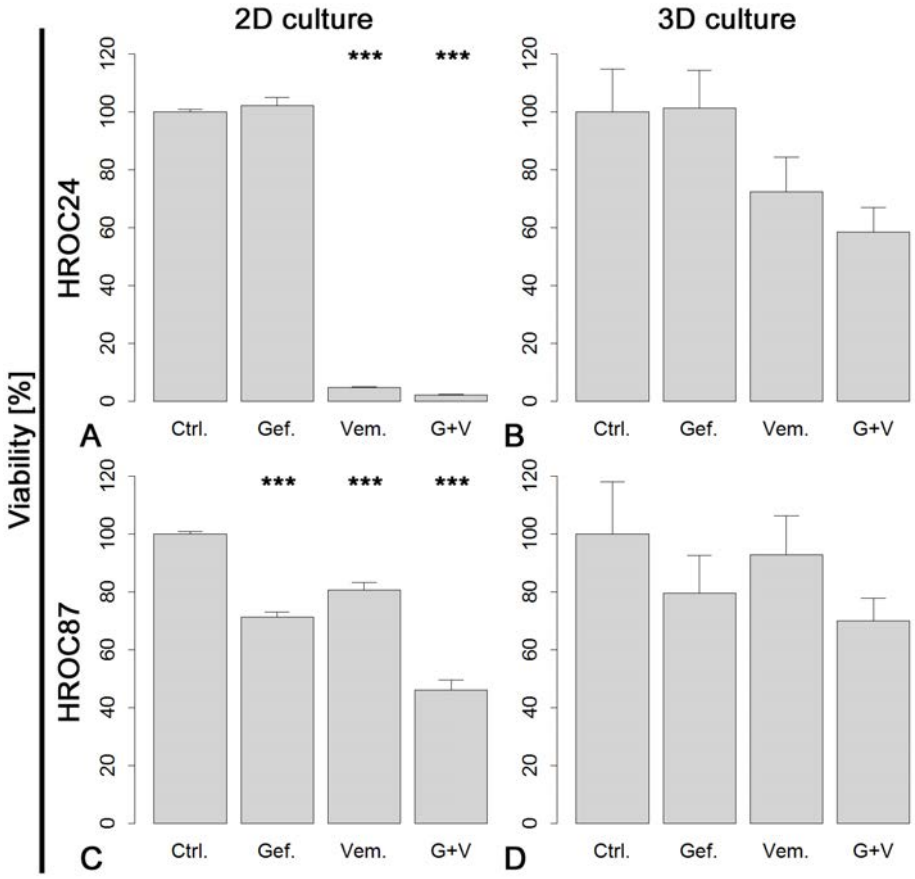

Figure 3.52: Quantitative MTT test of HROC24 cells (A–B) and HROC87 cells (C–D) cultured in 2D culture (A/C, n = 3) as well as in 3D culture (B/D, n = 6) and treated with gefitinib (Gef.), vemurafenib (Vem.) and the combination of both drugs (G+V). Displayed is the percentaged viability of the control (Ctrl.). In 2D culture, the cell line HROC24 showed no viability reduction when treated with Gef. (102.2 %, A). Vem. treatment decreased viability to 4.8 % and G+V therapy resulted in viability reduction to 2.1 % (A). HROC87 cells did not show a viability reduction in any treatment in 2D culture (A). Gef. therapy led to 71.2 %, Vem. to 80.7 % and G+V treatment to 46.0 % of viable cells compared to the Ctrl. (C). In comparison to 2D culture, both cell lines presented a lesser reduction of viability in 3D culture. HROC24 cells displayed a percentaged viability of 101.2 % with Gef., 72.4 % with Vem. and 58.4 % with G+V (B). The viability of the cell line HROC87 decreased to 79.4 %, 92.8 % and 70.1 % when treated with Gef., Vem. and G+V therapy, respectively (D). The error bars show the standard deviation of the mean in 2D culture (A/C) and the standard error of the mean in 3D culture (B/D). (Statistical significance values by pairwise student's t-test with Bonferroni correction: # $0.05<p<0.1$, * $p<0.05$, ** $p<0.01$, *** $p<0.001$)

proteins in common signalling pathways. The EGFR activation could be detected in both cell lines, it showed a weaker signal when the cells were treated with gefitinib. In HROC87 cells, HGFR (c-Met) activation could be detected in the untreated control and in cells treated with gefitinib or vemurafenib but not in the combination therapy. After vemurafenib treatment, the HGFR phosphorylation signal (pHGFR, pMet) was stronger compared to the control and a weak phosphorylation signal of ErbB3 could be detected (fig. S2). Furthermore, Erk1/2 showed a weaker signal in the combination treatment in comparison to the control or the treatment with gefitinib or vemurafenib (fig. S3). Because of the additional activation of the HGFR in the RTK array, the cell line HROC87 was chosen for further analyses by western blotting.

The results of western blot analysis of the cell line HROC87 and its respective xenografts are displayed in figure 3.53. Displayed are EGFR, Met (HGFR), Akt and Erk1/2 as well as the respective phosphorylated proteins for HROC87 cells cultured in conventional 2D culture (A) and in static 3D culture (B) as well as their xenografts (C). The cells responded to gefitinib treatment and its combination with vemurafenib by a signal reduction of the phosphorylated EGFR (pEGFR) in 2D culture (A) and in 3D culture (B) whereas vemurafenib alone did not reduce its activity. pMet was diminished when the cells were treated with gefitinib or its combination with vemurafenib in 2D culture (A). In 3D culture, only the combination of both drugs blocked pMet (B). The pAkt signal was not affected by any treatment in 2D culture but pErk1/2 signal was reduced (A). There could be observed a strong Akt activation (pAkt) of HROC87 cells cultured in 3D culture when being treated with the combination therapy (B). A weaker pAkt signal could be detected in untreated cells and in cells treated with gefitinib as well as with vemurafenib (B). pErk1/2 could be partially blocked by gefitinib and the combination treatment in 3D culture compared to the untreated control and vemurafenib therapy (B). The cytoskeleton protein α-tubulin served as a loading control.

Figure 3.53 C presents the western blot analysis for two different xenograft tumours (1 and 2) of the cell line HROC87. The xenograft tumour 1 responded to the different treatments by a decrease of the pEGFR, pErk1/2 and pAkt signals. In contrast, the xenograft tumour 2 showed a decreased pEGFR signal only when being treated with gefitinib or the combination therapy. Also, pErk1/2 was not blocked by the different treatments in the xenograft tumour 2. pAkt signal was weaker after gefitinib treatment and after the combination therapy compared to the control and vemurafenib treatment. In both xenograft tumours, the pMet signal could not be detected though Met was present.

Differences between two FCS batches regarding cell signalling in HROC87 cells are displayed in figure 3.54 for conventional 2D culture as well as static 3D

culture. HROC87 cells showed a stronger pEGFR signal in 3D culture than in 2D culture. Gefitinib treatment but not vemurafenib treatment could partially reduce the pEGFR signal in 2D culture and 3D culture. A complete inhibition of pErk1/2 could be observed in the combination therapy only in cells cultured in 2D culture with FCS Lot N° 8SB016 and in 3D culture with both FCS batches. Cells cultured in 2D culture with FCS Lot N° BS210601.5 did not show the complete inhibition of pErk1/2. The signal of pMet could be totally blocked by gefitinib or its combination with vemurafenib in 2D culture with FCS Lot N° 8SB016 but not with N° BS210601.5. In static 3D culture with FCS Lot N° 8SB016, gefitinib and the combination therapy blocked only partially pMet signalling. Overall, the pMet signal was weaker in 3D culture with FCS Lot N° BS210601.5 but could be totally blocked with the combination treatment. The pAkt signal was stronger in cells cultured with FCS Lot N° 8SB016 than in cells cultured with N° BS210601.5 in 2D culture as well as in 3D culture.

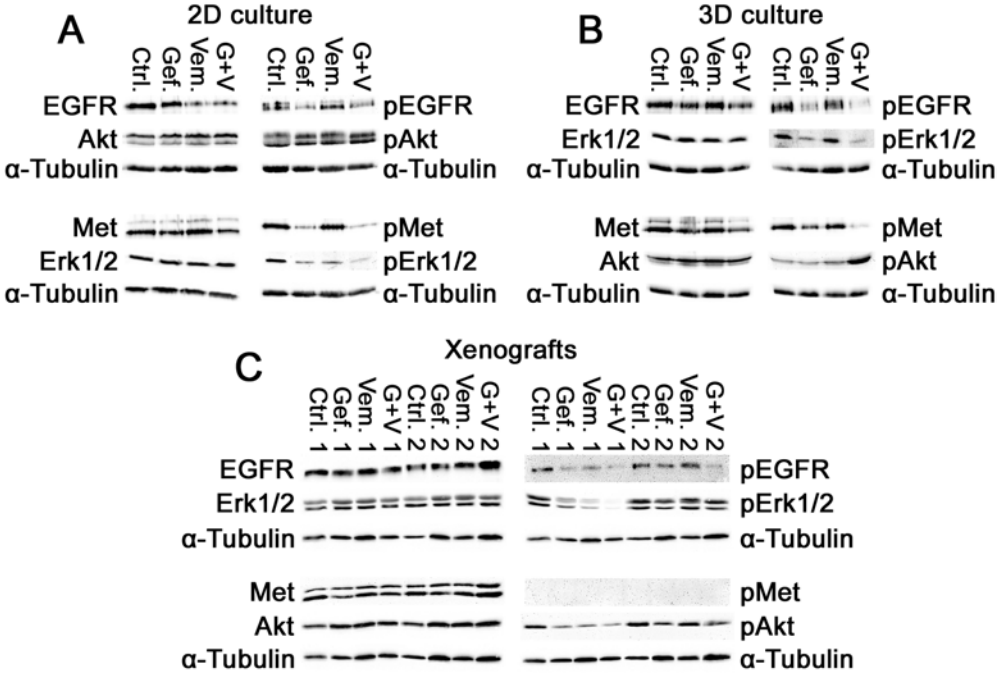

Figure 3.53: Western blot of the cell line HROC87 cultured in conventional 2D culture (A) and in static 3D culture (B, FCS Lot N° 8SB016) as well as of xenografts (C) treated with gefitinib (Gef.), vemurafenib (Vem.) and a combination of both drugs (G+V). The control (Ctrl.) shows untreated cells. Displayed are EGFR, Met (HGFR), Akt and Erk1/2 and their respective phosphorylated and active counterparts. Gefitinib and the combination therapy led to a weaker signal of the pEGFR in 2D culture as well as in 3D culture. pErk1/2 showed a weaker signal in 2D culture in any treatment approach. In comparison, pErk1/2 displayed weaker signals when the cells were treated either with gefitinib or the combination therapy in static 3D culture, vemurafenib treatment did not affect its activity. pAkt signal did not change during treatment in 2D culture whereas there was a strong signal of pAkt in the combination treatment in 3D culture. In the xenograft tumours of HROC87 cells (1 and 2), pEGFR signal could be detected but no pMet signal. pErk1/2 signal was visible in Ctrl. 1, Gef. 1 and weakly in Vem. 1 but not in G+V 1. In contrast, the second xenograft tumour showed a pErk1/2 signal independent of the treatment. α-Tubulin served as loading control.

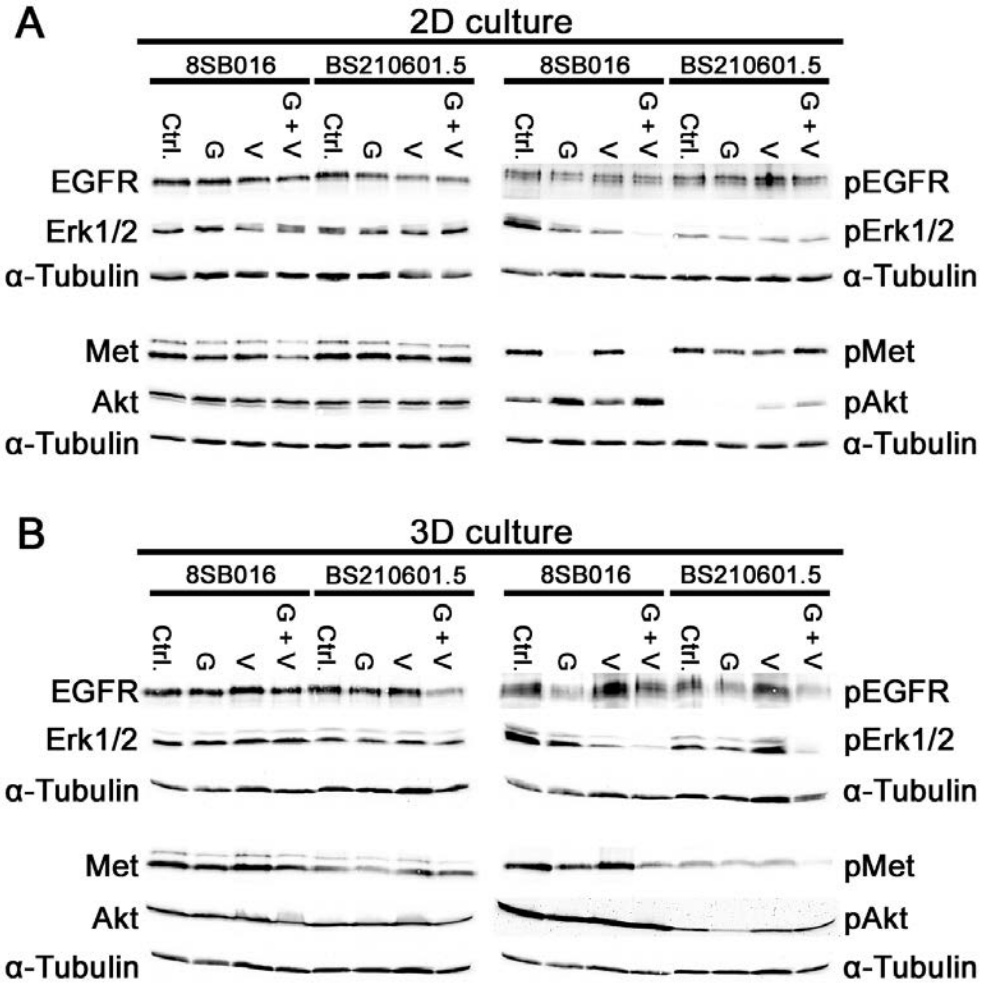

Figure 3.54: Western blot of HROC87 cells cultured in two different FCS batches (Lot N° 8SB016 and N° BS210601.5) and treated with the EGFR inhibitor gefitinib (G) or the BRAF inhibitor vemurafenib (V) or the combination of both drugs (G+V). In conventional 2D culture (A), the inhibition of pMet (pHGFR) could be only observed in gefitinib or in combination therapy treated cells cultured with FCS Lot N° 8SB016. In static 3D culture (B), pMet signal was more stable throughout the treatment approaches. There was no pMet signal detectable in HROC87 cells cultured under 3D conditions with FCS Lot N° BS210601.5 and treated with the combination therapy (B). Signalling of pAkt was more pronounced in medium containing FCS Lot N° 8SB016 in 2D culture (A) as well as in 3D culture (B). The pErk signal was partially blocked by gefitinib and vemurafenib treatment and totally blocked by the combination therapy in 2D culture with FCS Lot N° 8SB016. For FCS Lot N° BS210601.5, this effect could not be observed in 2D culture (B). The combination treatment successfully blocked pErk1/2 in 3D culture regardless of the used FCS batch. Ctrl. = control.

4 Discussion

The attrition rates for cancer drugs are much higher than in other therapeutic areas. Only 5 % of agents that show anticancer activity enter the market and get approved for registration [128]. Especially in the clinical trial phases II and III, 56 % of drugs fail because of their lack of efficacy and 28 % due to safety issues. About a third fail in the field of oncology [129]. A reason for this failure might lie in preclinical *in vitro* testing where usually conventional 2D models are used to assess the drug response of only one type of cell to an agens [130]. Furthermore, the current *in vivo* gold standard "mouse model" is still implemented in drug research for testing efficacy after successful drug responses of *in vitro* models, but this cannot sufficiently predict the outcome in humans [131–133]. Therefore new preclinical *in vitro* models for a better prediction of drug responses are urgently needed.

In this thesis, novel 3D colon cancer models on the basis of a decellularised porcine intestine were established. An overview of two different batches of the SISmuc is shown in figure 3.1. The H&E staining displays the preserved villi and crypt structures in the cell-free scaffold. The natural batch-to-batch variation is visible by the different thicknesses of submucosa and mucosa (fig. 3.1 A/C vs. B/D). Nevertheless, the SISmuc is prepared according to a standardised operating protocol (SOP) and its quality is proven by performing histological analyses (H&E and Feulgen stain) and quantitation of residues of bile acid prior to use. To prove that the scaffold still includes preserved basal laminae after the decellularisation process, an alcian blue-PAS staining was performed (fig. 3.2). It could be shown that these were present, lining the former crypts and blood vessels. This is a unique feature of the SISmuc compared to synthetic matrices and important for a tumour model as already published in Stratmann *et al.*, 2014 [78].

In the first part of the thesis, the cell line SW480 was used together with primary fibroblasts for the establishment of a complex 3D tumour model. After characterisation of the tumour model including stromal cells, a standard treatment with the chemotherapeutic 5-FU was performed under static and dynamic culture conditions. In the second part, two 3D colon cancer models with the early passage *BRAF*-mutant cell lines HROC24 and HROC87 were established and characterised regarding morphology, EMT marker expression, cancer

stem cell markers and markers of colorectal carcinoma. These stainings were compared to a primary adenocarcinoma of the colon and xenograft models of HROC87 cells. Subsequently, the established 3D models were treated with the BRAF inhibitor vemurafenib and the EGFR inhibitor gefitinib. The success of this targeted therapy was assessed by the evaluation of apoptosis, viability of the cells, proliferation and activation changes in the signalling pathways.

4.1 Establishment of a standardised 3D colon carcinoma model and treatment with 5-FU

There are several approaches to generate 3D colon cancer models, e.g. the use of hydrogel-based scaffolds [134–136] or electrospun scaffolds [137] as well as spheroid formation by hanging drop culture [138]. As mentioned above, the SISmuc as a matrix with preserved natural tissue architecture was used for the establishment of a 3D colon carcinoma model [78].

4.1.1 Characterisation of the standardised tumour model

Since SW480 cells are well characterised [114], they were chosen for the generation of the 3D tumour model. Primary dermal fibroblasts were added to the tumour model to increase its complexity and to examine the influence of stromal cells on tumour cells in a 3D environment. Subsequently, immunofluorescence stainings for the marker combinations E-cadherin/β-catenin and PCK/vimentin were performed to determine the EMT state of the tumour model.

4.1.1.1 Epithelial character of SW480 cells in a 3D environment

At first, the cells were stained for E-cadherin/β-catenin and PCK/vimentin in order to characterise the epithelial-mesenchymal state of the cells cultured in conventional 2D cell culture as well as in static and dynamic 3D culture. In 2D cell culture, SW480 MC exhibited a weak staining of the epithelial marker E-cadherin. Only few cells growing closely together were clearly stained (fig. 3.7 B and D). B-catenin could be detected primarily in the cell nuclei (fig. 3.7 C and D) where it functions as a transcription factor. These results indicate the mesenchymal characteristics of the cell line SW480 in 2D MC. In contrast, SW480 cells presented a more pronounced epithelial phenotype in static 3D MC (fig. 3.8 A–D) and dynamic 3D MC (fig. 3.9 A–D) regarding E-cadherin expression. Additionally, the β-catenin staining was lighter in the static 3D MC (fig. 3.8 A–D) than in conventional 2D MC. In normal epithelial

tissue, E-cadherin and β-catenin form a complex with actin filaments at the cell membrane in order to stabilise the epithelial layer. When a cell undergoes a shift towards a mesenchymal state, this complex is loosened and cells can leave the well-organised cell structure. The acquisition of mesenchymal characteristics and the loss of epithelial morphology are typical for cancer cells in late tumour progression and metastasis [139–141]. This process is reversed during the formation of metastases at distant sites where carcinoma cells regain epithelial features during MET [142, 143]. This could explain the cells' expression of E-cadherin in the 3D MC models. In the dynamic 3D MC model, there was an increased cell number and more cells stained for β-catenin than in the static 3D MC. This could be due to the influence of the medium flow in the bioreactor which promotes cell growth and hence altered the cells' behaviour by mechanical stimuli and a better nutrient supply.

The staining for PCK revealed that SW480 cells were not only expressing this epithelial marker in 2D MC (fig. 3.4 B) but also the mesenchymal filament protein vimentin (fig. 3.4 C). This displays the mesenchymal character of SW480 cells in 2D MC which tallies with the results of the E-cadherin/β-catenin staining, showing the cells' heterogeneity concerning the observed EMT marker expressions. In static 3D MC (fig. 3.5 A–D), the tumour cells still expressed both markers but vimentin staining was not as pronounced as in 2D MC. Interestingly, vimentin could not be detected in dynamic 3D MC (fig. 3.6 C) and the cells presented a complete epithelial phenotype regarding this marker combination. Together, these results indicate that the cell line SW480 shows more epithalial than mesenchymal characteristics when cultured in a 3D environment suggesting an underlying MET. Whether this is caused by the selection of a particular cell clone and/or change of the cells' phenotype remains unclear.

4.1.1.2 Co-culture changes the tumour cells' behaviour

As expected, fibroblasts in 2D MC were stained for vimentin (fig. 3.4 G) but negative for E-cadherin (fig. 3.7 F). Regardless of being cultured in conventional 2D culture or static/dynamic 3D culture, they expressed neither PCK (fig. 3.4, 3.5, and 3.6 F) nor β-catenin (fig. 3.7, 3.8, and 3.9 G). The 2D CC of SW480 cells and fibroblasts resulted in a change of the E-cadherin and β-catenin expression in the tumour cells which had shifted towards an epithelial state (fig. 3.7 I–L). This is indicated by a pronounced E-cadherin staining (fig. 3.7 J) and lighter β-catenin expression (fig. 3.7 K). Also, this was true for the static 3D CC of SW480 cells and fibroblasts (fig. 3.8) where fewer tumour cells were stained for β-catenin. The results for the PCK/vimentin staining in 2D

CC (fig. 3.4 I–L), static 3D CC (fig. 3.5 I–L), and dynamic 3D CC (fig. 3.6 I–L) suggest the same findings for the more epithelial character of the cell line SW480 under 3D culture conditions. The dermal fibroblasts seemed to prevent the EMT process (and/or promote MET) of the tumour cells. This could also be observed in another study with melanoma cells [144].

In contrast to the dynamic 3D MC, the tumour cells at the margins of the tumour-like cell masses were stained for β-catenin in dynamic 3D CC (fig. 3.9 L), thus indicating that the cells still kept mesenchymal characteristics of the canonical Wnt pathway which is important for the normal development during embryogenesis as well as for cell migration during tumour progression [145, 146]. This shows that SW480 cells can be influenced variably by (dermal) fibroblasts and that the tumour cells' behaviour displays high plasticity regarding a possible shift from EMT to MET as well as vice versa.

4.1.1.3 Dynamic 3D culture promotes an enhanced tumour cell growth

The H&E staining of dynamic 3D models revealed that fibroblasts altered the scaffold's natural collagen structure by flattening and remodelling the former crypts and villi extremely (fig. 3.3 B/E). Cells were growing on top of and inside the former mucosa. SW480 cells alone did not remodel the matrix itself (fig. 3.3 A/D) but their growth pattern was remarkably changed in the CC (fig. 3.3 C/F), thereby destroying the former crypt and villi structures. The fibroblasts intermingled with the tumour cells forming tumour-like cell aggregates which showed an invasive growth indicated by the remodelling of the mucosal structure. However, the cells still remained within the former mucosa and did not cross the *muscularis mucosae*. The remodelling of the scaffold could also be proven by a double staining for PCK and collagen IV which is a component of the basal membrane (fig. 3.10). Here, the natural former crypt borders were clearly stained for collagen IV and the tumour cells stayed within these structures (fig. 3.10 C). Fibroblasts grown alone and together with tumour cells could remodel the collagen-based matrix and crypt or villi structures were no longer visible (fig. 3.10 K). The more elaborate dynamic culture method promotes an increased cells growth and allows to enhance the effects observed in the static 3D culture, thereby mimicking the *in vivo* situation of a tumour more clearly and thus providing a suitable system for drug testing.

These results indicate that cells receive different stimuli in dynamic culture which probably influences gene expression and hence the cells' behaviour. The models show that normal fibroblasts, in this case dermal fibroblasts, can have a major impact on the characteristics of tumour cells as already known from conventional 2D cell culture [147, 148]. However, the formation of tumour cell

aggregates including fibroblasts was visible only in a 3D environment. There is growing evidence that normal fibroblasts can be activated by different stimuli such as growth factors (TGF-β, EGF, PDGF and FGF-2) or direct cell-to-cell communication [149]. Cancer cells are able to induce the activated phenotype of normal fibroblasts, thus converting them to cancer associated fibroblasts (CAFs) which then contribute to the tumour microenvironment by inhibiting cancer cell apoptosis, inducing cancer cell proliferation and stimulating tumour angiogenesis [149, 150]. Moreover, fibroblasts have the ability to remodel the surrounding extracellular matrix [149]. This could also be observed in the double staining of PCK and collagen IV (fig. 3.10) as well as in the H&E staining (fig. 3.3). Whether the fibroblasts in the presented 3D models were really CAFs, is material for further experiments, e.g. double stainings for fibroblast-activation protein (FAP) and vimentin as well as other comprehensive investigations [149].

Regarding morphological features, the 3D environment resembles the *in vivo* situation more closely. The conventional 2D culture cannot reflect these characteristics which are important for the understanding of tumour development and progression as well as therapy approaches. In conclusion, fibroblasts are an important cell type of the tumour stroma which can influence tumour growth and progression. They are an inalienable component for the development of further *in vitro* models which could be used for the prediction of drug testing outcomes *in vivo*. Additionally, as vascularised models are already available [74, 117, 151], endothelial cells could be integrated into the 3D tumour model in order to increase its complexity and to evaluate the meaning of the different cell types for treatment strategies.

4.1.2 Standard treatment with 5-FU

A standard treatment with 5-FU was performed in static MCs of SW480 cells and fibroblasts as well as in static and dynamic CCs (fig. 3.11) to show that this model is a useful tool in preclinical testing. The compound 5-FU is used as a commonly applied drug in clinical treatment of colorectal cancer [152].

In static 3D MC, SW480 cells were nearly insensitive to the treatment with 5-FU (fig. 3.11 A/E) [2]. This low sensitivity of SW480 cells against 5-FU has been reported in several studies before [153–155]. In contrast, the static 3D co-culture showed a visible reduction of the tumour cell mass when treated with 5-FU (fig. 3.11 C/G). This effect was even more pronounced in the dynamic CC (fig. 3.11 D/H), indicating that fibroblasts can produce drug sensitivity in cancer cells. In contrast to findings in other studies [156, 157], the drug sensitivity of the cancer cells was increased by the dermal fibroblasts in this

tumour model. Further experiments should find out if CAFs isolated from tumour biopsies can increase the resistance of tumour cells to 5-FU treatment compared to normal fibroblasts derived from the dermis [158].

Fibroblasts were not affected by the treatment with 5-FU in static 3D MC or in static and dynamic CC. Their cell number did not decrease compared to the control (fig. 3.11 B/F, C/G and D/H). This is in line with previous studies examining the effects of 5-FU on proliferating human fibroblasts *in vitro* and *in vivo* where concentrations of 0.2 µg/ml already affected proliferation but only concentrations above 100 µg/ml were found to be toxic [159, 160].

These results led to a shared first authorship in the article "Mimicking metastases including tumor stroma: A new technique to generate a three-dimensional colorectal cancer model based on a biological decellularized intestinal scaffold" of the journal Tissue Engineering Part C Methods [2]. The findings demonstrate that it is possible to create metastasis-like tissue by co-culturing fibroblasts and tumour cells in a dynamic culture system enabling analyses of drug responses in advanced tumour stages.

4.2 Targeted therapy of 3D *BRAF*-mutant colon carcinoma models

The two early passage *BRAF*-mutant cell lines HROC24 and HROC87 were chosen for the establishment of a 3D colorectal carcinoma model because of their well-characterised mutational status. After characterisation and comparison of cells grown in conventional 2D culture and static 3D culture, a targeted therapy was performed with the BRAF inhibitor vemurafenib (PLX4032, Zelboraf™) and the EGFR inhibitor gefitinib (Iressa®).

4.2.1 Characterisation of a 3D tumour model of *BRAF*-mutant colorectal carcinoma

The two cell lines HROC24 and HROC87 grew differently in conventional 2D culture as well as in static 3D culture. While HROC24 cells presented a more scattered growth in loose cell clusters in 2D culture, HROC87 cells grew in denser cell aggregates. In static 3D culture, HROC24 cells built monolayers on top of the SISmuc and partially grew inside the former crypts of the scaffold. In contrast, the cell line HROC87 tended to build multi-layered cell clusters which were scattered on top of the scaffold and grew inside the former crypts (fig. 3.12). These differences reflect the distinct tumour stages and different mutations of the two cancer cell lines: HROC24 cells are graded as G2T2N0M0

and HROC87 cells are graded as G3T3N0M0 [70, 113]. Therefore HROC87 cells present a more advanced tumour stage with a more dysplastic cell growth in the 3D tumour model.

Figure 3.14 shows an alcian blue-PAS stain of the 3D tumour models and of a tubular colon adenocarcinoma as well as of a healthy colon. The morphology of the 3D tumour models is more like the moderately differentiated adenocarcinoma where tumour cells grow irregularly within the connective tissue and the stroma. The organised glandular architecture as displayed in the healthy colon is almost completely lost in the adenocarcinoma. There were some single HROC87 cells stained for mucines showing the cells' adenocarcinomatous origin: carcinomas with more than 10 % but less than 50 % mucinous component are termed adenocarcinoma [23].

4.2.1.1 Immunohistochemical phenotype shows typical pattern for adenocarcinoma

CDX2, CK7 and CK20 are the most widely used immunhistochemical markers for colorectal adenocarcinoma [23]. Therefore both cell lines were stained for these markers (fig. 3.15, 3.16 and 3.17). HROC24 cells and HROC87 cells as well as the adenocarcinoma were stained for CDX2 which is positive in >90 % of colorectal adenocarcinoma and constitutes a marker of enteric differentiation [161, 162]. The cells within the adenocarcinoma were negative for CK7 and (partially) positive for CK20, which is the most common immunophenotype of colorectal adenocarcinoma [163]. Both cell lines, HROC24 cells and HROC87 cells, were CK7-negative in 2D culture as well as in 3D culture. However, only single tumour cells of both cell lines were stained for CK20 in 2D culture. In 3D culture also, only very few HROC24 cells were CK20-positive, but no HROC87 cell expressed this marker with FCS N° 8SB016. This reduced or absent CK20 expression in CRC is associated with the clinical characteristics of both cell lines which presented a spMMR-D with MSI-H [164], correlated to cells with a *BRAF* mutation [24]. The shown specimen of adenocarcinoma is therefore not comparable in this case and its exact histopathological variants (tumour type, TNM stage, etc.) as well as its molecular characteristics (mutational status, MMR-D, etc.) are unknown. In conclusion, the stainings of the 3D models show a typical immunohistochemical phenotype of the two *BRAF*-mutant cell lines with MSI.

4.2.1.2 The expression of putative tumour stem cell markers shows differences between 2D and 3D culture

The expression of stem cell markers, such as CD44, CD133, CD166 and EpCAM, is thought to be correlated to a cell's potency for tumour initiation [165] and significantly associated with the patients' survival [108]. Interestingly, both cell lines, HROC24 and HROC87, did not express the markers CD44 and CD166 in conventional 2D culture, only in static 3D culture (fig. 3.30 and 3.31 A–D and I—L). The expression of CD44 can be explained by the scaffold's properties of providing an ECM which is not existant on the plane surface of 2D culture: CD44 is an adhesion molecule with multiple isoforms that has pleiotropic roles in signalling, migration and homing [166]; it binds to hyaluronic acid which is a substantial part of the ECM. For this reason, most cells expressed this hyalurone receptor in the 3D model. Also, some but not all of the tumour cells in the specimen of the colon adenocarcinoma were found to be stained for CD44 (fig. 3.32 C). It is likely that stromal cells (e.g. fibroblasts) were stained too, as shown in the healthy colon where no glandular cells but only stromal cells were stained (fig. 3.32 D).

An explanation for the expression of CD166 in 3D culture might be the fact that this transmembrane marker is found at sites of cell-to-cell contacts and is involved in homotypic and heterotypic adhesion [109, 127]. In conventional 2D culture, cells cannot establish such cell-to-cell contacts which are naturally found in tissues, e.g. in colon adenocarcinoma or healthy colon (fig. 3.32 K and L). Therefore the 3D model offers a tool for identifying and examining markers which could not have been found in cells cultured in a 2D environment.

No differences could be found between 2D and 3D culture regarding the staining for CD133 (fig. 3.30 and 3.31 E–H). Accordingly, its expression does not depend on the cells' environment. The specimen of colon adenocarcinoma showed staining for CD133 in single cells only (fig. 3.32 G). Tumours highly expressing CD133 are correlated with the worst survival, regardless of the expression of CD44 and CD166 [108]. Furthermore, there is evidence that CD133-positive cells are enriched in cancer-initiating cells in many tissues, e.g. retinoblastoma [167, 168], teratocarcinoma [167], brain tumour [98, 100], kidney cancer [169], prostate tumour [170], hepatocellular [102] and colon carcinoma [103, 104]. These CD133-positive CRC cells were found to be resistant to apoptosis because they produce interleukin-4 [171]. Additionally, studies have found that colon cancer cell spheroids grown *in vitro* also express Msi-1 and consist of heterogeneous popultions of cells: even though all the cells express CD133, different subpopulations express CD166, CD44, CD29, CD24, or Lgr5 [172, 173]. On the other hand, there is one single study which states that CD133

is not a specific marker of organ-specific stem and progenitor cells but that it is ubiquitously expressed in differentiated colonic epithelium of adult mice and humans [174]. Hence, an exact conclusion cannot be made regarding the CD133 expression of the 3D tumour models. For a detailed analysis of CD133-positive cancer stem cells, double stainings for the other mentioned markers have to be performed.

The stainings showed that in the 3D model EpCAM was only detected in apical cells of the tumour cell clusters but almost all cells were stained in conventional 2D culture (fig. 3.30 and 3.31 M–P). Probably the 3D environment promoted cell polarity which goes in line with previous findings [175–178]. However, the tumour cells of the colon adenocarcinoma were stained with low intensity (fig. 3.32 O) and some enterocytes only were stained in the healthy colon (fig. 3.32 P). This is contrary to the normal expression of EpCAM in glandular cells of the colon which present rather strong staining [179, 180], but can probably be explained by the longer fixation times of the native tissues in comparison to the 3D tumour models. Longer fixation times result in a stronger cross-linking of proteins and hence antigen epitopes which may have to be treated longer by heat-induced antigen retrieval or by enzymatic antigen retrieval respectively, in order to obtain a sufficient staining intensity.

In conclusion, almost all HROC24 and HROC87 cells were stained for CD44, CD133 and CD166. It is unlikely that all those cells are really (cancer) stem cells since tumours are thought to consist of a heterogeneous cell population and CSCs are small in number within a tumour [107] but it shows that these cells might have stem cell-like properties. For the detection of "real" cancer stem cells, it is crucial to perform multiple immunofluorescence co-stainings for two or three out of a multitude of different stem cell markers already described [110, 165]. Nevertheless, the results show that cells change their behaviour and expression depending on the culture method which then changes the experiment's outcome regarding the classification of distinct cells. Hence, it is important to include a cell's natural 3D environment in *in vitro* models for a more exact representation of the actual *in vivo* characteristics. Otherwise, artefacts are examined leading to wrong assumptions which explains the high attrition rates of clinical trials.

4.2.1.3 Analysis of EMT markers of HROC24 and HROC87 cells cultured in 2D as well as in 3D culture

Both cell lines displayed the epithelial marker E-cadherin which was co-localised with β-catenin at the cell borders in 2D as well as in 3D culture (fig. 3.34). Together with the present PCK staining and the absence of the mesenchymal

marker vimentin (fig. 3.35) the results show a definite epithelial phenotype of both HROC24 and HROC87 cell lines.

For comparison, a specimen of a HROC87 xenograft tumour as well as of a colon adenocarcinoma were stained for PCK and vimentin (fig. 3.36). The staining shows that the dense growth of HROC87 cells in the 3D tumour model resembles PCK-positive adenocarcinoma cells, although tumour stroma is lacking in the 3D model. The xenograft tumour presented a more spongy morphology with single vimentin-positive stromal cells which were probably of murine origin.

Adding stromal cells, e.g. fibroblasts or endothelial cells, will in future be necessary for *in vitro* models in order to improve and mimic the microenvironment of a tumour more precisely [175]. But for characterisation purposes, monoculture can give important information for the understanding of basic cellular processes.

4.2.1.4 Influence of FCS: Selection of a distinct cell subpopulation?

The growth pattern of HROC24 cells did not differ between the two FCS batches N° 8SB016 and N° BS196368 used, neither in 2D culture (fig. 3.12 A/E and D/G) nor in static 3D culture (fig. 3.12 B/F and D/H). In contrast, the cell line HROC87 presented a more enhanced cell growth with FCS Lot N° 8SB016 in 2D culture as well as in 3D culture than with the succeeding batch N° BS196368 (fig. 3.12 I/M and J/N vs. K/O and L/P). There were less HROC87 cells on the scaffold when cultured with FCS Lot N° BS196368 (fig. 3.13).

The stainings for CDX2 and CK7 did not show any differences between the two FCS batches for HROC24 cells, regardless of 2D or 3D culture (fig. 3.18 and 3.20). However, there were slightly more HROC24 cells stained for CK20 in 2D as well as in 3D culture when using media containing FCS N° BS196368. The same results were found for the cell line HROC87: the staining for CDX2 and CK7 did not differ between the two FCS batches, neither in 2D nor in 3D culture (fig. 3.19 and 3.21). But there were more CK20-positive HROC87 cells in 2D culture with FCS N° BS196368 than with N° 8SB016. In 3D culture, no cell was found to be stained for CK20 with FCS N° 8SB016. However, there were some HROC87 cells stained for CK20 with FCS N° BS196368. Furthermore, the stainings for the tumour stem cell markers did not show any differences between the two FCS batches in the two cell lines.

These results show that FCS can have an influence on cell growth and marker expression which is already known for the differentiation of mesenchymal stem cells [181]. It might be that the FCS batches differed in their growth factor

content and/or composition, thus conferring different growth and differentiating advantages to certain cell subclones. Inevitably, this will influence an experiment's outcome and create artefacts. Hence, future cell culture media must not rely on FCS but have to be chemically defined in order to avoid such artefacts which are presented and discussed in the next sections.

4.2.2 Targeted therapy of *BRAF*-mutant 3D tumour models

In order to test the hypothesis that the presented 3D tumour model provides an advanced test system that is more reliable and exact than conventional 2D *in vitro* models, targeted therapies of the *BRAF*-mutant CRC cell lines were performed with the two approved drugs gefitinib and vemurafenib. The readout parameters included assaying (immuno-)histological changes, proliferation rate, apoptosis rate, cell viability, and activation changes of proteins in common signalling pathways.

4.2.2.1 Histological changes of the targeted treatment

In static 3D culture, the cell line HROC24 responded slightly to the BRAF inhibitor vemurafenib but not to an anti-EGFR therapy with gefitinib alone. Both inhibitors presented a synergistic effect causing a visible reduction of the cell number which is displayed in H&E stainings (fig. 3.37). Furthermore, the cells were still expressing E-cadherin and β-catenin after treatment with gefitinib but the staining for β-catenin was less pronounced when treated with vemurafenib or a combination of both inhibitors (fig. 3.39). Neither the stainings for PCK nor for vimentin changed during treatments. Only fewer cells were visible (fig. 3.41). It shows that no EMT process was activated and that the cells still kept their epithelial phenotype.

In contrast, the H&E stainings revealed that there was no visible response of HROC87 cells to any drug or the combination of both drugs (fig. 3.38). As for the cell line HROC24, no changes of the EMT markers E-cadherin of β-catenin were detected, only the staining for β-catenin was not as pronounced in the combination therapy approach (fig. 3.40). PCK staining showed that the cells expressed this epithelial marker throughout the different types of treatment. Interestingly, some single cells were stained for vimentin only in the vemurafenib approach (fig. 3.42). It seemed that some cells had gained mesenchymal characteristics. Similarly, such a phenotype switch towards a mesenchymal state has already been described for melanoma cells which responded to (chronic) vemurafenib treatment with an elevated Wnt signalling and increased expression of the EMT inducer Wnt5A [182]. On the other hand, it was reported

that gefitinib inhibits the development of an invasive phenotype and EMT in drug-resistant NSCLC cells [183]. However, the staining for PCK and vimentin of the CC of HROC87 cells and (dermal) fibroblasts revealed that only fibroblasts seemed to be stained for vimentin. The tumour cells were only stained for PCK showing the maintenance of their epithelial character (fig. 3.43).

These diverging results of the two *BRAF*-mutant cell lines reflect the individual mutations in other genes: while HROC24 cells harbour mutations in exon 15 of *APC* but are wildtype for *TP53*, HROC87 cells harbour mutations in exons 6 and 7 of *TP53*, but are wildtype for *APC* [113].

4.2.2.2 Proliferation rate changes with culture condition

The Ki-67 index was markedly reduced in 3D culture compared to conventional 2D culture. This can be explained by contact inhibition which the cells experience in a 3D environment. In 2D culture, the proliferation rate was artificially high and more than 90 % of the cells proliferated. Moreover, the cancer cells in the 3D model showed a heterogeneous distribution of proliferating cells which resembled the specimen of an adenocarcinoma (fig. 3.44) showing sections with high and low proliferation rates.

The phenotype and genomic differences of the two cell lines can also be observed in the results of the Ki-67 index: HROC24 cells did not respond to gefitinib treatment. The proliferation rate was not found to be decreased, neither in 2D culture nor static 3D culture, but treatment with vemurafenib or the combination therapy led to a significant reduction of the proliferation rate in 2D culture (fig. 3.45 A–H and 3.46 A–B). In contrast, HROC87 cells showed a significant reduction of the Ki-67 index in conventional 2D culture with gefitinib monotherapy and its combination with vemurafenib (fig. 3.45 I–P and 3.47 A). In static 3D culture, the combination therapy only led to a significant decrease of the proliferation rate (fig. 3.47 B). For both cell lines, the number of cells per image was in average lower in static 3D culture than in conventional 2D culture (fig. 3.46 and 3.47 C–D), but the median HROC87 cell number per image stayed the same for both culture methods.

It could be demonstrated that the 3D tumour presented overall lower proliferation rates which are comparable to those of native tumours where an average Ki-67 index of 49 % was found in colorectal adenomas [184]. Hence, the 3D tumour model is superior to conventional 2D culture and mimics the *in vivo* situation regarding cell proliferation more accurately.

4.2.2.3 Apoptosis rates and viability were decreased in 3D culture and treatment response is FCS dependent

Because most HROC24 and HROC87 cells were found to be stained for CK18 in 2D culture as well as 3D culture (fig. 3.48), the M30 CytoDeath™ ELISA was suitable for the assessment of the apoptosis rate (see section 2.2.4 on page 60).

Significant differences in the apoptosis rate 48 h after treatment with vemurafenib and the combination therapy were found in HROC24 cells cultured in conventional 2D conditions with FCS N° 8SB016. In static 3D culture, no differences were found (fig. 3.49 A–B). Interestingly, the apoptosis rate showed a significant difference for the combination treatment only in 2D cultured HROC87 cells, whereas in 3D culture, the apoptosis rates did not differ between the different treatment approaches (fig. 3.50 A–B). These results tally with the previously described impact of a 3D environment concerning phenotype and gene expression of CRC cells [185] and probably explain the increased drug resistance which can be observed in 3D models [78, 186–188].

The influence of different FCS batches could be observed in both cell lines. HROC24 cells showed the same results in 2D culture for both FCS batches; but in 3D culture with FCS N° BS196368, the combination treatment with gefitinib and vemurafenib showed a significantly increased apoptosis rate in comparison to their respective monotherapies (fig. 3.49 D). In contrast, the cell line HROC87 did not respond to any treatment approach, neither in conventional 2D culture nor in static 3D culture with FCS N° BS196368 (fig. 3.50 C–D). This again underlines the distinct differences between the two cell lines regarding phenotype and molecular characteristics. Possibly, the different FCS batches might provide a growth advantage to a certain cell subclone which is more or less sensitive to drug treatments. Additionally, HROC87 cells grew even more densely in 2D culture with FCS N° BS196368 (fig. 3.12 K and O) which could explain the higher drug resistance compared to cells cultured with FCS N° 8SB016 (fig. 3.12 I and M).

For quantitation and quality reasons, the variability of the MTT test between different "cell crowns" for both cell lines was assessed. It did not exceed the requested standard deviation of 18 % (fig. S1) as stated in the OECD guidelines 439 for the testing of chemicals which are used for *in vitro* skin irritation tests with reconstructed human epidermis test models [189].

The results of the viability assays CellTiter-Glo® (fig. 3.51) and MTT test (fig. 3.52) supported the observations of the M30 ELISA. The viability of the cell line HROC24 was significantly reduced after the treatment with vemuraf-

enib and its combination with gefitinib in 2D culture, whereas no significant decrease in viability was found in 3D culture. Interestingly, HROC87 cells responded to all treatments in 2D culture but not in 3D culture. However, the combination therapy was more effective than the respective monotherapies. The reason why HROC87 cells responded to all treatments in 2D culture might be due to the fact that viability assays rely on the cells' metabolic activity and are also dependent on the number of cells [190]. Probably, HROC87 cells were more directly affected metabolically by the treatments and/or there were less in number than the HROC24 cells but yet the cells were more resistant to apoptosis induction because of their *TP53* mutation.

4.2.2.4 3D culture changes protein activations in the signalling pathway

The ProteomeProfiler™ Human Phospho-RTK Array (fig. S2) showed that the EGFR was activated in both cell lines. Additionally, HROC87 cells displayed a strong activation of the HGFR (Met). Because of this and the more malignant phenotype of HROC87 cells, this cell line was chosen for further investigations of the signalling pathway. Moreover, this cell line represented the typical resistance to inhibition with vemurafenib which is described in the clinic for patients harbouring the $BRAF^{V600E}$ mutation. Therefore, only HROC87 xenografts were established in PD Dr. M. Linnebacher's lab.

For comparison of 2D and 3D cultured HROC87 cells, they were further screened by the ProteomeProfiler™ Human Phospho-Kinase Array (fig. S3) for an overview of the activated proteins in the signalling pathway. Eventually, the major RTKs EGFR and Met as well as the kinases Erk1/2 and Akt were selected for western blot analysis of 2D and 3D cultured HROC87 cells as well as of HROC87 xenografts (fig. 3.53). The results show that the EGFR was expressed and gefitinib treatment decreased its activation in 2D culture as well as 3D culture. Moreover, Met activation was reduced by gefitinib treatment as well, but the signal was weaker in 2D culture than in 3D culture where the cells are less exposed to drugs and therefore possess an increased chemoresistance. As expected, Met activation was not affected by the BRAF inhibitor vemurafenib, neither in 2D culture nor 3D cultur. However, the downstream kinase Erk1/2 was less activated in 2D culture only. This was also true for the inhibition of both pEGFR and pMet by the small molecule gefitinib. Akt was constitutively active in 2D culture independent of the treatment approach, but it showed a strong activation signal of 3D cultured cells treated with the combination therapy which was the most successful in both culture methods. These results demonstrate the survival strategies of cells cultured in 2D culture and 3D culture: because of being more exposed to drugs in 2D culture,

the cells activate Akt blocking TP53 which could induce apoptosis. Hence, the cells attain a higher chemoresistance through Akt activation which has already been described as a resistance mechanism for lung cancer cells after treatment with gefitinib [191]. A similar underlying cellular process mediating the resistance of gastric cancer cells to Met inhibition by Akt activation was published by Corso *et al.* in 2010 [192], and the activation of the HER family was additionally involved. Furthermore, Fritsche-Guenther *et al.* reported that RAF inhibitors caused a reactivation of Akt in *BRAF*- or *KRAS*-mutant CRC cells by activating the PI3K/Akt pathway [193]. Taken together, the present results suggest the existence of resistance mechanisms other than only EGFR-mediated reactivation of the MAPK signalling observed in *BRAF*-mutant CRC cells after vemurafenib treatment, as proposed previously by Prahallad *et al.* and Corcoran *et al.* [67, 68]: It is more likely that the inhibition of EGFR and/or Met and BRAF leads to a reactivation of Akt which could be STAT3-mediated [191] or possibly MEK-dependent. Furthermore, PI3K inhibition with LY294002 was not successful in blocking the pAkt signal in HROC87 cells (fig. S6). This indicates the existence of another yet unknown mechanism of Akt activation which has been reported for certain pancreatic cancer cell lines [194]. Cancer cells manage to escape drug treatments in many ways and their distinct mutations must be taken into account.

The most important difference between the xenograft tumours and both, 2D and 3D, *in vitro* models was the activation of Met which could not be detected in the *in vivo* models (fig. 3.53). Probably, murine HGF is not compatible with human HGFR [195] and therefore no activation occurs. Similar findings have already been reported before and even humanised mouse models cannot predict human pharmacokinetics in a quantitative sense [87]. Hence, xenograft models do not properly reflect the activations of the signalling pathways occurring in tumour cells. This can lead to false conclusions regarding treatment outcome and success, respectively. Together with the fact that the xenograft tumours showed high variations in their tumour weights (fig. S4) and no significant differences in the tumour volumes (fig. S5), the 3D *in vitro* model presents a more superior and reasonable tool for drug testing.

4.3 Conclusion

It could be shown that (dermal) fibroblasts can have an influence on cancer cells, such as SW480 cells, and that co-cultures resemble a native tumour more closely as it never lacks stromal cells. Furthermore, dynamic culturing promotes cancer cell growth and thereby comes nearer to the *in vivo* situation of

a tumour, The established 3D tumour model provides an alternative test system for drug research and development, which could be shown in a standard chemotherapeutic treatment with 5-FU. In future, this test system might help to produce better and more accurate predictions of the drug response of a targeted therapy of *KRAS*-mutant carcinomas which account for approximately 40 % of all CRCs [14, 54].

Furthermore, it was shown that it is possible to perform and evaluate a targeted therapy for *BRAF*-mutant CRCs on basis of the here established 3D *in vitro* tumour model which is superior to conventional 2D culture methods or common *in vivo* models: While HROC24 cells were sensitive to treatment with the BRAF inhibitor vemurafenib which resembles the response of *BRAF*-mutant malign melanoma to inhibition of this kinase [62, 63], the cell line HROC87 showed resistance as previously described by Kopetz *et al.* [65, 66]. This difference in drug response might be caused by the distinct mutations of both early passage cell lines showing different grades of the original tumours [70]. The results suggest that it is not advisable to consider single driver mutations, e.g. $BRAF^{V600E}$, as isolated. Individual mutations have to be taken into account when treating patients with a targeted therapy in order to achieve the best possible outcome, which is in accordance to patient stratification in the context of personalised medicine [40].

In conclusion, the developed 3D *in vitro* CRC model in this study provides a basic tool for drug testing which might in future help to reduce the huge drug development costs by reflecting the processes of the signalling pathways more precisely and thereby providing more exact predictions of efficacy. By computational approach, this test system may provide the basis for further *in silico* models. Its modular setting allows to incorporate not only cancer cells but also stromal cells, such as fibroblasts, endothelial cells or lymphocytes, thus allowing to copy a tumour's microenvironment more precisely. Additionally, the 3D model may reduce animal experiments as these cannot truly reflect the processes occurring in a human tumour.

References

1. American Cancer Society. *Global Cancer Facts & Figures* https://www.cancer.org/research/cancer-facts-statistics/global.html, last access: 12.10.2017. 2017.
2. Nietzer, S., Baur, F., Sieber, S., Hansmann, J., Schwarz, T. *et al.* Mimicking Metastases Including Tumor Stroma: A New Technique to Generate a Three-Dimensional Colorectal Cancer Model Based on a Biological Decellularized Intestinal Scaffold. eng. *Tissue Eng Part C Methods* **22,** 621–635 (June 2016).
3. Lee, G., Malietzis, G., Askari, A., Bernardo, D., Al-Hassi, H. & Clark, S. Is right-sided colon cancer different to left-sided colorectal cancer? - A systematic review. *European Journal of Surgical Oncology* **41,** 300–308 (2015).
4. Hounnou, G., Destrieux, C., Desmé, J., Bertrand, P. & Velut, S. Anatomical study of the length of the human intestine. *Surgical and Radiologic Anatomy* **24,** 290–294 (2002).
5. Krogh, D. *Biology: a guide to the natural world* Fifth edition (Benjamin Cummings, 2011).
6. Young, B., O'Dowd, G. & Woodford, P. *Wheater's Functional Histology: A text and colour atlas.* 6th edition (Churchill Livingstone, 2013).
7. Sipos, F., Molnár, B., Zágoni, T., Berczi, L. & Tulassay, Z. Growth in epithelial cell proliferation and apoptosis correlates specifically to the inflammation activity of inflammatory bowel diseases: ulcerative colitis shows specific p53- and EGFR expression alterations. *Diseases of the Colon and Rectum* **48,** 775–786 (2005).
8. Sipos, F., Leiszter, K. & Tulassay, Z. Effect of ageing on colonic mucosal regeneration. *World Journal of Gastroenterology* **17,** 2981–2986 (2011).
9. Colussi, D., Brandi, G., Bazzoli, F. & Ricciardiello, L. Molecular pathways involved in colorectal cancer: Implications for disease behavior and prevention. *International Journal of Molecular Sciences* **14** (2013).

10. Siegel, R. L., Miller, K. D., Fedewa, S. A., Ahnen, D. J., Meester, R. G., Barzi, A. & Jemal, A. Colorectal cancer statistics, 2017. eng. *CA Cancer J Clin* **64,** 104–117 (2017).

11. International Agency for Research on Cancer (IARC). *GLOBOCAN 2012: Cancer fact sheets: Colorectal cancer - Estimated incidence, mortality and prevalence worldwide in 2012.* http://globocan.iarc.fr/Pages/fact_sheets_cancer.aspx?cancer=colorectal, last access: 01.10.2017. 2012.

12. Siegel, R. L., Miller, K. D. & Jemal, A. Cancer statistics, 2017. *CA Cancer J Clin* **67,** 7–30 (2017).

13. International Agency for Resarch on Cancer (IARC). *GLOBOCAN 2012: Population fact sheets: Estimated cancer incidence, mortality and prevalence worldwide in 2012.* http://globocan.iarc.fr/Pages/fact_sheets_population.aspx, last access: 01.10.2017. 2012.

14. Vogelstein, B., Fearon, E. R., Hamilton, S. R., Kern, S. E., Preisinger, A. C., Leppert, M., Nakamura, Y., White, R. & Smits Alida ande Bos, J. L. Genetic alterations during colorectal-tumor development. *The New England Journal of Medicine* **319,** 525–532 (1988).

15. Fearon, E. R. & Vogelstein, B. A genetic model for colorectal tumorigenesis. *Cell* **61,** 759–767 (1990).

16. American Cancer Society. *Colorectal Cancer Facts & Figures 2017-2019* (Atlanta: American Cancer Society, 2017).

17. Schatzkin, A., Freedman, L. S., Dawsey, S. M. & Lanza, E. Interpreting precursor studies: What polyp trials tell us about large-bowel cancer. *Journal of the National Cancer Institute* **86,** 1053–1057 (1994).

18. Levine, J. S. & Ahnen, D. J. Adenomatous polyps of the colon. *The New England Jounal of Medicine* **355,** 2551–2557 (2006).

19. Morson, B. C. Evolution of cancer of the colon and rectum. *Cancer* **34,** 845–849 (1974).

20. Risio, M. The natural history of adenomas. *Best Practise & Research. Clinical gastroenterology.* **24,** 271–280 (2010).

21. Pickhardt, P., Kim, D., Pooler, B., Hinshaw, J., Barlow, D., Jensen, D., Reichelderfer, M. & Cash, B. Volumetric growth rates of small colorectal polyps: Longitudinal investigation of natural history using CT colonography. *Lancet Oncology* **14,** 711–720 (2013).

22. Stryker, S., Wolff, B., Culp, C., Libbe, S., Ilstrup, D. & MacCarty, R. Natural history of untreated colonic polyps. *Gastroenterology* **93,** 1009–1013 (1987).

23. Fleming, M., Ravula, S., Tatishchev, S. F. & Wang, H. L. Colorectal carcinoma: Pathologic aspects. eng. *J Gastrointest Oncol* **3,** 153–173 (Sept. 2012).

24. Weisenberger, D., Siegmund, K., Campan, M., Young, J., Long, T. *et al.* CpG island methylator phenotype underlies sporadic microsatellite instability and is tightly associated with BRAF mutation in colorectal cancer. *Nature Genetics* **38,** 787–793 (2006).

25. Boland, C. R. & Goel, A. Microsatellite instability in colorectal cancer. eng. *Gastroenterology* **138,** 2073–2087.e3 (June 2010).

26. Chan, T. L., Zhao, W., Leung, S. Y. & Yuen, S. T. BRAF and KRAS mutations in colorectal hyperplastic polyps and serrated adenomas. *Cancer Research* **63,** 4878–4881 (2003).

27. Samowitz, W., Albertsen, H., Herrick, J., Levin, T., Sweeney, C., Murtaugh, M., Wolff, R. & Slattery, M. Evaluation of a large, population-based sample supports a CpG island methylator phenotype in colon cancer. *Gastroenterology* **129,** 837–845 (2005).

28. Nosho, K., Irahara, N., Shima, K., Kure, S., Kirkner, G. *et al.* Comprehensive biostatistical analysis of CpG island methylator phenotype in colorectal cancer using a large population-based sample. *PLoS One* **3.** doi:10.1371/journal.pone.0003698 (2008).

29. Roth, A. D., Tejpar, S., Delorenzi, M., Yan, P., Fiocca, R. *et al.* Prognostic role of KRAS and BRAF in stage II and III resected colon cancer: results of the translational study on the PETACC-3, EORTC 40993, SAKK 60-00 trial. eng. *J Clin Oncol* **28,** 466–474 (Jan. 2010).

30. Rajagopalan, H., Bardelli, A., Lengauer, C., Kinzler, K., Vogelstein, B. & Velculescu, V. Tumorigenesis: RAF/RAS oncogenes and mismatch-repair status. *Nature* **418** (2002).

31. Bouzourene, H., Hutter, P., Losi, L., Martin, P. & Benhattar, J. Selection of patients with germline MLH1 mutated Lynch syndrome by determination of MLH1 methylation and BRAF mutation. *Familial Cancer* **9,** 167–172 (2010).

32. National Institutes of Health (NIH). *Advances in colorectal cancer research: Stages of colorectal cancer.* https://www.nih.gov/research-training/advances-colorectal-cancer-research, last access: 04.10.2017. 2015.

33. Winawer, S. & Zauber, A. The advanced adenoma as the primary target of screening. *Gastroinstestinal Endoscopy Clinics of North America* **12,** 1–9 (2002).

34. Zauber, A. G., Winawer, S. J., O'Brien, M. J., Lansdorp-Vogelaar, I., van Ballegooijen, M. *et al.* Colonoscopic polyectomy and long-term prevention of colorectal-cancer deaths. *The New England Journal of Medicine* **366,** 687–696 (2012).

35. Sargent, D., Sobrero, A., Grothey, A., O'Connell, M. J., Buyse, M. *et al.* Evidence for cure by adjuvant therapy in colon cancer: Observations based on individual patient data from 20,898 patients on 18 randomized trials. *Journal of Clinical Oncology* **27,** 872–877 (2009).

36. Baudino, T. A. Targeted cancer therapy: The next generation of cancer treatment. *Current Drug Discovery Technologies* **12,** 3–20 (2015).

37. Van Cutsem, E., Nordlinger, B. & Cervantes, A. Advanced colorectal cancer: ESMO clinical practice guidelines for treatment. *Annals of Oncology* **21,** 93–97 (2010).

38. Hanahan, D. & Weinberg, R. The hallmarks of cancer. eng. *Cell* **100,** 57–70 (Jan. 2000).

39. Hanahan, D. & Weinberg, R. A. Hallmarks of cancer: the next generation. eng. *Cell* **144,** 646–674 (Mar. 2011).

40. (ed European Commission, D. R.) *Biomarkers for patient stratification.* (European Commission, Health Research Directorate, Brussels, 2010).

41. Whang, J., Frei, E. I., Tjio, J., Carbone, P. & Brecher, G. The distribution of the philadelphia chromosome in patients with chronic myelogenous leukemia. *Blood* **22,** 664–667 (1963).

42. Elefanty, A., Hariharan, I. & Cory, S. bcr-abl, the hallmark of chronic myeloid leukaemia in man, induces multiple haematopoietic neoplasms in mice. *EMBO Journal* **9,** 1069–1078 (1990).

43. National Cancer Institute. *Targeted cancer therapies: What targeted therapies have been approved for specific types of cancer?* https://www.cancer.gov/about-cancer/treatment/types/targeted-therapies/targeted-therapies-fact-sheet, last access: 03.10.2017. 2017.

44. US Food and Drug Administration. *Iressa ® (gefitinib)* https://www.accessdata.fda.gov/drugsatfda_docs/label/2005/021399s008lbl.pdf, last access: 03.10.2017. 2004.
45. US Food and Drug Administration. *Tarceva ® (erlotinib)* https://www.accessdata.fda.gov/drugsatfda_docs/label/2016/021743s025lbl.pdf, last access: 03.10,2017. 2016.
46. Gazdar, A. Activating and resistance mutations of EGFR in non-small-cell lung cancer: role in clinical response to EGFR tyrosine kinase inhibitors. *Oncogene* **28 (Suppl. 1),** S24–31 (2009).
47. US Food and Drug Administration. *Erbitux ® (cetuximab)* https://www.accessdata.fda.gov/drugsatfda_docs/label/2012/125084s225lbl.pdf, last access: 03.10.2017. 2012.
48. US Food and Drug Administration. *Vectibix ® (panitumumab)* https://www.accessdata.fda.gov/drugsatfda_docs/label/2009/125147s067lbl.pdf, last access: 03.10.2017. 2008.
49. US Food and Drug Administration. *Avastin ® (bevacizumab)* https://www.accessdata.fda.gov/drugsatfda_docs/label/2014/125085s305lbl.pdf, last access: 03.10.2017. 2014.
50. US Food and Drug Administration. *Cyramza (Ramucirumab)* https://www.accessdata.fda.gov/drugsatfda_docs/label/2015/125477s011lbl.pdf, last access: 03.10.2017. 2015.
51. US Food and Drug Administration. *Opdivo (nivolumab)* https://www.accessdata.fda.gov/drugsatfda_docs/label/2017/125554s034lbl.pdf, last access: 03.10.2017. 2017.
52. US Food and Drug Administration. *Stivarga ® (regorafenib)* https://www.accessdata.fda.gov/drugsatfda_docs/label/2017/203085s007lbl.pdf, last access: 03.10.2017. 2017.
53. US Food and Drug Administration. *Zaltrap ® (ziv-aflibercept)* https://www.accessdata.fda.gov/drugsatfda_docs/label/2012/125418s000lbl.pdf, last access: 03.10.2017. 2012.
54. Andreyev, H., Norman, A., Cunningham, D., Oates, J., Dix, B. *et al.* Kristen ras mutations in patients with colorectal carcinoma: the 'RASCAL II' study. *British Journal of Cancer* **85,** 692–696 (2001).
55. Arnold, D. & Seufferlein, T. Targeted treatments in colorectal cancer: state of the art and future perspectives. eng. *Gut* **59,** 838–858 (June 2010).

56. Davies, H., Bignell, G. R., Cox, C., Stephens, P., Edkins, S. *et al.* Mutations of the BRAF gene in human cancer. eng. *Nature* **417,** 949–954 (June 2002).

57. Wilhelm, S., Carter, C., Lynch, M., Lowinger, T., Dumas, J., Smith, R., Schwartz, B., Simantov, R. & Kelley, S. Discovery and development of sorafenib: a multikinase inhibitor for treating cancer. *Nature Reviews. Drug Discovery.* **5,** 835–844 (2006).

58. Gysin, S., Salt, M., Young, A. & McCormick, F. Therapeutic strategies for targeting Ras proteins. *Genes Cancer* **2,** 359–372 (2011).

59. Pratilas, C. & Solit, D. Targeting the mitogen-activated protein kinase pathway: physiological feedback and drug response. *Clinical Cancer Research* **16,** 3329–3334 (2010).

60. Li, H., Chen, Y., Rao, S., Chen, X., Liu, H., Qin, J., Tang, W., Yue-Wang, Zhou, X. & Lu, T. Recent advances in the research and development of B-Raf inhibitors. *Current Medicinal Chemistry* **17,** 1618–1634 (2010).

61. US Food and Drug Administration. *Zelboraf ™ (vemurafenib, PLX4032)* https://www.accessdata.fda.gov/drugsatfda_docs/label/2011/202429s000lbl.pdf, last access: 03.10.2017. 2011.

62. Flaherty, K. T., Puzanov, I., Kim, K. B., Ribas, A., McArthur, G. A. *et al.* Inhibition of mutated, activated BRAF in metastatic melanoma. eng. *N Engl J Med* **363,** 809–819 (Aug. 2010).

63. Chapman, P. B., Hauschild, A., Robert, C., Haanen, J. B., Ascierto, P. *et al.* Improved survival with vemurafenib in melanoma with BRAF V600E mutation. eng. *N Engl J Med* **364,** 2507–2516 (June 2011).

64. Yuen, S. T., Davies, H., Chan, T. L., Ho, J. W., Bignell, G. R. *et al.* Similarity of the phenotypic patterns associated with BRAF and KRAS mutations in colorectal neoplasia. *Cancer Research* **62,** 6451–6455 (2002).

65. Kopetz, S., Desai, J., Chan, E., Hecht, J., O'dwyer, P., Lee, R., Nolop, K. & Saltz, L. *PLX4032 in metastatic colorectal cancer patients with mutant BRAF tumors.* in *ASCO Annual Meeting Proceedings* **28** (2010), 3534.

66. Kopetz, S., Desai, J., Chan, E., Hecht, J. R., O'Dwyer, P. J. *et al.* Phase II Pilot Study of Vemurafenib in Patients With Metastatic BRAF-Mutated Colorectal Cancer. eng. *J Clin Oncol* **33,** 4032–4038 (Dec. 2015).

67. Corcoran, R. B., Ebi, H., Turke, A. B., Coffee, E. M., Nishino, M. *et al.* EGFR-mediated re-activation of MAPK signaling contributes to insensitivity of BRAF mutant colorectal cancers to RAF inhibition with vemurafenib. eng. *Cancer Discov* **2,** 227–235 (Mar. 2012).

68. Prahallad, A., Sun, C., Huang, S., Di Nicolantonio, F., Salazar, R., Zecchin, D., Beijersbergen, R. L., Bardelli, A. & Bernards, R. Unresponsiveness of colon cancer to BRAF(V600E) inhibition through feedback activation of EGFR. eng. *Nature* **483,** 100–103 (Mar. 2012).

69. Yaeger, Rona (Memorial Sloan Kettering Cancer Center). *Vemurafenib and panitumumab combination therapy in patients with BRAF V600E mutated metastatic colorectal cancer.* https://clinicaltrials.gov/ct2/show/study/NCT01791309?view=results, last access: 09.10.2017. 2015.

70. Maletzki, C., Stier, S., Gruenert, U., Gock, M., Ostwald, C., Prall, F. & Linnebacher, M. Establishment, characterization and chemosensitivity of three mismatch repair deficient cell lines from sporadic and inherited colorectal carcinomas. eng. *PLoS One* **7,** e52485 (2012).

71. Langer, P. & Vacanti, J. Tissue engineering. *Science* **260,** 920–926 (1993).

72. Caddeo, S., Boffito, M. & Sartori, S. Tissue engineering approaches in the design of healthy and pathological in vitro tissue models. *Frontiers in Bioengineering and Biotechnology* **5** (2017).

73. O'Brien, F. J. Biomaterials & scaffolds for tissue engineering. *Materials today* **14,** 88–95 (2011).

74. Mertsching, H., Walles, T., Hofmann, M., Schanz, J. & Knapp, W. H. Engineering of a vascularized scaffold for artificial tissue and organ generation. eng. *Biomaterials* **26,** 6610–6617 (Nov. 2005).

75. Schanz, J. *Etablierung einer biologischen vaskularisierten Matrix als Grundlage für ein in vitro Lebertestsystem* PhD thesis (Universität Stuttgart, Fakultät für Geo- und Biowissenschaften, 2007).

76. Pusch, J. *Etablierung einer 3D-Darmgewebestruktur zur in vitro Untersuchung der Resorption potentieller Wirkstoffe auf Basis einer natürlichen Kollagenmatrix.* PhD theses (Universität Konstanz, Mathematisch-Naturwissenschaftliche Sektion, Fachbereich Biologie, 2009).

77. Schanz, J., Pusch, J., Hansmann, J. & Walles, H. Vascularised human tissue models: a new approach for the refinement of biomedical research. eng. *J Biotechnol* **148,** 56–63 (July 2010).

78. Stratmann, A. T., Fecher, D., Wangorsch, G., Göttlich, C., Walles, T., Walles, H., Dandekar, T., Dandekar, G. & Nietzer, S. L. Establishment of a human 3D lung cancer model based on a biological tissue matrix combined with a Boolean in silico model. eng. *Mol Oncol* **8,** 351–365 (Mar. 2014).

79. Moreno, L. & Pearson, A. D. How can attrition rates be reduced in cancer drug discovery. *Expert Opinion on Drug Discovery* **8,** 363–368 (2013).

80. Waring, M. J., Arrowsmith, J., Leach, A. R., Leeson, P. D., Mandrell, S. *et al.* An analysis of the attrition of drug candidates from four major pharmaceutical companies. *Nature Reviews Drug Discovery* **14,** 475–486 (2015).

81. Schuhmacher, A., Gassmann, O. & Hinder, M. Changing R&D models in research-based pharmaceutical companies. *Journal of Translational Medicine* **14** (2016).

82. Ghajar, C. M. & Bissell, M. J. Tumor engineering: The other face of tissue engineering. *Tissue Engineering: Part A* **16,** 2153–2156 (2010).

83. Kimlin, L. C., Casagrande, G. & Virador, V. M. In vitro three-dimensional (3D) models in cancer research: An update. *Molecular Carcinogenesis* **52,** 167–182 (2013).

84. Russel, W. & Burch, R. *The principles of humane experimental technique.* (Methuen, London, 1959).

85. The Commission to the Council and the European Parliament. *Seventh Report on the Statistics on the Number of Animals used for Experimental and other Scientific Purposes in the Member States of the European Union.* http://eur-lex.europa.eu/legal-content/EN/TXT/?uri=CELEX:52013DC0859, last access: 23.10.2017. 2013.

86. Shanks, N., Greek, R. & Greek, J. Are animal models predictive for humans? *Philosophy, Ethics, and Humanities in Medicine* **4** (2009).

87. Lin, J. Applications and limitations of genetically modified mouse models in drug discovery and development. *Current Drug Metabolism* **9,** 419–438 (2008).

88. Kalluri, R. & Neilson, E. Epithelial-mesenchymal transition and its implications for fibrosis. *Journal of Clinical Investigation* **112,** 1776–1784 (2003).

89. Kalluri, R. & Weinberg, R. A. The basics of epithelial-mesenchymal transition. *Journal of Clinical Investigation* **119,** 1420–1428 (2009).

90. Hay, E. D. An overview of epithelio-mesenchymal transformation. *Acta Anatomica* **154,** 8–20 (1995).

91. Zeisberg, M. & Neilson, E. G. Biomarkers for epithelial-mesenchymal transitions. *Journal of Clinical Investigation* **119,** 1429–1437 (2009).

92. Lamouille, S., Xu, J. & Derynck, R. Molecular mechanisms of epithelial-mesenchymal transition. *Nature Reviews Molecular Cell Biology* **15,** 178–196 (2014).

93. Singh, a. & Settleman, J. EMT, cancer stem cells and drug resistance: an emerging axis of evil in the war on cancer. *Oncogene* **29,** 4741–4751 (2010).

94. Raymond, W. & Leong, A. Vimentin–a new prognostic parameter in breast carcinoma? *Journal of Pathology* **158,** 107–114 (1982).

95. Clevers, H. The intestinal crypt, a prototype stem cell compartment. *Cell* **154,** 274–284 (2013).

96. Batlle, E. & Clevers, H. Cancer stem cells revisited. *Nature Medicine* **23,** 1124–1134 (2017).

97. Lapidot, T., Sirard, C., Vormoor, J., Murdoch, B., Hoang, T., Caceres-Cortes, J., Minden, M., Paterson, B., Caligiuri, M. A. & Dick, J. E. A cell initiating human acute myeloid leukaemia after transplantation into SCID mice. *Nature* **367,** 645–648 (1994).

98. Singh, S., Clarke, I., Terasaki, M., Bonn, V., Hawkins, C., Squire, J. & Dirks, P. Identification of a cancer stem cell in human brain tumors. *Cancer Research* **63,** 5821–5828 (2003).

99. Al-Hajj, M., Wicha, M., Benito-Hernandez, A., Morrison, S. & Clarke, M. Prospective identification of tumorigenic breast cancer cells. *Proc Natl Acad Sci USA* **100,** 3983–3988 (2003).

100. Singh, S., Hawkins, C., Clarke, I., Squire, J., Bayani, J., Hide, T., Henkelman, R., Cusimano, M. & Dirks, P. Identification of human brain tumor initiating cells. *Nature* **432,** 396–401 (2004).

101. Hermann, P., Huber, S., Herrler, T., Aicher, A., Ellwart, J., Guba, M., Bruns, C. & Heeschen, C. Distinct population of cancer stem cells determine tumor growth and metastatic activity in human pancreatic cancer. *Cell Stem Cell* **1,** 313–323 (2007).

102. Yin, S., Li, J., Hu, C., Chen, X., Yao, M. *et al.* CD133 positive hepatocellular carcinoma cells possess high capacity for tumorigenicity. *International Journal of Cancer* **120,** 1444–1450 (2007).

103. O'Brien, C., Pollett, A., Gallinger, S. & Dick, J. A human colon cancer cell capable of initiating tumour growth in immunodeficient mice. *Nature* **445,** 106–110 (2007).

104. Ricci-Vitiani, L., Lombardi, D., Pilozzi, E., Biffoni, M., Todaro, M., Peschle, C. & De Maria, R. Identification and expansion of human colon-cancer-initiating cells. *Nature* **445,** 111–115 (2007).

105. Dubrovska, A., Kim, S., Salamone, R., Walker, J., Maira, S., García-Echeverría, C., Schultz, P. & Reddy, V. The role of PTEN/Akt/PI3K signaling in the maintenance and viability of prostate cancer stem-like cell populations. *Proc Natl Acad Sci USA* **106,** 268–273 (2009).

106. Clarke, M. F., Dick, J. E., Dirks, P. B., Eaves, C. J., Jamieson, C. H., Jones, D. L., Visvader, J., Weissman, I. L. & Wahl, G. M. Cancer Stem Cells–Perspectives on current status and future directions: AACR workshop on cancer stem cells. *Cancer Research* **66** (2006).

107. Ishawata, T. Cancer stem cells and epithelial-mesenchymal transition: Novel therapeutic targets for cancer. *Pathology International* **66,** 601–608 (2016).

108. Horst, D., Kriegl, L., Engel, J., Kirchner, T. & Jung, A. Prognostic significance of the cancer stem cell markers CD133, CD44, and CD166 in colorectal cancer. *Cancer Investigation* **27,** 844–850 (2009).

109. Weidle, U., Eggle, D., Klostermann, S. & Swart, G. ALCAM/CD166: cancer-related issues. *Cancer Genomics & Proteomics* **7,** 231–243 (2010).

110. Wahab, S., Islam, F., Gopalan, V. & Lam, A. The identification and clinical implications of cancer stem cells in colorectal cancer. *Clinical Colorectal Cancer* **16,** 93–102 (2017).

111. The Human Protein Atlas. *CD133 (Prominin 1)* https://www.proteinatlas.org/ENSG00000007062-PROM1/tissue, last access: 12.10.2017.

112. Lugli, A., Iezzi, G., Hostettler, I., Muraro, M., Mele, V., Tornillo, L., Carafa, V., Spagnoli, G., Terracciano, L. & Zlobec, I. Prognostic impact of the expression of putative cancer stem cell markers CD133, CD166, CD44s, EpCAM, and ALDH1 in colorectal cancer. *British Journal of Cancer* **103,** 382–390 (2010).

113. Maletzki, C., Klier, U., Marinkovic, S., Klar, E., Andrä, J. & Linnebacher, M. Host defense peptides for treatment of colorectal carcinoma - a comparative in vitro and in vivo analysis. eng. *Oncotarget* **5,** 4467–4479 (June 2014).

114. Leibovitz, A., Stinson, J., McCombs 3rd, W., McCoy, C., Mazur, K. & Mabry, N. Classification of human colorectal adenocarcinoma cell lines. eng. *Cancer Res* **36,** 4562–4569 (Dec. 1976).

115. Fogh, J., Wright, W. & Loveless, J. Absence of HeLa cell contamination in 169 cell lines derived from human tumors. *J Natl Cancer Inst* **58,** 209–214 (Feb. 1977).

116. ATCC. *SW480* http://www.lgcstandards-atcc.org/Products/all/CCL-228.aspx#characteristics, last access: 18.09.2017.

117. Mertsching, H., Schanz, J., Steger, V., Schandar, M., Schenk, M., Hansmann, J., Dally, I., Friedel, G. & Walles, T. Generation and transplantation of an autologous vascularized bioartificial human tissue. eng. *Transplantation* **88,** 203–210 (July 2009).

118. Schultheiss, D., Gabouev, A. I., Cebotari, S., Tudorache, I., Walles, T. *et al.* Biological vascularized matrix for bladder tissue engineering: matrix preparation, reseeding technique and short-term implantation in a porcine model. eng. *J Urol* **173,** 276–280 (Jan. 2005).

119. Linke, K., Schanz, J., Hansmann, J., Walles, T., Brunner, H. & Mertsching, H. Engineered liver-like tissue on a capillarized matrix for applied research. eng. *Tissue Eng* **13,** 2699–2707 (Nov. 2007).

120. Mosmann, T. Rapid colorimetric assay for cellular growth and survival: application to proliferation and cytotoxicity assays. eng. *J Immunol Methods* **65,** 55–63 (Dec. 1983).

121. Berridge, M. V., Tan, A. S., McCoy, K. D. & Wang, R. The Biochemical and Cellular Basis of Cell Proliferation Assays That Use Tetrazolium Salts. *Biochemica* **4.** https://lifescience.roche.com/wcsstore/RASCatalog%20AssetStore/Articles/BIOCHEMICA_96_4_p14-19.pdf (1996).

122. Schutte, B., Henfling, M., Kölgen, W., Bouman, M., Meex, S. *et al.* Keratin 8/18 breakdown and reorganization during apoptosis. eng. *Exp Cell Res* **297,** 11–26 (July 2004).

123. Leers, M., Kölgen, W., Björklund, V., Bergman, T., Tribbick, G. *et al.* Immunocytochemical detection and mapping of a cytokeratin 18 neo-epitope exposed during early apoptosis. eng. *J Pathol* **187,** 567–572 (Apr. 1999).

124. Gerdes, J., Lemke, H., Baisch, H., Wacker, H., Schwab, U. & H, S. Cell cycle analysis of a cell proliferation-associated human nuclear antigen defined by the monoclonal antibody Ki-67. *The Journal of Immunology* **133,** 1710–1715 (1984).

125. Lowry, O., Rosebrough, N., Farr, A. & Randall, R. Protein measurement with the Folin phenol reagent. eng. *J Biol Chem* **193,** 265–275 (Nov. 1951).

126. Wessel, D. & Flügge, U. A method for the quantitative recovery of protein in dilute solution in the presence of detergents and lipids. eng. *Anal Biochem* **138,** 141–143 (Apr. 1984).

127. Sanders, M. A. & Majumdar, A. P. Colon cancer stem cells: implications in carcinogenesis. *Front Biosci* **16,** 1651–1662 (2014).

128. Kola, I. & Landis, J. Can the pharmaceutical industry reduce attrition rates? *Nature Reviews Drug Discovery* **3,** 711–716 (2004).

129. Arrowsmith, J. & Miller, P. Trial Watch: Phase II and Phase III attrition rates 2011-2012. *Nature Reviews Drug Discovery* **12,** 569 (2013).

130. Fu, J., Fernandez, D., Ferrer, M., Titus, S. A., Buhler, E. & Lal-Nag, M. A. RNAi high-throughput screening of single- and multi-cell-type tumor spheroids: A comprehensive analysis in two and three dimensions. *SLAS Discovery* **22,** 525–536 (2017).

131. Sharpless, N. E. & DePinho, R. A. The mighty mouse: genetically engineered mouse models ins cancer drug development. *Nature Reviews Drug Discovery* **5,** 741–754 (2006).

132. Francia, G. & Kerbel, R. S. Raising the bar for cancer therapy models. *Nature Biotechnology* **28,** 561–562 (2010).

133. Begley, C. G. & Ellis, L. M. Drug development: Raise standards for preclinical cancer research. *Nature* **483,** 531–533 (2012).

134. Dainiak, M. B., Savina, I. N., Musolino, I., Kumar, A., Mattiasson, B. & Galaev, I. Y. Biomimetic macroporous hydrogel sscaffold in a high-throughput screening format for cell-based assays. *Biotechnology Progress* **24,** 1373–1383 (2008).

135. Chandrasekaran, S., Deng, H. & Fang, Y. PTEN deletion potentiates invasion of colorectal cancer spheroidal cells through 3D matrigel. *Integrative Biology* **7,** 324–334 (2015).

136. Ivanovska, J., Zehnder, T., Lennert, P., Sarker, B., Boccaccini, A. R., Hartmann, A., Schneider-Stock, R. & Detsch, R. Biofabrication of 3D alginate-based hydrogel for cancer research: Comparison of cell spreading, viability, and adhesion characteristics of colorectal HCT116 Tumor cells. *Tissue Engineering: Part C* **22,** 823–835 (2016).

137. Kim, T.-E., Kim, C. G., Kim, J. S., Jin, S., Yoon, S., Bae, H.-R., Kim, J.-H., Jeong, Y. H. & Kwak, J.-Y. Three-dimensional culture and interaction of cancer cells and dendritic cells in an electrospun nano-submicron hybrid fibrous scaffold. *International Journal of Nanomedicine* **11,** 823–835 (2016).

138. Bender, B. F., Aijian, A. P. & Garrell, R. L. Digital microfluidics for spheroid-based invasion assays. *Lab on a Chip* **16,** 1505–1513 (2016).

139. Jouanneau, J., Tucker, G., Boyer, B., Vallés, A. & Thiery, J. Epithelial cell plasticity in neoplasia. *Cancer Cells* **3,** 525–529 (1991).

140. Boyer, B. & Thiery, J. Epithelium-mesenchyme interconversion as an example of epithelial plasticity. *APMIS* **101,** 257–268 (1993).

141. Birchmeier, C., Birchmeier, W. & Brand-Saberi, B. Epithelial-mesenchymal transitions in cancer progression. *Acta Anatomica* **156,** 217–226 (1996).

142. Wells, A., Yates, C. & Shepard, C. E-cadherin as an indicator of mesenchymal to epithelial reverting transitions during the metastatic seeding of disseminated carcinomas. *Clin Exp Metastasis* **25,** 621–628 (2008).

143. Yao, D., Dai, C. & Peng, S. Mechanism of the mesenchymal-epithelial transition and its relationship with metastatic tumor formation. *Molecular Cancer Research* **9,** 1608–1620 (2011).

144. Zhou, L., Yang, K., Randall Wickett, R. & Zhang, Y. Dermal fibroblasts induce cell cycle arrest and block Epithelial-mesenchymal transition to Inhibit the early stage melanoma development. *Cancer Medicine* **5,** 1566–1579 (2016).

145. Rao, T. P. & Kühl, M. An updated overview on Wnt signaling pathways. *Circulation Research* **106,** 1798–1806 (2010).

146. Micalizzi, D. S., Farabaugh, S. M. & Ford, H. L. Epithelial-mesenchymal transition in cancer: Parallels between normal development and tumor progression. *J Mammary Gland Biol Neoplasia* **15,** 117–134 (2010).

147. Santos, R., Benvenuti, T., Honda, S., Del Valle, P., Katayama, M. *et al.* Influence of the interaction between nodal fibroblast and breast cancer cells on gene expression. *Tumor Biology* **32,** 145–157 (2011).

148. Iacopino, F., Angelucci, C. & Sica, G. Interactions between normal human fibroblasts and human prostate cancer cells in a co-culture system. *Anticancer Research* **32,** 1579–1588 (2012).

149. Kalluri, R. & Zeisberg, M. Fibroblasts in cancer. *Nature Reviews Cancer* **6,** 392–401 (2006).

150. Orimo, A. & Weinberg, R. A. Heterogeneity of stromal fibroblasts in tumor. *Cancer Biology and Therapy* **6,** 618–619 (2007).

151. Moll, C., Reboredo, J., Schwarz, T., Appelt, A., Schürlein, S., Walles, H. & Nietzer, S. Tissue engineering of a human 3D in vitro tumor test system. eng. *J Vis Exp.* doi:10.3791/50460 (2013).

152. Herdrich, K. & Weinberger, H. *Selected schedules in the therapy of malignant tumors* 16th edition (Baxter Oncology, 2011).

153. Yoshikawa, R., Kusunoki, M., Yanagi, H., Noda, M., Furuyama, J., Yamamura, T. & Hashimoto-Tamaoki, T. Dual antitumor effects of 5-fluorouracil on the cell cycle in Colorectal carcinoma cells: a novel target mechanism concept for pharmacokinetic modulating chemotherapy. *Cancer Research* **61,** 1029–1037 (2001).

154. Bracht, K., Nicholls, A., Liu, Y. & Bodmer, W. 5-Fluorouracil response in a large panel of colorectal cancer cell lines is associated with mismatch repair deficiency. *British Journal of Cancer* **103,** 340–346 (2010).

155. Mhaidat, N., Bouklihacene, M. & Thorne, R. 5-Fluorouracil-induced apoptosis in colorectal cancer cells is caspase-9-dependent and mediated by activation of protein kinase C-delta. *Oncology Letters* **8,** 699–704 (2014).

156. Gonçalves-Ribeiro, S., Díaz-Maroto, N., Berdiel-Acer, M., Soriano, A., Guardiola, J. *et al.* Carcinoma-associated fibroblasts affect sensitivity to oxaliplatin and 5FU in colorectal cancer cells. *Oncotarget* **7,** 59766–59780 (2016).

157. Tao, L., Huang, G., Wang, R., Pan, Y., He, Z., Chu, X., Song, H. & Chen, L. Cancer-associated fibroblasts treated with cisplatin facilitates chemoresistence of lung adenocarcinoma through IL-11/IL-11R/STAT3 signaling pathway. *Scientific Reports* **6.** doi:10.1038/srep38408 (2016).

158. Harati, K., Daigeler, A., Hirsch, T., Jacobsen, F., Behr, B., Wallner, C., Lehnhardt, M. & Becerikli, M. Tumor-associated fibroblasts promote the proliferation and decrease the doxorubicin sensitivity of liposarcoma cells. *International Journal of Molecular Medicine* **37,** 1535–1541 (2016).

159. Lee, D. A., Shapourifar-Tehrani, S. & Kitada, S. The effect of 5-fluorouracil and cytarabine on human fibroblasts from tenon's capsule. *Investigative Ophthalmology & Visual Science* **31,** 1848–1855 (1990).

160. Ophir, A. Effects of 5-fluorouracil on proliferating fibroblasts in vivo. *Experimental Eye Research* **53,** 799–803 (1991).

161. Werling, R., Yaziji, H., Bacchi, C. & Gown, A. CDX2, a highly sensitive and specific marker of adenocarcinomas of intestinal origin: an immunohistochemical survey of 476 primary and metastatic carcinomas. *American Journal of Surgical Pathology* **27,** 303–310 (2003).

162. Kaimaktchiev, V., Terracciano, L., Tornillo, L., Spichtin, H., Stoios, D. *et al.* The homeobox intestinal differentiation factor CDX2 is selectively expressed in gastrointestinal adenocarcinomas. *Modern Pathology* **17,** 1392–1399 (2004).

163. Chu, P. & Weiss, L. Keratin expression in human tissues and neoplasms. *Histopathology* **40,** 403–439 (2002).

164. McGregor, D., Wu, T., Rashid, A., Luthra, R. & Hamilton, S. Reduced expression of cytokeratin 20 in colorectal carcinomas with high levels of microsatellite instability. *American Journal of Surgical Pathology* **28,** 712–718 (2004).

165. Willis, N., Przyborski, S., Hutchinson, C. & Wilson, R. Colonic and colorectal cancer stem cells: progress in the search for putative biomarkers. *Journal of Anatomy* **213,** 59–65 (2008).

166. Visvader, J. E. & Lindeman, G. J. Cancer stem cells in solid tumours: accumulating evidence and unresolved questions. eng. *Nat Rev Cancer* **8,** 755–768 (Oct. 2008).

167. Miraglia, S., Godfrey, W., Yin, A., Atkins, K., Warnke, R., Holden, J., Bray, R., Waller, E. & Buck, D. A novel five-transmembrane hematopoietic stem cell antigen: isolation, characterization, and molecular cloning. *Blood* **90,** 5013–5021 (1997).

168. Maw, M., Corbeil, D., Koch, J., Hellwig, A., Wilson-Wheeler, J. *et al.* A frameshift mutation in prominin (mouse)-like 1 causes human retinal degeneration. *Human Molecular Genetics* **9,** 27–34 (2000).

169. Bussolati, B., Bruno, S., Grange, C., Buttiglieri, S., Deregibus, M., Cantino, D. & Camussi, G. Isolation of renal progenitor cells from adult human kidney. *American Journal of Pathology* **166,** 545–555 (2005).

170. Collins, A., Berry, P., Hyde, C., Stower, M. & Maitland, N. Prospective Identification of tumorigenic prostate cancer stem cells. *Cancer Research* **65,** 10946–10951 (2005).

171. Todaro, M., Alea, M., Di Stefano, A., Cammareri, P., Vermeulen, L. *et al.* Colon cancer stem cells dictate tumor growth and resist cell death by production of interleukin-4. *Cell Stem Cell* **1,** 389–402 (2007).

172. Todaro, M., Perez Alea, M., Scopelliti, A., Medema, J. & Stassi, G. IL-4-mediated drug resistance in colon cancer stem cells. *Cell Cycle* **7,** 309–313 (2008).

173. Vermeulen, L., Todaro, M., de Sousa Mello, F., Sprick, M., Kemper, K., Perez Alea, M., Richel, D., Stassi, G. & Medema, J. Single-cell cloning of colon cancer stem cells reveals a multi-lineage differentiation capacity. *Proc Natl Acad Sci U S A* **105,** 13427–13432 (2008).

174. Shmelkov, S., Butler, J., Hooper, A., Hormigo, A., Kushner, J. *et al.* CD133 expression is not restricted to stem cells, and both CD133+ and CD133- metastatic colon cancer cells initiate tumors. *Journal of Clinical Investigation* **118,** 2111–2120 (2008).

175. Kim, J. B. Three-dimensional tissue culture models in cancer biology. *Seminars in Cancer Biology* **15,** 365–377 (2005).

176. Yamada, K. M. & Cukierman, E. ModModel tissue morphogenesis and cancer in 3D. *Cell* **130,** 601–610 (2007).

177. Eritja, N., Llobet, D., Domingo, M., Santacana, M., Yeramian, A., Matias-Guiu, X. & Dolcet, X. A novel three-dimensional culture system of polarized epithelial cells to study endometrial carcinogenesis. *American Journal of Pathology* **176,** 2722–2731 (2010).

178. Inman, J. L. & Bissell, M. J. Apical polarity in three-dimensional culture systems: where to now? *J Biol* **9** (2010).

179. Schmelzer, E. & Reid, L. EpCAM expression in normal, non-pathological tissues. *Front Biosci* **13,** 3096–3100 (2008).

180. The Human Protein Atlas. *EPCAM - Colon* https://www.proteinatlas.org/ENSG00000119888-EPCAM/tissue/colon#imid_14811802, last access: 18.09.2017.

181. Yokoyama, M., Miwa, H., Maeda, S., Wakitani, S. & Takagi, M. Influence of fetal calf serum on differentiation of mesenchymal stem cells to chondrocytes during expansion. *Journal of Bioscience and Bioengineering* **106,** 46–50 (2008).

182. Zhentao, F. L., Dhillon, A. S., Anderson, R. L., McArthur, G. & Ferrao, P. T. Phenotype switching in melanoma: Implications for progression and therapy. *Front O* **5** (2015).

183. La Monica, S., Caffarra, C., Saccani, F., Galvani, E., Galetti, M. *et al.* Gefitinib inhibits invasive phenotype and Epithelial-mesenchymal transition in drug-resistant NSCLC cells with MET amplification. *PLoS One* **8** (2013).

184. de Sousa, W., Rodrigues, L., Silva Jr., R. & Vieira, F. Immunohistochemical evaluation of p53 and Ki-67 proteins in colorectal adenomas. *Arquivos de gastroenterologia* **49,** 35–40 (2012).

185. Luca, A., Mersch, S., Deenen, R., Schmidt, S., Messner, I. *et al.* Impact of the 3D microenvironment on phenotype, gene Expression, and EGFR inhibition of colorectal cancer cell lines. *PLoS One* **8.** doi:10.1371/journal.pone.0059689 (2013).

186. Trédan, O., Galmarini, C., Patel, K. & Tannock, I. Drug resistance and the solid tumor microenvironment. *J Natl Cancer Inst* **99,** 1441–1454 (2007).

187. Longati, P., Jia, X., Eimer, J., Wagman, A., Witt, M. R., Rehnmark, S., Verbeke, C., Toftgård, R., Löhr, M. & Heuchel, R. L. 3D pancreatic carcinoma spheroids induce a matrix-rich, chemoresistant phenotype offering a better model for drug testing. *BMC Cancer* **13** (2013).

188. Edmondson, R., Jenkins Brogli, J., Adcock, A. F. & Yang, L. Three-dimensional cell culture systems and their applications in drug discovery and cell-based biosensors. *Assay and Drug Development Technologies* **12,** 207–218 (2014).

189. OECD iLibrary: Organisation for Economic Co-operation and Development. *OECD guidelines for the testing of chemicals: 439 - In vitro skin irritation: Reconstructed human epidermis test method* http://www.oecd-ilibrary.org/docserver/download/9715291e.pdf?expires=1506600233&id=id&accname=guest&checksum=, last access: 28.09.2017. 2015.

190. *Cell Viability Assays - Methods and Protocols* (eds Gilbert, D. F. & Friedrich, O.) (Humana Press, 2017).

191. Wu, K., Chang, Q., Lu, Y., Qiu, P., Chen, B., Thakur, C., Sun, J., Li, L., Kowluru, A. & Chen, F. Gefitinib resistance resulted from STAT3-mediated Akt activation in lung cancer cells. *Oncotarget* **4,** 2430–2438 (2013).

192. Corso, S., Ghiso, E., Cepero, V., Sierra, J. R., Migliore, C., Bertotti, A., Trusolino, L., Comoglio, P. M. & Giordano, S. Activation of HER family members in gastric carcinoma cells mediates resistance to MET inhibition. *Mol Cancer* **9** (2010).

193. Fritsche-Guenther, R., Witzel, F., Kempa, S., Brummer, T., Sers, C. & Blüthgen, N. Effects of RAF inhibitors on PI3K/AKT signalling depend on mutational status of the RAS/RAF signalling axis. eng. *Oncotarget* **7,** 7960–7969 (Feb. 2016).

194. Matsumoto, J., Kaneda, M., Tada, M., Hamada, J.-i., Okushiba, S., Kondo, S., Katoh, H. & Moriuchi, T. Differential mechanisms of contitutive Akt/PKB activation and its influcence on gene expression in pancreatic cancer cells. *Japanese Journal of Cancer Research* **93,** 1317–1326 (2002).

195. Weinberg, R. *The Biology of Cancer* (Garland Science: New York, 2006).

Supplementary data

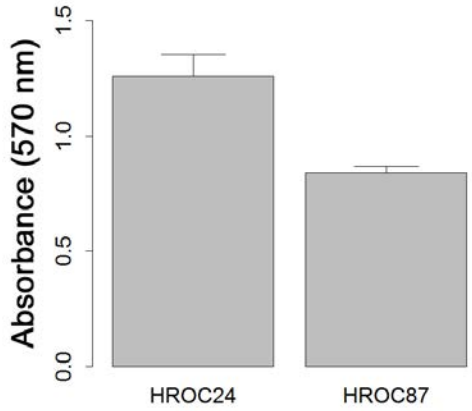

Figure S1: Quantitative MTT test for the evaluation of the deviation between different experimental approaches of HROC24 cells and HROC87 cells cultured in static 3D culture. When MTT is being metabolically reduced to formazan, it forms water-insoluble crystals within the cells. These can be solubilised with isopropanol and quantitatively measured by absorptiometry. Shown here are the mean absorbances at 570 nm for the solubilised formazan of both cell lines. HROC24 cells displayed a mean absorbance of 1.25985 with a standard deviation of the mean of 7.37 % (n = 4). The cell line HROC87 presented a standard deviation of 3.34 % of the mean absorbance of 0.84115 (n = 4). Error bars show the standard deviation of the mean absorbance: 0.09280318 for HROC24 cells and 0.02807045 for HROC87 cells.

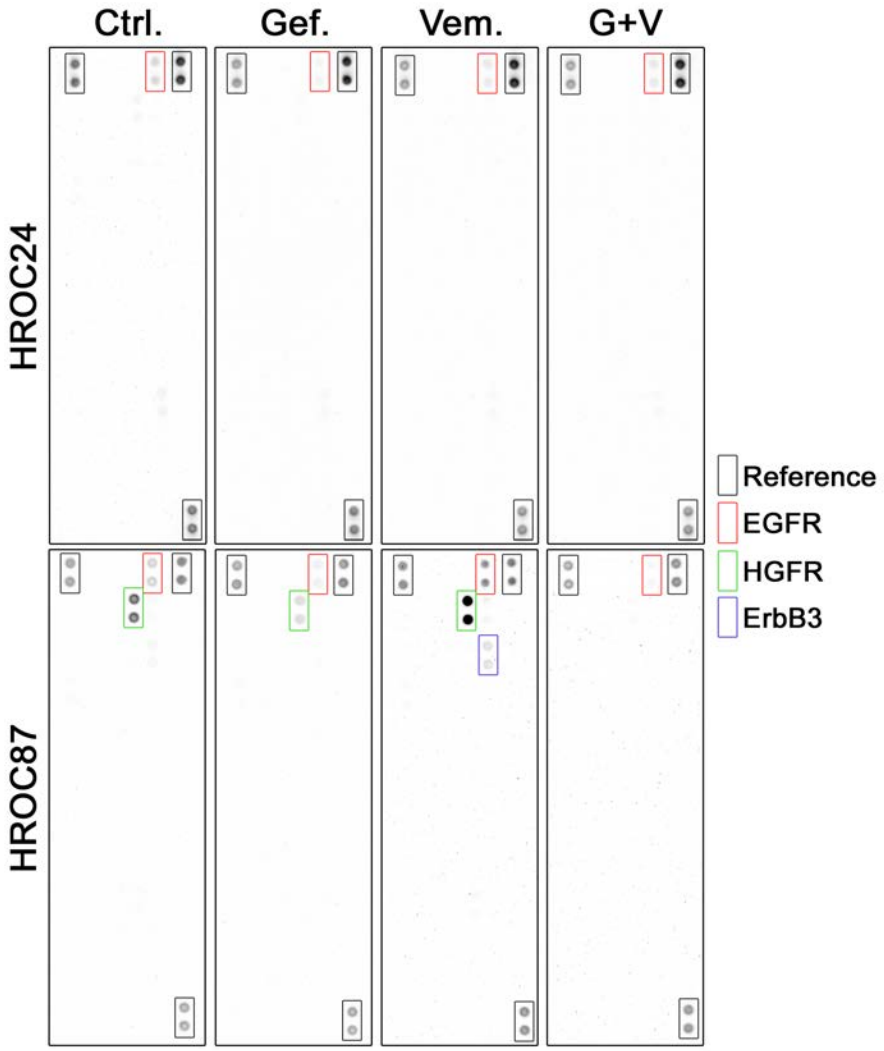

Figure S2: ProteomeProfiler™ Human Phospho-RTK Array of HROC24 cells and HROC87 cells cultured in static 3D culture (FCS Lot N° 8SB016) and treated with gefitinib (Gef.), vemurafenib (Vem.) and a combination of both drugs (G+V). Displayed are the reference spots (black rectangles), the spots of the epidermal growth factor receptor (EGFR, red rectangles), the spots of the hepatocyte growth factor receptor (HGFR/c-Met, green rectangles) and the spots of the EGFR family type B3 (ErbB3/Her-3, blue rectangle). Gef. therapy resulted in a reduction of the EGFR signal. HGFR was not detectable in HROC24 cells but in HROC87 cells. Vem. treatment resulted in an activation of HGFR and ErbB3 in HROC87 cells. The G+V therapy blocked the activation of HGFR as well as of EGFR in the cell line HROC87.

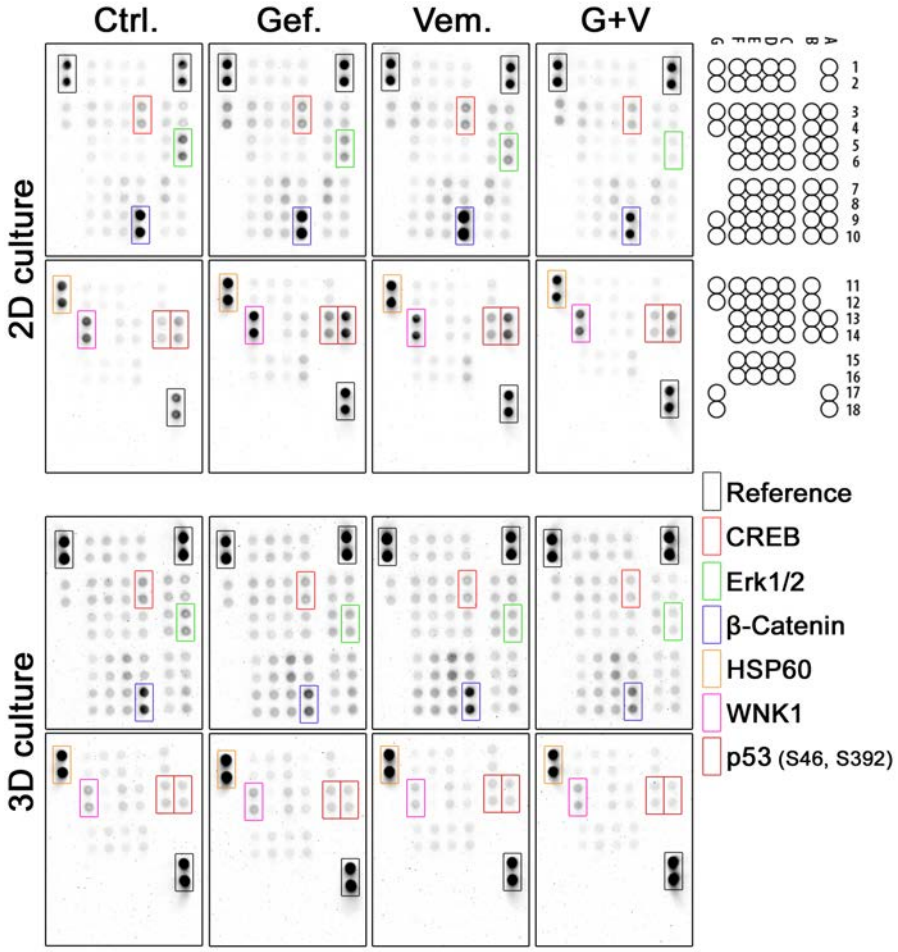

Figure S3: ProteomeProfiler™ Human Phospho-Kinase Array (R&D Systems) of HROC87 cells cultured in conventional 2D culture as well as in static 3D culture (FCS Lot N° 8SB016). Displayed are the spots showing a stronger signal (coloured rectangles) of the control (Ctrl.) as well as of cells being treated with gefitinib (Gef.), vemurafenib (Vem.) or a combination of both drugs (G+V). The coordinates of the array are depicted in the upper right corner of the figure. The targets of the antibodies' spots are listed in table S1.

Table S1: Coordinates of the Proteome Profiler™ Human Phospho-Kinase Array displayed in figure S3. (neg. ctrl. = negative control)

Coordinate	**Target/Control**	**Coordinate**	**Target/Control**
A1, A2	Reference spot	A13, A14	p53 (S392)
A3, A4	p38α	A17, A18	Reference spot
A5, A6	Erk1/2	B11, B12	Akt 1/2/3 (T308)
A7, A8	JNK 1/2/3	B13, B14	p53 (S46)
A9, A10	GSK-3α/β	C11, C12	p70 S6 Kinase (T389)
B3, B4	EGFR	C13, C14	p53 (S15)
B5, B6	MSK1/2	C15, C16	c-Jun
B7, B8	AMPKα1	D11, D12	p70 S6 Kinase (T241/S424)
B9, B10	Akt 1/2/3 (S473)	D13, D14	RSK 1/2/3
C1, C2	TOR	D15, D16	eNOS
C3, C4	CREB	E11, E12	STAT3 (Y705)
C5, C6	HSP27	E13, E14	p27
C7, C8	AMPKα2	E15, E16	PLC-γ1
C9, C10	β-Catenin	F11, F12	STAT3 (S727)
D1, D2	Src	F13, F14	WNK1
D3, D4	Lyn	F15, F16	PYK2
D5, D6	Lck	G11, G12	HSP60
D7, D8	STAT2 (Y689)	G17, G18	PBS (neg. ctrl.)
D9, D10	STAT5a (Y694)	—	—
E1, E2	Fyn	—	—
E3, E4	Yes	—	—
E5, E6	Fgr	—	—
E7, E8	STAT6	—	—
E9, E10	STAT5b	—	—
F1, F2	Hck	—	—
F3, F4	Chk-2	—	—
F5, F6	FAK	—	—
F7, F8	PDGFRβ	—	—
F9, F10	STAT5a/b	—	—
G1, G2	Reference spot	—	—
G3, G4	PRAS40	—	—
G9, G10	PBS (neg. ctrl.)	—	—

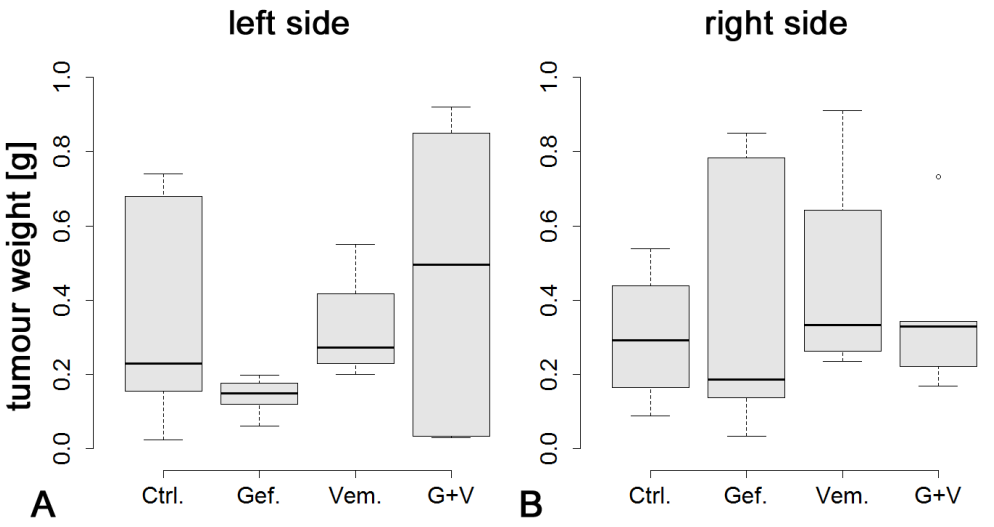

Figure S4: Tumour weight of HROC87 xenografts. Displayed are the tumour weights of HROC87 cells injected subcutaneously into the left side (A) and right side (B) of male NMRI Foxn1nu mice which were treated for 21 days with gefitinib (Gef., 100 mg/kg, 3x per week i.p.), vemurafenib (Vem., 417 mg/kg, ad libitum) or a combination of both drugs (G+V). The control group (Ctrl.) received 28 µl DMSO i.p. 3x per week. The median weights of the left sided tumours of Ctrl., Gef., Vem., and G+V were 0.230 g, 0.149 g, 0.2725 g, and 0.4950 g, respectively. The tumours on the right side weighed in median 0.2915 g (Ctrl.), 0.187 g (Gef.), 0.3325 g (Vem.), and 0.329 g (G+V). Data comprises n = 5 for each treatment group.

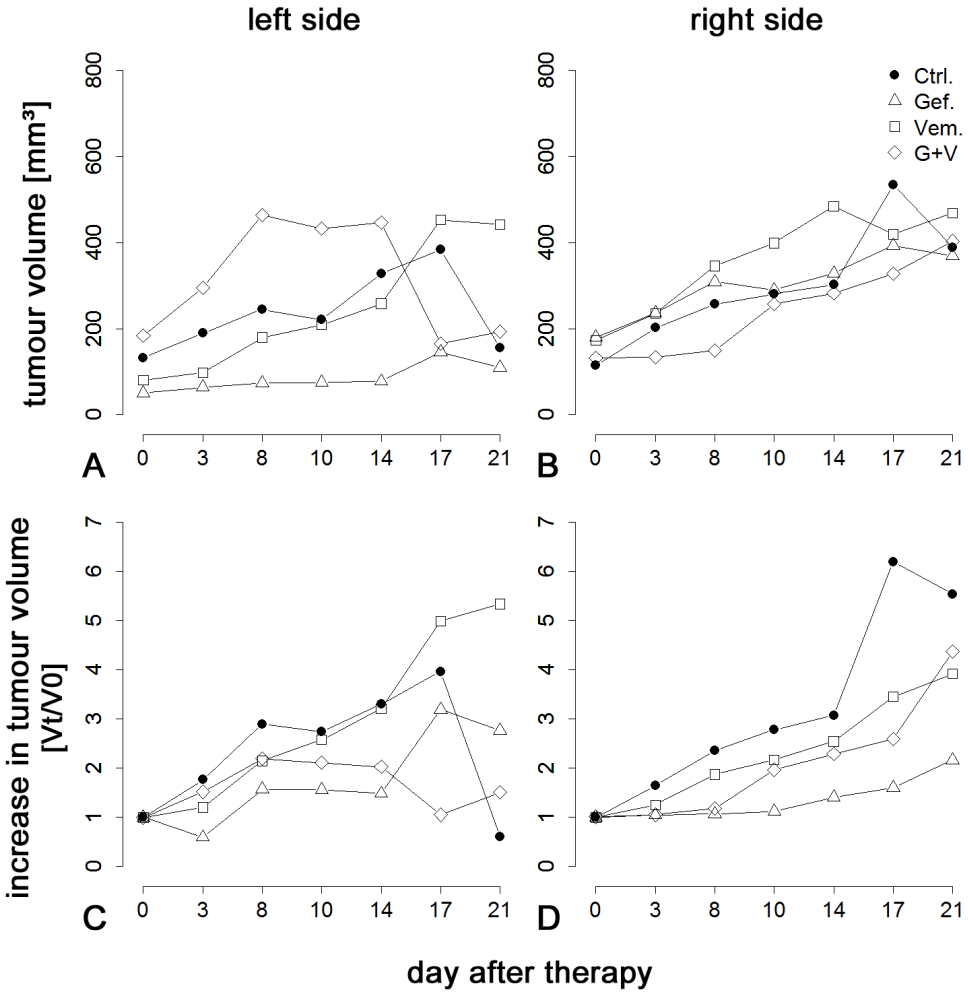

Figure S5: Absolute tumour volume (A–B) and increase in the tumour volume (C–D) of HROC87 xenografts. Displayed are the absolute tumour volumes of HROC87 cells injected subcutaneously into the left side (A) and right side (B) of male NMRI Foxn1nu mice as well as the increase in the tumour volumes (Vt/V0) over the treatment time of 21 days for left sided (C) and right sided (D) tumours. Data comprises n = 5 for each treatment group.

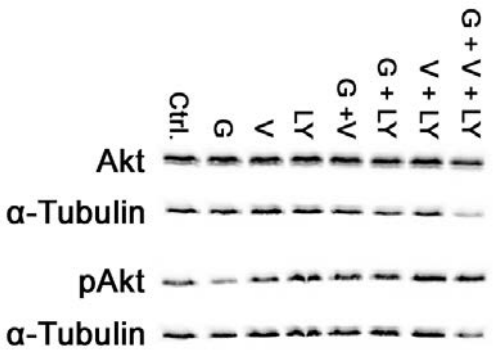

Figure S6: Western blot analysis for Akt and pAkt of HROC87 cells cultured in 2D conditions and treated with 1 µM gefitinib (G), 1 µM vemurafenib (V) and/or 10 µM LY294002 (LY). The signal of phosphorylated Akt (pAkt) was not reduced by treatment with its upstream activator PI3K inhibitor LY. This indicates either an insensitivity of PI3K to the drug LY294002 for the used concentration of 10 µM or a rescue mechanism to restore Akt activation via another signalling pathway kinase.

Affidavit/Eidesstattliche Erklärung

Affidavit

I hereby confirm that my doctoral thesis entitled "Establishment of a 3D tumour model and targeted therapy of *BRAF*-mutant colorectal carcinoma" is the result of my own work. I did not receive any help or support from commercial consultants. All sources and/or materials applied are listed and specified in the thesis.

Furthermore, I confirm that this thesis has not yet been submitted as part of an examination process neither in identical nor in similar form.

Place, Date	Signature

Eidesstattliche Erklärung

Hiermit versichere ich an Eides statt, dass meine Dissertation mit dem Titel „Establishment of a 3D tumour model and targeted therapy of *BRAF*-mutant colorectal carcinoma" eigenständig, d.h. insbesondere selbständig und ohne Hilfe eines kommerziellen Promotionsberaters angefertigt und keine anderen als die von mir angegebenen Quellen und Hilfsmittel benutzt habe.

Die vorgelegte Dissertation wurde bisher bei keinem anderen Prüfungsverfahren in gleicher oder ähnlicher Form eingereicht; sie ist nicht identisch mit der von mir verfassten Diplomarbeit.

Die meinem Promotionsverfahren zugrunde liegende Promotionsordnung für die Fakultät für Biologie der Julius-Maximilians-Universität Würzburg ist mir bekannt.

Ort, Datum	Unterschrift

Publications and conference contributions

Articles

Sarah Nietzer*, Florentin Baur*, Stefan Sieber, Jan Hansmann, Thomas Schwarz, Carolin Stoffer, Heide Häfner, Martin Gasser, Ana Maria Waaga-Gasser, Heike Walles, and Gudrun Dandekar. Mimicking metastases including tumor stroma: A new technique to generate a three-dimensional colorectal cancer model based on a biological decellularized intestinal scaffold. Tissue Engineering: Part C, Volume 22, Number 7, 2016.
(* Authors contributed equally to this article.)

Oral presentations

Florentin Baur, Sarah Nietzer, Gudrun Dandekar, Heike Walles. Targeted therapies of two different *BRAF*-mutated cell lines and the establishment of a 3D tumor model on the basis of a decellularized intestinal matrix. World Conference on Regenerative Medicine (WCRM) 2015, Congress Center Leipzig, Leipzig, Germany.

Posters

Florentin Baur, Gudrun Dandekar, Sarah Nietzer, Heike Walles. Targeted therapies of two different *BRAF*-mutated cell lines and the establishment of a 3D tumor model on the basis of a decellularized intestinal matrix. 31. Deutscher Krebskongress (DKK) 2014 (February 19–22), Messe Berlin: Messegelände Süd, Berlin, Germany.

Florentin Baur, Gudrun Dandekar, Sarah Nietzer, Heike Walles. Targeted therapies of two different *BRAF*-mutated cell lines and the establishment of a 3D tumor model on the basis of a decellularized intestinal matrix. DECHEMA

3D Cell Culture 2014: Advanced Model Systems, Applications & Enabling Technologies (June 25–27), Konzerthaus Freiburg, Freiburg, Germany.

Florentin Baur, Gudrun Dandekar, Sarah Nietzer, Heike Walles. Targeted therapies of two different *BRAF*-mutated cell lines and the establishment of a 3D tumor model on the basis of a decellularized intestinal matrix. European Association for Cancer Research (EACR) Conference Series 2014: Goodbye Flat Biology – 3D Models & the Tumour Microenvironment (November 2–5), Harnack House Berlin, Berlin, Germany.

Florentin Baur, Gudrun Dandekar, Sarah Nietzer, Heike Walles. Targeted therapies of two different *BRAF*-mutated cell lines and the establishment of a 3D tumor model on the basis of a decellularized intestinal matrix. 18th International AEK Cancer Congress 2015 (March 18–20), EMBL Heidelberg, Heidelberg, Germany.

Florentin Baur, Gudrun Dandekar, Sarah Nietzer, Heike Walles. Targeted therapies of two different *BRAF*-mutated cell lines and the establishment of a 3D tumor model on the basis of a decellularized intestinal matrix. Cambridge Health Institute's 3rd annual Functional Analysis & Screening Technologies (FAST) Congress 2015 (November 9–11), Renaissance Waterfront Hotel Boston, Boston (MA), USA.

Florentin Baur, Gudrun Dandekar, Sarah Nietzer, Heike Walles. Targeted therapies of two different *BRAF*-mutated cell lines and the establishment of a 3D tumor model on the basis of a decellularized intestinal matrix. 32. Deutscher Krebskongress (DKK) 2016 (February 24–27), Messe Berlin: City Cube Berlin, Berlin, Germany.

Florentin Baur, Gudrun Dandekar, Sarah Nietzer, Heike Walles. Targeted therapies of two different *BRAF*-mutated cell lines and the establishment of a 3D tumor model on the basis of a decellularized intestinal matrix. DECHEMA 3D Cell Culture 2016: How close to 'in vivo' can we get? Models, applications & translation (April 19–21), Konzerthaus Freiburg, Freiburg, Germany.

Acknowledgement

I wish to begin by expressing my sincerest gratitude to Prof. Dr. Heike Walles for giving me the great opportunity to conduct my PhD thesis at the Chair of Tissue Engineering & Regenerative Medicine of the University Hospital Würzburg.

Furthermore, I would like to express my warmest thanks to Prof. Dr. Thomas Dandekar for being my second supervisor as well as for the incredibly fast proofreading and constructive criticism of my thesis.

For their guidance during the experimental and the write-up phase of the thesis as well as for their enthusiasm and patience, I am especially grateful to Dr. Sarah Nietzer and Dr. Gudrun Dandekar. I always enjoyed working with and for you and I appreciated your constant encouragement.

Besides my supervisors, I would like to thank the whole team of the Chair of Tissue Engineering & Regenerative Medicine for providing a great and pleasant atmosphere to work in. There always was an open ear, an encouraging word or a helping hand if you needed anything.

Special thanks go to Heide Häfner, Heike Oberwinkler, Sabine Gätzner, Sabine Graiff, Sabine Wilhelm and Christa Amrehn for assisting me in SISmuc preparation, cell culture, histology, protein chemistry and bioreactor issues as well as for helping out in holidays or illness.

Huge thanks go to Lena Nelke for having always an open ear and for her moral support during any crisis as well as for chatting in the lab about everything what is out there in the world. Also, I would like to thank Claudia Göttlich for sharing her experience and for her organisational skills. I also thank you both for helping out in cell culture during holidays or illness.

Furthermore, I wish to express heartfelt thanks to the “Internationals”, Reem, Melva, Jihyoung, Miguel, Ives, Claudia S., Markus, and Maria V., for their support and the nice atmosphere in the office where I always felt welcome. I will miss the chats and the fun we used to have, the laughing and our jokes

about anything as well as learning important words and phrases in a multitude of languages “to survive on the streets”.

I would like to express my deepest gratitude to my wife Veronica for sharing all my ups and downs, for giving me unlimited support, strength and confidence and for just being who you are.

Last but not least, I want to thank my parents, Irene and Philipp, and my grandparents as well as the rest of my family for supporting me during my studies and in all situations along my way.